TECHNISCHE UNIVERSITÄT MÜNCHEN
Munich School of Engineering
Forschungsgruppe „Energy Efficient and Smart Cities“

Integration of Decentralized Battery Storage in Low Voltage Systems

Akhila Jambagi

Vollständiger Abdruck der von der Munich School of Engineering der Technischen Universität München zur Erlangung des akademischen Grades eines

Doktor–Ingenieurs (Dr.-Ing.)

genehmigten Dissertation.

Vorsitzender:		Prof. Dr. Thomas Hamacher
Prüfer der Dissertation:	1.	Vicky Albert-Seifried, Ph.D.
	2.	Prof. Dipl-Ing. Thomas Auer
	3.	Prof. Dr.-Ing. Andreas Jossen

Die Dissertation wurde am 20.11.2019 bei der Technischen Universität München eingereicht und durch die Munich School of Engineering am 09.03.2021 angenommen.

Acknowledgements

First, I would like to thank my supervisor Dr. Vicky Cheng for providing the opportunity to work in the Energy Efficient and Smart Cities group, and for her support throughout my time at the TUM. I would also like to express my gratitude to Professor Thomas Hamacher for the guidance and humorous discourse. I am also grateful to the MSE, and the Energy Valley Bavaria program, which supplied support and funding throughout my research.

My gratitude also goes to all my colleagues at the TUM, for the collaborations and good times. A special thanks is owed to Michael Kramer, whose friendship and close teamwork has been so valuable to me throughout the last six years. In addition I would like to express my gratitude to the Cleanvelope team, particularly Lisa, Lea and Claudia for the great atmosphere and moral support during the final stage of my PhD.

A further thanks to my friends and family, who have cheered me on during this long process. My most sincere love and gratitude to my mother Usha, and sister Neesha, who never fail to inspire me and give me strength.

The most important thank you goes to my partner Dom, who has helped me through so many challenges. Thank you for your endless patience and support.

Abstract

In the movement towards a more sustainable energy system, increasing the share of renewable generation is an important step. Amongst the many options for renewable generation, distributed PV has seen significant growth, particularly in Germany. Battery storage can be used to support distributed generation, for instance by increasing the amount of local self-consumption and preventing grid overload. So far, the implementation of distributed battery storage has not been widespread mainly due to high cost.

The focus of this thesis is the "Optimal Planning Problem" of battery storage, which refers to the identification of cost optimal capacity and location of battery units in the grid. Emphasis is placed on decentralized storage, as it is shown to be successful at preventing curtailment of intermittent renewables by balancing out unacceptable voltages or currents. A number of novel modelling tools are developed to study the optimal planning problem using two case study distribution grids for demonstration.

A highly detailed and flexible load profile generator is presented, that provides statistically accurate representative profiles for residential loads for the case studies. The first planning algorithm presented is an annual optimisation problem that includes energy price, feed in tariff and storage price to determine the cost optimal battery storage capacity at each node in the grid. Solving this optimisation problem is time consuming, and the optimal storage results are highly sensitive to price. Due to unreasonable solving time, this method cannot be applied to large distribution grids.

A novel algorithm is proposed, which is suitable for use on large grids and provides results for a wide array of price scenarios. This method is labelled the Two Stage algorithm, as it decomposes the planning problem into a sizing stage and a placement stage. The sizing stage uses a heuristic method to approximate the total optimal storage capacity, and the placement stage distributes the storage amongst the nodes in the grid.

The Two Stage algorithm results can be used identify total optimal storage for a wide range of price scenarios instantly. This feature is used to investigate the effect of price trends on optimal storage, showing that as both storage prices and feed in tariffs reduce, storage becomes a lot more profitable quickly. At some level of storage penetration the marginal benefit of additional storage reduces.

The Two Stage algorithm is also used for more detailed investigation regarding the prevention of overvoltage in distribution grids. This application is shown to be highly compatible with the increase of self-consumption. It is also shown that as the PV penetration increases, the need for storage increases although the marginal benefit reduces. Finally, analysis of placement strategies shows the benefit of decentralized storage over centralized storage in its ability to provide grid support and reduce losses.

Contents

Abstract v

Contents vi

List of Figures ix

List of Tables xiii

List of Acronyms xv

Nomenclature xvii

Notation xxi

1 Introduction 1
1.1 Motivation . . . 1
1.2 Investigation Overview and Thesis Structure . . . 2
1.3 Contributions . . . 3

2 Background 5
2.1 Mathematical Modelling and Optimisation . . . 5
2.2 Battery Storage Applications . . . 7
2.3 Battery model . . . 11
2.4 Distribution Grid Modelling . . . 20

3 Introduction 25
3.1 Background and Motivation . . . 25
3.2 Literature . . . 26
3.3 Methodology . . . 29
3.4 REM Output . . . 43
3.5 Validation . . . 46

4 Annual Optimal Storage Planning 55
4.1 Literature Survey . . . 56
4.2 Planning Algorithm as an Optimisation Problem . . . 57
4.3 Case Study 1 : Rural sample grid . . . 66

5 Two Stage Algorithm 73
5.1 System Prerequisites . . . 73
5.2 Methodology . . . 75
5.3 Demonstration using Case Study 1 Results . . . 79

5.4 Case Study 2 : Hittistetten grid . . . 83
5.5 Modelling inaccuracies and approximations . . . 88
5.6 Time Resolution . . . 93

6 Cost Analysis **97**
6.1 Feed-in Tariff . . . 97
6.2 Battery prices . . . 100
6.3 Realistic Solar Home Battery Options . . . 103

7 Scenario Analysis **109**
7.1 Grid parameters . . . 109
7.2 PV Feed-in . . . 119
7.3 Placement Scenarios: Centralized Storage . . . 124

8 Conclusion and Outlook **131**
8.1 Summary . . . 131
8.2 Conclusions . . . 133
8.3 Outlook . . . 134

Bibliography **146**

A REM Background Data **149**

List of Figures

1.1 Investigation overview with chapter references . . . 3

2.1 Overview of several storage applications, and probable interactions with various stakeholders. The blue arrows indicate the stakeholder that operates the storage, and the pink arrows indicate the stakeholder that benefits from the storage . . . 7
2.2 Battery stack model as a voltage source (left), and the function of open circuit voltage and charge . . . 13
2.3 Illustration of the principles behind the two charge wells described by the Kinetic Battery model (KiBaM) [1] . . . 14
2.4 Plotting the discrete KiBaM model against sample time using a logarithmic scale. The state matrix A_d entries are plotted in subplot (a), and the input matrix B_d values are plotted in (b) . . . 17
2.5 Convex hull of the degradation map based on [2] . . . 18
2.6 Power line π-model without shunt elements . . . 20

3.1 REM workflow . . . 30
3.2 Composition of the load categories (LC) for each of the household categories (HC) [3] 32
3.3 Probability distributions for event start time and event duration for activity based loads, based on TUS data . . . 34
3.4 Workflow for generation of activity based loads (cooking, television and desktop computer) . . . 35
3.5 Probability distributions used for the lighting loads are clearly highly dependent on the daylight hours of the day being simulated . . . 36
3.6 Simulation of 1000 Households with the time resolution of 1 minute, on a winter working day. The scaled SLP shows the aggregate load profile for the day, and the dotted blue line shows the sum of the activity and lighting loads which corresponds correctly with the peaks that appear in the SLP . . . 37
3.7 Example fridge load simulated using a 1 minute resolution . . . 38
3.8 Representative smart meter measured cyclical loads normalised to a maximum magnitude of 1. For use in the REM all loads are scaled in magnitude, and the fridge/freezer waveform is also scaled in cycle duration . . . 40
3.9 Dryer cycle, with the magnitude normalised to a maximum of 1. This cycle is multiplied by the respective appliance power rating. The stages of the reactive load are indicated, and the corresponding reactive load is shown in red . . . 41
3.10 Load categories for a simulation of 1000 households with a 15 minute time resolution using the SLP for the 2nd of January 2018 in Ulm, Bavaria . . . 43
3.11 Variation of the aggregate load with increasing number of households. Simulation time resolution is one minute, using the SLP for the second of January 2018 in Ulm, Bavaria . . . 44

3.12 Profiles displayed with different time resolutions 45
3.13 Volatility comparison of the REM simulated profiles to the measured profiles of the HES 46
3.14 Comparison of the spread of load magnitudes of measured data versus simulated REM profiles 47
3.15 Comparison of the spread of the total daily energy demand of the HES versus the simulated REM profiles 48
3.16 (a) Shows the average ADMD for the measured data and the simulated data for 1 to 300 profiles, using 600 combinations for each data point. (b) Shows the range of ADMD for 1 to 15 households, highlighting the lowest and highest values for ADMD out of the 600 combinations 49
3.17 Spread of annual loads using an annual simulation of 1000 households per category. The dotted lines are indicative of the trend of the REM annual loads, and the solid lines display a normal distribution with the mean used from the REM and the standard deviation from [4] 50
3.18 (a) Plot of the difference between the aggregate REM profiles for 1000 households of each category and the corresponding SLP for each day of the year. (b) the aggregate profile for the best match, five household members on the 1st of Jan. (c) the worst case aggregate profile, five household members on the 1st of Jan. . . 52
3.19 Power factor and power values for an aggregate load of 1000 households for 1 day 53

4.1 Linear approximation of a quadratic function using 7 points in the full power range 59
4.2 Case study 1 grid from [5] with node numbering 66
4.3 Optimal storage for CS1 nodes for the different price scenarios 68
4.4 The positive impact of storage on the grid depicted by plotting the percentage of self-consumption and self-supply against the amount of storage. The x axis states the total amount of storage in the network in the first line, and the price scenario on the second line. 69
4.5 Results of simulations using PS2, with restricted and unrestricted inter day transfer. Subplots (a) and (b) shows the daily storage use in terms of total discharging and charging energy, for the restricted (a) and unrestricted (b) simulations. Subplot (c) shows the net daily storage energy in the unrestricted case 70

5.1 Procedure for the Two Stage annual planning algorithm 78
5.2 Sample day selection method 79
5.3 Results of subsystem optimisation of CS1 aggregated over all days of the year shown in plot (a), plot (b) shows an example of the objective function for PS3 . . 80
5.4 CS1 results for optimal storage comparing the annual problem, Two Stage problem and the use of only the sample days 81
5.5 Case study 1: Energy characteristics of the whole year in a solid lines, and dotted lines for the sample days in plot (a). Plot (b) shows the objective function evaluation for PS5 81
5.6 The non-geographical topology of the Case Study 2 grid, showing the annual load (a) and annual PV generation (b) 83
5.7 The node voltages of the Case Study 2 grid with no storage, using a colormap to depict all the voltages in (a), and instances of over-voltage highlighted in (b) . . . 84
5.8 Storage planning using the Two Stage planning algorithm for price scenarios 1-6 . 86
5.9 Comparison of the Case Study 2 properties for the Two Stage Simulation 87

5.10 Comparison of results using the Two Stage algorithm compared to using the sample days. Plot (a) shows the difference in total storage for each of the price scenarios, and plot (b) shows the amount of storage per node for PS5 as an example 88
5.11 Energy characteristics of the whole year in a solid lines, and dotted lines for the sample days in plot (a). Plot (b) shows the objective function evaluation for price scenario 6 89
5.12 The errors in bus voltage (a) and angle (b) are plotted as a function of the true voltage and angle respectively. The plot colour are scaled to the nodes, to see if there is a correlation between nodes and error 90
5.13 Demonstration of the line power for a branch in the Case Study two sample day simulation on a day where the line constraint is active 91
5.14 The effect of the degradation on the planning result is demonstrated firstly in plot (a) with a comparison of optimal storage capacity when the degradation model is included and excluded. Plot (b) shows the total degradation for each of the sample days, and part (c) shows the difference in degradation per storage unit . . 92
5.15 Difference in a single row of $\mathcal{M}_{\text{buy}}$ and $\mathcal{M}_{\text{FI}}$ for the Two Stage algorithm performed with the different time resolutions. The row depicted above is characterised by: $E_{tot} = 34\text{kWh}$ 94
5.16 Standard deviation and mean for the difference between the matrices $\mathcal{M}_{\text{buy}}$, $\mathcal{M}_{\text{FI}}$ and $\mathcal{M}_{\text{loss}}$ for each of the rows 95

6.1 Historical values for the FiT in Germany since their introduction in 2001, since after 2012 the FiT varies slightly between months, a corrected annual value is used for this graphic [6] 98
6.2 Results for the planning algorithm applied to Case Study 1 and Case Study 2 for a range of storage costs and FiTs. The total optimal storage in the network is plotted against the FiT 99
6.3 Bloomberg New Energy Finance calculations for average price of Lithium Ion Batteries [7] 100
6.4 Case Study 1 and Case Study 2 sensivity of total optimal storage to storage cost assuming a battery lifetime of 5 years 101
6.5 Surface plot of optimal storage results for Case Study one varying both the FiT and storage cost, based on 20% of capital cost of storage 102
6.6 Price comparison of some of the major suppliers of lithium ion batteries for solar applications, prices available with online retailers on 21.03.2019. *Sonnen eco batteries have an built in inverter, and it was not possible to find the price of the battery alone. **The Tesla Powerwall cannot be bought as a standalone battery, the entire system equipment cost €8800, although this does not include mandatory installation costs 104

7.1 In a PF simulation with no storage and no curtailment, plot (a) shows the lines that have overcurrent and plot (b) shows the location of nodes that face overvoltage 110
7.2 Optimal Power Flow with no storage in the network results in curtailment of PV to maintain limits 111
7.3 Results of the Two Stage algorithm for the energy characteristics (a), and an evaluation of the cost function for PS2 in (b). The dashed lines show the corresponding results for the base case results 112
7.4 Cost Sensitivity of the simulation with reduced voltage tolerance (a) and the difference to the base case (b) 114
7.5 Effect of modifying the slack bus voltage to 1.05 pu in for PS1-3 116

7.6 Effect of modifying the slack bus voltage to 1.05 pu in for PS4-6 117
7.7 Change in optimal storage as PV is scaled for CS1 in plot (a) and CS2 in plot (b) 120
7.8 Cost Sensitivity surface plot CS2 for a PV scaling factor of 1.5 121
7.9 Sensitivity to PV scaling without a FiT, for a range of storage costs 122
7.10 Results of adding a 95 kWp PV installation to each node in the network besides substation nodes, using the sample day algorithm for CS2 with PS4. Plot (a) shows the total optimal network storage, against the node to which the PV is added. Plot (b) classifies the total network storage in 4 bins and indicates the total storage results for the respective nodes. The diamond plots are nodes that previously had no PV, and the square plots indicate nodes with existing PV, to which the 95 kWp installation is added 123
7.11 The effect of the placement scenarios on the total storage for each of the price scenarios, for CS1 (a) and CS2 (b) 125
7.12 Annual total network losses for each of the placement scenarios plotted against the total storage in the network 126
7.13 Energy characteristics for the various placement scenarios with a slack bus voltage of 1.05 pu 127
7.14 Cost Surface difference plots showing in plot (a) the effect of reducing the voltage tolerance for centralized storage, subtracting the normal voltage tolerance results from the reduced. Plot (b) shows the difference between centralized and distributed storage by subtracting the surface for free placement from placement scenario 1. The free placement surface is shown in Figure 7.4(a) 128

List of Tables

2.1 Battery parameters overtaken from [2] 15

3.1 Population composition used for the synthetic population [8], the average annual energy demand per household category [3], and the average living area per person [9] 31

4.1 Time Specific Planning Constraints 64
4.3 Case study 1 profile properties by node 67
4.4 Fixed parameters used for all case study simulations 67
4.5 Price scenario cost parameters 67

6.1 Comparison of Home Battery Lines 105
6.2 LG Chem Battery Range 107

7.1 Line upgrade simulation for all six price scenarios, including the total storage and the storage increase compared to the base case in chapter 3, and the total curtailment. 111
7.2 Modified slack bus voltage simulation results including aggregate network storage, the comparison to the base case in chapter 5, and the total curtailment. 113

List of Acronyms

AC	Alternating Current
ADMD	After Diversity Maximum Demand
BMS	Battery Management System
BTM	Behind the Meter
CS1	Case Study 1
CS2	Case Study 2
DC	Direct Current
DSO	Distribution System Operator
EV	Electric Vehicle
FI	Feed-In
FiT	Feed-in Tariff
GDP	Gross Domestic Product
HC	Household Category
HES	Household Electricity Survey
HHdb	Household Database
KCL	Kirchhoffs Current Law
KiBaM	Kinetic Battery Model
LC	Load Category
LP	Linear Program
LV	Low Voltage
MILP	Mixed Integer Linear Program
MIP	Mixed Integer Program

MIQP	Mixed Integer Quadratic Program
MPOPF	Multi Period Optimal Power Flow
MV	Medium Voltage
ODE	Ordinary Differential Equation
OPF	Optimal Power Flow
PF	Power Flow
PV	Photovoltaic
QP	Quadratic Program
RAM	Random-Access Memory
REM	Residential Electricity Model
RHC	Receding Horizon Control
SLP	Standard Load Profile
SoC	State of Charge
SoE	State of Energy
TSO	Transmission System Operator
TUS	Time Use Survey

Nomenclature

Battery Variables

η_{cap}	Range of recommended Depth of Discharge
η_{ch}	Charging Efficiency
η_{dis}	Discharging Efficiency
$\mathcal{P}$	Vector of battery prices for each size option
$\mathcal{S}$	Vector of battery size options
b	Number of discrete battery size options considered
C_Q	Maximum available charge (Ah)
c_r	Recovery Factor (sec^{-1})
c_w	Charge Well Factor
c_{st}	Cost of storage per kWh of capacity
E_{cap}	Battery Storage Capacity (kWh)
E_{deg}	Capacity loss due to Degradation (kWh)
E_{int}	Integer variable for number of storage units of discrete sizes
E_{st}	Energy level of battery (kWh)
I_{bat}	Battery Current (A)
P_{bat}	Battery Power (kW)
P_{ch}	Charging Power (kW)
P_{dis}	Discharging Power (kW)
Q	Amount of charge in battery (Ah)
R_{int}	Internal Resistance (Ohms)
V_t	Terminal Voltage (V)
V_{oc}	Open Circuit Voltage (V)
x	Amount of charge in the wells (Ah)

x_E Amount of charge in the wells (kWh)

Grid Variables

$\mathbf{I_{km}}$ Complex current in the line between nodes k and m (kA)

$\mathbf{S_{km}}$ Complex power flow in the line between nodes k and m (kVA)

$\mathbf{V_j}$ Complex voltage of node k(V)

Π_j The set of adjacent nodes to node k

θ Vector of all bus angles in a network

θ_j Angle of node k (rad)

B_l Admittance matrix of a network

b_{km} Susceptance in the line (Ohms^{-1})

C_f Connectivity matrix mapping busses to the beginning of the lines (from)

C_g Connectivity matrix mapping generators to the busses

C_t Connectivity matrix mapping busses to the end of the lines (to)

C_{inj} Connectivity matrix mapping lines to the node injection

G_l Conductance matrix of a network

g_{km} Conductance in the line (Ohms^{-1})

n_{br} Number of branches in the network

n_{bus} Number of busses or nodes in the network

n_g Number of generators in the system

P_j^{net} The set of adjacent nodes to node k

P_l Vector of active line powers in all lines in a network

$P_{\overline{sq}}$ Overapproximated upper limit for square magnitude of active line power for all lines in network

P_{gen} Vector of all active generation at all generation nodes in a network

P_{inj} Vector of active bus injection at all nodes in a network

P_{km} Active power flow in the line between nodes k and m (kW)

P_{km}^{loss} Active power losses in the line between nodes k and m (kW)

P_{load} Vector of active loads at all nodes in a network

Q_l Vector of reactive line powers in all lines in a network

$Q_{\overline{sq}}$ Overapproximated upper limit for square magnitude of reactive line power for all lines in network

Q_{gen} Vector of all reactive generation at al generation nodes in a network

Q_{inj} Vector of reactive bus injection at all nodes in a network

Q_{km} Reactive power flow in the line between nodes k and m (kVA)

Q_{load} Vector of reactive loads at all nodes in a network

r_{km} Resistance in the line between nodes k and m (Ohms)

$S_{\overline{sq}}$ Overapproximated upper limit for square magnitude of apparent line power for all lines in network

V Vector of all bus voltage magnitudes in a network in radians

V_j Voltage magnitude of node k (V)

x_{km} Reactance in the line between nodes k and m (Ohms)

y_{km} Complex admittance in the line, inverse of impedance (Ohms^{-1})

z_{km} Complex impedance in the line between nodes k and m (Ohms)

Other Symbols

Δt The time step used between samples (hours)

c_{FiT} Cost of storage per kWh sold to the distribution operator from distributed generation

c_{gen} Cost of storage per kWh bought from the distribution operator

k Time instance referenced the the optimisation problem, i.e. $k = 1$ refers to the first sample

M_p Vector of gradients for a hyperplane approximation for plane p

N The number of time samples in an optimisation problem

Y_p Vector of y-axis intercept points for a hyperplane approximation for plane p

Notation

$f(...)$	Function of variables inside brackets
$\dot{x}$	Derivative of variable$x$ with respect to time
$\mathbf{I}, \mathbf{V}, \mathbf{S}$	Complex quantity for current, voltage and apparent power
$\mathbf{x}^*$	Complex Conjugate of x
$\|x\|$	Magnitude of x
$\underline{x}, \overline{x}$	Lower and upper limit for x respectively
$x \in \{...\}$	x is a set whose members are listed in the curly brackets
$\forall$	for all
$\mathbb{R}$	The set of real numbers
$\mathbb{I}$	The set of integers
$x \in \mathbb{R}^{n_1 \times n_2}$	x is a matrix of real numbers with n_1 rows and n_2
$a \otimes b$	The Kronecker product of a and b, i.e. a kron b
I^n	Identity matrix of the size $n \times n$
$\approx$	Approximately equals

Chapter 1

Introduction

1.1 Motivation

Recent years have seen widespread political and social acceptance that climate change is one of the most pressing global issues. The Paris agreement of 2015 [10] represented a major global commitment to combat climate change, with a concrete goal of limiting global temperature rise to 2°C above pre-industrial levels. Reducing carbon emissions, also referred to as decarbonisation, is a crucial measure towards limiting the rise of global temperatures. Due to the reliance on fossil fuels, the energy system is one of the major sources of carbon emissions. In 2016 electricity and heat generation was the largest emitting sector, accounting for 42% of global emissions [11]. For this reason, many countries are actively working towards decarbonising the energy system, for which one of the key strategies is increasing the amount of renewable energy generation.

Germany in particular has set very ambitious targets with the "Energiewende" concept, a transition strategy to achieve an environmentally sustainable energy supply [12]. This will involve a phase-out of nuclear reactors by 2022, along with a reduction of greenhouse gas emissions of 80-95% by 2050 and a renewable energy target of 60%. In the context of this movement, research that investigates how renewables can best be integrated into the energy sector is important.

Although the majority of the renewable energy generation will be large scale solar, wind and hydro, there is also a strong case for distributed generation [13]. Renewable generation connected to the distribution grid does not rely on transmission infrastructure to transport energy to end users, thereby reducing transmission losses and saving on potential network upgrade requirements. Distributed solar is particularly widespread in Germany. In 2017 over 53% of solar energy was generated by installations connected to the distribution grid [14], amounting to 10% of total renewable generation.

Large quantities of distributed PV can cause problems in distribution grids, as it results in periods where local generation significantly exceeds local load. Generally, distribution grids are designed for uni-directional power flow, delivering power from a connection to the transmission network to the end-user. During times of excess generation however, the distribution grid is required to transport energy in the opposite direction. This can result in major overloading of distribution grids, particularly since they are usually not designed for bi-directional power flow.

Traditionally the response to grid overload is network upgrade, however this is a very expensive solution. An alternative strategy is to create more flexibility in the energy system by including technologies with flexible operation. Energy storage is one such technology that can be used to support distributed generation, for instance by absorbing energy during times of excess generation and releasing energy at other times.

Many studies have listed battery storage as a promising technology for improving renewable penetration, including the IPCC report on renewable energy sources in 2012 [15]. So far, the implementation of distributed battery storage has not been widespread mainly due to high cost. The last years have seen a rapid decrease in battery prices, potentially making them increasingly financially attractive [6].

The purpose of this work is to use simulations and mathematical models to investigate the use of distributed battery storage to integrate more PV in the distribution grid. The main research goals are:

- Development of modelling tools for simulation of battery storage in a distribution network that are suitable for optimisation, and can be used to evaluate trends. Energy systems are complex, and the difficulty lies in the development of a model that is complex enough to capture the relevant dynamics whilst also being computationally efficient.
- Since prices are such a complex and rapidly changing parameter, a goal of this work is to develop methods to gain insight into simulation results that are generally applicable for any price scenario. Prices cannot be left out in a work about energy storage, as cost has been the main barrier so far, therefore it is necessary to find a way to gain general insights from the results.
- Gain insight in the profitability of storage under various conditions, such as increasing PV generation, and changes in network parameters.

1.2 Investigation Overview and Thesis Structure

The focus of this thesis is the "Planning Problem" of battery storage in a distribution grid. This refers to the identification of cost optimal storage capacity and location of battery units in the grid. Simulation results of the planning problem are examined for more detailed analysis that addresses the research questions related to use of battery storage to support renewable integration. A diagram of the investigation overview is shown in Figure 1.1.

First it is necessary to mention the case studies that are used in this thesis to demonstrate results. Case Study 1 (CS1) is a small radial grid, and Case Study 2 (CS2) is a larger meshed grid. To assign load profiles to the case studies, a Residential Electricity demand Model (REM) is developed in chapter 3. The model is highly detailed and can be used for many applications outside of this thesis. Chapter 3 also contains a validation of the REM against measured data.

A basic optimal planning algorithm based on several models found in literature is formulated in Chapter 4 and performed on CS1. One year is considered to be representative, therefore the simulations performed are annual planning simulations. The annual optimal planning algorithm cannot be performed on CS2 as it is too computationally intensive. A novel algorithm that is suitable for use on larger grids is formulated in Chapter 5, and referred to as the Two Stage algorithm. The Two Stage algorithm is shown to give a good approximation of the results for CS1, and it can also solve the planning problem for CS2.

The planning algorithms developed in this thesis is used to run simulations that address relevant research questions in chapters 6 and 7. Chapter 6 focusses on a cost analysis, where the rapidly changing price trends are investigated. Using the Two Stage simulation, their effect on storage

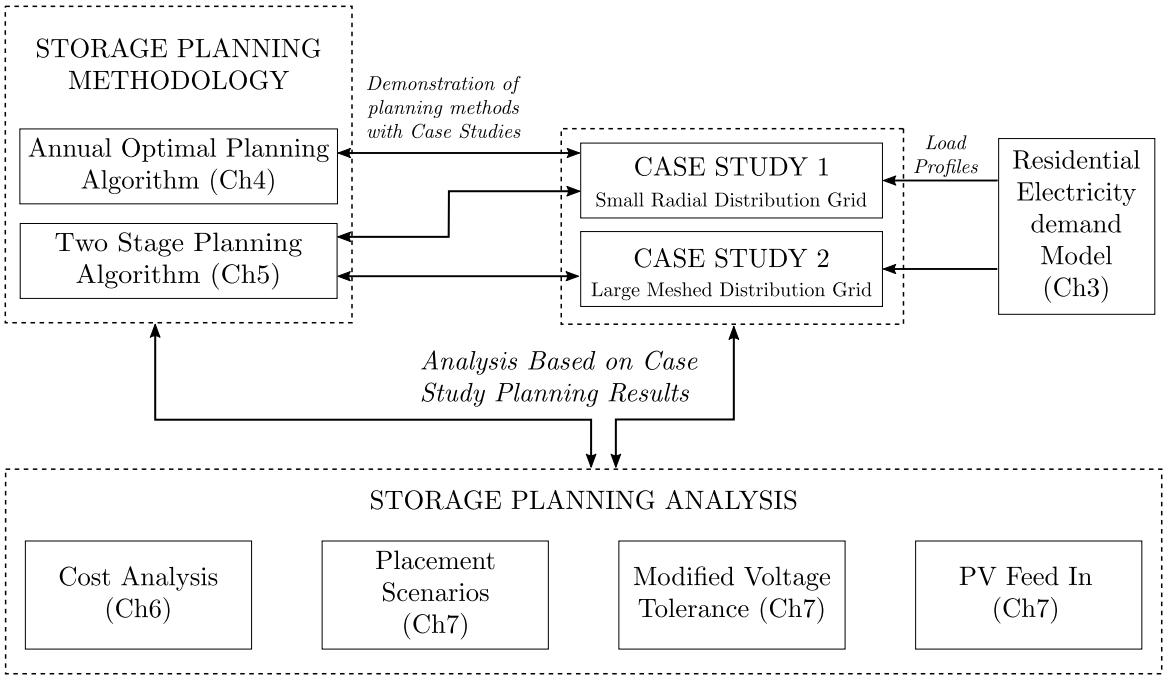

Figure 1.1: *Investigation overview with chapter references*

planning is examined.

Three further points are addressed in chapter 7. Firstly, the effect of a change in reference voltage on optimal storage is shown. Secondly, the dependence of optimal storage on the amount of PV in the grid is shown. Finally, an investigation into various possible placement scenarios takes place.

Besides the investigation modules that are shown in Figure 1.1, Chapter 2 includes some relevant background, and Chapter 8 gives a conclusion and outlook.

1.3 Contributions

The contributions of this work consist both of the modelling tools and algorithms developed for simulations, and the resulting analysis that takes place by evaluating simulation results.

- **Residential Electricity Demand Model (REM)** : In order to accurately represent distribution grids, an important component is residential load. The methodology is presented for a highly detailed and flexible load profile generator, that has many uses beyond the scope of this work.
- **Planning algorithm for battery storage in large distribution grids** : Academic literature contains many examples of planning algorithms for distribution grids, however they are generally not suitable for large or complex networks due to computational difficulty. The algorithm developed in this work decomposes the larger planning problem in such a way that it can be applied to larger and more complex networks.
- **Storage sizing results for a wide range of price scenarios** : It will be shown in this work that both battery costs and feed in tariffs strongly determine the amount of total cost

optimal storage in a network. As these are changing significantly, both geographically and over time, it is more valuable to obtain results apply to a range of price scenarios. The algorithm developed in this work allows for immediate evaluation of total optimal storage in a network for a range of prices, which allows for a more valuable way to compare different scenarios.

- **Case Study based evaluation of modelling choices** : In any modelling exercise, it is necessary to make decisions to approximate the reality appropriately. In this work some of these decisions are examined further with respect to energy systems at the distribution grid level. For instance, the effect of different time resolutions is shown, as well as the effect of various modelling simplifications. This can be useful for future studies, as validation or justification for these choices.
- **Case Study and scenario based investigations** : The modelling tools developed are used to carry out scenario based simulations on case study grids, including increasing PV, changing grid parameters and different placement strategies.

Chapter 2

Background

In this chapter, an overview of the context and some of the technical fundamentals is given, starting with a description of the mathematical formulation used in Section 2.1. Section 2.2 provides an overview of various possible battery storage applications in the grid at different scales. Section 2.3 contains a short description of battery fundamentals, as well as a description of the battery model used for this thesis. Finally, in Section 2.4 an introduction to grid modelling is given, along with the linearisation techniques used for this thesis.

2.1 Mathematical Modelling and Optimisation

Mathematical modelling and optimisation are two powerful tools for studying the behaviour of systems. In an abstract sense, mathematical modelling involves describing a system using mathematical concepts and language, in order to gain useful insight. In this thesis, descriptive mathematical models are built to approximate the behaviour of several energy system components. The models are used to run simulations to analyse how the system could work under different conditions.

Optimisation techniques can be performed on mathematical models with specific formulations, with the purpose of choosing the best amongst a set of solutions. Specific notation is often used in optimisation, for instance the problem formulation is referred to as the 'optimisation problem'. Optimisation problems generally have three components; an objective function, inequality constraints and equality constraints. In one commonly used description, these components are applied to a set of optimisation variables stacked in a vector x as shown in Equation 2.1.

$$\begin{aligned} \underset{x}{\text{minimize}} \quad & f(x) && \text{objective function} \\ \text{subject to} \quad & g(x) \leq 0, && \text{inequality constraints} \\ & h(x) = 0, && \text{equality constraints} \end{aligned} \tag{2.1}$$

Solving the optimisation problem means identifying the values for the optimisation variables that yield the minimum value of the objective function, within the domain of possible solutions determined by the constraints.

There are two steps to mathematical optimisation. Mathematical modelling refers to the definition of the optimisation problem, and mathematical programming refers to finding the optimal solution. This thesis is only concerned with the mathematical modelling stage, and uses existing 'solvers' to obtain solutions.

Optimisation problems can be classified based on the forms of the functions $f(x), g(x)$ and $h(x)$. In this thesis, only problems with linear constraints are utilised, as good solvers are available for this type of problem. Two common classes of problems with linear constraints are Linear Programs (LP) and Quadratic Programs (QP), which differ only in the cost function:

Linear Program	**Quadratic Program**
$f(x) = c^T x$	$f(x) = \frac{1}{2} x^T Q x + c^T x$
$A_{ineq} x - b_{ineq} \leq 0$	$A_{ineq} x - b_{ineq} \leq 0$
$A_{eq} x - b_{eq} = 0$	$A_{eq} x - b_{eq} = 0$

Within this formulation A_{ineq}, A_{eq} and Q are matrices, and b_{ineq}, b_{eq} and c are vectors, ensuring that all the constraints are linear.

Another class of problems are Mixed Integer Programming (MIP) problems, where some of the optimisation variables are integers. MIPs can be used to describe systems that contain discrete elements. Examples of inherently discrete optimisation problems include, optimal operation of systems with discrete operating ranges, distribution of discrete resources, or selection of technologies that are mutually exclusive. A specific type of useful integer variable is the binary variable, which can only take the value of 0 or 1. As the solving methods for MIPs are more complicated, incorporating integer variables results in a much more computationally intensive and time consuming problem. The choice of linear or quadratic cost function is still available, as many solvers have the capabilities to solve Mixed Integer Linear Programs (MILP) and Mixed Integer Quadratic Programs (MIQP), which take the form:

MILP	**MIQP**
$f(x) = c^T x$	$f(x) = \frac{1}{2} x^T Q x + c^T x$
$A_{ineq} x - b_{ineq} \leq 0$	$A_{ineq} x - b_{ineq} \leq 0$
$A_{eq} x - b_{eq} = 0$	$A_{eq} x - b_{eq} = 0$
$x_i \in \mathbb{Z}, \forall i \in \mathcal{I}$	$x_i \in \mathbb{Z}, \forall i \in \mathcal{I}$

The set $\mathbb{Z}$ refers to the set of integers, and the set $\mathcal{I}$ refers to the set of all integer variables in the problem.

Chapters 4-5 of this thesis deal with the description of the planning problem of battery storage in the distribution grid as an optimisation problem, using the programming problems above. The optimisation problem is solved using either GUROBI [16] or CPLEX [17], two commercially available solvers. Using MATLAB [18] to describe the problem, it is possible to use the toolbox Yalmip [19] to describe the problem with assigned variable names, so that it is unnecessary to create the matrices and vectors A, Q, c and b explicitly.

2.2 Battery Storage Applications

As a very flexible technology, there are a lot of potential applications for battery storage in the grid. Although research within this field mostly looks into strategies for single applications, there are some studies on multi-application application strategies using multi-objective optimisation. There are many ways to classify the applications for battery storage, such as size of storage units as in [20] or potential revenue sources such as in [21]. A useful classification is the definition of 'application families' by Hesse in [22]. Figure 2.1 shows some of the most common stakeholders involved with each of the application families. The application families defined in [22] include:

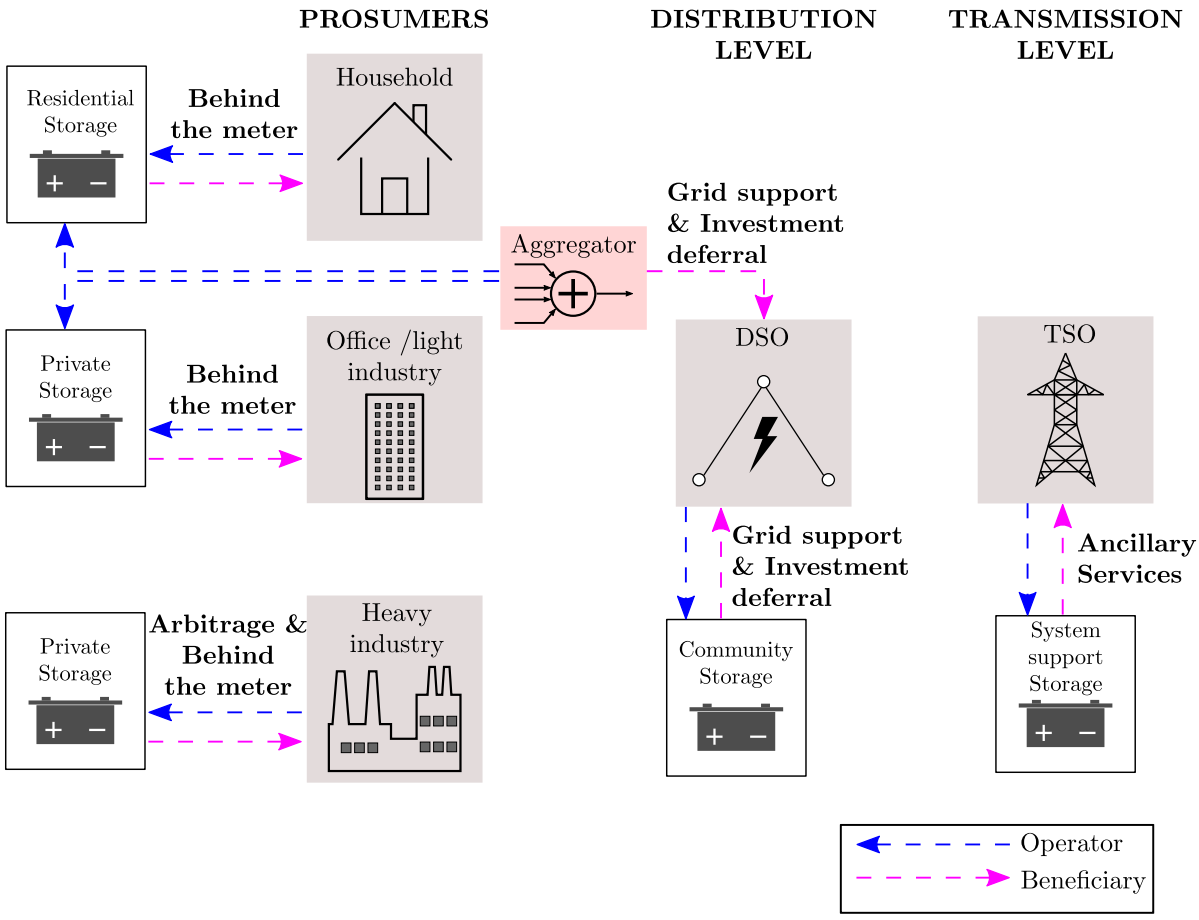

Figure 2.1: *Overview of several storage applications, and probable interactions with various stakeholders. The blue arrows indicate the stakeholder that operates the storage, and the pink arrows indicate the stakeholder that benefits from the storage*

- **Ancillary services:** defined as services necessary to support the transmission of electricity from its generation site to the customer. Although the beneficiaries for these applications are typically transmission system operators (TSO), the system support storage may be privately owned and can participate in providing ancillary services by participating in reserve auctions for example.

- **Behind the meter:** the purpose of the storage is to provide financial benefits to the owner on-site, at the home, office or other commercial facility. These applications utilize the storage only for saving money on bills or as a source of profit by selling energy.

- **Arbitrage:** also known as energy trade, refers to buying and selling energy from markets with the aim of exploiting price differences across the day. Currently the only markets with variable electricity prices are wholesale markets like the EEX, where the size of the individual trades is so large that participation is generally only feasible for very large storage units. Regulatory issues may be complex, since generally there are strict regional specifications for stakeholders to participate.

- **Grid support and investment deferral:** involves actively operating storage to maintain network limits, or to make more efficient use of existing infrastructure such as transformers and power lines. This can be achieved by using an aggregator that coordinates privately owned small scale storage in an area, or a larger 'community' storage that is owned and operated by the network operator.

2.2.1 Literature survey of applications

Ancillary Services

Frequency control is required to enable stable operation of the power supply system by maintaining a frequency of 50 Hz. Quick changes in supply and demand, or power outages can lead to fluctuations in frequency. This is particularly relevant within the context of large scale renewable generation with intermittent natures such as wind and PV. Frequency control takes place at three time scales, known as primary, secondary and tertiary control, and literature is found investigating the use of battery storage for all three applications. In particular, the primary control market has been shown to be a viable application for large scale battery systems in a number of studies, such as [23]. The Smarter Network Storage project [24] has identified it as an important market for storage in the UK, whilst a range of operational strategies are developed in [25–27]. Other reserve markets with longer timescales have also been investigated, such as secondary reserve [28, 29] and day ahead markets [30].

Another application for large scale battery storage in the system is to restore power generation after a power outage or technical defect. This is known as black start capability, and studies [31,32] have shown promise for the use of Li-Ion batteries particularly for this application due to their high nominal power and low self-discharge. There are some ongoing projects implementing this functionality, of which the WEMAG project has successfully implemented a Li-Ion battery bank capable of black-starting the grid [33].

Behind The Meter (BTM)

For BTM applications the potential for cost saving depends highly on the specific case conditions, and as of now no universal cost saving benefit has been identified. The most common and obvious application is to use batteries to reduce energy bills by increasing the self-consumption of locally generated PV or other renewable generation. Although this is a very reasonable application, the potential for profit depends highly on the local generation capacity, load, feed-in tariff and energy price. There is a great deal of research in this field particularly for use with PV at home, such as [34–37], as well as for industrial customers [38].

There are certain types of energy contracts for industrial consumers that charge for both peak power demand as well as total energy consumption, thereby offering a financial incentive for reducing the peak consumption. Energy storage can be utilised for peak shaving to considerably

reduce energy bills, as investigated in [39–41]. Currently there is no market that offers an equivalent financial incentive for residential consumers.

Batteries can also be used to increase energy autonomy, and reduce the dependence on local grid infrastructure thereby protecting the user from blackouts. This is particularly valuable for certain kinds of commercial users like hospitals and computer servers, where a reliable energy supply is critical. This has been investigated in [42, 43]. In certain cases there can also be financial benefits for smoothing of generation with very strong fluctuations as shown in [44].

The marketing for existing domestic storage solutions on the market, such as the Tesla Powerwall and VARTA energy storage systems, revolve primarily around increasing local self consumption to reduce energy bills and secondarily to provide an uninterrupted power supply. Energy autonomy is also often mentioned as a benefit, although when local infrastructure is reliable this is not financially beneficial, it is possibly more of an ideological objective.

Energy Trade

Energy trade has been an application in the past for pumped hydro storage, when the main influence on energy prices was that lower demand during the night resulted in lower energy prices at this time [45]. Recent work shows that arbitrage with fluctuations over a short time scale can be a viable application for batteries now and in future [46–48].

Grid support and Investment Deferral

The usage of battery systems for investment deferral for the grid is a more complicated application in reality. Often network components are sized to deal with an expected worst case load, with additional redundancy in some cases. When demand exceeds the rated capacity of transformers and/or power lines, the traditional response is to upgrade the network. Utilizing battery storage along with other demand side management techniques to reduce peak loads, can be a viable alternative to increasing network capacity. The difficulty is in valuing these alternative measures and providing appropriate financial compensation. The technical aspects and potential economic models are investigated in [49, 50].

Another problem due to increasing amounts of renewable feed-in in distribution grids is voltage deviation. Many studies look into the viability of using battery systems to provide voltage support and thereby increase the amount of renewable in-feed in a distribution network, [51–54]. The same issue arises as it does for investment deferral: it is difficult to create a financial incentive for voltage support for private battery operation. A simpler and more realistic economic model may be that the DSO themselves own and operate the batteries.

Another future issue that relates to this application family is the increased electricity demand due to emergence of electric vehicles (EV), and the resulting need for charging infrastructure. Fast charging solutions in particular, have a very high power demand, and have the potential to overload the system [55]. There is a great deal of academic and industrial research investigating appropriate solutions for integrating EV and charging infrastructure, including the studies in [56, 57]. Utilising batteries has been proposed in [58] to support EV charging and in [59] to support electric bus charging.

Combined Applications

Utilizing batteries for multiple applications is considered to be important to the economic viability of energy storage [24] even though it poses many technical, logistical and regulatory challenges. Different applications concern different stakeholders, making it difficult to create a market model. Regulatory constraints also pose an issue, for example market unbundling regulations prevent certain stakeholders from collaborating [60, 61].

Academic research aimed at developing operational algorithms for batteries using multi-objective optimisation is common in recent years, although approaches vary significantly. One example exploits the difference in timescales of different applications, by combining energy arbitrage and frequency regulation for a financial optimisation [62] . Another approach, as taken in [52], combines the constraint management of voltage regulation along with peak power reduction.

A more common multi-application study involves using batteries to support microgrid operation. Since this allows more freedom, batteries can be operated to simultaneously offer control reserve, voltage regulation and act as a balancing unit to ensure autonomy, [63, 64].

2.2.2 Application concept for this thesis

The research into many of these applications has shown promise for the use of energy storage in the grid. However studies concerning each of these applications requires the use of models of vastly different scales. For investigating BTM applications, electricity price models may be required, as well as models of residential loads. For grid support applications, distribution grid models are key. Whereas for investigating ancillary services, the transmission grid models are very important. It is not possible to investigate all possible applications within the scope of this work, even though many of the applications are valid research directions. It is necessary to identify the scale of the study, and then select the appropriate applications.

This thesis focusses on the distribution grid level, therefore BTM and grid support applications are considered. BTM is included, in the sense that energy price, storage price and feed in tariffs are considered and a solution is found to optimise the self consumption of local PV. An aggregator is implicit, as the model coordinates the operation of all the storage units in a distribution grid to achieve the best outcome for the whole system. However, it includes elements of community storage, as the grid model also enforces that network limits, particularly line current and voltage limits. Investment deferral as such is not modelled, instead the storage is used to make better use of existing grid infrastructure. Storage is placed anywhere in the grid, not only at residential locations. The application in this thesis can therefore be considered a combination of community storage, residential and private storage with a BTM application.

2.3 Battery model

The research field of battery modelling has seen a lot of activity in recent years. Since it is not within the scope of this thesis to develop new battery models, suitable models that have been adequately validated are selected from the body of academic literature. In the following text some principles of battery operation are outlined, as well as some types of battery models that exist in literature. Finally the two models used in this thesis are specified. The first describes the dynamic behaviour, and the second model describes the degradation of the battery. Battery degradation refers to the diminishing of storage capacity from the rated value, due to various reasons including time and usage.

Battery model selection
The challenge of modelling batteries is that they are electrochemical devices ruled by highly non-linear processes. Battery models that accurately describe behaviour exist within the electrochemical domain, and use partial differential equations on the variables of current, voltage and charge. These models are often not suitable for classical optimisation as they are non-linear and have many parameters.

For engineering studies it is sometimes more useful to use a battery model in the power and energy domain. The challenge is to identify the relevant dynamics, and to linearise them appropriately. The dynamic model used in this thesis is based on the Kinetic Battery Model (KiBaM) [1], developed for lead acid batteries. Fortenbacher, in [2], adapts the KiBaM for energy system studies, and provides a validated parametrisation for lithium ion batteries. The degradation model is also based on [2]. These models will be described in more detail in the following pages, however it is required to briefly justify the use of these specific models.

Firstly both models are linear and include both the dynamics and the degradation in a form that is easy to implement within an optimisation framework. This is a major advantage considering that this thesis involves multi-period optimisation problems for systems with upto 200 nodes, for which complex models would result in intractable problems. Secondly the models have been extensively verified using the high fidelity electrochemical model DUALFOIL [65] for parameter selection and to identify if the dynamics produce accurate results.

Finally, the degradation model lends itself well to sizing algorithms as it has a linear term for the size of storage. This is uncommon, as a major determining variable for degradation is depth of discharge, which is a non-linear function of storage size. The Fortenbacher model has decoupled the state of charge from the storage size providing a degradation model that can easily be implemented for sizing problems.

2.3.1 Battery models in literature

The battery models in literature can be categorized into five basic types: electrochemical models, electrical circuit based models, stochastic models, semi-empirical models and analytic models. The electrochemical models are based on the chemical reactions that take place, and are used by chemists to develop batteries. These models are very complex and unsuitable for optimisation problems due to their large number of parameters and non-linear differential equations. An example of this is the Doyle, Fuller and Newman model [66]. Another commonly used model is the

DUALFOIL [65] as it is freely available on the internet, and has more than 30 parameters that the user can set. It is often used to verify other analytic models, as an alternative to verification using measurements.

Electrical circuit models are sometimes used in electrical engineering, by representing batteries with components like resistors and capacitors to describe various behaviours, for example the Pspice model for lithium ion batteries in [67]. These are generally less complex than the electrochemical models, but are still too complex for the system studies that take place in this thesis.

Stochastic models describe the amount of charge left in a battery using Markov chains and use probabilities to determine whether the battery gains, loses or recovers charge. The most common model of this kind is published by Chiasserine and Rao, in a series of papers culminating in [68]. Semi-empirical models describe battery degradation by fitting analytic functions to experimental data.

Analytical models use more general functions to describe battery behaviour. The most useful analytical model is the Kinetic Battery Model (KiBaM) developed by Manwell and McGowan [1, 69, 70]. This model will be described in this chapter, as it provides the foundation for the battery model used in this thesis. Another option is the diffusion model first published in [71] which models the diffusion of ions with simple differential equations. In [72] it is shown that the diffusion model is the continuous version of the KiBaM model.

2.3.2 Battery terminology and principles

In many electrical engineering applications, batteries are represented as a voltage source as illustrated in Figure 2.2. The modelling challenge is to accurately represent the available energy, power and current-voltage (IV) characteristics. The image refers to a battery stack, which usually consists of multiple cells, controlled by a Battery Management System (BMS). The open circuit voltage V_{oc} drops over the internal resistance R_{int}, and the terminal voltage V_t, indicates the amount of power available. The battery current I_{bat} is effectively an input to the system as it is externally determined by the application requirement, and is used to calculated how much power is required from the battery.

The open circuit voltage drops as charge is delivered, as shown in Figure 2.2, although this shape changes depending on the battery current. In order to charge and discharge the battery in a way that the full available charge can be utilized, specific currents need to be used. This is known as Constant Current Constant Voltage (CC-CV) charging. The open circuit voltage remains between the cut off voltages $\underline{V}_{oc}$ and $\overline{V}_{oc}$, which will depend on the electrochemical properties of the battery.

Battery degradation is characterised by the maximum available charge C_Q reducing over time, as indicated by the curve shift from time zero to time t^1 in Figure 2.2. There are various processes that result in such capacity fade, some of which are discussed in Section 2.3.4.

One term that is often used in regard to battery operation is State of Charge (SoC), which refers to the proportion of remaining available charge left in the battery. It is generally defined as $\text{SoC} = \frac{Q}{C_Q}$, where Q refers to the amount of charge in the battery, measured in Ah. Between the states of 0 (fully discharged) and 1 (fully charged), it is difficult to estimate the SoC, and this is a research field on its own.

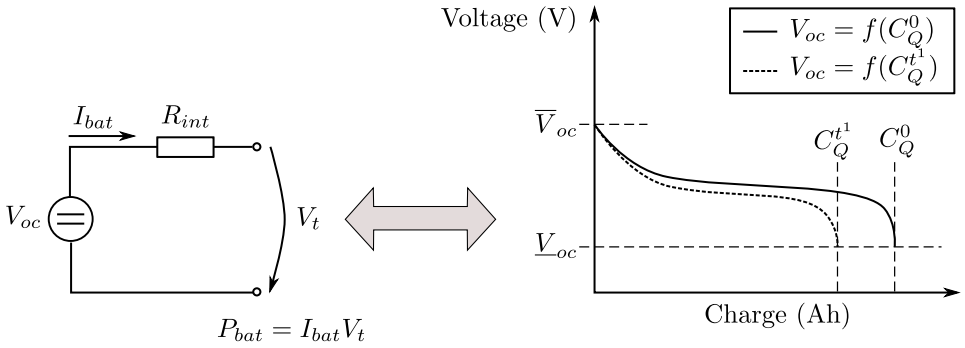

Figure 2.2: *Battery stack model as a voltage source (left), and the function of open circuit voltage and charge*

The relationships described so far exist in the current and voltage domain, however for energy system modelling it is necessary to define the terms that are used in the power and energy domain. In energy terms the total energy capacity of the battery E_{cap} is given in kWh and is defined as the integral of the open circuit voltage over the range of charge as in Equation 2.2.

$$E_{cap} = Q \times \frac{1}{Q} \int_0^{C_Q} V_{oc}\,\mathrm{d}Q = \int_0^{C_Q} V_{oc}\,\mathrm{d}Q \tag{2.2}$$

The energy domain equivalent of Q is E_{st}, which refers to the amount of energy stored in the battery, measured in kWh. The energy domain equivalent of SoC is sometimes defined as the State of Energy (SoE) $= E_{st}/E_{cap}$. Although the SoC and SoE are often used interchangeably, this is technically incorrect as V_{oc} is a non-linear function of the remaining charge. Battery degradation can also be expressed in terms of a loss of energy capacity.

The equivalent to battery current is charging and discharging power P_{ch} and P_{dis}. The simplest linear model for the evolution of the energy level in a battery is given in Equation 2.3, which includes the charging and discharging efficiencies η_{ch} and η_{dis}. The efficiencies include the battery loss due to the internal resistance, and the inverter losses. Therefore P_{ch} and P_{dis} refer to the power that can be measured outside the battery.

$$\dot{E}_{st} = -P_{bat} = \eta_{ch}P_{ch} + \eta_{dis}^{-1}P_{dis} \tag{2.3}$$

Although the simple dynamic battery model described by Equation 2.3 is used in many power system studies, there are certain additional dynamics that may be relevant. Firstly, the recovery effect, whereby batteries regain some of the lost charge during idle periods where there is no battery current. Secondly, the rate capacity effect, which refers to the fact the effective capacity is lower under a higher load.

2.3.3 Kinetic Battery model and application

The Kinetic Battery Model (KiBaM) [1] is an analytical model developed for lead-acid batteries, so named because it models a chemical kinetics process. The model distributes the total available charge over two wells, as shown in Figure 2.3. A fraction of the charge is in an available

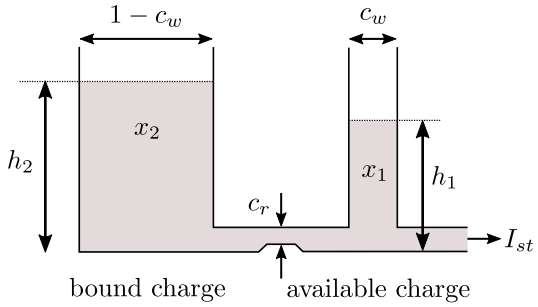

Figure 2.3: *Illustration of the principles behind the two charge wells described by the Kinetic Battery model (KiBaM) [1]*

charge well, with a width of c_w, and the rest is in a bound charge well with a width of $1 - c_w$. The bound charge well only supplies charge into the available charge well, whereas the available charge well supplies to the load I_{st}. The charge flows from the bound well into the available well through a valve, of which the flow rate is characterised by the recovery factor c_r given in sec^{-1}. The rate at which the charge flows also depends on the difference in height of two wells $h_2 - h_1$. The amount of charge in the bound and available wells are given in Ah by x_1 and x_2 respectively.

This model takes into account the recovery effect, as it captures the dynamic that more overall charge is available if instead of a continuous load, the battery has some time to recover i.e. to refill the available charge well. It also captures the rate capacity effect, since the available charge well will be drained faster for higher discharge currents without having the time to recharge, and therefore for higher currents there is less available charge. The change of charge in the two wells is given by the Ordinary Differential Equations (ODE) in equations 2.4 and 2.5 .

$$\dot{x}_1 = c_r(h_2 - h_1) - I_{st} \tag{2.4}$$

$$\dot{x}_2 = -c_r(h_2 - h_1) \tag{2.5}$$

By identifying the definitions of the heights as $h_1 = x_1/c_w$ and $h_2 = x_2/(1 - c_w)$ the model can be rewritten as a state space model with the state variable $x = [x_1, x_2]^T$.

$$\dot{x} = \begin{bmatrix} -\frac{c_r}{c_w} & \frac{c_r}{1-c_w} \\ \frac{c_r}{c_w} & -\frac{c_r}{1-c_w} \end{bmatrix} x - \begin{bmatrix} 1 \\ 0 \end{bmatrix} I_{st} \tag{2.6}$$

The state space model in equation 2.6 exists within the voltage/current domain, as the unit for x is Ah. For this thesis however, the equivalent model in the power domain is required. A new state space variable is used $x_E = [x_{E1}, x_{E2}]^T$, which gives the capacity in each of the wells in kWh. The energy level of the storage is the summation of the charge in the wells as in Equation 2.7. The efficiencies η_{ch} and η_{dis} refer to the charging and discharging efficiencies. Although in reality they vary with the charging power, it is reasonable to fix them between the charging and discharging limits. The resulting ODE is given in Equation 2.8.

$$E_{st} = x_{E1} + x_{E2} \tag{2.7}$$

$$\begin{bmatrix} \dot{x}_{E1} \\ \dot{x}_{E2} \end{bmatrix} = \begin{bmatrix} -\frac{c_r}{c_w} & \frac{c_r}{1-c_w} \\ \frac{c_r}{c_w} & -\frac{c_r}{1-c_w} \end{bmatrix} \begin{bmatrix} x_{E1} \\ x_{E2} \end{bmatrix} + \begin{bmatrix} \eta_{ch} & \eta_{dis}^{-1} \\ 0 & 0 \end{bmatrix} \begin{bmatrix} P_{ch} \\ P_{dis} \end{bmatrix} \tag{2.8}$$

Although the KiBaM model was developed for lead acid batteries, it has been verified in [2] that it is also suitable for modelling lithium ion batteries using the parameters in Table 2.1. The

charge well recovery c_w and recovery factor c_r are obtained using a least squares approximation of the equivalent DUALFOIL model.

Table 2.1: *Battery parameters overtaken from [2]*

c_w	0.15	charge well factor
c_r	1-e3 sec^{-1}	recovery factor
η_{ch}	0.98	charge efficiency
η_{dis}	0.97	discharge efficiency

Discretisation of KiBaM

The model in Equation 2.8 is a continuous time model, which describes the system in Ordinary Differential Equations (ODE) in the form:

$$\dot{x} = Ax + Bu \tag{2.9}$$

In the state space formulation in Equation 2.9, x is a vector containing the state variables, u is a vector containing the input variables, and A and B are matrices, making the system linear. In the case of the KiBaM, the state variables are the amount of energy in each of the wells and the input variables are the charging and discharging powers. Equation 2.10 is used to evaluate the system states at any given time t_1. Time t_1 is given in seconds measured from time zero t_0, and the initial condition x_0 is the system state at time zero.

$$x(t_1) = e^{At_1}x_0 + e^{At_1}\int_0^{t_1} e^{-A\tau}Bu(\tau)d\tau \tag{2.10}$$

For the simulations in this work, a discrete form of the state space model is required, which has the format:

$$x(k+1) = A_d x(k) + B_d u(k) \tag{2.11}$$

In the discrete time form, there is a fixed sample time Δt, and the next state, i.e. the state at time $(k+1)\Delta t$ is evaluated as a linear function of the current state at the time $k\Delta t$. The discrete time matrices can be calculated with equations 2.12 and 2.13.

$$A_d = e^{A\Delta t} \tag{2.12}$$

$$B_d = \int_0^{\Delta t} e^{A\lambda}d\lambda B \tag{2.13}$$

It is assumed that the inputs remain constant over the time step, i.e. for the battery model the charging power remains the same until the next time step.

Some simple models, like the 2.3 can be very simply discretized by multiplying the linear terms with the sample time as shown in Equation 2.14.

$$E_{st}(k+1) = E_{st}(k) + \eta_{ch}\Delta t P_{ch} + \eta_{dis}^{-1}\Delta t P_{dis} \tag{2.14}$$

There is an inherent loss of information with a discretisation of a system, as the states can only be evaluated at discrete time intervals, whereas the continuous time model can evaluate the

states at any time. However, in many studies it is necessary to model a system over a period of time, and using a discrete model it is possible simultaneously calculate the system states for a long period of time in discrete intervals based only on the initial condition and inputs. For instance, using a charging profile given in 15 minute intervals for a week, and an initial SoE, it is possible to calculate the SoE for the entire week in a single calculation. This is important for the optimisation problems that will be defined in this thesis.

For the KiBaM model the discretisation is applied using the built in MATLAB command `c2d`, which takes the continuous time matrices and converts them into discrete time matrices. Using the parameters in Table 2.1 the continuous-time state-space matrices in Equation 2.8 is evaluated. The discrete-time model will have to be derived depending on the sample time. As an example, for a sample time of 15 minutes the value used for Δt is 60×15, and the resulting system model is given in Equation 2.15.

$$\begin{bmatrix} x_{E1}(k+1) \\ x_{E2}(k+1) \end{bmatrix} = \underbrace{\begin{bmatrix} 0.1507 & 0.1488 \\ 0.8493 & 0.8501 \end{bmatrix}}_{A_d} \begin{bmatrix} x_{E1}(k) \\ x_{E2}(k) \end{bmatrix} + \underbrace{\begin{bmatrix} 238.4162 & 250.8060 \\ 643.5838 & 677.0291 \end{bmatrix}}_{B_d} \begin{bmatrix} P_{ch}(k) \\ P_{dis}(k) \end{bmatrix} \tag{2.15}$$

The model is very consistent, as the columns of the state matrix sum to 1, which means that the wells are only equalising and no energy is gained or lost. The change in total energy comes from the charging power, for which the columns sum to $\eta_{ch}\Delta t$ and $\eta_{dis}\Delta t$ respectively. In other words, the simple linear model in Equation 2.14 is still true, the KiBaM model only gives additional information on how the energy is split between the wells, and therefore how much is energy is available.

Since different sample times are used within this work, the discrete time matrices will be derived as part of the algorithm using the built in MATLAB command. It is useful to examine how the model changes with sample time by plotting the values of the matrices against sample time, as shown in Figure 2.4. Some commonly used sample times for energy system studies are marked in the plots. Figure 2.4 (a) shows that the state matrix converges to a point where the height of the wells equalise within one time step, where the values for a_{11} and a_{12} are equal to the value for c_w 0.15. The majority of the convergence occurs between a 1 minute and 15 minute time scale, and at 15 minutes the equalisation happens within one time step.

Figure 2.4 (b) is more demonstrative of the charge recovery effect, as it shows how much of the charging power fills both the wells. For time resolutions between 1 second and 1 minute the b_{11} and b_{12} are dominant, i.e. most to all of the charging or discharging power fills the available charge well x_{E1}. At larger time resolutions above 15 minutes however the wells are charged and discharged almost proportionally to their respective widths.

The conclusion is that the sample times at which the charge recovery effect is relevant are very different for the time resolutions that will be considered in this work. For 1 hour the effect is almost non-existent, and for 15 minutes the effect is negligible. Time resolutions of 1 minute will be impacted more strongly by the charge recovery, as the amount of available charge may be different than if the simple model were to be used. Sample times of less than 1 minute are not used in this work, as the studies require simulations for long time durations, and using a sample time of 1 second would result in very large optimisation problems.

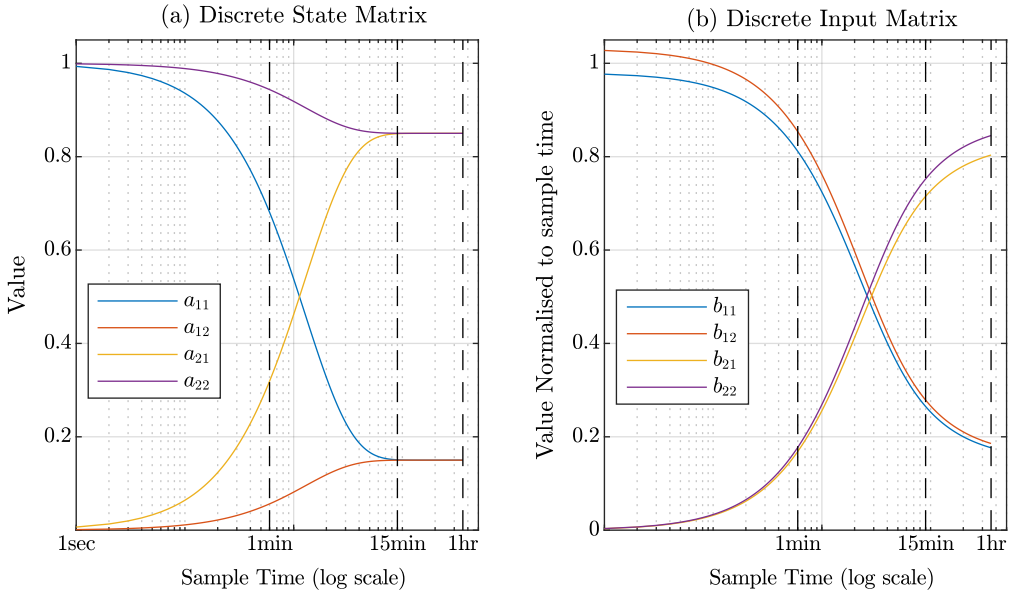

Figure 2.4: *Plotting the discrete KiBaM model against sample time using a logarithmic scale. The state matrix A_d entries are plotted in subplot (a), and the input matrix B_d values are plotted in (b)*

2.3.4 Battery degradation

Battery degradation occurs because of various chemical processes, also referred to as side reactions, that occur within the battery that lead to active material loss. Degradation is often split into the categories of calender ageing and cycle ageing. Calendar ageing is due to non operational factors such as ambient temperature, ambient humidity, and simply the passing of time. Cycle ageing is due to operational factors, and can be greatly reduced by appropriately operating the battery. The physical process can be characterised by the growth of cracks in the active materials, and is analogous to the fatigue in materials subjected to cyclic mechanical loading [73]. Overall, the battery degradation depends very heavily on the type of battery chemistry and materials in question.

There are many stress factors that can contribute to the cyclic ageing of the battery, including:

- Cycle depth: It has been demonstrated for some lithium ion batteries that operating within a smaller window of the capacity, the battery has a much longer lifetime. For example the study in [74] showed that a Lithium Nickel Manganese Cobalt Oxide battery cell can perform upto 50,000 cycles at 10% cycle depth and only 500 at 100% cycle depth.

- Current rate: The battery currents affect how the battery degrades

- Extreme SoC levels : A short time of overcharging or over discharging of the batteries can result in a dramatic loss of capacity, however in power system applications it is sufficient to assume the BMS manages this aspect.

- Average SoC : The average SoC does have a minor effect on the degradation [74]

- High operating temperatures : Many of the chemical reactions in batteries change with temperature, and high operating temperature can cause a fast capacity loss. Similarly to the SoC levels however, it is sufficient to assume that the BMS avoids this.

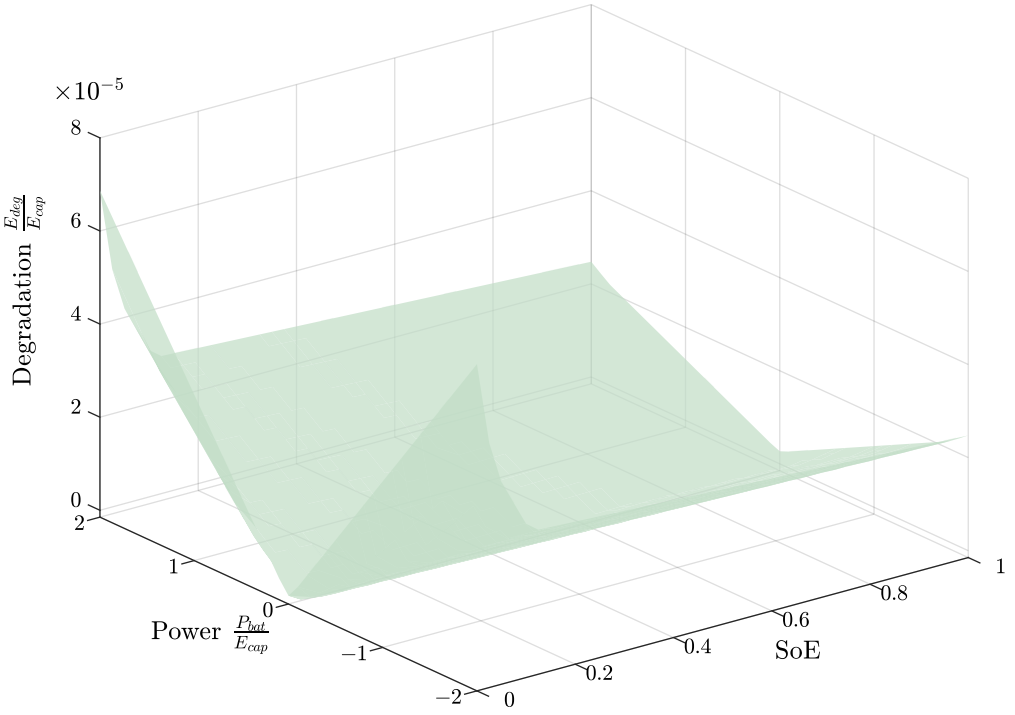

Figure 2.5: *Convex hull of the degradation map based on [2]*

These processes are difficult to model due to the complex nature of the chemical reactions. Most electrochemical models use differential equations on a large number of parameters to determine the ageing. This is not suitable for use within power system studies, as it is not reasonable to include so many parameters. It is also valuable to have models that describe behaviour not specific to a type of battery chemistry. Particularly within optimisation studies it is necessary to have only linear or quadratic terms that are dependent on the control actions of charging and discharging. For a planning study, the energy capacity is also an optimisation variable, therefore depth of discharge is a non-linear function of the optimisation variables.

Degradation model

The degradation model used in this thesis was published by Fortenbacher [2], who developed empirical degradation maps for lithium ion batteries. This model is selected for a number of reasons. Firstly the maps have been developed for optimal control sizing methods and have independent cost terms for power, energy levels and battery size. Secondly the piecewise affine maps are easy to implement and are not very computationally demanding. Thirdly, the method has been extensively verified with the high fidelity model DUALFOIL.

Degradation maps refer to the mapping of degradation to the desired control variables, so that it is not necessary to understand or analytically model the processes that result in degradation. To develop the models, firstly a system identification method was developed to quantify the amount of degradation for the DUALFOIL model. Then the system was run using a random current output and the capacity loss was mapped to the control variables of nominal battery current and SoC. The model is then discretised and transformed to the energy domain, making the active variables nominal battery power and SoE. The resulting map is not convex, and so a convex hull

of the degradation map is defined. Finally, a Piece-Wise Approximation (PWA) of the convex hull is derived.

The expression for capacity loss in kWh E_{deg} relative to the storage capacity is given in Equation 2.16, and by multiplying by E_{cap} it is possible to separate the control variables from the storage size. The hyperplanes that approximate the convex hull are given by the vectors $\mathbf{a}_1$, $\mathbf{a}_2$ and $\mathbf{a}_3$.

$$\frac{E_{deg}}{E_{cap}} = max\left(\mathbf{a}_1\frac{P_{bat}}{E_{cap}} + \mathbf{a}_2\frac{E_{st}}{E_{cap}} + \mathbf{a}_3\right) \tag{2.16}$$

The convex hull of the degradation map can then be used for optimisation problems, and verified by checking the degradation calculated in the optimisation with the same input in the DUALFOIL model. Because the PWA is of the convex hull, and not of the degradation itself, there are some errors, which lie within an acceptable range.

2.4 Distribution Grid Modelling

2.4.1 Power Flow Analysis

Power Flow (PF) analysis is used to calculate voltages and currents in the power system, and is important for analysing the steady-state operation of electrical networks. Power flow can also be implemented as an optimisation problem, identifying the most economical generation options and reducing system losses.

Within the field of power systems analysis, an electrical grid network may be described by busses, and the branches that connect them. Busses, also known as nodes, are fixed in location and typically can have loads, generators or other attached components such as PV generation. The branches that connect the nodes reflect overhead lines or underground cables with a current carrying capacity rating. Branches have a certain resistance and reactance, resulting in a voltage drop over the line due to current flowing through it. Busses at the end of a long line, or busses with large loads and/or feed-in can experience major voltage deviations, resulting in network stability issues. Battery storage can help with voltage issues by increasing local consumption at the nodes and thereby reducing the branch flows and resulting voltage deviations.

For the planning of storage systems it is necessary to determine which lines in the grid will approach current limits, and which nodes will face over- or undervoltage issues. Optimal planning takes into account the PF in the lines to introduce storage in the locations that help voltages to remain within the limits.

PF in a line is fundamentally non-linear, and significant research has been done to approximate power flow equations in order to allow linear optimisation. The most common linearisation is known as the DC approximation, but since this method does not calculate voltages, reactive power or losses, it is unsuitable for many applications. The following text deals with the derivation of line flows and the power PF problem, as well as a linear approximation to allow multi-period optimisation of a grid.

Power Line Model

Modelling a power line typically starts with the commonly used pi-equivalent model of a line, for which a graphical representation is shown in Figure 2.6. A line between the nodes k and m is parametrised by its complex impedance z_{km}, which can be decomposed into the resistance r_{km} and reactance x_{km}.

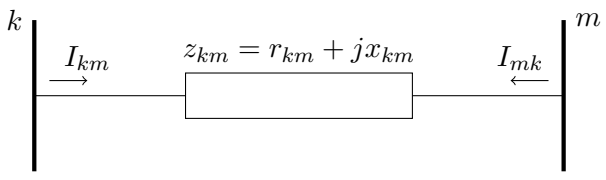

Figure 2.6: *Power line π-model without shunt elements*

For ease of formulation it is also useful to refer to the admittance equation given in Equation 2.17, which is the inverse of impedance. Admittance is measured in Siemens, and consists of a real component called conductance, g_{km} and imaginary component susceptance b_{km}, for which the formulae are given in Equation 2.18,

$$y_{km} = z_{km}^{-1} = g_{km} + jb_{km} \tag{2.17}$$

$$g_{km} = \frac{r_{km}}{r_{km}^2 + x_{km}^2} \qquad b_{km} = \frac{-x_{km}}{r_{km}^2 + x_{km}^2} \tag{2.18}$$

Any node k is characterised by a complex voltage $\mathbf{V_k}$, and as shown in Equation 2.19 it is expressed in terms of its magnitude V_k and angle θ_k. The complex currents in both directions as shown in Figure 2.6 can be expressed in terms of the voltages at the branch terminal nodes and the line admittance, as in equations 2.20 and 2.21 [75].

$$\mathbf{V_k} = V_k e^{j\theta_k} \tag{2.19}$$

$$\mathbf{I_{km}} = y_{km}(\mathbf{V_k} - \mathbf{V_m}) \tag{2.20}$$

$$\mathbf{I_{mk}} = y_{km}(\mathbf{V_m} - \mathbf{V_k}) \tag{2.21}$$

The complex power flow in a line, $\mathbf{S_{km}}$ is given in Equation 2.22, and can be formulated in terms of the bus voltages and branch resistance and reactance using equations 2.19 and 2.20.

$$\begin{aligned} \mathbf{S_{km}} = \mathbf{V_k I_{km}^*} &= \frac{V_k^2 - V_k V_m \cos\theta_{km} - jV_k V_m \sin\theta_{km}}{r_{km} - jx_{km}} \\ &= P_{km} + jQ_{km} \end{aligned} \tag{2.22}$$

The unit for complex power is VA, and it can be decomposed into the real component P_{km} and reactive component Q_{km}, for which the expressions are given in equations 2.23 and 2.24.

$$P_{km} = \frac{r_{km}V_k^2 - r_{km}V_k V_m \cos\theta_{km} + x_{km}V_k V_m \sin\theta_{km}}{r_{km}^2 + x_{km}^2} \tag{2.23}$$

$$Q_{km} = \frac{-r_{km}V_k V_m \sin\theta_{km} + x_{km}^2 V_k^2 - x_{km}V_k V_m \cos\theta_{km}}{r_{km}^2 + x_{km}^2} \tag{2.24}$$

Another important definition is power injection, which is the sum of power flows of all adjacent branches. The formula for power injection at node k is given by Equation 2.25.

$$P_k^{inj} = \sum_{l \in \Pi_k} P_{kl}, \qquad \text{where } \Pi_k \text{ is the set of nodes adjacent to } k \tag{2.25}$$

The last thing to quantify is the real power loss in a line, which is derived in Equation 2.26.

$$P_{km}^{loss} = |\mathbf{I_{km}}|^2 r_{km} = \frac{|\mathbf{S_{km}}|^2}{|\mathbf{V_m}|^2} r_{km} = \frac{P_{km}^2 + Q_{km}^2}{V_m^2} r_{km} \tag{2.26}$$

Power Flow and Optimal Power Flow problems

The objective of a Power Flow (PF) study is to determine the bus voltages and angles of all nodes in the system, and thereby deduce the power flows in the lines. For convenient notation, the numbers of busses, branches and generators are referred to as n_{bus}, n_{br} and n_{gen} respectively. All nodes in a network are at any given time characterized by four variables. The variables for the bus k are:

- θ_k : bus angle
- V_k : bus voltage

- P_k^{net} : net active power - the sum of all real loads, generation and storage power at node k
- Q_k^{net} : net reactive power - the sum of all reactive loads, generation and storage power at node k

The first step is to identify the known quantities, which will depend on the type of node. Typically three types of nodes are relevant:

- PQ nodes - the real and reactive net powers are known, generally load busses
- PU nodes - the real power and voltage is known, generally generation busses
- reference node or slack bus - serves as the voltage and angle reference, the active power is unknown and used to balance generation, load and losses. For any PF the network needs to have one slack bus, in many systems any PU bus can be selected as the slack bus.

The next step is to deduce the constraints that describe the system. Two equality constraints are used to describe the nodal balance based on Kirchhoff's Current Law (KCL), enforcing that the sums of real and reactive power flowing out of each node sum to zero, as shown in equations 2.27 and 2.28.

$$\sum_{l \in \Pi_k} P_{kl} + P_k^{net} = P_k^{inj} + P_k^{net} = 0 \quad \forall k = 1...n_{bus} \tag{2.27}$$

$$\sum_{l \in \Pi_k} Q_{kl} + Q_k^{net} = Q_k^{inj} + Q_k^{net} = 0 \quad \forall k = 1...n_{bus} \tag{2.28}$$

The bus voltages and angles in the system are calculated against a reference bus s:

$$\theta_s = 0 \tag{2.29}$$

$$V_s = 1 \tag{2.30}$$

A PF calculation involves using numerical analysis to calculate the values of all the unknown variables for a network, where the constraints 2.27, 2.28, 2.29 and 2.30 are maintained. Using the expressions for power flow in a line 2.23 and 2.24, results in a highly non-linear problem known as the ACPF. Generally the ACPF cannot be solved analytically, and so iterative solutions have been developed.

Whereas in a PF calculation the generation is fixed, an Optimal Power Flow (OPF) calculation assumes that all voltages, angles and generation capabilities are free within the limits. The OPF solution includes the "optimal dispatch", which gives the cost-optimal output powers for all generators.

For the OPF it is therefore necessary to specify the network constraints shown in Equation 2.31. All bus voltages need to remain within a range of $\pm$ 10% of 1 pu for all nodes. Generator limits are given by their rating, and there may be a limit for real and reactive generation separately. Although in reality generator limits may be more complex and P and Q cannot be decoupled, this simplification is adequate for this study. The branch limits do apply to the magnitude of apparent power and are specific to each branch, in this case it is assumed that the limits are bidirectional, i.e. $\underline{S_{km}} = -\overline{S_{km}}$.

$$\underline{V} \leq V_k \leq \overline{V} \quad \forall k = 1...n_{bus}, k \neq s \tag{2.31a}$$

$$\underline{P_{gen,k}} \leq P_{gen,k} \leq \overline{P_{gen,k}} \quad \forall k = 1...n_{gen} \tag{2.31b}$$

$$\underline{Q_{gen,k}} \leq Q_{gen,k} \leq \overline{Q_{gen,k}} \quad \forall k = 1...n_{gen} \tag{2.31c}$$

$$\underline{S_{km}} \leq |S_{km}| \leq \overline{S_{km}} \quad \forall \text{network lines} \tag{2.31d}$$

The results of a PF or OPF calculation provide a snapshot status of the grid under specific loading conditions. For many studies it is necessary to calculate and optimize over a period of time, requiring a multi period OPF (MPOPF). This is particularly relevant when there are components of the network that have time dependencies, such as energy storage or any other flexible loads. An MPOPF for a system containing energy storage can provide a schedule for optimal charging and discharging of the storage units in the network. Due to the nonlinearities, this can be a very difficult problem to solve. Therefore it is necessary to approximate the equations to make the problem more tractable.

2.4.2 Linearised Power Flow

The most well known linear PF approximation is the DC power flow, or DCPF, which reduces the problem by assuming that the voltage is always 1 pu, thereby also neglecting the reactive power flow. Furthermore the network is assumed to be purely reactive, and therefore the losses are ignored as well. The resulting problem is entirely linear, and therefore allows an analytical solution to be easily calculated. However, many important properties are not part of the model. Since alleviating overvoltage issues and reducing overall line losses in a network are two significant uses of energy storage, the DC approximation is not suitable for use in this study.

The linearisation method presented in [76] is more detailed and complex than the DCPF, although the initial assumptions are similar. Equations 2.23 and 2.24 are non-linear, and to linearise them two key approximations are used. Firstly, the small angle approximation is used, which assumes that $\theta_{km} \approx 0$. This allows for the following linearisation:

$$\sin\theta_{km} \approx \theta_{km} = \theta_k - \theta_m \qquad \cos\theta_{km} \approx 1 \tag{2.32}$$

The second approximation uses the fact that $V_k \approx 1$ and $V_m \approx 1$, and therefore multiplying by the voltage is the same as multiplying by 1. To linearise the power flows using these approximations, both real and reactive power are separated into two parts, to separate the dependency of voltage and angles.

$$\begin{aligned} P_{km} &= \frac{r_{km}}{r_{km}^2 + x_{km}^2} V_k (V_k - V_m \cos\theta_{km}) &&+ \frac{x_{km}}{r_{km}^2 + x_{km}^2} V_k V_m \sin\theta_{km} \\ &= g_{km}(V_k - V_m) &&- b_{km}(\theta_k - \theta_m) \end{aligned} \tag{2.33}$$

For ease of notation the admittance model of a line is used where the expressions for conductance and susceptance are given in Equation 2.18. The same process is applied to the reactive power flow.

$$\begin{aligned} Q_{km} &= \frac{-r_{km}}{r_{km}^2 + x_{km}^2} V_k V_m \sin\theta_{km} &&+ \frac{x_{km}}{r_{km}^2 + x_{km}^2} V_k (V_k - V_m \cos\theta_{km}) \\ &= -g_{km}(\theta_k - \theta_m) &&- b_{km}(V_k - V_m) \end{aligned} \tag{2.34}$$

The linearised line flow given in equations 2.33 and 2.34 can be used to linearise the PF problem

by implementing the line limits as linear constraints, as well as providing a linear expression for bus injection. The assumptions made in this approximation results in inaccuracies in the final result, and the error is evaluated using the case study results in Section 5.5.1. The most severe approximation is assuming the voltage is approximately 1 p.u., and the results are more inaccurate the further the actual voltage deviates from this value. However, since the constraints limit the voltage at all nodes to remain within 10% on either side of 1 p.u. the error is low and the approximation is considered acceptable.

Chapter 3

Introduction

This chapter presents a model that is an extension of the one published by the same author in [77].

3.1 Background and Motivation

For studying the planning and operation of battery storage at the distribution level, it is necessary to realistically represent residential loads. Although energy system studies often use Standard Load Profiles (SLP) to represent loads, there are a number of reasons why this is not suitable for the investigations in this thesis. SLPs provide a highly accurate representation of aggregate loads, as they are usually based on measured data at substations or common connection points. They are good at representing seasonal differences, and differences between weekends and weekdays. However, it is shown in this chapter that for higher time and spatial resolutions, they do not provide a realistic representation of loads. Aggregate loads, like the SLP, are much smoother than individual household profiles because load peaks occur at different times. This phenomenon is known as 'diversity'. Furthermore, since SLPs typically provide profiles at a 15 minute resolution, studies that take place on a minute or second basis need a more detailed load profile than the SLP.

For the energy storage studies in this thesis, the case studies have between 10 and 200 residential loads, and the SLP may not be a good representation of the load behaviour. The real load is much more spiky than the SLP, and the SLP does not represent diversity between households.

Besides using SLPs to represent loads, planning studies are often carried out by accounting for the worst case to ensure system robustness. For example, when planning for new cables, transformers or other essential electrical equipment, they are sized according to the highest expected load. For energy storage this is not appropriate, since security issues are typically not the main priority for operation. When sizing for maximum profits for example, the typical load scenario is much more relevant than the worst case.

Within the research group, 'Energy Efficient and Smart Cities', a very detailed residential electricity demand profile generator called REM has been developed, of which the active power model is published in [77]. The REM is built to be flexible and provide profiles that are suitable for a wide range of studies. The REM incorporates a large variety of data to provide as much detail as possible, so that scenarios involving changing behaviour or changing technology can be reflected. The REM provides profiles for active and reactive power, at a time resolution upto 1 second, modelling individual appliances to provide accurate details, whilst incorporating SLPs to ensure the aggregate load is also correct.

This chapter is structured as follows; Section 3.2 outlines some of the most commonly cited load models that have been published in academic literature. Section 3.3 describes the methodology used to create the REM, including the data sources utilized, the load categories used, and the way active and reactive loads are modelled. Section 3.4 shows the REM output and points out some major features. Finally in Section 3.5 an extensive validation is carried out on the REM profiles, on an individual basis by comparing the statistical properties to measured load profiles, and on an aggregate basis by investigating the properties of the aggregate profiles.

3.2 Literature

As mentioned previously, it is still common to use the SLP to model electricity loads in academic studies. However, with the growing focus on Demand Side Management and the effects on the network of increased distributed generation the need for more detailed load models is increasing. This has led to a number of published models for generating statistically accurate electricity demand profiles in academic literature, that aim to represent household loads in greater detail.

The most common way of classifying methods for residential load models is by grouping them into top down and bottom up models, as in the the review paper by Grandjean [78]. The terminology references the hierarchical position of the input data. Top down models consider characteristics of the entire housing sector, and attribute energy consumption behaviour to these characteristics [79]. Commonly used characteristics include macroeconomic indicators such as GDP and employment rates as well as weather conditions. Many top down models take the form of a deterministic statistical disaggregation model: this approach consists of disaggregating measured load profiles to identify various appliances. Diversity is not modelled at all because it is embedded, in a deterministic way, in the measured data. This type of modelling produces profiles that are a highly accurate representation of the input profiles, however they do require large amounts of measured data to work.

Commonly cited examples of top down models include that of Aigner et al [80], which is a regression based model that attempts to determine the hourly variation of the load curve with respect to the mean daily power value. The parameters considered include temperature, size of the dwelling, and appliance penetration. Another commonly cited model is the Delmod [81]. Delmod includes the same information as Aigner's model, but includes socioeconomic factors like occupant numbers and income, as well as behavioural changes.

More recent examples of top down models includes one by Wang [82], whose model produces half hourly profiles. The focus is placed on extracting patterns at different time scales, including seasonality, days of the week, and diurnal patterns. McLoughlin [83] uses a multiple linear regression model to describe total electricity consumption, maximum demand, load factor and time of use. Socio-economic factors like dwelling type, number of bedrooms, head of household age and household size are used as model input. Besides applying regression in the time-domain, another approach is modelling the profile characteristics based on the frequency domain. An example is the work of Magnano [84], where the relationship of load to temperature is modelled and Fourier analysis is used to reflect seasonal changes. Another commonly cited method is that of Stephen [85], where a Gaussian mixture model is used to cluster measured load profiles and generate synthetic load profiles from the learned clusters.

The disadvantage of top down models is that there is no internal logic, i.e. all samples within the profile time period have no logical relationship to one another. This does not allow for much

extrapolation or insight into how behavioural or technological changes can influence the total load.

Bottom up models are often referred to as data-driven models, as the approach involves collecting data to build up a picture of the individual households. Bottom up models are able to create accurate profiles with very high time resolutions for a small number of households. Many bottom up models include technical information about household appliances, and often attempt to model human behaviour in some form or other. There are many different approaches to bottom up modelling, differing by which information they include, and the method used to model human behaviour. A common feature of bottom up models is an occupancy model, that determines when households are occupied and therefore certain appliances can be switched on. The review paper by Grandjean [78] seperates bottom up models into statistical random models, probabilistic empirical models, and time of use based models.

An example of a statistical random model is published by Yao and Steemers [86], whose model is focused on simulating the worst possible case in households, which involves all appliances running on a given day. The times that the devices are used are randomly generated and do not incorporate any data on domestic habits.

An example of a probabilistic empirical model is that of Stokes [87], where a three layered approach is used to provide per-consumer, 1-minute averaged loads on an end-use basis. Stokes develops a mathematical formula based on a sinusoid for normalised power demand, and uses socio-economic differences between households to create diversity. The Stokes model only provides a high resolution profile for one of the households, and the aggregate load of the remaining households. Another example is the Paaterson and Lund model [88], where the starting of individual appliances is modelled as a random process, depending on season and a social factor. Due to the input data, the model is only able to calculate load curves for households living in flats.

The largest category according to the Grandjean classification is the time of use based models, which is also the category that the REM falls under. The first published model of this category was by Walker and Pokoski [89], who use an activity based model to create profiles at a 15 minute time resolution. The model includes the ideas of availability of appliances and occupancy, and the probability that certain loads will occur at certain times due to human behaviour. The next early model of this category is by Capasso [90], who incorporates more data into the model and also attempts to model the interactions between the load categories. This model is geared towards planning, and therefore focuses on peak load days.

Another time of use based model is published by Armstrong [91], who develops a model to generate 5 minute profiles for households living in single-family detached houses. The model groups the consumers into low, medium and high consumers all having a different power factor. Based on total energy use statistics and normalised energy use profiles, a random process is used to determine the time of a switching event.

After the Capasso and Walker models, the Markov-chain approach became popular for time of use models. Two of the most well-known models are those of Richardson and Widen. The Markov-chain approach constructs probabilities from the TUS survey about which activities follow one another, or 'transition probabilities', and then construct appliance loads based on the activity. The Richardson model [92–94] describes occupancy, light usage and domestic electricity demand at a time resolution of 10 minutes. The model is built in Excel and is available as a free down-

load. The Widen and Wackelgard model, [95–97] also employs transition probabilities to create occupancy, light, electricity and domestic hot water models, at a high time resolution of 1 minute.

There have been many other published load models, although the most significant and highly cited ones have been listed above. There is one lesser known model created by Molitor [98], that has influenced the structure of the REM. It is also a bottom up model in the sense that the various load categories are modelled separately. However, it utilizes only the SLP to generate probability distributions for starting times of loads. It does not take into account the fact that different loads occur at different times, as the bottom up models that employ the Time Use Surveys do.

A model published at the same time as the REM was created by Fischer [99]. Like the REM, it uses the Time Use Survey to create activity based loads, and uses elements of the SLP. Unlike the REM, it does not use the SLP to create probabilities for loads that are not well reflected in the TUS.

One of the main distinguishing factors of the REM is that it does not model households individually, rather it models the entire population and assigns loads randomly. The advantage of this approach is that the aggregate load is very accurate. The only inaccuracy of the REM compared to the Markov chain approach is that the internal logic, i.e. the links between the various activities is not incorporated in the model.

Unfortunately, utilising profiles from existing models is often not a reasonable option, even those that have been made readily available such as the Richardson model. Firstly there is little control over the parameters that are included in modelling, for example the SLP or appliance ownership statistics used. The background data may also not be updated, and since electricity loads do change with time and depend heavily on location, it is often unreasonable to use other models. The REM is developed to be extremely flexible, in order to facilitate a wide array of studies. For this reason the time resolution can be set by the user, and all the load categories can be incorporated. The REM can therefore be used to investigate the effect of changes in behaviour of consumers, or change in technologies by replacing individual load categories.

3.3 Methodology

3.3.1 High Level Overview

A high level workflow of the REM configured to create daily profiles is shown in Figure 3.1. The minimum user input includes the number of households, the desired time resolution of the resulting profiles (seconds or minutes), and the date to be simulated (e.g. the first of January). The REM is based on a large variety of data, that can be updated or changed by the user if more specific data is available.

The first step is to generate a synthetic population that details the household members and appliances of each of the simulated households. Then the aggregate profile for the entire population for the selected day is calculated, and the population is divided into Household Categories (HCs) based on the household size. The load for each HC is modelled independently. Before calculating load profiles, the household occupancy is modelled. Occupancy profiles specify the presence of households members in the dwelling throughout the day. Occupancy is required for certain activity loads that can only occur with the presence of an 'occupant', for example television and cooking.

The total daily energy consumption is distributed amongst the various Load Categories (LCs), which are individually simulated based on which modelling bracket they fall into. The LCs belong to one of the following five brackets: activity dependent loads, lighting load, base loads, turn-on loads and miscellaneous. Activity dependent loads, like television and cooking are modelled based on occupant behaviour. Lighting is a special type of activity dependent load, which is modelled to include the daylight hours as well as occupancy. Activity independent loads, or base loads, are those like the fridge and freezer, whose energy consumption does not significantly depend on the behaviour of the occupants. These three loads are added and the remaining load comprise of turn-on and miscellaneous loads. Turn-on loads include washing machines, dryers and dishwashers, whose usage are related to the occupant behaviour but cannot be linked to a specific activity. Finally, the loads that cannot be categorized are classified as miscellaneous. The profiles modelled in each LC are added to make up the total household profile, and the household profiles are added to give the aggregate results.

Annual profiles are generated by looping all steps besides the synthetic population, ensuring the household characteristics and appliance ownership remain the same. The LC profiles and household profiles are written to memory after each day to ensure the simulation does not run out of RAM.

Summary of main data sources

Any of the following data can be updated by the user to reflect a different region, time or population. Currently the REM Uses the following statistics to create the synthetic population and load profiles.

- **Population Composition**: [8] Munich - the household sizes of the synthetic population are assigned according to average Munich percentage breakdown, as published by the city of Munich.
- **Annual load according per HC**: the average annual energy demand per HC published by the energy agency EnergieAgentur.NRW [3].

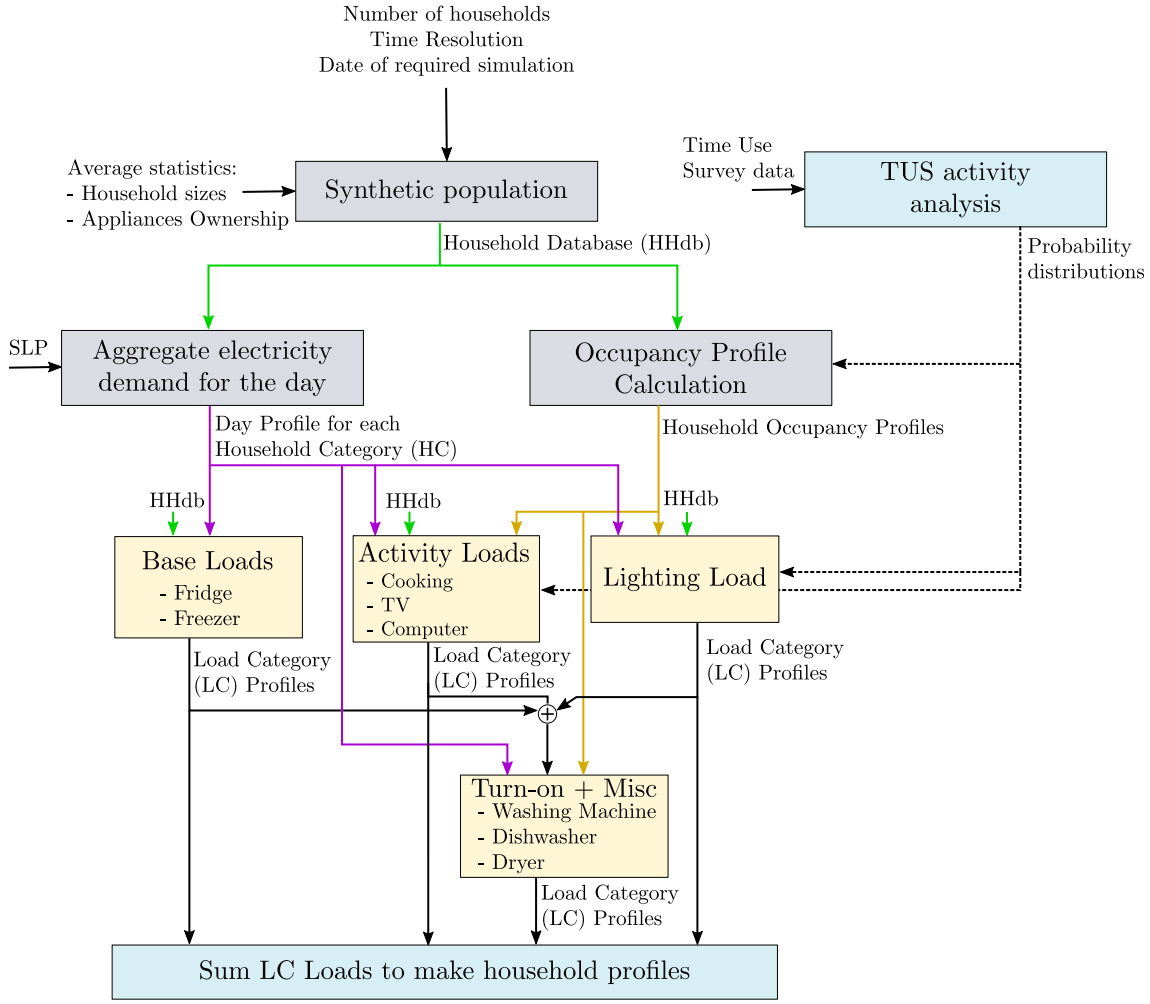

Figure 3.1: *REM workflow*

- **Average living area**: the average living area per person published by the German Federal Statistical Office [9].
- **Appliance Ownership**: Depending on the household size, the number of relevant devices owned is assigned based on national statistics of device ownership as published in a study by the Bavarian state office for statistics [100].
- **Standard Load Profile (SLP)**: The SLP used is a file that gives a timeseries for the average household energy consumption for the entire year of 2018 in 15 minute increments, as published by the utility company SWU for the city of Ulm [101].
- **Load Category (LC) Shares**: Percentage of the total energy consumption of each LC depending on the HC, published in the same study by the EnergieAgentur.NRW [3], given in full in Appendix A.
- **Time Use Survey**: Survey taken in 2012 where subjects filled in diaries in 10 minute intervals, recording their activities. The TUS in 2001 is also used as it contains information regarding location that is missing from the 2012 survey. The Research data centres of the Federal statistical office offer a scientific use file that was used for this study [102, 103].
- **Tracebase**: Smart meter measurements of various household devices taken at a time

resolution of at least a second [104] .

- **Appliance Power Rating**: To determine the appliance power ratings two main sources are used, the energy use calculator [105], and a study on smart appliances [104]
- **Reactive Power**: Reactive power is determined using many smart meter databases, although most data is derived from measurements published in [106, 107].

3.3.2 Model Breakdown

Synthetic population, appliance ownership and energy profile

There are a large number of factors that influence the energy consumption and behaviour of households, such as income, age, employment status and region. It would certainly be possible to assign all these properties to the synthetic population, as they are all factors that will contribute towards the electricity consumption characteristics of the households. However, it is very difficult to determine how these factors interact with one another. It is important to be able to judge which factors can effectively be represented in the model with the available data. Household size was judged to have the most important influence on total energy consumption, and data is available to estimate the difference in appliance ownership, load composition and annual load based on this parameter.

The household size is significant to the output, since the annual energy consumption as well as the breakdown of the load categories vary substantially with the household size. The population composition can be given as input by the user. If no input is given, the default values are the average Munich statistics shown in Table 3.1. The model assigns a number of members to each household according to the composition, and separates the synthetic population into these HCs that are then modelled separately.

Household Category (members)	1	2	3	4	5+
Population composition Munich 2017 (percentage)	54.1	25.1	10.3	7.5	3.1
Annual electricity demand without DHW (kWh)	1714	2812	3704	4432	5317
Average living area per person (m^2)	69.6	48.7	35	30.3	25.7

Table 3.1: *Population composition used for the synthetic population [8], the average annual energy demand per household category [3], and the average living area per person [9]*

The appliance ownership varies greatly between HCs, and the statistics used for the model are based on a study carried out by the Bavarian state office of statistics (Bayerisches Landesamt für Statistik) in 2016 [100]. This study shows the variation of appliance ownership based on household size, income, status of main earner (employed, unemployed or retired), age of main earner, family status, and housing ownership status.

Based on the study on ownership of household appliances published by the Bavarian statistical office [100], relevant appliances are assigned to each of the households. Based on the population statistics published in [9], a living area is assigned to each household. Finally a parameter for lighting power per square meter in W/m^2 is assigned based on [108]. Within the REM, all household information is summarized in a table called Household Database (HHdb) which is used for internal consistency in the rest of the model.

Category breakdown
Just as the households are categorised based on the number of household members, the loads are also divided into categories (LCs) based on the energy uses that make up residential loads. The percentage make-up of each of these LCs varies strongly based on the HC, as shown in Figure 3.2 [3]. The circulation pump is a load category that relates to circulation of water in a building. Since this is highly building specific, this category is excluded from the REM by subtracting the circulation pump load percentage from the total.

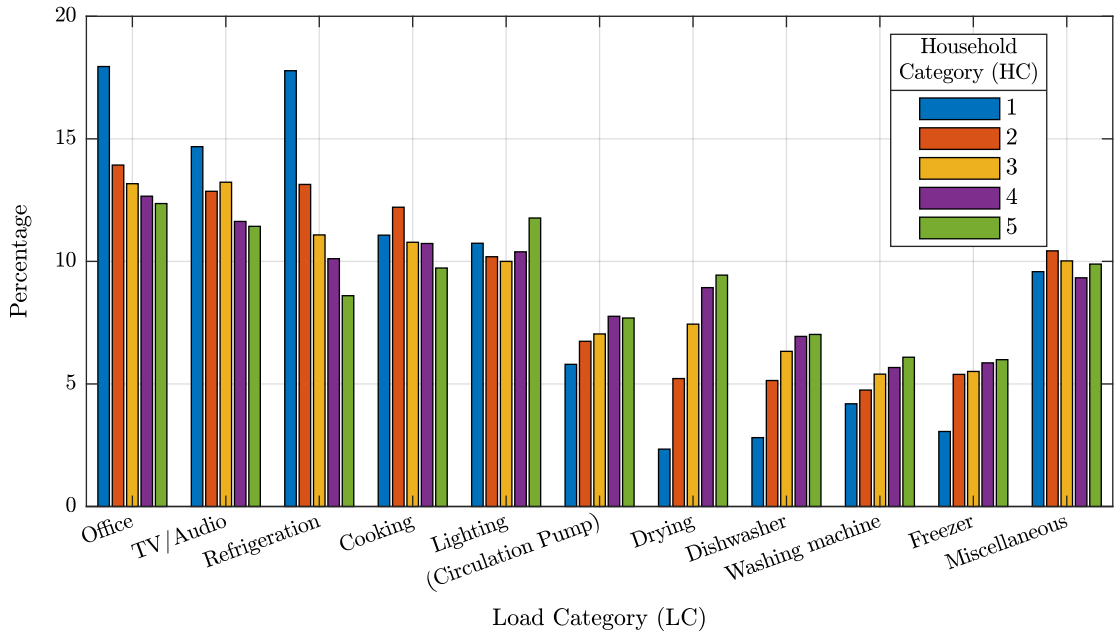

Figure 3.2: *Composition of the load categories (LC) for each of the household categories (HC) [3]*

Based on the statistics in Figure 3.2, each load category is modelled separately for each household category. Five different procedures are used for the different types of categories, as shown in Figure 3.1. These are:

- Activity Based Loads: Cooking, TV/Audio, Office (desktop computer)
- Base Loads: Refrigeration, Freezing
- Turn on loads: Washing machine, Dishwasher
- Lighting loads
- Miscellaneous: Miscellaneous, Office (non desktop computer)

Within this chapter, the methodology for modelling each of the procedures listed above is explained in further detail.

TUS Activity analysis
For the activity based loads, Time Use Surveys (TUS) are used to create probability functions for when certain events are likely to occur. For the activity analysis, the TUS taken in 2012/2013 is used, which surveys 5000 German households corresponding to over 11000 individuals. An extensive questionnaire is filled out by the participants, including age, income levels, jobs, details

on living space, car ownershop, hobbies, educational background and more. The participants also fill out a diary for three days, describing what they are doing in 10 minute intervals. Participants choose from a range of activity codes, and can list one or two activities per time interval.

The TUS is used to derive probability distributions for activities that relate to the activity based LCs in Figure 3.2. For example, the activity "Preparation of food" is linked to cooking, and the activity "Television and Video/DVD" is linked to the television LC. Although this does not account for times where devices might be running without the person being actively involved in this category, it does give a lot of insight into which devices are likely on at which times. Since the number of household members is also known, it is possible to distinguish between the behaviour of different HCs.

The TUS also gives insight into the duration for which certain activities are performed. Therefore for cooking, computer use and television, duration probabilities are also derived from the TUS.

Figure 3.3 shows the distributions derived from the TUS for Cooking, TV/Audio and Computer use. The time probabilities in plot (a) show that there are clear peaks for each LC, such as 12:00 for cooking, and 20:00 for television. The duration plot in, Figure 3.3 (b) is also helpower factorul. Cooking loads are usually short, the majority of time spent preparing food is less than 1 hour. The duration plots for both television and computer show peaks every 30 minutes, and in the case of television, even stronger peaks for 1 hour.

The probability distributions are not calculated during each REM simulation as the identical probability distributions are used for each REM calculation. Instead, the distributions are precalculated and stored within the REM files as background data. It is not necessary to work with the TUS data directly within the REM simulation. As for any of the REM background data, the distributions in Figure 3.3 can also be substituted with other data to assess the effect of changes of human behaviour on load profiles.

The TUS is also used for creating occupancy profiles for the households. The 2001/2002 TUS [102] has a corresponding diary entry for location, where participants fill in locations including, home, at work, travelling and more. Unfortunately the updated TUS in 2012/2013 does not have a location entry for the diaries, and so the old TUS is used for the occupancy. The profiles for occupants being at home is extracted from the TUS diaries to create a boolean table. Each household is given an occupancy profile by randomly selecting a number of profiles corresponding to the number of household members and combining them to give profile indicating whether or not a household is occupied at a certain time.

3.3.3 Active Power Load Profile Generation

Creating the load profiles starts with the determination of the day-specific total energy demand, and aggregate load profile for each HC of the synthetic population. This is derived from the annual load profile, which is calculated for each HC using the SLP. The SLP gives the average annual profile for households scaled to 1000 kWh in 15 minute intervals. Equation 3.1 shows how the annual load profile per HC is calculated, where Household(HC) refers to the total number of households per HC in the synthetic population.

$$\text{Annual Profile(HC)} = \frac{\text{SLP} \times \text{Annual Load(HC)} \times \text{Households(HC)}}{1000} \quad \forall HC \in \{1, ..., 5\} \quad (3.1)$$

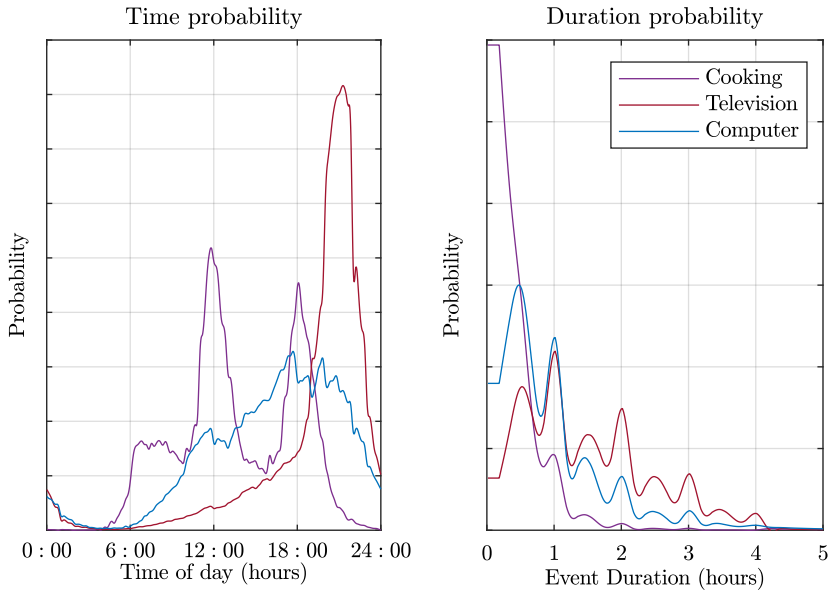

Figure 3.3: *Probability distributions for event start time and event duration for activity based loads, based on TUS data*

The annual profile is required because the SLP also includes seasonal variation and variation between workdays and weekends. Equation 3.1 is performed separately for each HC, facilitating the separate load profile calculation for each HC as well. The required day is then selected from the annual profiles per HC. The result is the total day load per HC, and corresponding profiles, referred to as 'day profiles'. The SLP therefore delivers not only the shape of the daily profile, but also the total daily energy.

The HHdb, occupancy profiles, day profiles and the TUS distributions are used to calculate the base loads, activity loads and lighting loads independently of each other.

Activity Based Loads

For the activity based loads, it is first necessary to determine the total LC energy consumption for the day for each HC. This is done by taking the day load per HC, and multiplying it by the LC percentage shown in Figure 3.2. For example, cooking loads takes up an average of 9.6 % of the total load for single person households, so the daily load for the HC = 1 category is multiplied by 0.096 to determine the total cooking energy consumption for all single person households in the population.

The overall work-flow for generating activity-based loads is shown in Figure 3.4. The principle is that events are generated randomly, assigned to a household and this action is repeated until the total amount of LC energy has been reached. The events generated have three properties, start time, duration and magnitude. The start time and duration are derived by using the probability distributions from the TUS, shown in Figure 3.3. The magnitude, i.e. power, is determined using a distribution of power ratings based on typical appliances. To determine cooking events for instance, a range of powers of typical stove events is estimated. Where simple square waves are not sufficient, appropriate noise signals are added.

The range of load magnitudes for the various appliances are based on the source [105]. The mag-

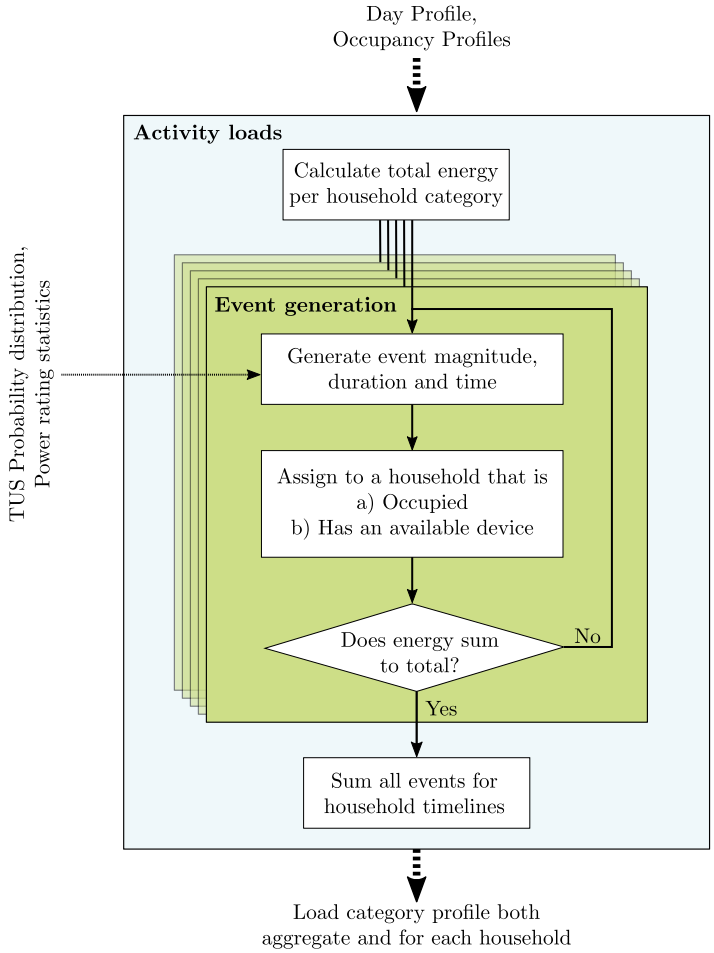

Figure 3.4: *Workflow for generation of activity based loads (cooking, television and desktop computer)*

nitude is not fixed per device, as the same device can have load events with different magnitudes.

- Electric stoves: Magnitudes are generated with a normal random distribution with a mean of 3 kW and a standard deviation of 1 kW, and are forced to be positive by repeating the generation until a positive value is found.
- Television: Magnitudes are generated with a normal random distribution with a mean of 150 W and a standard deviation of 10 W, repeating the generation until the answer is positive. A white noise signal is added, ranging from 20 % to 100 % of the generated magnitude
- Desktop computers: Magnitudes are chosen using a uniform distribution within the limits of 50 W and 150 W.

Once the event has been generated, a list is made of all the households that both have an available cooking appliance and are occupied for the entire event duration. One of the eligible households is randomly selected, and the event is added to the load profile of that household. The device in question will be marked as 'in use' for the event duration, and cannot be assigned another load event during this time. The total event energy is added to a counter, and the process continues until the counter reaches the total amount of cooking energy.

Office loads are subdivided further, since the types of devices involved in this category have very different energy consumptions. Based on a study into the components of office loads in households in the UK [109] there are ten appliances that make up household office loads, of which the three largest make up 73% of total office load. The three largest components are desktop computers, fax/printers and modems. Of these three devices, the desktop accounts for 27% of office loads and is the only appliance that can be directly linked to an activity. The remaining office loads are added to the miscellaneous loads.

Lighting Loads

Lighting loads are more complicated to model, since typical households have a large number of lighting devices. Although lighting is highly activity dependent, additional data regarding daylight times is also needed. Lighting events have the same structure as the activity based loads, in the sense that they have three parameters: start time, duration and magnitude. The process for determining these three parameters is different from activity loads, since for lighting the parametrization is based on distributions derived from various different sources. The distributions used for the lighting model are shown in Figure 3.5.

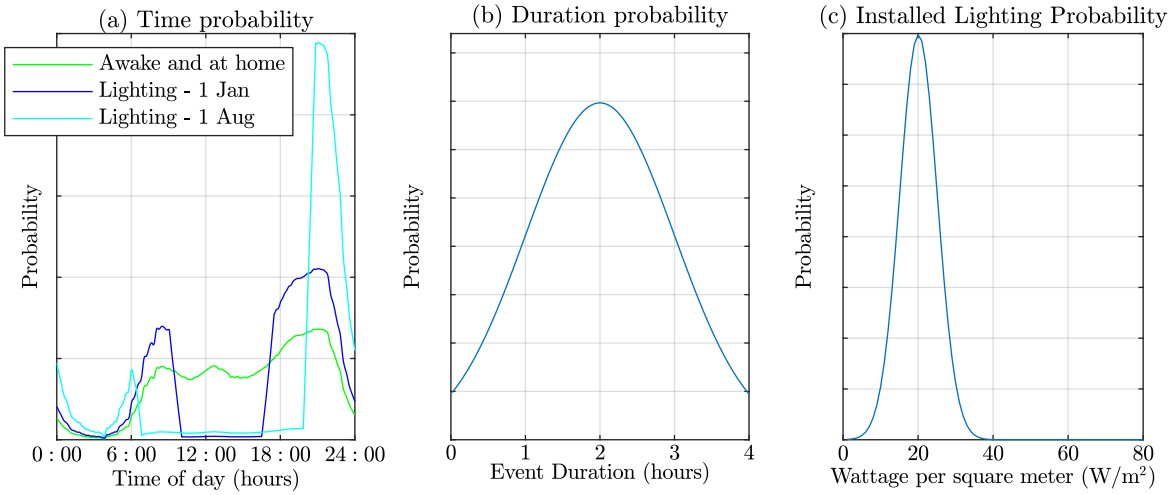

Figure 3.5: *Probability distributions used for the lighting loads are clearly highly dependent on the daylight hours of the day being simulated*

The start time of lighting events is based on a probability distribution that combines active occupancy with daylight time. The day of the year is given as user input, the respective daylight times for Munich are loaded from a table. As with any of the REM background data, this data can be replaced to model a different region. The daylight distribution includes a buffer time of 40 minutes, outside of which lights have only a small probability of being turned on. The probability distribution for active occupancy is derived from the 2001 TUS, extracting the times that the participants are awake and in the house. The distribution for start time of a lighting event is calculated by multiplying the probabilities for active occupancy with the daylight probability. As shown in Figure 3.5, the probability distribution of start time is highly dependent on the day of the year that is being modelled.

The probability distribution for the duration of lighting events uses a study based on the household electricity survey in the UK, focused on lighting loads specifically [110]. The study gives

insight into the amount of time that lights are left on based on measured data. The study indicates that a suitable distribution for duration is a normal distribution with a mean of 2 hours, and a standard deviation of 1 hour, truncated between 0 and 4 hours. Lighting event magnitudes are randomly generated using a uniform distribution between 10 W and 100 W.

For loads besides lighting, a number of relevant appliances is assigned to each household. For lighting, a value for installed lighting power per square meter is assigned instead, measured in W/m^2. Using the respective household living area, a maximum lighting power is calculated for each household. Based on statistics in England installed lighting is assigned according to a normal distribution with a mean 24 W/m^2, and standard deviation 5 W/m^2, truncated between 5 W and 85 W. In this way, lighting events are generated and assigned to any household that is not lit to its full capacity at the event time. Figure 3.6 shows that the activity based loads and lighting account for some of the peaks that are seen in the SLP.

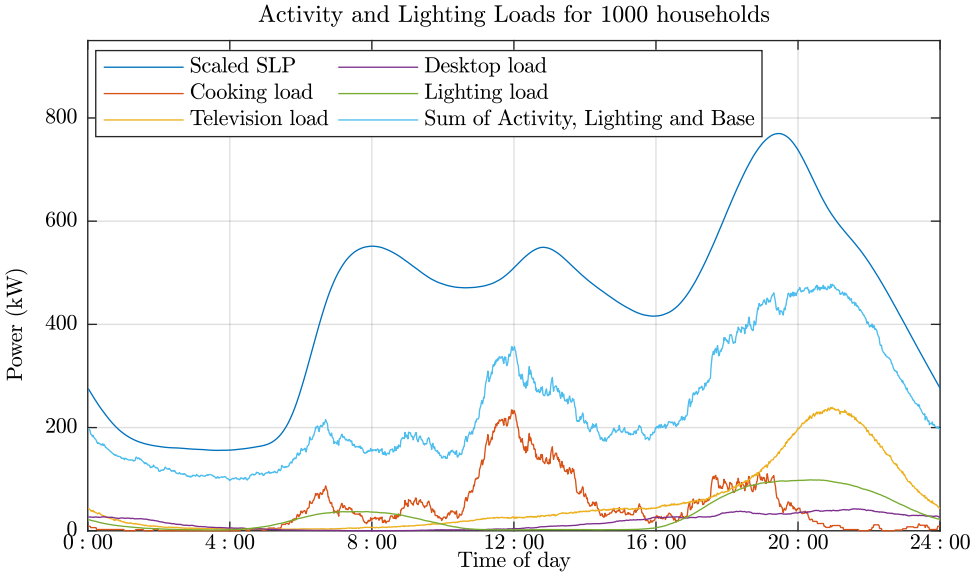

Figure 3.6: *Simulation of 1000 Households with the time resolution of 1 minute, on a winter working day. The scaled SLP shows the aggregate load profile for the day, and the dotted blue line shows the sum of the activity and lighting loads which corresponds correctly with the peaks that appear in the SLP*

Base Loads

Base loads are assumed to be independent of resident behaviour and household occupancy. The appliances modelled with the base load procedure are refrigerators and freezers. The typical waveforms of these cooling devices follow a cyclical pattern of on- and off-times of the appliance compressor. Besides technical and environmental factors (e.g. capacity, ambient temperature conditions, and placement within the dwelling), the energy demand of cooling appliances is also dependent on consumer driven factors such as the frequency of door opening or the inside temperature settings. For simplicity, such details are not taken into account in the modelling. However, they could be added in case of need for more accurate appliance models, such as studies on demand side management of thermostatically controlled loads.

The modelling of cooling devices is very different from the event based load modelling used for

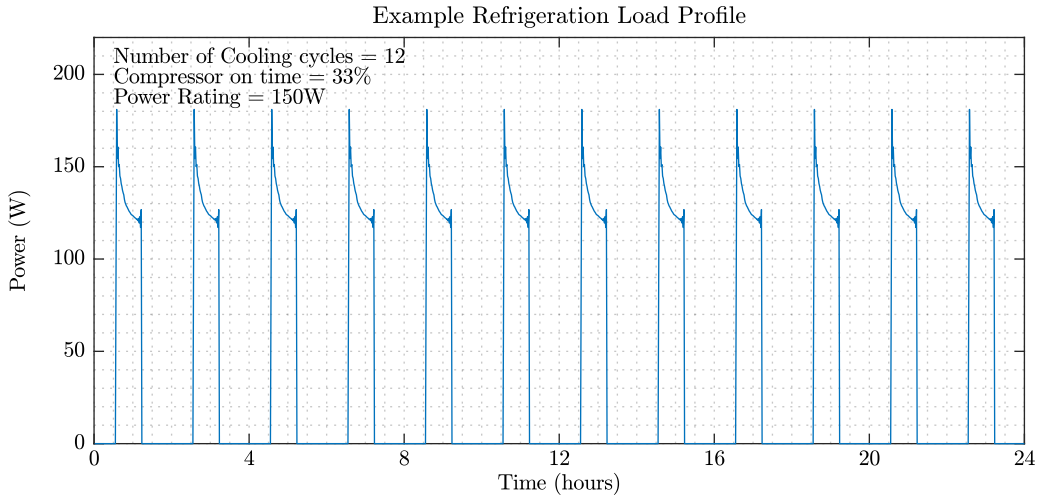

Figure 3.7: *Example fridge load simulated using a 1 minute resolution*

activity based loads and lighting loads, in which events are generated until the total load has been achieved. As cooling devices are not event based, a different strategy is taken to ensure the total amount of energy is correct. The daily load of each device is made up by resampling the typical cycle based on a 33 % on-time for the compressor. Knowing the annual refrigeration load for each HC, it is possible to calculate the mean power for all fridges in the HC using the Equation 3.2.

$$\text{Mean Fridge Power} = \frac{\text{Annual refrigeration demand(HC)}}{\text{Number of fridges (HC)} \times 365 \times 24} \tag{3.2}$$

Based on this mean, a normal distribution is created with a standard deviation of 30 W, and truncated between 50 W and 300 W based on [104]. From this distribution, the power ratings of all the fridges for each household categories are assigned and stored in the HHdb. The assignment of power ratings for freezing are very similar, except a normal distribution is created using a standard deviation of 10 W, and the power is truncated from 20 W to 200 W.

To generate the load profile for the cooling devices, each cooling device in the synthetic population is modelled sequentially and added to the respective household load profile. The first step is to assign a number of cooling cycles. Based on the data in [104] it is deduced that cooling devices typically have between 8 and 32 cooling cycles per day. The daily profile uses a measurement of one typical cooling cycle from the tracebase measured data [111], which is shown in 3.8(d). This typical cooling cycle is then resampled to fit the number of cycles, and scaled to match the appliance power rating. The load profile uses a 33% on time, padding the rest of the profile with zeros, and then shifting it in time randomly to ensure that the on-times of all the fridges in the population vary.

An example of a resulting waveform is shown in Figure 3.7, with the number of cooling cycles and the power ratings varying between households.

Turn-on and miscellaneous loads

The turn-on load methods are applied to LCs that consist of appliances with cycles, where the only action the user takes is to turn on the device. These appliances are dishwashers, washing machines and dryers. Generally these appliances also have a delay or timer functionality,

therefore it is not possible to use the activities in the TUS to determine when the load events take place. Even though there are activities in the TUS that relate to washing clothes or dish washing, since the cycle turn on can be delayed, the activities do not necessarily relate to the load times.

Miscellaneous loads are all other household loads that are too small to have their own LC, this may include appliances such as irons, vacuum cleaners, phone chargers and non desktop office loads.

Since timing information cannot reliably be deduced using the TUS, the SLP is used to make up the turn-on and miscellaneous loads. The activity, lighting and base loads take up 45% -52% of the total load depending on the HC. The aggregate remainder is the scaled SLP minus the sum of activity, lighting and base loads, shown in Figure 3.6. It is from this remainder that the probability distribution for events is derived for the turn on loads. The same process is repeated for miscellaneous load, in order to ensure that the total load matches the scaled SLP as closely as possible.

The load forms for each turn-on device are cyclical, as the devices vary between spin cycles that have different energy characteristics. Therefore these loads are modelled by extracting typical cycles shown in 3.8 using the tracebase database [111], which contains smart meter measurements of a vast array of household devices. From these measurements upto 5 typical load cycles for each turn-on device were selected and replicated for the load events with randomly selected magnitudes.

The magnitudes are assigned to the devices not the individual events, and are kept consistent by assigning them to the HHdb. Based on [104] the magnitudes are assigned using the following distributions:

- Dryer: uniform probability between 2000 W and 2500 W.
- Washing machine: uniform probability between 1800 W and 2500 W.
- Dishwasher: uniform probability between 1200 W and 2400 W.

3.3.4 Reactive Power Load Model

An extension to the REM is developed that models corresponding reactive power profiles, based on the type of appliance and load category. Reactive load can be calculated when the active load and the power factor of the appliance in question is known using Equation 3.3.

$$Q = P \tan\theta = P \tan \arccos(\text{power factor}) \tag{3.3}$$

Although Equation 3.3 gives the magnitude of the reactive power, it is also important to know the sign. There is a difference between a lagging and leading power factor. The terms refer to whether the phase of the current is leading or lagging the phase of the voltage. A lagging power factor signifies that the load is inductive, as the load will consume reactive power, and therefore the reactive component Q is positive as reactive power travels through the circuit and is consumed by the inductive load. A leading power factor signifies that the load is capacitive, as the load supplies reactive power, and therefore the reactive component Q is negative as reactive

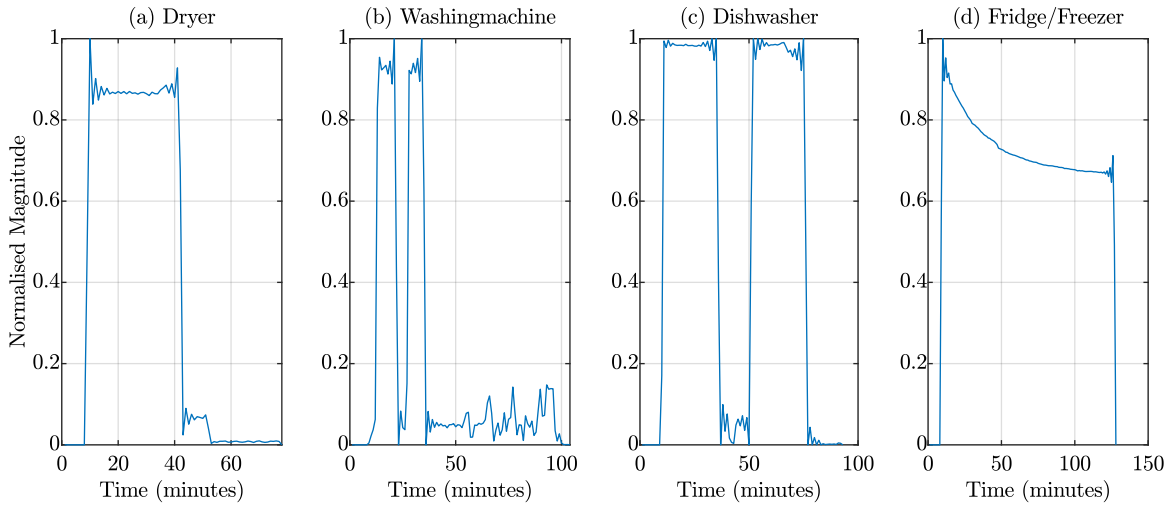

Figure 3.8: *Representative smart meter measured cyclical loads normalised to a maximum magnitude of 1. For use in the REM all loads are scaled in magnitude, and the fridge/freezer waveform is also scaled in cycle duration*

power is being supplied.

Various data sources are used to select the correct power factor for each appliance. One of the main sources of data is the ACS-f2 [106], a large database of smart-meter data providing measurements of real and reactive loads in very high time resolutions. This data is used to gain insight into the reactive loads of a number of devices. Another main source of data is a report on the power signatures of home appliances written by the Finnish research institute SGEM [112]. The following list shows the power factor used for different appliances in the REM, and the data sources used to deduce them. It is important to note that even though these are estimates taken from representative appliances, the aggregate reactive power matches lies within the expected range.

- **Cooking**: The only device modelled for this category is the electric stove, and based on the ACS-f2 [106] it is deduced that stoves have an average power factor 0.9997, which means a very small phase angle, and almost no reactive load at all. Furthermore it is a capacitive load which means the reactive component is negative.
- **Television** : The power factor of the television depends on the magnitude of the active power; the higher the active power, the higher the power factor. Televisions are also capacitive loads, and therefore have a negative reactive load. Based on both measurements from [113] and the analysis in [106] the following ranges are defined:
  - Active power $\leq$ 5W $\rightarrow$ power factor = 0.23
  - Active power 5W - 40W $\rightarrow$ power factor = 0.70
  - Active power $>$ 40W $\rightarrow$ power factor = 0.9376
- **Desktop Computer**: The reactive power for desktop computers is also capacitive, and is modelled by defining two magnitude ranges of active power with different power factors based on [106, 107]
  - Active power $\leq$ 5W $\rightarrow$ power factor = 0.172

  - Active power > 5W → power factor = 0.91

- **Lighting**: Lighting loads are inductive, and modelled with amplitude-dependent power factors based on [112]
  - Active power ≤ 10W → power factor = 0.339
  - Active power 10W - 100W → power factor = 0.6484
  - Active power > 100W → power factor = 0.8636

- **Dishwasher**: The reactive load is inductive, and the power factor depends on the stage of the cycle, as the power consumption for heating the coil, washing and rinsing are different. For this reason the power factor is adjusted according to the magnitude of the active power, based on [113, 114].
  - Active power ≤ 10W → power factor = 0.83
  - Active power 10W - 100W → power factor = 0.26
  - Active power > 100W → power factor = 0.99

- **Dryer**: The dryer has a more complicated inductive reactive load profile, where each spin cycle is characterized by a surge, or peak load, and a decay portion where the reactive load remains constant. For the remainder, the power factor depends on the active load magnitude. The following values are deduced from the Umass Trace Repository dataset [107, 115].
  - The surge is found by the maximum active power = 100% → power factor = 0.979
  - The decay is when active power is 75%-100% of the maximum → Reactive power is constant, calculated by applying the power factor = 0.85 to the active power at the first time instance that this stage of the cycle occurs
  - Outside of the surge and decay, the power factor is 0.514 if the active power ≥ 20W, and power factor = 0.901 otherwise

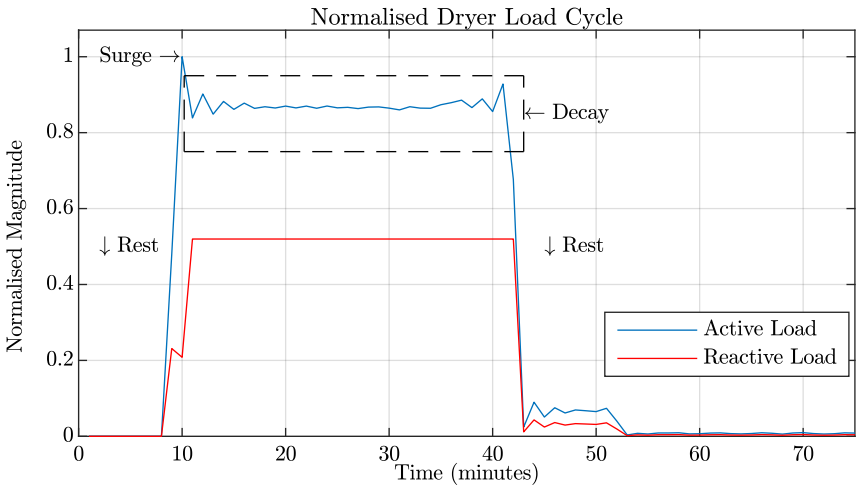

Figure 3.9: *Dryer cycle, with the magnitude normalised to a maximum of 1. This cycle is multiplied by the respective appliance power rating. The stages of the reactive load are indicated, and the corresponding reactive load is shown in red*

- **Freezer**: The reactive power load of the freezer is similar to that of the dryer, as it is inductive and the waveform includes a surge, a decay and remainder. The following power factors are based on data from [106, 113]
  - The surge, defined as the point where the active power is 100% of the maximum cycle power, has a power factor of 0.72
  - The decay portion is defined as the active power bracket of 66% upto but not including 100% of the maximum, and during this time the reactive power is constant, calculated by applying a power factor of 0.65 to the active power in the first instant where the decay portion begins.
  - the remainder of the load has a constant power factor of 0.63
- **Fridge**: The refrigerator is similar to the dryer, as its reactive load is inductive and has a surge, decay, and a remainder based on [107]
  - For the surge the load has a power factor of 0.74
  - The decay portion is defined as the active power bracket of 64% - 100% of the maximum, and during this time the reactive power is constant, calculated by applying a power factor of 0.61 to the first power value directly after the surge.
  - the remainder of the load has a constant power factor of 0.63
- **Washing machine**: The reactive load model is inductive and has a similar structure to that of the dishwasher. It has different power factors for different stages of the washing cycle that are distinguished by the magnitude of the active power load based on [107]
  - Active power $\leq$ 10W $\rightarrow$ power factor = 0.80
  - Active power 10W - 750W $\rightarrow$ power factor = 0.51
  - Active power $>$ 750W $\rightarrow$ power factor = 0.69
- **Printing**: Printing loads have a constant power factor of 0.661
- **Miscellaneous**: A constant power factor of 0.9 is used, as this is generally assumed to be the general power factor of households

To illustrate the reactive load of the cyclical loads, Figure 3.9 illustrates the cycle and the way the reactive load is modelled for the dryer. The freezer and fridge loads are modelled similarly to the dryer. For other cyclical loads, like the washing machine and dishwasher the different power factors are distinguished by the magnitude of the active power.

3.4 REM Output

The REM has several outputs that are useful for different applications. Below is a list of the data generated by the REM for daily or annual simulations:

- `HHdb` - the household database that contains the details of the synthetic population, including the number of household members (the HC), the appliances and respective power ratings.
- `HH_Timeline` - A set of matrices with the waveforms of each of the LCs for every household in the synthetic population. This can be used for studies into the effects of the specific LCs, for example load shifting of turn-on loads.
- `Reactive_HH_Timeline` - The corresponding reactive loads for each household, in the form of a matrix for each LC.
- `Timeline` - The aggregate load for all categories for each household. This is most useful for the studies in this work, as household loads can be assigned to nodes in a network.
- `Reactive_Timeline` - The aggregate reactive load of all categories for each household.
- `HH_Occupancy` - The occupancy profiles that correspond with the load profiles. These can be used to create a corresponding heating or domestic hot water load model. It can also be used to investigate the effect of occupancy on aggregate load.

There are various aspects of the REM output to investigate, and in the following analysis several aspects of the load profiles are visually presented, along with some limitations of the REM. The first output one can look at in more detail is the contribution of the various LCs to the aggregate load as shown in Figure 3.10.

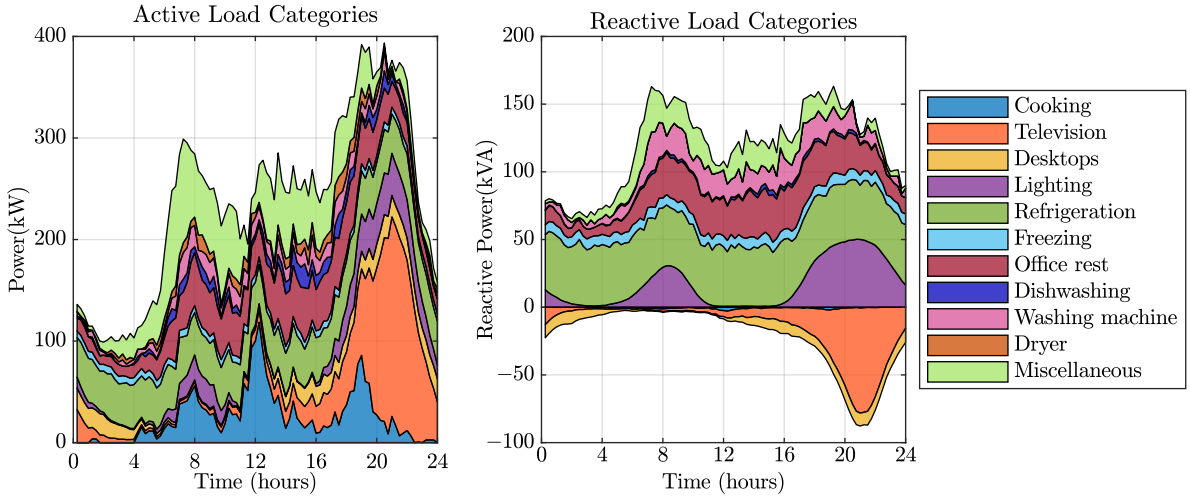

Figure 3.10: *Load categories for a simulation of 1000 households with a 15 minute time resolution using the SLP for the 2nd of January 2018 in Ulm, Bavaria*

First of all it is clear that the activity based loads significantly contribute to the aggregate load peaks, as shown previously in Figure 3.6. Freezing and refrigeration provide rather constant loads throughout the day. One limitation of the REM is that it does not include any information on how the make-up of LCs changes with the seasons. Using the SLP inherently includes the

seasonal variation of total load, which is a reasonable trend for many of the LCs. For example it is realistic that lighting loads will reduce in the summer, along with the total load. There are however, some loads that would oppose this, such as refrigeration and freezing, however it is difficult to obtain reasonable data quantify the annual trend of the LC proportions.

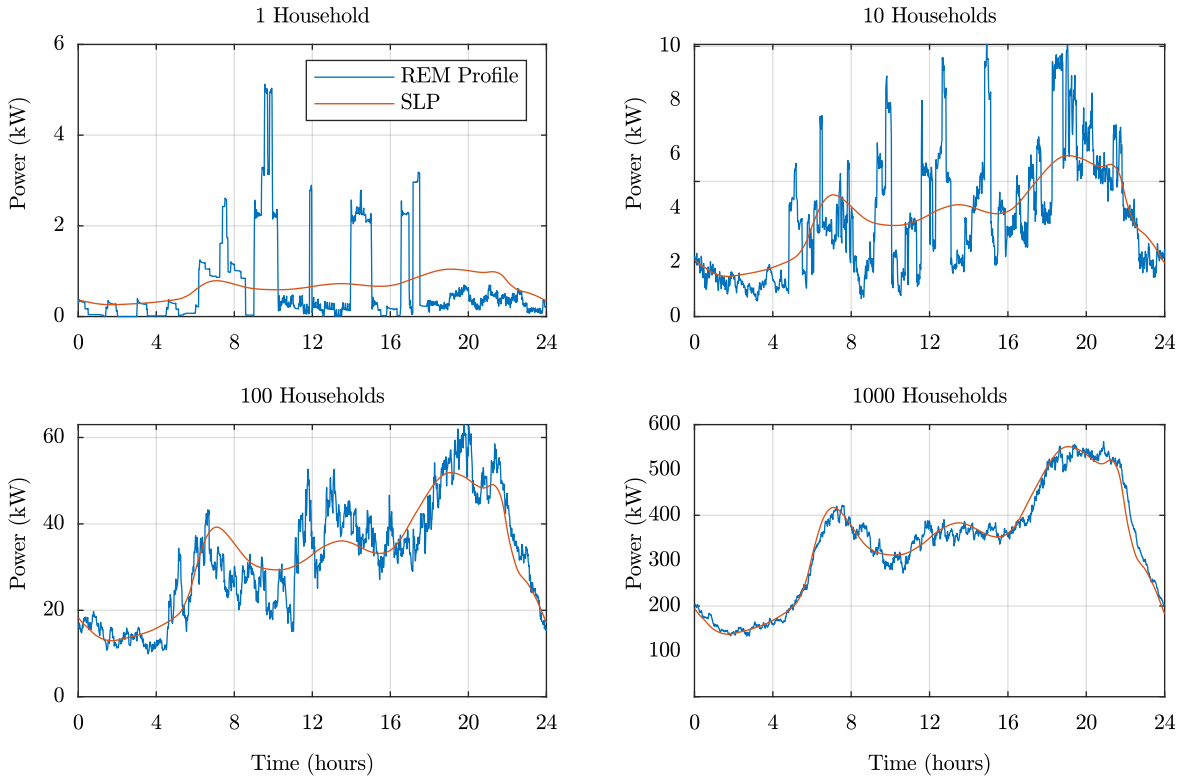

Figure 3.11: *Variation of the aggregate load with increasing number of households. Simulation time resolution is one minute, using the SLP for the second of January 2018 in Ulm, Bavaria*

The added value of the REM increases with the degree of spatial detail required, as shown in Figure 3.11. As expected, the more households are in the synthetic population, the closer the aggregate load profile resembles the SLP. For many energy studies, the load profile is calculated by scaling the SLP to the total energy consumption. Figure 3.11 clearly shows that this is not an accurate representation of aggregate load, for less than 100 households.

The other major added value is that of a higher time resolution. Figure 3.12 shows what an example load profiles looks with some commonly used time resolutions. From 1 second to 1 minute, there is not much difference in overall shape, because events that last less than 1 minute are uncommon and therefore infrequently modelled in the REM. These would be activity based loads or miscellaneous loads where the event duration is modelled by a distribution, with a small probability that the selected duration is less than one minute. The two main causes of the difference between 1 second and 1 minute can be identified firstly as the difference in the measured waveforms of the cyclical loads, like the fridge and the dryer, and secondly in the added noise signals to loads like the television.

From 1 minute to 15 minutes, the difference is also minor, and the curves remain roughly the same. However, there are some peaks that are missed out, and the noise signals are completely

gone. This may not be a big issue if the main concern is energy, but for use cases where power is the main issue, it might be more relevant. A significant loss of information occurs when reducing the time resolution to 1 hour, the peaks and shapes of the high resolution load profile are no longer clear. This is to be expected, as the duration of many household loads is less than an hour, so it is difficult to get an accurate representation of loads at this time resolution.

The outlook for 100 households is much better. Because of the diversity, even the profiles at high time resolutions are much smoother than for 1 household de to two main reasons. Firstly the probability for peaks is much smaller as there are more loads that will distribute themselves evenly. Secondly, noise is a much smaller percentage of the total load. Still it is clear that there is still significant loss of accuracy with the hourly profiles.

Based on Figures 3.11 and 3.12 it is clear that the lower the sample size, the more added value there is by having a lot of detail. A discussion on the appropriate time resolution for storage planning studies is included in chapter 5.6.

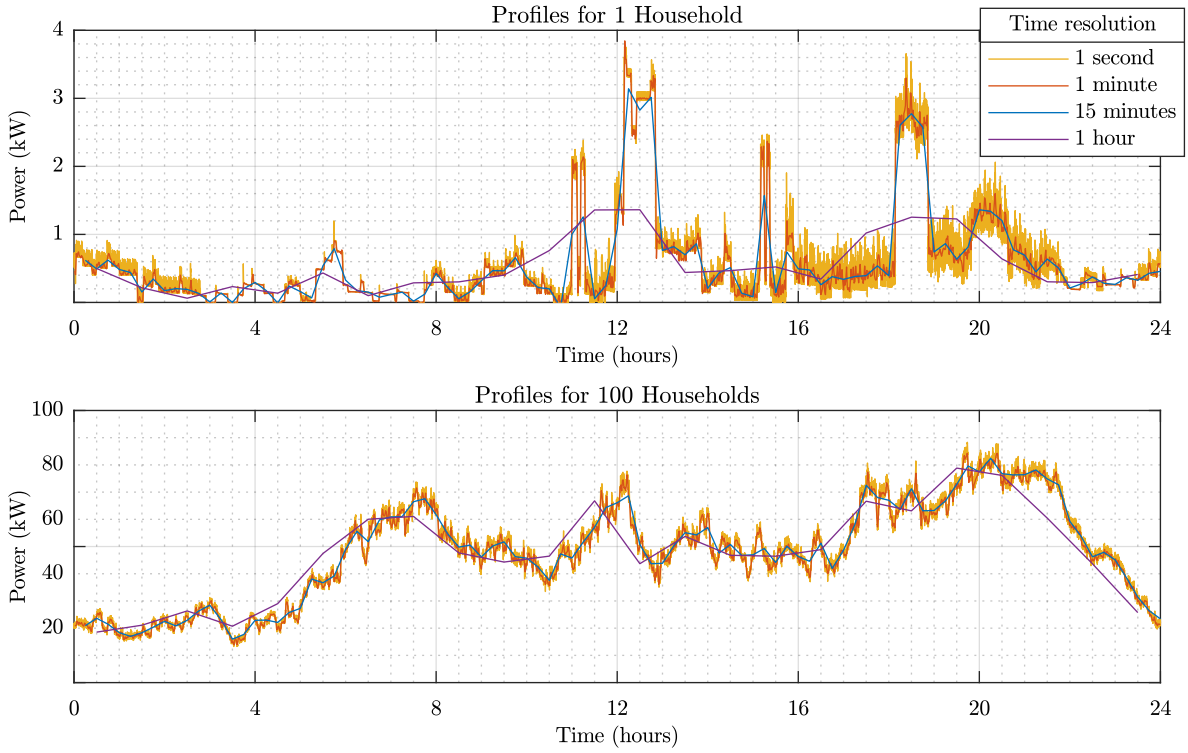

Figure 3.12: *Profiles displayed with different time resolutions*

3.5 Validation

Although the REM incorporates a lot of data from various sources to add details, there are still certain underlying assumptions and estimations within the process of creating load profiles. It is therefore important to assess if the simulated profiles are representative of real household loads. For this reason, an extensive validation is carried out to determine the strengths and weaknesses of the REM in two stages. Firstly, in Section 3.5.1 the validation of the active power load profiles for individual households is considered. Various statistical properties of a measured set of household loads are compared to a comparable set of REM profiles to show that the REM has similar properties. Secondly, in 3.5.2, an assessment takes place of the annual aggregate profiles for the entire population by examining the spread of annual loads that the REM produces, the consistency of SLP matching throughout the year, and the average power factor.

3.5.1 Individual Profiles

The data used for validation is based on the Household Electricity Survey (UK HES) [116], a project that collected a large amount of smart meter data. The survey includes a data set of electricity demand profiles of 235 households measured in two minute intervals for a month, giving 4060 daily profiles.

To simulate a set of profiles that can be compared to the HES, a set of 4060 profiles is generated by the REM using the population statistics of Munich with a time resolution of one minute. The profiles are then down-sampled to create profiles with a two minute resolution. Since the annual load used in Munich is very high compared to the annual load of the HES profiles, the daily load of the 4060 profiles are set to match that of the total HES so that the statistical properties can be compared more fairly.

Minute to Minute Volatility
One of the main objectives of the REM is to emulate the spikiness of real household load profiles. One way to judge if this is successful is by comparing the volatility of the HES profiles to that of the REM. Volatility in this case refers to the magnitude of the difference in power from one minute to the next.

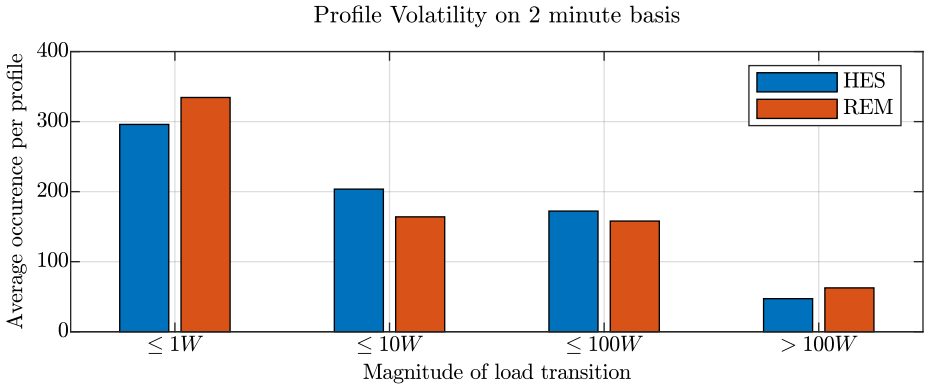

Figure 3.13: *Volatility comparison of the REM simulated profiles to the measured profiles of the HES*

A daily profile in a two minute time resolution has 720 samples, and the volatility is assessed by measuring the absolute difference between each sample and the next consecutive sample, referred

to as load transition. This can be expressed as: load transition $= |P(k+1) - P(k)| \forall k = 1...719$, where $P(k)$ is the load in W. Volatility can be compared by calculating all load transitions for each profile in the HES and the REM profiles, and counting if they fall within similar ranges. The results are plotted in Figure 3.13. It shows that the REM profiles are statistically very similar to the measured profiles. Load transitions less than 1 W are likely to be a result of noise, which is added to the TV loads, or the smaller variations from the measured profiles shown in Figure 3.8. The largest proportion of transitions are less than 1 W, and they are very accurately represented by the REM profiles.

Load transitions between 1 W and 10 W are likely to be caused by the variations in the measured cycle profiles, along with some of the smaller loads randomly generated for miscellaneous and office loads. These are slightly underestimated by the REM, which may indicate that more of the miscellaneous loads are smaller. Load changes between 10 W and 100 W are caused by some of the activity loads (TV and Desktop), all the lighting loads and some of the base and turn-on loads. This range is also well represented by the REM.

Larger load transitions of more than 100 W are slightly overestimated by the REM, indicating that there may be more large devices in the synthetic population of the REM than in the HES households. Overall the REM profiles have a satisfactory volatility.

Spread of Load Magnitudes

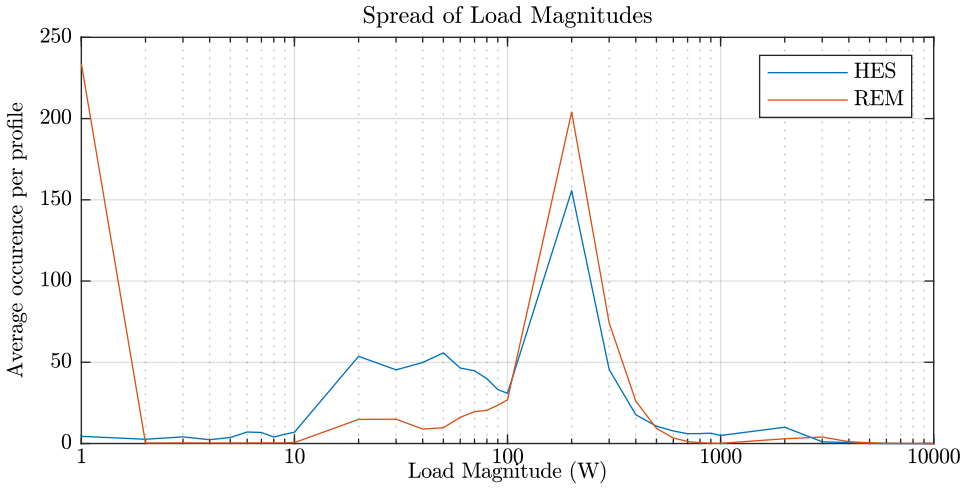

Figure 3.14: *Comparison of the spread of load magnitudes of measured data versus simulated REM profiles*

The conclusions reached by examining the volatility are confirmed by further investigating spread of load magnitudes, as shown in Figure 3.14. There are a number of conclusions to be drawn from this plot. Firstly, the REM has a large count of loads that are less than 1 W. Upon closer investigation many of these values are zero, indicating a lack of base and standby loads. The REM does not include devices such as routers, night lights, and standby power of devices that are plugged in. The REM is a heavily event based model, and thereby these constant loads are neglected. Since the loads in question are very small, this is not an important issue for most applications.

Secondly, it is clear that loads between 10 W and 100 W are under-represented, which could

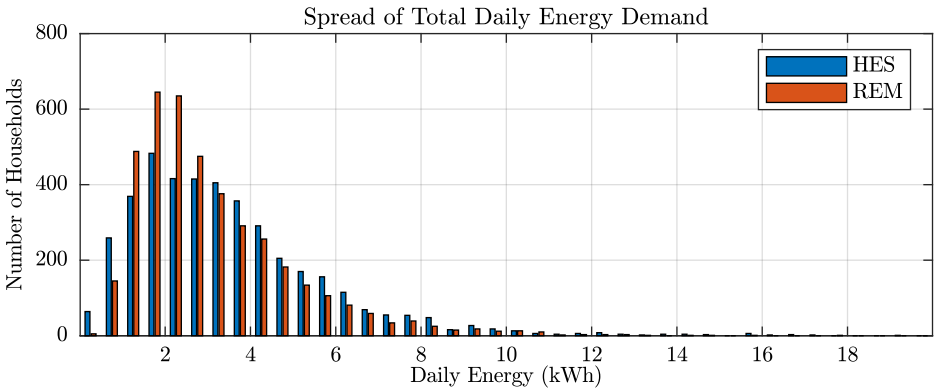

Figure 3.15: *Comparison of the spread of the total daily energy demand of the HES versus the simulated REM profiles*

indicate that the magnitudes assigned in the REM are too large, or that loads in the UK have smaller magnitudes. There is insufficient information to appropriately modify the REM. Despite the under-representation of smaller loads, the peak of loads that are 100 W - 200 W are very well represented. Since larger loads are more important for model accuracy, it is judged that the REM provides sufficiently representative load magnitudes for households.

Spread of total daily energy demand

Besides the power demand, it is important that the variation of total daily energy consumption between households is also accurately represented. Figure 3.15 shows that the spread of daily energy demand of the REM profiles is comparable to that of the real profiles. The spread of the HES profiles is a little wider, as it also includes certain anomaly cases, for example households with zero measured load. This will not be included in the REM profiles.

After Diversity Maximum Demand

An accurate representation of the After Diversity Maximum Demand (ADMD) is important for load profiles as it represents how peak demand drops as more profiles are aggregated. ADMD is calculated as the maximum demand, per customer, as the number of customers connected to the network approaches infinity. Figure 3.16 shows the calculated ADMD for the REM data versus the HES.

To calculate the ADMD of a series of profiles the procedure is as follows. The first value is calculated by choosing 600 random profiles, identifying the maximum power and then calculating the average maximum demand. The next value is calculated by randomly choosing 600 combinations of 2 profiles, and identifying the maximum demand of the sum of the two profiles divided by two. For this comparison this is performed upto the sum of 300 profiles, i.e. 600 random combinations of 300 profiles are chosen and their average maximum demand calculated.

The average maximum demand is shown in Figure 3.16 (a). The shapes of the curves are very similar, with a slight mismatch at higher number of profiles. This results from the fact that the aggregate profile has a higher maximum demand compared to the REM profiles, since the SLP used does not match the HES aggregate. This is not a reflection on the REMs ability to represent ADMD.

Part (b) shows the range of maximum demands from the 600 combinations of profiles chosen

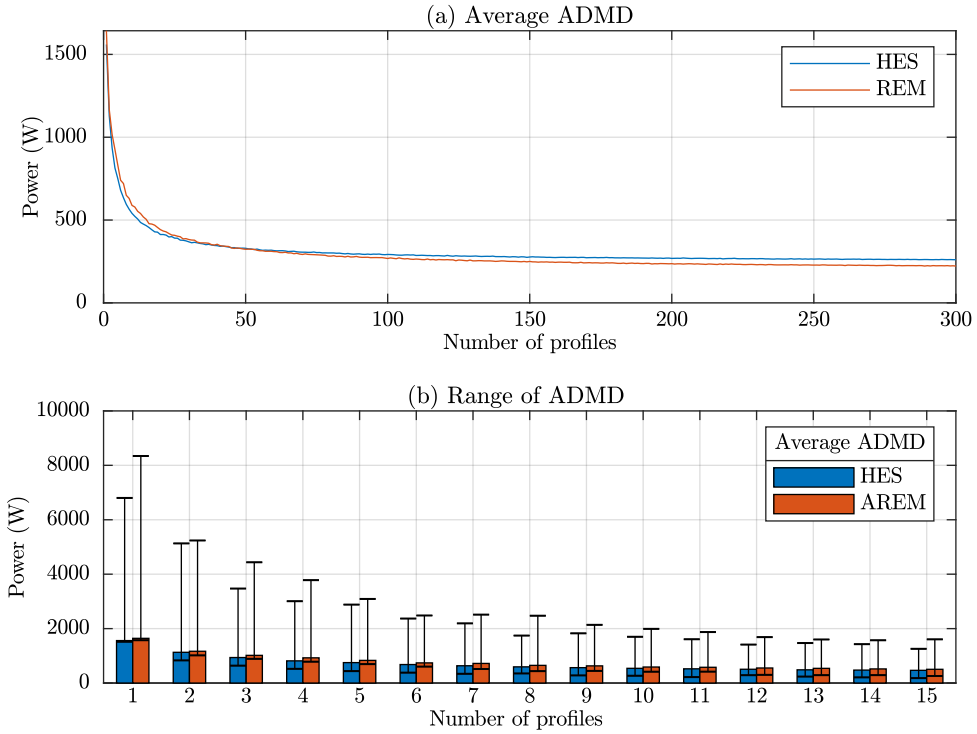

Figure 3.16: *(a) Shows the average ADMD for the measured data and the simulated data for 1 to 300 profiles, using 600 combinations for each data point. (b) Shows the range of ADMD for 1 to 15 households, highlighting the lowest and highest values for ADMD out of the 600 combinations*

for 1 to 15 profiles. The REM has a slightly larger range, which is to be expected since it has already been shown that the REM has more large loads than the HES. For this reason, it is not unexpected that for fewer profiles the maxima are a little higher. It does however still reflect the trend very well as it reduces the variation at a very similar rate.

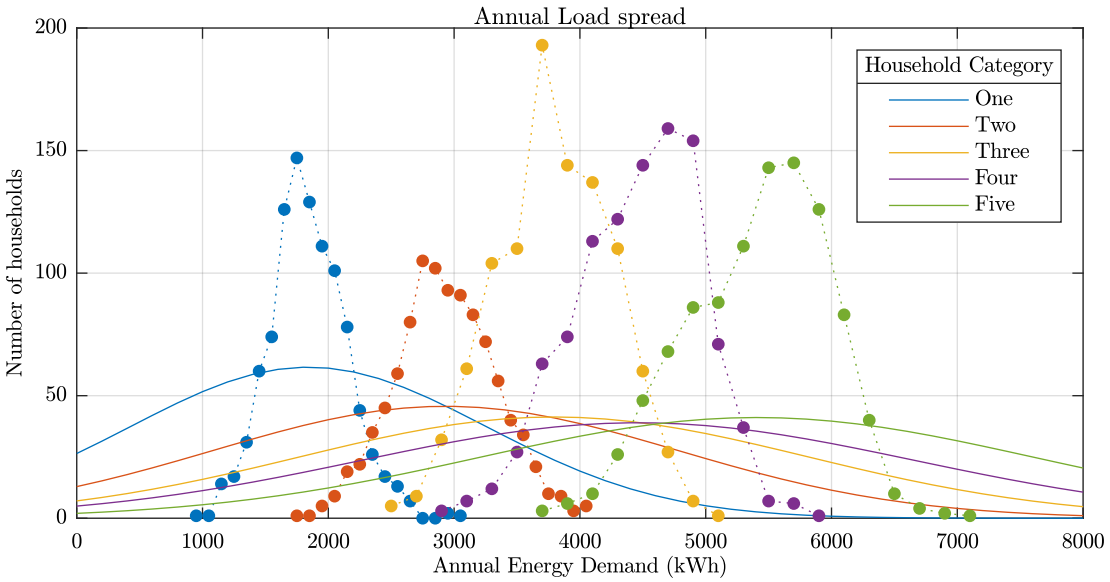

Figure 3.17: *Spread of annual loads using an annual simulation of 1000 households per category. The dotted lines are indicative of the trend of the REM annual loads, and the solid lines display a normal distribution with the mean used from the REM and the standard deviation from [4]*

.

3.5.2 Aggregate profiles

Besides the statistical properties of the individual profiles, it is also necessary to compare the aggregate profile to assess if large populations can be accurately modelled using the REM. For this assessment a large REM simulation was carried out, generating load profiles for 1000 households of each household category, i.e. 5000 households altogether, for an entire year. The standard load profile for Ulm for 2018 is used, and the annual load values stated in Table 3.1.

Variation of Annual loads

One of the major contributions of this model is combining the top down and bottom up approach, so that unlike bottom up models each profile is not worked to achieve the average annual load. This means that there is some variation within the population of each category. It is difficult to find realistic data to compare the spread of annual load amongst households. The data used, is a study published in 2015 [4] involving an analysis of the annual load of 2100 households in Germany using data measured in 2012. This study does not separately consider the HC of 5 person households, as all households with more than four people were categorised together. The data is therefore a little outdated and mismatched. Most importantly, the average annual load does not match the one used in the profiles. It is still useful however, to compare the REM to generate some insight.

Figure 3.17 shows the spread of annual loads of the 5000 simulated REM profiles, alongside the solid lines which display a probability distribution using the standard deviations deduced in [4]. Clearly the real loads have much more variation than the REM profiles. This is interesting as the daily variation matched the measured data of the HES very well as shown in Figure 3.15. The reason the REM does not represent the spread of annual loads as accurately as daily loads, is that the low consumption behaviour of one day is not carried on to the next. This is because when event based loads are distributed amongst the eligible households they are assigned with equal probabilities. This means that there is no distinguishing between high consumption and

low consumption households which exists in reality. The same goes for appliances, they are distributed with even probability. In reality the case is much more likely to be dependent on factors such as income or dwelling size, as wealthier households will have more appliances and higher annual loads. As mentioned in the introduction, it is not reasonable to model income and other factors that affect loads as it is difficult to obtain data to deduce the relationships between the factors.

The lack of diversity in total loads of the profiles is a drawback of the REM, that needs to be considered when using the profiles for studies. There are two possible solutions that have been employed so far depending on the setting. The first setting occurs when the study is for a real neighbourhood or district, and the annual loads of each household is known, possibly including the number of occupants. In this case an extremely large number of profiles are simulated, and a selection is made based on the profiles with the closest annual load to that of the real household. This is a good solution that will result in realistic profiles, the only drawback being the extra simulation time required for such a large synthetic population.

The second setting occurs if the required annual loads are unknown. In this case a realistic selection of annual loads can be generated using the statistics from [4]. Then the same procedure can be followed and a realistic selection of profiles can be made. It does however depend on the nature of the study, as in some cases it may not be important if the diversity is accurately modelled and the REM can be used without generating extra profiles.

Matching the SLP

One of the main features of the REM is the use of the SLP to ensure that aggregate loads are accurate. Based on the data used to create the REM, the only seasonal differences are the total daily energy, based on the SLP, and the shift in the lighting load. Behavioural changes due to changing occupancy or changes in the proportions of the load categories are not reflected. Another aspect of the aggregate profiles, is the consistency of the ability of the REM to match the SLP. The annual profiles of 1000 households per HC are compared to the SLP, to see if household size or seasonality affects the results. To illustrate the results the 2-norm of the difference between the simulated profiles is plotted for each day of the year in figure 3.18 (a).

There are three conclusions to be drawn from Figure 3.18(a). Firstly, if the total daily load is factored out by division, there is a slight seasonal variation. There is a much higher total daily load in the colder months compared to the summer months. When this is accounted for, the summer months are matched a little better than the winter months. Secondly, the HC has a minimal effect on the ability of the REM to match the SLP.

The third point is that there are some very regular peaks, and upon closer examination this stems from the weekly variations in the shape of the SLP. The REM is able to match weekdays a little better than weekends, Sundays being particularly difficult. This is to be expected as the TUS is used to determine activity loads, which factor heavily in the daily peaks. Two thirds of the profiles were weekday profiles, and it was considered to build different probability distributions for the weekends. This path was not taken however, since it would have made some of the sample of diary entries very small. It was judged to be more important to distinguish between household sizes, than between weekdays and weekends. Furthermore Figure 3.18 also shows the profiles of the best and worst matches to the REM, and even the worst match is still considered acceptably accurate. Overall ability of aggregate REM profiles to match the SLP is evaluated to

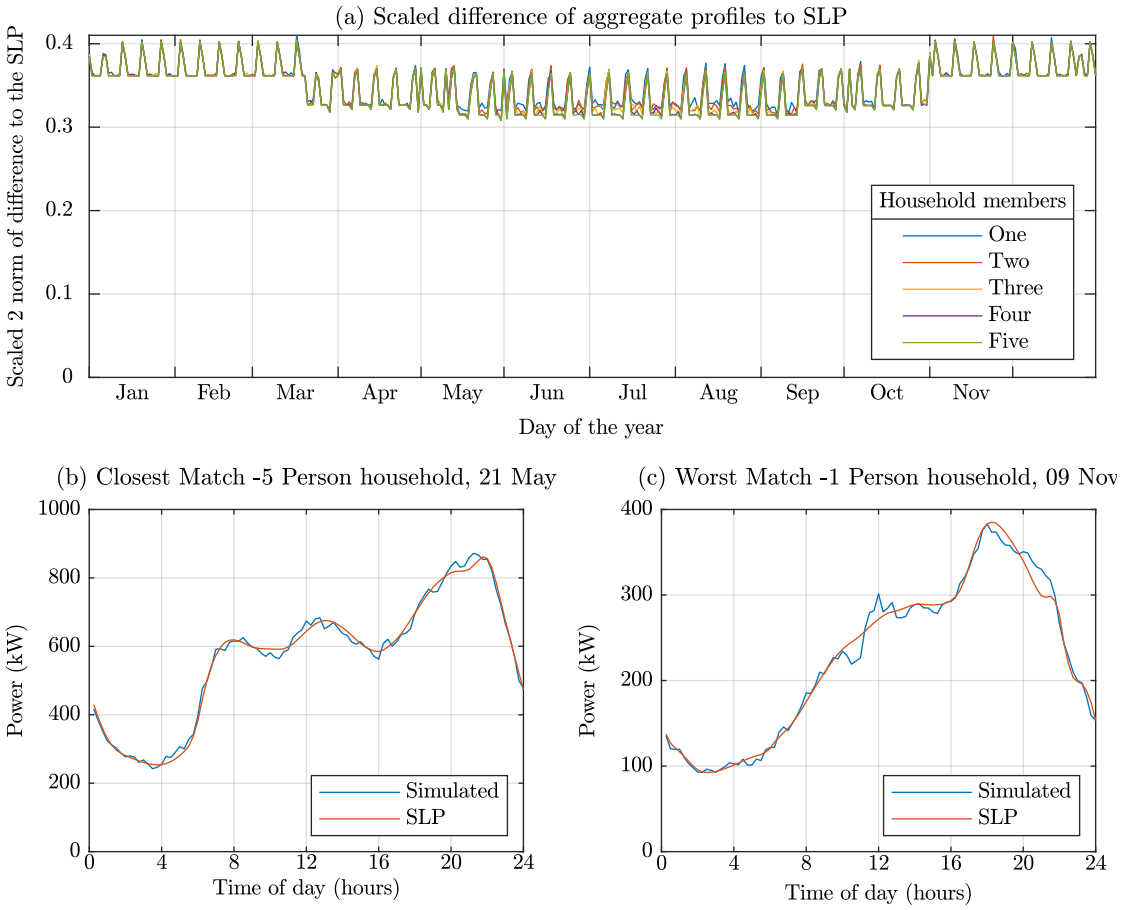

Figure 3.18: *(a) Plot of the difference between the aggregate REM profiles for 1000 households of each category and the corresponding SLP for each day of the year. (b) the aggregate profile for the best match, five household members on the 1st of Jan. (c) the worst case aggregate profile, five household members on the 1st of Jan.*

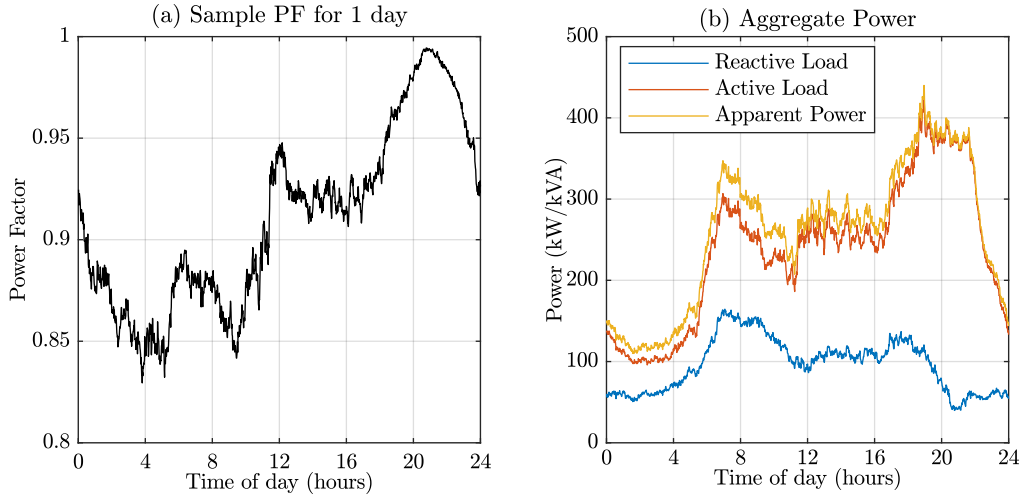

Figure 3.19: *Power factor and power values for an aggregate load of 1000 households for 1 day*

be sufficient.

Power Factor

There is not much data available to determine the average power factor of residential load profiles. However commonly used power factors are between 0.9 and 0.95. The REM profiles tend to average around 0.91, which is within the normal range. For studies involving power networks the most important thing is that the apparent power is not significantly increased, to remain within the line power limits. As shown in Figure 3.19 (a), the power factor is higher in the night and early morning as the proportion of cooling devices is higher. This is good because at the times where the active power is high, the power factor is also very good and so the overall apparent power is not increased much due to the reactive load.

Chapter 4

Annual Optimal Storage Planning

In this thesis, optimal storage planning refers to the identification of cost optimal storage capacity of batteries at each node in a distribution network. The following chapter documents how the planning problem is formulated as one of the optimisation problems defined in section 2.1. All the relevant system elements are formulated as linear equations, and a solver is used to calculate the optimal solution.

To formulate the optimisation problem it is necessary to identify which of the battery applications described in section 2.2 is included. As mentioned in section 2.2, this study takes place at the distribution level, therefore the battery storage is used for grid support and 'Behind The Meter' (BTM) applications. BTM in this context involves using battery storage to absorb energy during times of excess generation, and release the energy at times of excess load. The financial motivation for this load shifting is to reduce the cost of energy consumption, as the Feed in Tariff (FiT) is lower than the energy price. The grid support function of the storage is not modelled with financial incentives, but is included with the use of constraints. The system is constrained to make sure that line power and node voltage remain within an acceptable range.

The barrier for battery storage in these applications has primarily been high battery costs. Currently batteries are still a relatively expensive component, and therefore developing a methodology for optimal planning of energy storage is a focus of this work.

Within this chapter an annual optimal planning algorithm that simultaneously determines optimal battery sizes and locations within the network is developed and demonstrated. A linearised distribution grid model is included in the optimisation problem in the form of constraints. The planning algorithm implements a 'welfare optimisation', meaning it identifies the most economical solution for the entire network, neglecting any conflict of interest that may exist between different stakeholders and operators. The algorithm uses a simple objective function based on energy price, FiT, and storage cost that sums total costs for the network.

The structure of this section is as follows; in section 4.1 a literature survey is carried out outlining planning algorithms that have been published within the body of academic work. Section 4.2 outlines how the planning algorithm is formulated as an optimisation problem, using both a discrete model for storage sizes and a continuous model. The planning algorithm includes both the grid model presented in section 2.4.1, and the battery model in section 2.3.

To demonstrate the planning algorithm and evaluate the accuracy of the linearisation method, the algorithm is applied to case studies. Case Study 1, presented in section 4.3, uses a synthetic grid developed by Lindner in [5]. The results for optimal storage using six different price scenarios are compared, and their grid improvements in terms of self sufficiency and network losses

are examined. An investigation is performed to determine if the storage is mainly sized to shift energy between days or within a daily cycle.

4.1 Literature Survey

Previous academic work on planning algorithms for storage units in an electrical network differ in terms of the level of detail of the grid model, the battery model, as well as the size of network to which they are applied. Methods that use very complex grid and battery models tend to be unsuitable for use on larger systems due to high computational demand, whereas highly simplified models may not capture the important dynamics relevant for storage planning. A tradeoff is required between computational demand, and system complexity.

As shown in section 2.4.1, the full AC power flow equations are non-linear, and therefore a linear approximation is used for most planning algorithms. The algorithms in [117–119] use the DC approximation which neglects network voltages and line losses. It is shown in this thesis that this is unsuitable for use in distribution networks with voltage issues as they are crucial in storage planning. Other works such as [120, 121] use second order cone approximations which are much more computationally intensive compared to the approximation in this work. Second order cone programming is also applied to larger systems in [122], using Benders decomposition to reduce the problem size by dividing it into subproblems. A drawback of this approach is that it is only suitable for radial operation, which is enforced by the problem constraints. A power flow method called forward-backward sweep was used for storage planning in [2]. This approximation is also only suitable for radial networks, and is only applied to very small grids in the paper.

Besides algorithms designed purely for storage planning, there has been research into grid planning for multiple technologies, particularly for microgrids where autarchy is important. In [123] a Mixed Integer Linear Program (MILP) is used to choose optimal sizes of various technologies in a microgrid. The model used is highly detailed and includes both heating and cooling, using the grid model from [124] that provides good approximations of voltages and complex currents. However the algorithm is highly computationally intensive and is only applied to a 5 node system. Similarly in [125] a mixed integer program is used to size storage units in a microgrid, but is applied to only a six bus system.

A rather detailed battery model is used in [126], although the non linear model is not suitable for use in large optimisation problems. The presented sizing methodology does not include the distribution network at all, but rather focuses on a single grid-connected load and generation point. Similarly [127] focuses on a single PV and load point, and although an optimisation is used this comes at the cost of a highly simplified battery model.

A more full grid representation is used in [128]. In this study the sizing methodology does not involve optimisation, instead an iterative approach is taken where many scenarios are calculated through to choose the best one. This is an adequate methodology for the 14 bus case study that is used, but for larger networks it is not a reasonable method.

A more sophisticated approach may involve the use of a genetic algorithm such as in [129], where the focus is on using storage to manage grid imbalances. The methodology uses two steps, firstly a case reduction to identify some reasonable operating ranges, and secondly a genetic algorithm to select the best option. The difficulty in this method is in assessing the optimality. The same

is true for the heuristic approach proposed by [130], where energy storage is used to alleviate grid issues in both the distribution grid and transmission grid. The main purpose is ensuring grid stability, and neural networks are used to predict the system voltages. Optimal locations are found by identifying the sensitive busses in the network.

The linear models for batteries and distribution grids used in this thesis are presented in Chapter 2. The grid model is simple enough to use in an annual optimisation problem for a 16 node grid, and complex enough to give a good representation of the bus angles and voltages. The discrete-time KiBaM battery model is complex enough to characterise the most important battery dynamics, whilst still being simple enough to include in an annual simulation.

4.2 Planning Algorithm as an Optimisation Problem

The planning algorithm contains all the network and technical constraints of the system within an optimisation problem. In the following pages, the formulation of the optimal storage planning problem including a Multi Period Optimal Power Flow (MPOPF) is detailed.

The planning algorithm is formulated as one of the programming problems described in Section 2.1. It is necessary to formulate all system dynamics as linear constraints, including the power flow equations, using the linearisation in section 2.4.2, as well as the linearised storage equations. The choice between linear and quadratic cost function depends on the line loss model, and it will be shown that the quadratic cost function is most useful. Integer variables can be used to provide more accurate cost models of batteries, although this results in a much more computationally demanding problem.

4.2.1 Linearised Multi Period Optimal Power Flow

The PF and OPF provide a snapshot of the network status. For the sizing problem it is necessary to optimise the behaviour over a period of time, therefore a Multi Period OPF (MPOPF) is required. The length of the simulation is sampled with an appropriate time step, and in an MPOPF all the time instances are modelled simultaneously. This ensures that all the constraints in equations 2.27, 2.28, 2.31 are maintained at every sample in the simulation. For the results in this chapter a simulation duration of 1 year and a 15 minute time resolution is used, i.e. $\Delta t = 0.25$h. This means the total number of samples in the simulation is $4 \times 24 \times 365 = 35040$. Profiles corresponding to this time duration are required for the inputs: active load, reactive load and PV generation per node. In chapter 5.6, the impact of the chosen time resolution is examined, and three different time resolutions are compared.

For multi-period problems, the notation is as follows. The time instance reference of variables is given in the brackets following the variable. The time instance is typically referred to as k, where $k = 1$ is the first instance of the series. Sometimes initial conditions of variables are required, and these are referred to as the values at time $k = 0$. The total number of time instances, also referred to as samples, in the simulation is N, which equals 35040 for an annual simulation. The total duration of time included within the simulation is $N\Delta t$. To simplify the notation, the reference to the busses is removed and the variables refer to the stacked versions as shown in 4.1.

$$\theta(k) = \begin{bmatrix} \theta_1(k) \\ \vdots \\ \theta_{n_{bus}}(k) \end{bmatrix} \quad V(k) = \begin{bmatrix} V_1(k) \\ \vdots \\ V_{n_{bus}}(k) \end{bmatrix} \quad P_{gen}(k) = \begin{bmatrix} P_{gen,1}(k) \\ \vdots \\ P_{gen,n_g}(k) \end{bmatrix} \quad Q_{gen}(k) = \begin{bmatrix} Q_{gen,1}(k) \\ \vdots \\ Q_{gen,n_g}(k) \end{bmatrix} \tag{4.1}$$

The branch flows in a system at time instance k are summarized in the vector $P_l(k)$, where the lines in the system are numbered from 1 to n_{br}. Note that the numbering does not relate to the connecting nodes, instead the branches are numbered independently. When multiplying by the variables in Equation 4.1, the connectivity matrices $C_f \in \mathbb{R}^{n_{br} \times n_{bus}}$ and $C_t \in \mathbb{R}^{n_{br} \times n_{bus}}$ are defined, which indicate the branches that connect from and to the busses. For calculating the branch flow in terms of bus properties θ and V, the connectivity matrices are multiplied by a diagonal of the branch conductance and admittance, as shown in equations 4.2 and 4.3. For ease of notation the matrices are summarized as matrices of conductance G_l and the admittance B_l.

$$\begin{aligned} P_l(k) = \begin{bmatrix} P_{l_1}(k) \\ \vdots \\ P_{l_{n_{br}}}(k) \end{bmatrix} &= -\underbrace{\begin{bmatrix} b_{l_1} & \cdots & 0 \\ \vdots & \ddots & \vdots \\ 0 & \cdots & b_{l_{n_{br}}} \end{bmatrix}}_{B_l} (C_f - C_t)\,\theta(k) + \underbrace{\begin{bmatrix} g_{l_1} & \cdots & 0 \\ \vdots & \ddots & \vdots \\ 0 & \cdots & g_{l_{n_{br}}} \end{bmatrix}}_{G_l} (C_f - C_t)\,V(k) \\ &= -B_l\theta(k) + G_l V(k) \qquad \forall k = 1...N \end{aligned} \tag{4.2}$$

$$\begin{aligned} Q_l(k) = \begin{bmatrix} Q_{l_1}(k) \\ \vdots \\ Q_{l_{n_{br}}}(k) \end{bmatrix} &= -\begin{bmatrix} g_{l_1} & \cdots & 0 \\ \vdots & \ddots & \vdots \\ 0 & \cdots & g_{l_{n_{br}}} \end{bmatrix} (C_f - C_t)\theta(k) - \begin{bmatrix} b_{l_1} & \cdots & 0 \\ \vdots & \ddots & \vdots \\ 0 & \cdots & b_{l_{n_{br}}} \end{bmatrix} (C_f - C_t)V^k \\ &= -G_l\theta(k) - B_l V(k) \qquad \forall k = 1...N \end{aligned} \tag{4.3}$$

An expression for the bus injection, equal to the net power flow in all lines connected to a given bus is defined using the injection matrix $C_{inj} \in \mathbb{R}^{n_{bus} \times n_{br}}$ as shown in equations 4.4 and 4.5.

$$P_{inj}(k) = \underbrace{(C_f - C_t)'}_{C_{inj}}(P_l(k)) = -C_{inj}B_l\theta(k) + C_{inj}G_l V(k) \qquad \forall k = 1...N \tag{4.4}$$

$$Q_{inj}(k) = \underbrace{(C_f - C_t)'}_{C_{inj}}(Q_l(k)) = -C_{inj}G_l\theta(k) - C_{inj}B_l V(k) \qquad \forall k = 1...N \tag{4.5}$$

The nodal balance equations can be similarly stacked using the equations 2.27 and 2.28, and adding any other controllable components $P_X(k)$, which could refer to storage, PV or any other component. The connectivity matrix $C_g \in \mathbb{R}^{n_{bus} \times n_g}$ is used to connect generators to their respective busses. The same applies to any other controllable component X, where the connectivity matrix is $C_X \in \mathbb{R}^{n_{bus} \times n_X}$.

$$P_{inj}(k) - C_g P_{gen}(k) + P_{load}(k) + C_X P_X(k) = 0 \qquad \forall k = 1...N \tag{4.6}$$

$$Q_{inj}(k) - C_g Q_{gen}(k) + Q_{load}(k) + C_X Q_X(k) = 0 \qquad \forall k = 1...N \tag{4.7}$$

4.2.2 Branch Limits

The branch limits are determined by the size of installed cable or overhead line, and is a limit on the magnitude of the apparent power in a line. In a branch connecting nodes k and m, the magnitude of apparent power $|S_{km}|$ is given in Equation 4.8.

$$|S_{km}| = \sqrt{|P_{km}|^2 + |Q_{km}|^2} \tag{4.8}$$

Since the $|S_{km}|^2$ is a quadratic function of the active and reactive power flow in a line, it would require quadratic constraints to model correctly. Solving large problems with quadratic constraints is very difficult, therefore in this case it makes more sense to utilise a hyperplane approximation of $|P_{km}|^2$ and $|Q_{km}|^2$. Figure 4.1 shows the hyperplanes used to approximate both the squares of active and reactive power in every line, depending on the respective line limit $\overline{S_{km}}$.

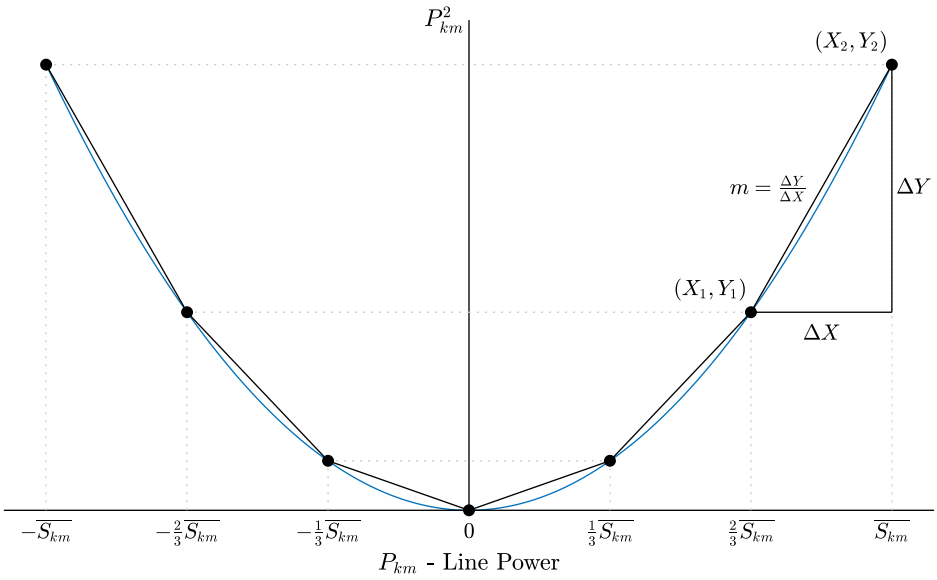

Figure 4.1: *Linear approximation of a quadratic function using 7 points in the full power range*

Note that the hyperplanes are also above the actual values, so the approximation is conservative. The formula for a hyperplane between points X_1, Y_1 and X_2, Y_2 is given in Equation 4.9.

$$\begin{aligned} y &= \frac{Y_2 - Y_1}{X_2 - X_1}(x - X_1) + Y_1 = m(x - X_1) + Y_1 \\ y &= \underbrace{m}_{\text{gradient}} x + \underbrace{Y_1 - mX_1}_{y \text{ intercept}} \end{aligned} \tag{4.9}$$

The approximation for $y = x^2$ based on the six hyperplanes with the gradients $m_1 - m_6$ and y intercepts $y_1^{int} - y_6^{int}$ can be given by the equation:

$$x^2 \approx y = max(m_p x + y_p^{int}) \qquad \forall p \in 1...6 \tag{4.10}$$

The constraint implementation is made a little easier because it is not necessary to find an explicit expression for the approximation of $|P_{km}|^2$. It is only necessary to constrain the apparent power, and this can be achieved with a few inequality constraints per line. For every line, seven points are selected equally spaced within the power limit as shown in Figure 4.1. This results in six hyperplanes to enforce the power limit. The line power limits are given by the vector $\overline{S_l} = [\overline{S_{l_1}}, ..., \overline{S_{l_{n_{br}}}}]^T$. To implement the hyperplane method, two vectors are calculated: $M_{1-6} \in \mathbb{R}^{n_{br} \times 1}$, and $Y_{1-6} \in \mathbb{R}^{n_{br} \times 1}$, which give the gradients and Y intercepts for the hyperplanes of each of the branch powers. The approximated square power flows are calculated with the equation 4.11.

$$\begin{aligned} P_{\overline{sq}}(k) &\geq M_p \odot P_l(k) + Y_p \quad \forall p = 1:6 \\ Q_{\overline{sq}}(k) &\geq M_p \odot Q_l(k) + Y_p \quad \forall p = 1:6 \end{aligned} \tag{4.11}$$

The symbol $\odot$ refers to element-wise multiplication. The variables $P_{\overline{sq}}$ and $Q_{\overline{sq}}$ are always greater than the actual squared active and reactive power, therefore the sum of these can be used to enforce the apparent power limit. The element wise squared line power limit can then be applied to ensure that the line limits are maintained.

$$P_{\overline{sq}}(k) + Q_{\overline{sq}}(k) \leq \overline{S_l} \odot \overline{S_l} \tag{4.12}$$

This method does require significant computation because it involves multiple constraints per branch per time instance (4.11, 4.12), and therefore it makes sense to implement the approximation only to the lines that have overcurrent issues. The application and outcome will be shown in section 5.5.2, where an active apparent power constraint is demonstrated.

4.2.3 Losses

The full expression for active line losses is given by Equation 2.26, showing that losses are proportional to the squared real and reactive power flow through a line. Using the same voltage approximation ($V_m \approx 1$), the line losses can be approximated to Equation 4.13. There are two methods for including losses, depending on whether it is suitable to use a quadratic program (QP) or not. A QP has linear constraints and a quadratic cost function, therefore the losses can be minimised in the cost function using the Equation 4.13 without requiring the calculation of losses using the constraints.

$$P_{km}^{loss} \approx (P_{km}^2 + Q_{km}^2) r_{km} \tag{4.13}$$

The second option is to use a linear program (LP) and use hyperplane approximations for each of the line losses, and minimise them. For the sizing problem it has been experimentally determined that using a QP is faster than the LP, because of the large number of constraints required to implement the hyperplane approximation.

4.2.4 Storage Model

Storage is added using the KiBaM model outlined in Section 2.3, including the discretised dynamic model and the degradation map. The vector $P_{st}(k)$ includes the storage power for every candidate node in the system similar to the variables in Equation 4.1. The storage power is separated into the charging $P_{ch}(k)$ and discharging $P_{dis}(k)$ components, as in Equation 4.14, and the limits in Equation 4.15 are enforced.

$$P_{st}(k) = P_{ch}(k) + P_{dis}(k) \qquad \forall k = 1...N \tag{4.14}$$

$$\begin{bmatrix} 0 \\ P_{st} \end{bmatrix} \leq \begin{bmatrix} P_{ch}(k) \\ P_{dis}(k) \end{bmatrix} \leq \begin{bmatrix} \overline{P_{st}} \\ 0 \end{bmatrix} \qquad \forall k = 1...N \tag{4.15}$$

Since there are two variables for each storage unit, they are stacked first per unit, and then for each unit in the network, as shown in 4.16 where n_{st} refers to the number of candidate storage nodes in the network.

$$x_{st}(k) = \begin{bmatrix} x_{E1,1}(k) \\ x_{E2,1}(k) \\ \vdots \\ x_{E1,n_{st}}(k) \\ x_{E2,n_{st}}(k) \end{bmatrix} \tag{4.16}$$

The size of the vector is $x_{st}(k) \in \mathbb{R}^{2n_{st}\times 1}$, and the update is calculated based on the dynamic model in equation 2.15. The discrete charging matrix B_d, is seperated into the first and second row, referred to as $B_{d,ch}$ and $B_{d,dis}$ respectively in order to multiply with the correct variables. The full expression is given in Equation 4.17.

$$x_{st}(k+1) = \begin{bmatrix} A_d & \cdots & 0 \\ \vdots & \ddots & \vdots \\ 0 & \cdots & A_d \end{bmatrix} x_{st}(k) + \begin{bmatrix} B_{d,ch} & \cdots & 0 \\ \vdots & \ddots & \vdots \\ 0 & \cdots & B_{d,ch} \end{bmatrix} P_{ch}(k) + \begin{bmatrix} B_{d,dis} & \cdots & 0 \\ \vdots & \ddots & \vdots \\ 0 & \cdots & B_{d,dis} \end{bmatrix} P_{dis}(k) \tag{4.17}$$

The large matrices in equation 4.17 are diagonals using the same smaller matrices, and can therefore be simplified using the Kroneckor tensor product.

$$x_{st}(k+1) = \underbrace{(I^{n_{st}} \otimes A_d)}_{\mathcal{A}_d} x_{st}(k) + \underbrace{(I^{n_{st}} \otimes B_{d,ch})}_{\mathcal{B}_{d,ch}} P_{ch}(k) + \underbrace{(I^{n_{st}} \otimes B_{d,dis})}_{\mathcal{B}_{d,dis}} P_{dis}(k) \tag{4.18}$$

Storage elements are the only components in the model that link the time instances, i.e. that link step k to $k+1$. They offer the only source of flexibility in balancing generation and demand over the course of the day. The discrete time update for the SoE E_{st} is given in Equation 4.19.

$$E_{st}(k) = \underbrace{(I^{n_{st}} \otimes [1 \quad 1])}_{\mathcal{C}_d} x_{st}(k) \tag{4.19}$$

For the sizing problem, the storage capacity E_{cap} is a decision variable as well, meaning its optimal value is given by the optimal solution. Depending on the type of battery used, the manufacturer tends to give a range of the charge level that is recommended for the battery operation. Charge levels outside of this range will result in highly accelerated battery degradation, and so the constraint enforces the charge to remain within this level using the limit for depth of discharge η_{cap}. Typical values are above $\eta_{cap} = 0.8$, although for many Lithium Ion batteries the full capacity can be safely used i.e. $\eta_{cap} = 1$.

$$0 \leq E_{st}(k) \leq \eta_{cap} E_{cap} \qquad \forall k = 1...N \tag{4.20}$$

The battery degradation is also included in the planning problem using the piecewise approximation of the convex hull depicted in 2.5. By enforcing a set of limits for each plane, at every time instant as in Equation 4.21 the upper limit for degradation can be obtained. For optimisation it is necessary to work with a convex hull, as a non-convex approximation could not used with an inequality constraint.

$$E_{deg}(k) \geq \mathbf{a}_1 P_{st}(k) + \mathbf{a}_2 E_{st}(k) + \mathbf{a}_3 E_{cap} \qquad \forall \mathbf{a}_1, \mathbf{a}_2, \mathbf{a}_3 \tag{4.21}$$

The variable E_{deg} can then be used in the cost function, in order to minimise battery degradation.

Battery Size Models
Within this thesis two models for battery sizes are used, firstly a continuous model allowing any battery size with a fixed price per kWh, secondly a discrete model with distinct sizes and prices that vary per kWh. The continuous variation allows E_{cap} to take any value greater than or equal to 0, with a cost c_{st}.

$$E_{cap} \geq 0, \qquad E_{cost} = c_{st} \sum^{Nodes} E_{cap} \tag{4.22}$$

The second cost model utilizes two vectors that refer to the available battery sizes $\mathcal{S} = [\mathcal{S}_1, \ldots, \mathcal{S}_b]^T$ and their respective prices $\mathcal{P} = [\mathcal{P}_1, \ldots, \mathcal{P}_b]^T$, where b is the number of size options. An integer variable $E_{int} \in \mathbb{Z}^{n_{st} \times b}$ is introduced which gives the number of storage units of each size at each candidate storage node.

$$E_{cap} = E_{int} \times \mathcal{S}, \qquad E_{cost} = \sum^{Nodes} (E_{int} \times \mathcal{P})$$

4.2.5 Planning Algorithm Formulation

Optimisation Variables
Formulating the planning algorithm as an optimisation problem requires all the components of the LP/QP to be defined, starting with the optimisation variable x, which involves all variables that are determined by the optimisation problem. Since the planning algorithm is a multi-period problem, it is most helpful to determine a time specific optimisation variable x_k as a set that includes all the time specific system variables:

$$x_k := \{\theta, V, P_{gen}, Q_{gen}, P_l, Q_l, P_{\overline{sq}}, Q_{\overline{sq}}, S_{\overline{sq}}, P_{PV}, P_{ch}, P_{dis}, x_{st}, E_{st}, E_{deg}\} \quad \text{at time } k$$

The variable P_{PV} is introduced here, referring to the PV feed-in at each node. Including it as a decision variable enables curtailment of PV when it is not economical or when it involves violating system constraints.

There are two additional variables that appear only once in the model, which relate to the battery capacity levels. Firstly the storage starting level E_0, i.e. the storage capacity $E_{st}(k)$ at $k = 0$. Secondly the storage capacity itself, E_{cap}. Therefore the full set of optimisation variables is:

$$x := \{x_k | \forall k = 1 : N, \quad E_{cap}, \quad E_0\}$$

Cost function
The objective function used for the planning algorithm is cost based, meaning that the unit for the cost function is euros. The scalar cost value c_{gen} refers to the cost of energy bought from the grid in €/kWh, the cost c_{st} refers to the cost of storage in €/kWh, and c_{FiT} refers to the FiT. The time specific component of the objective function f_k shown in equation 4.23.

$$
\begin{aligned}
f_k = & c_{gen}\Delta t \sum_{k=1}^{N}\sum^{nodes} P_{gen,+} && \text{Grid Energy cost} \\
& + c_{gen}\Delta t \sum_{k=1}^{N}\left((P_l)^T R_l P_l + (Q_l)^T R_l Q_l\right) && \text{Cost of losses} \\
& + c_{FiT}\Delta t \sum_{k=1}^{N}\sum^{nodes} P_{gen,-} && \text{Feed in earnings} \\
& + c_{st}\Delta t \sum_{k=1}^{N}\sum^{nodes} E_{deg} && \text{Degradation cost}
\end{aligned}
\tag{4.23}
$$

The objective function is a summation of the time specific components f_k and the storage cost component, as given in equation 4.24. For the annual simulation, the annual cost is calculated as 20% of the capital cost of storage. This could be interpreted as a linear discount on a battery with a lifetime of 5 years. The degradation in 4.23 is not discounted, as the cost of lost capacity cannot be spread over time. Even though battery lifetimes are typically longer than 5 years, a conservative annual cost is used for the simulations in this thesis.

$$
f = \sum_{k=1}^{N} f_k + 20\% \times E_{cost} \tag{4.24}
$$

Constraints

The constraints have been mostly summarized in this chapter already, and similarly to the cost function they consist of a time-specific component and a global component. The time specific components include the line power equations, the line constraints, nodal balance, network limits, storage equations and storage costing depending on whether the continuous or discrete model is used. A full list of time specific constraints is shown in Table 4.1, and clearly all these constraints are suitable for use within linear optimisation.

All of the constraints in Table 4.1 have been derived in previous chapters besides the constraint on PV. This is simply implemented to allow the system to curtail PV in case it is a more economical way to maintain the other constraints. The upper limit $\overline{P_{PV}}(k)$ is the PV profile time series.

The only constraint that is not time specific is the charge transfer for the energy storage, and within this work two options are compared. The first option enforces the constraint that the charge levels at the end of the simulations equal the charge level at the beginning, as in 4.25. This constraint ensures that the battery does not bring free energy into the system by discharging over the simulation duration. Using this constraint allows the battery to store energy between days, allowing the storage to save energy on a day of high PV feed in for a day with low PV.

$$
E_0 = E_{st}(k = N) \tag{4.25}
$$

The second option is implementing a constraint forcing the charge level at the beginning and end of every day to be equal. The advantage of this method is that it is more reflective of the control strategy that would actually be applied, as long term forecasts are not always good. Furthermore it provides more consistency with the approximations that will be introduced in

Table 4.1: *Time Specific Planning Constraints*

Line Flow	$P_l = -B_l\theta + G_l V$ $Q_l = -G_l\theta - B_l\theta$
Line Limits	$P_{\overline{sq}} \geq M_p \odot P_l + Y_p \qquad \forall p$ $Q_{\overline{sq}} \geq M_p \odot Q_l + Y_p \qquad \forall p$ $S_{\overline{sq}} = P_{\overline{sq}} + Q_{\overline{sq}}$ $S_{\overline{sq}} \leq \overline{S_l} \odot \overline{S_l}$
Nodal Balance	$P_{inj} - C_g P_{gen} + P_{load} + C_{st} P_{st} + C_{PV} P_{PV} = 0$ $Q_{inj} - C_g Q_{gen} + Q_{load} = 0$
Network Limits	$\begin{bmatrix} 0 \\ \underline{P_{gen}} \\ \underline{Q_{gen}} \\ \underline{V} \\ 0 \end{bmatrix} \leq \begin{bmatrix} P_{gen,+} \\ P_{gen,-} \\ Q_{gen} \\ V \\ P_{PV} \end{bmatrix} \leq \begin{bmatrix} \overline{P_{gen}} \\ 0 \\ \overline{Q_{gen}} \\ \overline{V} \\ \overline{P_{PV}} \end{bmatrix}$
Slack bus	$\theta_s = 0$ $V_s = 1$
Storage Equations	$P_{st} = P_{ch} + P_{dis}$ $x_{st}(k) = \mathcal{A}_d x_{st}(k-1) + \mathcal{B}_{d,ch} P_{ch} + + \mathcal{B}_{d,dis} P_{dis}$ $E_{st}(k) = \mathcal{C}_d x_{st}$ $\begin{bmatrix} 0 \\ \underline{P_{st}} \\ 0 \\ 0 \end{bmatrix} \leq \begin{bmatrix} P_{ch} \\ P_{dis} \\ x_{st} \\ E_{st} \end{bmatrix} \leq \begin{bmatrix} \overline{P_{st}} \\ 0 \\ \eta_{cap} E_{cap} \\ \eta_{cap} E_{cap} \end{bmatrix}$ $E_{deg} \geq \mathbf{a}_1 P_{st} + \mathbf{a}_2 E_{st} + \mathbf{a}_3 E_{cap} \qquad \forall \mathbf{a}_1, \mathbf{a}_2, \mathbf{a}_3$
(Discrete Sizes)	$E_{cap} = E_{int} \times \mathcal{S}$ $E_{cost} = \sum_{Nodes} (E_{int} \times \mathcal{P})$
(Continuous Sizes)	$E_{cost} = c_{st} \sum_{Nodes} E_{cap}$

future chapters. The disadvantage is that even with a 24 hour prediction window, it would be possible to transfer energy between days. In fact it will be shown that although this constraint makes a big difference in the way the storage is used, it does not make a big difference to the results for optimal storage amounts. The second option, where intra day storage is restricted, is mostly used in this work as it is a more reasonable method particularly when sample days are used.

The use of the program Yalmip [19] allows all variables to be written explicitly, and therefore it is not necessary to derive the matrices for the cost function and the constraints.

Algorithm 1 outlines the procedure for calculating the optimal storage using the annual optimal storage algorithm.

Algorithm 1 Annual Optimal Planning Algorithm

Require: Grid Data
Require: Annual Profiles for Active Load, Reactive Load, PV
1: $N = 365 \times 24 \times \Delta t$
2: Objective = cost of bought energy - cost of feed in energy + cost of storage
3: Net Storage Constraint : $E_0 = E_{st}(k = N)$
4: **for** $k = 1$ to N **do**
5: Build time specific network constraints (Table 4.1)
6: Objective += Cost of line losses
7: Objective += Storage Degradation
8: **end for**
9: OPTIMIZE system over the year
10: Optimal result: E_{cap}

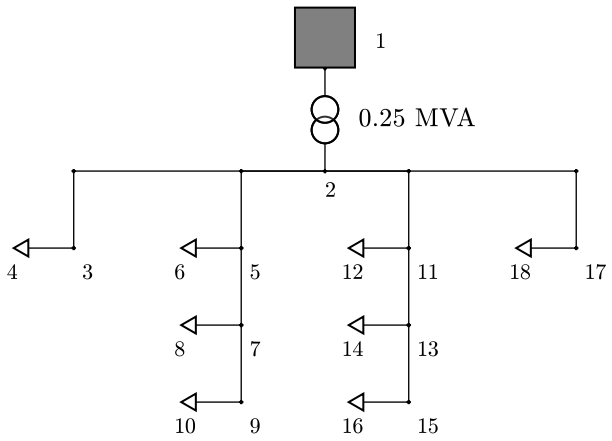

Figure 4.2: *Case study 1 grid from [5] with node numbering*

4.3 Case Study 1 : Rural sample grid

In the following pages, the planning algorithm described in this chapter is applied to Case Study 1 (CS1), a synthetic sample grid for a rural network based on the publication by Lindner [5]. In the study, 5 synthetic sample distribution grids are produced based on the analysis of 358 real distribution grids in Germany with the purpose of investigating voltage problems. The real grid data is used to classify the samples into three categories: rural, village, and suburban based mainly on the distance between load points and transformer apparent power ratings. Urban grids are not included in the study as they are generally very meshed, and the study focus is on radial grids. The rural and village grids are further separated into cable-dominated and overhead line dominated grids, as the respective impedances are very different.

The synthetic grids are generated based mainly on the median cable technologies and cross-section areas, and the likelihood of direct connections to the substation. Statistics on distributed generation are also used to determine the most likely placement and quantities of the PV, which is given in terms of peak production (W_p).

The topology for CS1 is shown in Figure 4.2. The grid has eight household loads and four nodes with distributed generation. The only form of distributed generation considered is PV, since PV is the dominant source of distributed generation in Germany [14].

The publication [5] indicates that all loads are residential, although it does not provide an annual load or a specific SLP to use. Loads are assigned by using the REM to generate a set of 5000 annual profiles with a range of household sizes, and choosing randomly out of the set for the loads. The PV profiles are generated using the installed PV amount from [5] and weather data from rural Bavaria.

The profile characteristics used for the first set of results are shown in Table 4.3.

4.3.1 Case Study 1 Results

The annual planning algorithm is performed on CS1 for six different price scenarios. The annual simulation takes a long time, therefore only six simulations were performed for this section. The solution of the optimisation problem includes the optimal size of battery at each node, as well

Table 4.3: *Case study 1 profile properties by node*

Node number	Annual Load	Annual PV	Peak PV
1	-	-	-
2	-	-	-
3	-	-	-
4	4.52 MWh	7.4 MWh	29.6 kW
5	-	-	-
6	4.77 MWh	-	-
7	-	-	-
8	2.82 MWh	-	-
9	-	-	-
10	4.77 MWh	6.35 MWh	25.5 kW
11	-	-	-
12	4.07 MWh	-	-
13	-	-	-
14	2.75 MWh	6.25 MWh	25 kW
15	-	-	-
16	3.17 MWh	2.5 MWh	10 kW
17	-	-	-
18	3.85 MWh	-	-

Table 4.4: *Fixed parameters used for all case study simulations*

Parameter	$\overline{P_{st}}$	$\underline{P_{st}}$	$\overline{V}$	$\underline{V}$	η_{cap}	η_{ch}	η_{dis}	Lifetime	c_{gen}
Value	10kW	-10kW	1.1	0.9	0.8	0.98	0.97	5 years	€0.285/kWh

as a schedule for the charging of the storage units. The schedule is not useful for operation as it is only valid for the specific load and PV profiles used, and is only valid if perfect prediction is available. Furthermore all grid values, including the node voltages and angles, the transformer power flows as well as the line flows are all given by the optimisation results and can be examined.

In the following pages a number of features of the results for the six price scenarios will be examined. The model parameters for CS1 are given in Table 4.4, and the costs for each of the price scenarios are summarized in Table 4.5.

The results in this section use the continuous price model for batteries, meaning there is a fixed price per kWh and a continuous range of storage sizes are allowed. The highest price used is €230/kWh, which is based on the estimated cost for Lithium Ion batteries in 2016 (273 dollars) [131]. In reality this is not a price that is available for residential battery units, as it is the average price of all Lithium Ion batteries sold, and is highly skewed by the wholesale prices of batteries available to the automotive industry for electric vehicles. However, there is a clear trend that battery prices are reducing, which is discussed in detail in chapter 6.2, so the prices 150 and 100 are also included. FiTs in Germany are currently around €0.12/kWh, which are amongst the highest in the world. It is not expected that future energy systems will have such

Table 4.5: *Price scenario cost parameters*

Price Scenario	PS1	PS2	PS3	PS4	PS5	PS6
Battery Cost (€/kWh)	230	150	100	230	150	100
FiT (€/kWh)	0.12	0.12	0.12	0.05	0.05	0.05

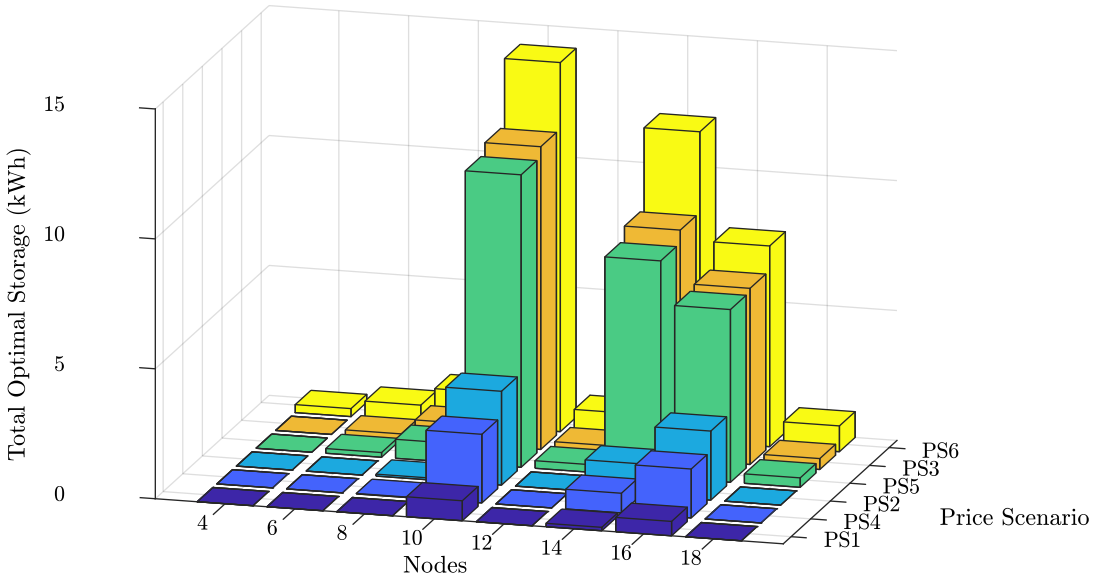

Figure 4.3: *Optimal storage for CS1 nodes for the different price scenarios*

high FiTs, for this reason a lower tariff of €0.05/kWh is also used.

A much more detailed cost analysis will take place in chapter 6.2.

In the following pages it will be shown that the price scenario has a high impact on the optimal storage in the system, which in turn has a strong effect on the self-sufficiency properties of the system. Furthermore, it is shown that allowing intraday energy transfer using the storage does not change the results for optimal storage.

The optimal storage results for each node is shown in Figure 4.3. Since in the optimal storage results only the even nodes have batteries, the odd nodes were left out of the plot. This is because only the even nodes contain loads or PV, and therefore storage is placed at these nodes to reduce losses.

Positive Impact of Storage on Network

In order to assess the positive impact of the amount of storage on the self-sufficiency and losses of the network, quantities such as self-supply, self-consumption, autarchy and network losses can be extracted from the results. To gain insight into the effect of storage on the system, the properties can be plotted against the total amount of network storage. This is shown in Figure 4.4.

The self-consumption refers to the percentage of generated PV energy that is consumed within the network itself, and the results indicate a roughly linear relationship to the amount of storage in the network, where around 45% is achieved without any storage upto 75% with 38kWh. Similarly, the self-supply plots the percentage of the total load covered by local generation. Self-supply also seems to follow a linear relationship to amount of storage, starting at 33% with no storage, and reaching 54% with 38kWh of storage.

Autarchy refers to the amount of time the grid is completely self-sufficient i.e. the entirety of the load is supplied from local generation. It is shown that this does improve with increased

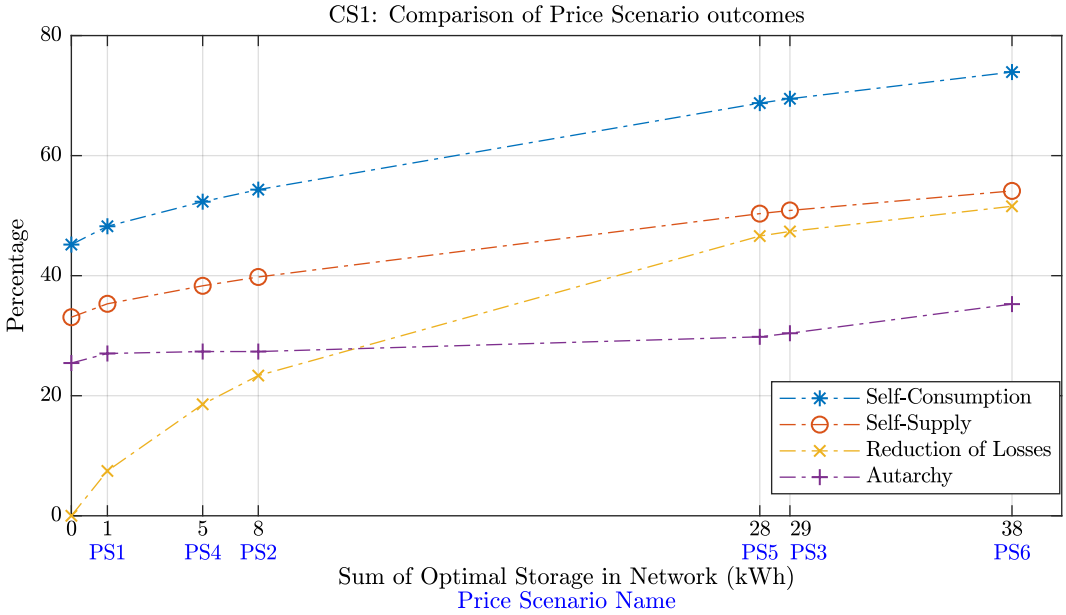

Figure 4.4: *The positive impact of storage on the grid depicted by plotting the percentage of self-consumption and self-supply against the amount of storage. The x axis states the total amount of storage in the network in the first line, and the price scenario on the second line.*

storage, but with a non-linear relationship. The autarchy is also rather low, achieving only 35% with 38kWh of storage, up from a base case of 25%.

The largest improvement is identified in reduction of losses, although the gradient of improvement does reduce with more storage. This makes sense as from a cost perspective losses are minor compared to the bought energy, and to eliminate losses completely it would be necessary to reduce all line flows to 0.

It is important to recognise that these results are a strong reflection of the cost function used. For these results a pure cost optimisation is used, which means that the storage is primarily used to increase self-consumption and reduce losses in order to save electricity costs. With the same amount of storage, a different cost function could lead to more autarchy.

Self-supply and autarchy are qualities that are important when assessing the potential of the network to be a self-sufficient microgrid. Figure 4.4 shows that for this grid, the cost-efficient optimal storage is very far away from achieving autarchy, even with price conditions that are much more favourable for storage than those of today.

inter day transfer

It is important for the rest of this work to establish whether the optimal storage provides cost savings by load shifting within a day or between days. To investigate whether the storage is sized to shift intra-day or inter day energy, the simulations are performed twice for all price scenarios. The first set of simulations allows the SoE to be free within the simulation time, and is only restricted to be the same at the beginning and end of the simulation. The second set restricts the daily net charge level of the individual storage units to zero.

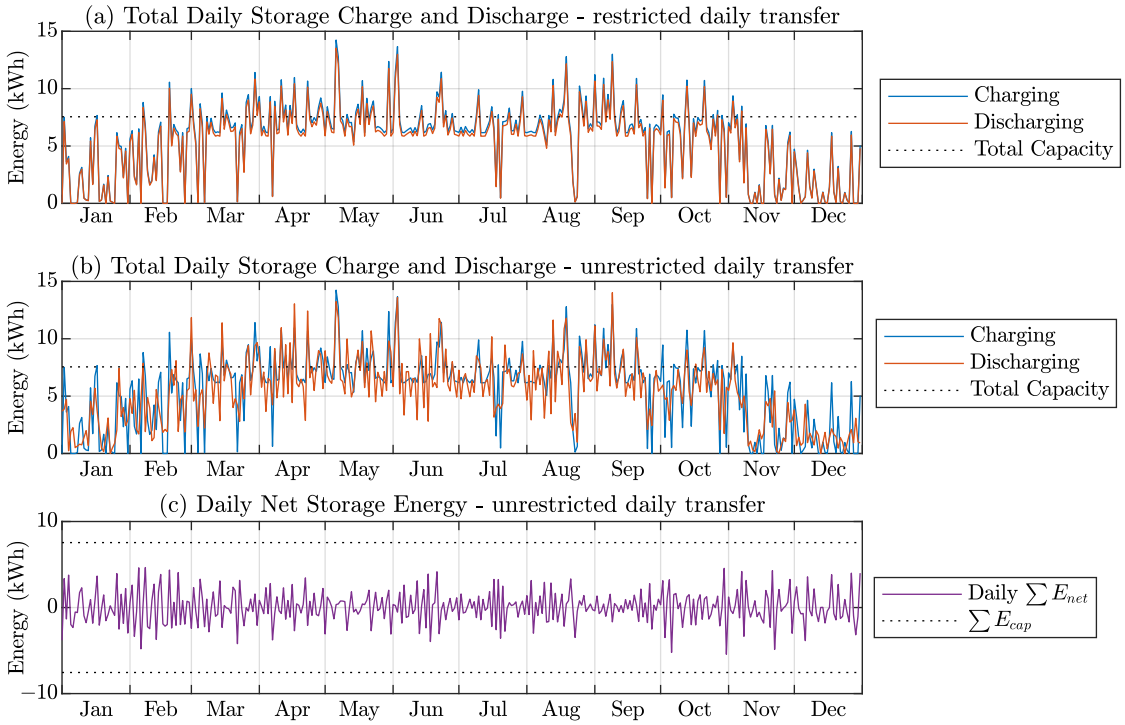

Figure 4.5: *Results of simulations using PS2, with restricted and unrestricted inter day transfer. Subplots (a) and (b) shows the daily storage use in terms of total discharging and charging energy, for the restricted (a) and unrestricted (b) simulations. Subplot (c) shows the net daily storage energy in the unrestricted case*

The charging and discharging behaviour is compared in Figure 4.5, and is shown to be quite different. Plot (a) and (b) show that the sum of the charging and discharging powers per day for the entire year. Plot (a) shows that when the SoE is restricted per day the charging and discharging are the same and the only difference is due to losses. The total charging and discharging power can exceed the storage capacity showing that the storages may be charged and discharged several times a day. Plot (b) shows that when the freedom is available the storage is charged quite differently and there are greater differences between charging and discharging. Subplot (c) plots the difference between the SoE at the beginning and end of the day for the unrestricted simulation, and shows that there are many instances of high differences proving that significant intraday transfer takes place.

Despite the difference in charging behaviour, the storage planning results are practically identical for the restricted and unrestricted simulations. The result is less than 1% different for every simulated price scenario.

It is undesirable that inter day transfer has a strong effect on optimal storage, as it implies that the results for optimal storage are highly dependent on accurate long term predictions of PV and load. In reality predictions for both are very difficult. Furthermore operation of residential batteries will typically take place using shorter control horizons of 24 hours or less. Fortunately, the results show that for the typical profiles used, inter day transfer has a very minimal effect on optimal storage.

Chapter Summary

In Chapter 4 an algorithm is presented for annual optimal planning of storage in a distribution grid, using input data in the form of a grid model, and load and PV profiles. The focus of this chapter is the linearisation of various modelling elements, and the properties of the results of the algorithm applied to a simple case study.

- Inclusion of a distribution grid model requires a number of linear approximations that provide an appropriate trade-off between computational simplicity and accuracy. These include:
  - A linearisation for power flow in a line from literature, [76], that allows bus voltage as well as reactive power flow to be included in a linear grid model;
  - A conservative hyperplane approximation enforces limits on the magnitude of apparent power in lines;
  - Network losses are included in the cost function, as it is more reasonable to incorporate a quadratic term in the cost function than in the constraints.
- Battery storage is incorporated using a discrete KiBaM model, where the storage capacity at every node is an optimisation variable. The optimal solution identifies the cost optimal storage capacity at every candidate node in the network.
- All modelling elements are formulated within a quadratic program, where all the physical components are written as constraints and all system costs are included in the objective function. The problem is modelled in MATLAB [18], using the yalmip [19] package to enable semantic formulation.
- The annual planning algorithm is performed on a case study (CS1), an 18 node radial grid from [5]. The REM is used to assign household loads to the nodes, and the PV capaci ty is specified by the authors.
- As the annual algorithm is time consuming, it can only be performed on a limited number of price scenarios. Six price scenarios are selected based on current prices and future trends. It is shown that the cost scenario has a significant impact on the total optimal storage in the network.
- Based on the optimisation results, four quantities are evaluated against the total optimal storage: self-sufficiency, self-consumption, loss reduction and autarchy. Although there is a positive correlation between them, the algorithm is shown to improve some more than others. This is likely a result of the cost function used, which in this case is effective at improving self-consumption more so than autarchy.
- By restricting the net daily SoE, and comparing the results to a simulation where the daily net SoE is unrestricted it is possible to evaluate whether or not inter day load shifting has a significant impact on the optimal storage. This is relevant for two reasons, firstly because the reality of inter day load shifting requires accurate predictions of loads and PV which is not always reasonable. Secondly, the approximations used in following chapters exclude inter day load shifting entirely, and it is therefore necessary to validate this approximation. The results using CS1 show that when the option is available, there is some inter day load shifting, however the impact on the optimal storage is negligible.

Chapter 5

Two Stage Algorithm

Although it is possible to perform an annual simulation on CS1, using the annual planning algorithm on larger networks can be extremely computationally demanding i.e. requiring too much memory or taking too much time. The former is the case for Case Study 2 (CS2), as the available resources for this work were not sufficient to simulate CS2 for one year. In this chapter an alternative heuristic method for planning of storage is proposed, that can also be applied to large networks, and that produces very similar results to the algorithm in Chapter 4. This method is referred to as the Two Stage planning algorithm, as it decomposes the planning problem into two subproblems dealing sizing and placement. This method includes a procedure for the selection of sample days, required for the placement stage. It is shown that the sample days can be used for the entire planning problem (sizing and placement) to obtain an approximation of the annual planning results. The methodology presented in this chapter constitutes one of the major contributions of this dissertation.

This chapter is structured as follows: in Section 5.1, the system properties that are necessary for the Two Stage algorithm are described. In Section 5.2 the methodology is presented for the Two Stage algorithm, including the procedure for selecting sample days. In section 5.3 the algorithm is applied to CS1 and the results are compared to those of the full annual problem presented in the Section 4.3. A third set of results is compared to the Two Stage and the annual planning results, which are obtained by using only the sample days for planning. A second case study network (CS2) is presented in Section 5.4 and the results of both the Two Stage and sample day algorithms are presented.

The results of the Two Stage algorithm applied to CS2 are used to examine various a number of modelling approximations and linearisation techniques in Section 5.5. Finally, in Section 5.6 the topic of time resolution is addressed using Two Stage algorithm results.

5.1 System Prerequisites

The annual planning algorithm presented in Chapter 4 involves solving an optimisation problem to determine the cost optimal amount of storage capacity at every node, for a given price scenario. The solver minimises an objective function, which sums the cost of buying energy, profit from selling locally generated energy, network losses, the annualised cost of storage, and the cost of degradation, as shown in Equation 4.24. The solution of the optimisation problem includes not only the storage at every node (E_{cap}), but also the entire solution for the MPOPF, including how much energy is bought and sold.

The Two Stage algorithm exploits the fact that if the total storage in the system is fixed, the

optimal solution is almost entirely insensitive to price. This can be tested by fixing $\sum E_{cap}$, and solving the optimisation problem for different price scenarios. The results show that despite the different price scenarios, the MPOPF solution is the same, most importantly P_{gen} and P_{loss} are identical for all solutions. It is therefore useful to think of the cost function components in 4.24 as being functions of total network storage instead of functions of price.

It is important to note that this system property is only true if c_{gen} is greater than c_{FiT}. If this condition is true, the optimisation identifies a solution that maximises the self-consumption with the available storage. The total amount of optimal storage is highly sensitive to price, as the potential profit is weighed against the cost of storage. All the other decision variables, including those that appear in the cost function, are dependent on the total network storage.

Another property of the system behaviour that is exploited by the Two Stage algorithm, is the weak link between days of the year. This has already been indicated for CS1 in Section 4.3.1, by the fact that total optimal storage does not change if the storage is not allowed to shift energy between days. This allows the annual problem to be decomposed into daily problems, which can be solved independently of one another.

At this point it is important to mention that determining the total optimal storage is not the same as determining the optimal storage at each node. In fact it is shown that the two can be identified sequentially. This leads to the separation that provides the foundation of the Two Stage algorithm: first an optimal solution is found for total network storage in the sizing stage, and second, the total storage is distributed amongst the nodes in the placement stage.

Optimal placement of storage in the network affects the value of the cost function in two significant ways. Firstly, it minimises the system losses, by placing storage in a way that minimises power flow in lines. Secondly, it can be used to maintain system constraints by supporting nodes with over-voltage or lines with over-current. This can reduce curtailment, and thereby increase the amount of energy sold back into the grid.

For the systems that are relevant for this thesis, it is shown that placement has a relatively minor effect on the total optimal storage. There are two intuitive reasons for this. Firstly, the losses are a relatively minor component of the cost function. The majority of the profit derived from storage is related to the cost savings achieved by increasing self consumption. Secondly, curtailment is typically a result of excess PV generation due to weather conditions. The nodes that have large PV installations, are likely to suffer from grid overload. Since the problematic node are often those with large PV installations, the optimal placement will be the same for many grid conditions.

To summarize, the prerequisites for system behaviour that are required for the Two Stage algorithm are:

- **Requirement 1**: For the range of price scenarios considered, system behaviour is independent of price if the total storage is fixed;
- **Requirement 2**: The link between days of the year is weak, i.e. the profitability of storage does not significantly change if the storage is allowed to load-shift between days;
- **Requirement 3**: Losses are a relatively small percentage of the cost function value;
- **Requirement 4**: There is consistency in the nodes that suffer from over-voltage.

Using the results of the Two Stage algorithm, it will be shown that all these properties of system behaviour can be verified.

5.2 Methodology

The methodology for the Two Stage algorithm is presented in pseudocode form in Algorithm 2, and graphically in Figure 5.1. The two stages of the algorithm are referred to as the sizing stage, and the placement stage. The purpose of the sizing stage is to find the optimal value for total network storage, and the purpose of the placement stage is to optimally distribute the storage amongst the nodes in the grid. It is useful to define a variable for total storage, for which the expression is given in Equation 5.1.

$$E_{tot} = \sum^{Nodes} E_{cap} \tag{5.1}$$

As mentioned in Section 5.1, the Two Stage algorithm exploits the fact that three components of the function, bought energy, sold energy, and line losses, are insensitive to price if E_{tot} is fixed. This makes it possible to iterate over a range of values of E_{tot} and calculate these three components. The number of iterations for the total storage is referred to as $n_{E_{tot}}$, and the range of total storage values is referred to as $\mathcal{E}_{tot} \in \mathbb{R}^{n_{E_{tot}}}$. Degradation has a minor effect on the placement of storage, but a negligible effect on total storage, and is therefore left out of the sizing stage.

By exploiting the fact that there is only a weak link between days, the annual problem can be decomposed into 365 daily problems. The sizing stage uses the results of $n_{E_{tot}} \times 365$ subproblems, extracting the values of the three cost function components to determine how they change with total network storage.

Lines 1 to 17 of Algorithm 2 show the sizing stage steps to calculate the optimal E_{tot}, referred to as E^*_{tot}. Firstly, the length of the optimisation problem N of the daily subproblem is calculated depending on the time resolution. A 15 minute time resolution, i.e. $\Delta t = 0.25$h, results in $N = 96$. The decomposition into daily subproblems is implemented with a for loop in Line 2. The daily profiles for active load, reactive load and PV are extracted, and used to build the network constraints listed in Table 4.1 and Equation 4.25.

For each daily problem another for loop is implemented in line 5, fixing E_{tot} to every value in $\mathcal{E}_{tot}$. An optimal result is calculated, and the optimisation results are used to populate the matrices that describe bought energy $\mathcal{M}_{\text{buy}}$, feed-in energy $\mathcal{M}_{\text{FI}}$ and losses $\mathcal{M}_{\text{loss}}$ as shown in lines 7-9. These matrices are of the size: $\mathcal{M} \in \mathbb{R}^{365 \times n_{E_{tot}}}$ and are populated with the quantity of energy bought, sold and the line losses for each fixed E_{tot}, for each day. The calculation for each of the matrices is given in equations 5.2, 5.3 and 5.4. The indices d and m identify the sub-problem as they are defined in Algorithm 2, d refers to day and m refers to the index of $\mathcal{E}_{tot}$. The matrix entries are calculating using the sub-problem optimisation results P_{gen} and the line losses. The bought energy is calculated by summing the positive values of P_{gen}, i.e. the energy flowing in from the MV network and multiplying it by the time resolution. Similarly, the feed-in energy uses the sum of the negative energy, i.e. the energy flowing out of the distribution grid. The losses are calculated using Equation 4.13.

Algorithm 2 Two Stage Planning Algorithm

Require: Grid Data
Require: Annual Profiles for Active Load, Reactive Load, PV

STAGE 1 : Sizing

$N = 24 \times \Delta t$
for $d = 1$ to 365 **do**
    Extract daily profiles from annual profiles
    Build Network Constraints: 1 Day
    for $m = 1$ to $n_{E_{tot}}$ **do**
        OPTIMIZE system over one day using the constraint $E_{tot} = \mathcal{E}_{tot}(m)$
        $\mathcal{M}_{\text{buy}}(d, m) = \Delta t \sum_{k=1}^{N} P^{+}_{gen}(k)$
        $\mathcal{M}_{\text{FI}}(d, m) = \Delta t \sum_{k=1}^{N} P^{-}_{gen}(k)$
        $\mathcal{M}_{\text{loss}}(d, m) = \Delta t \sum_{k=1}^{N} P_{loss}(k)$
    end for
end for
for $m = 1$ to $n_{E_{tot}}$ **do**
    $\mathcal{E}_x(m) = \sum_{d=1}^{365} \mathcal{M}_x(d, m) \quad \forall x = \{\text{buy, FI, loss}\}$
    $\mathcal{O}(m) = c_{gen}(\mathcal{E}_{\text{buy}}(m) + \mathcal{E}_{\text{loss}}(m)) + c_{FiT}\mathcal{E}_{\text{FI}}(m) + c_{st}\mathcal{E}_{tot}(m)$
end for
$m^* \rightarrow \mathcal{O}(m^*) = \min(\mathcal{O})$
$E^*_{tot} = \mathcal{E}_{tot}(m^*)$

STAGE 2: Placement

Require: Sample Day Profiles
$N = 36 \times 24 \times \Delta t$
Build Network Constraints: 36 Days
OPTIMIZE system over sample days using the constraint $\sum E_{cap} = E^*_{tot}$
Optimal result : E^*_{cap}

$$\mathcal{M}_{\text{buy}}(d,m) = \Delta t \sum_{k=1}^{N} P_{gen}^{+}(k) \tag{5.2}$$

$$\mathcal{M}_{\text{FI}}(d,m) = \Delta t \sum_{k=1}^{N} P_{gen}^{-}(k) \tag{5.3}$$

$$\mathcal{M}_{\text{loss}}(d,m) = \Delta t \sum_{k=1}^{N} P_{loss}(k) \qquad \forall d \in \{1,...,365\}, \quad \forall m \in \{1,...,n_{E_{tot}}\} \tag{5.4}$$

The matrices can then be summed over the days, yielding the vectors $\mathcal{E}_{\text{buy}}$, $\mathcal{E}_{\text{FI}}$ and $\mathcal{E}_{\text{loss}}$, which are referred to as the energy characteristics ($\mathcal{E}$). The value of the cost function can now be calculated for every value of m, by multiplying the energy characteristics and total storage by their respective costs. The objective function $\mathcal{O} \in \mathbb{R}^{n_{E_{tot}} \times 1}$ is calculated using Equation 5.5.

$$\mathcal{O}(m) = c_{gen}(\mathcal{E}_{\text{buy}}(m) + \mathcal{E}_{\text{loss}}(m)) + c_{FiT}\mathcal{E}_{\text{FI}}(m) + c_{st}\mathcal{E}_{tot}(m) \qquad \forall m \in \{1,...,n_{E_{tot}}\} \tag{5.5}$$

It is now possible to derive the optimal value of total storage, referred to as E_{tot}^{*}, as the value that minimises the objective function $\mathcal{O}$. The optimality of the solution is correct to the step size used in $\mathcal{E}_{tot}$.

Choosing the range of total storage values $\mathcal{E}_{tot}$, and an appropriate step size requires some insight into the system. Greater precision can be achieved by using a smaller step size, however for most practical applications a high precision is not required. The larger the step size, the smaller $n_{E_{tot}}$ is, and the quicker the algorithm can be performed. The selection of these parameters is extremely case study specific, and may require some trial and error.

Assuming the time resolution is 15 minutes, the sizing problem decomposes one annual problem with a duration of $N = 35040$ to $365 \times n_{E_{tot}}$ subproblems of the size $N = 96$. In general, the Two Stage algorithm is significantly quicker than the annual optimal planning algorithm, as solving time scales badly for optimisation problems. There is another powerful advantage of this sizing approach. Much of the calculation, including all the optimisation, needs to be performed only once in order to calculate E_{tot}^{*} for any price scenario. The vectors $\mathcal{E}$ can be multiplied by any combination of costs to evaluate any objective function, and thereby can identify the minimising value E_{tot}^{*}.

The placement stage of the algorithm utilises sample days to represent the annual problem. The annual problem is scaled down by a factor of 10 by selecting 36 sample days throughout the year. Fixing the total storage to the optimal value calculated in the sizing stage, the optimal E_{cap}^{*} is approximated by performing the optimisation over 36 days.

The Two Stage algorithm can yield near-optimal results if the four prerequisites of system behaviour listed Section 5.1 are true. The first requirement is the independence of system behaviour if total storage is fixed, and the second requirement is the weak link between of the days of the year. Both are important, as the algorithm calculates the values of the matrices $\mathcal{M}$ separately, requiring them to be independent. For sizing and placement to be calculated in two stages, the third and fourth requirements are important. Since each subsystem optimisation recalculates E_{cap}, each daily solution has a different optimal location that calculates the grid losses of that day. For placement to be separately calculated, the loss minimisation must be a small component compared to the buy-sell components, so as not to influence the total optimal storage. Similarly, if voltage issues are causing curtailment of PV, it is important that the same nodes are always

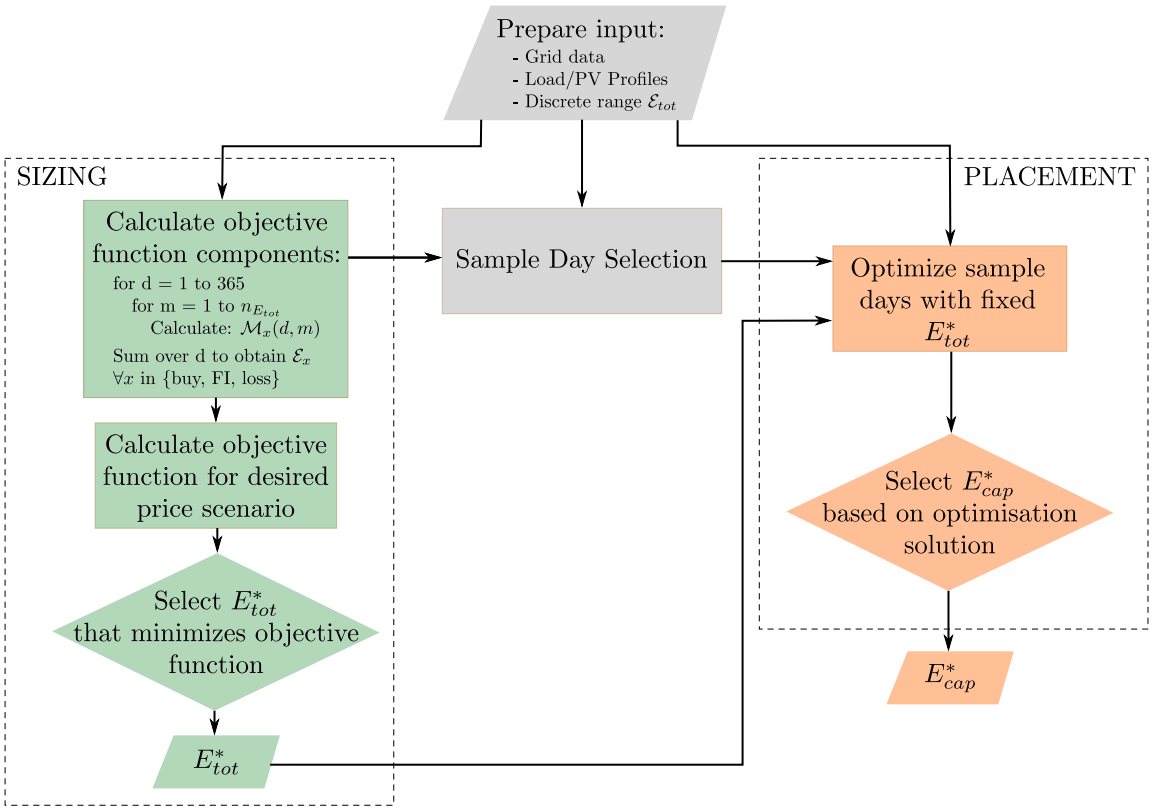

Figure 5.1: *Procedure for the Two Stage annual planning algorithm*

problematic, so as not to affect the total storage. If E^*_{tot} is only optimal if it can be constantly rearranged in the grid, then it is not valid as an optimal result.

The procedures that can be used for checking these four conditions are presented along with two case studies, after a brief overview of the method used for selecting sample days.

Sample Day Selection

The selection of representative days for investigations that use optimisation is a research field in its own right. Since large optimisation problems are so time consuming to solve, it is useful to be able to reduce the problem size by choosing sample days to represent the whole year. Studies like [132], [133], develop methods for sample day selection using clustering, for planning problems specifically. It is not within the scope of this thesis to implement and verify clustering methods, therefore a simple method is used for selecting 36 sample days throughout the year. The Two Stage algorithm is compatible with any sample days selection method, including a clustering method.

The method for selecting sample days is illustrated in Figure 5.2. The system is optimised over 10 chronological days, to find the optimal total storage for that time period, referred to as $E_{tot,10}$. Then each of the days is optimised individually, to obtain ten values for total storage for each day, referred to as $E_{tot,1}$. The day that has an optimal storage closest to $E_{tot,10}$ is selected as the representative day for that ten day period. This is repeated throughout the year: 365 days

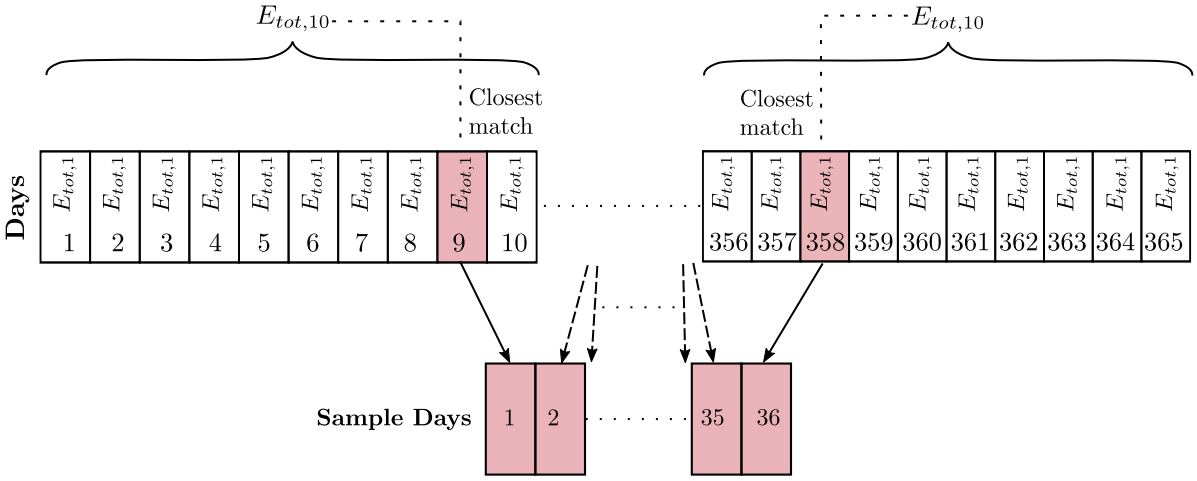

Figure 5.2: *Sample day selection method*

are broken down into 36 sets of 10 (and some 11) day periods, and a sample day is selected for each of these periods. This yields 36 sample days.

For the Two Stage algorithm, the sample days are used to optimally distribute a fixed amount of total storage in the grid. It is also possible to use the sample days for both sizing and storage, i.e. to approximate the basic annual planning algorithm. This method of planning is referred to as the sample day method. Using the case studies, it is shown that the sample day method yields inferior results compared to the Two Stage algorithm.

5.3 Demonstration using Case Study 1 Results

The Two Stage algorithm is applied to CS1 to approximate the results shown in Figure 4.3. The range of total storage is 0-65kWh with a step size of 1kWh. This means the vector $\mathcal{E}_{tot} = [0\text{kWh}, 1\text{kWh}, ..., 65\text{kWh}]$, and the number of total storage iterations is $n_{E_{tot}} = 66$. The sizing stage calculates the energy characteristics: $\mathcal{E}_{\text{buy}}$, $\mathcal{E}_{\text{FI}}$ and $\mathcal{E}_{\text{loss}}$. These vectors can be plotted against total storage, as shown in Figure 5.3 (a). The figure shows that the bought energy and sold energy follow the same curve, and flatten out around 50kWh. This means that above 50kWh, there is less marginal self-consumption benefit of adding more storage.

The y axis for Figure 5.3(a) is energy, and to obtain the cost optimal storage it is necessary to multiply the energy values by the relevant prices. This is shown in Figure 5.3(b) for PS3, which shows the plot for objective function $\mathcal{O}$ versus total storage. It also breaks down the costs of the individual components: $\mathcal{E}_{\text{buy}}$ and $\mathcal{E}_{\text{loss}}$ are multiplied by €0.285 and $\mathcal{E}_{\text{FI}}$ by €0.12. The full cost function is the sum of these three components plus $\mathcal{E}_{tot}$ multiplied by 20% of €100. The value for E^*_{tot} is identified by finding the location of the minimum function of $\mathcal{O}$, in this case 29kWh, which matches the optimal result from Chapter 4.

Once the value for E^*_{tot} is selected, the placement is determined by performing the optimisation over the sample days fixing $\sum E_{cap}$ to 29kWh. The sample day method is also applied to CS1, by optimising over the sample days without fixing E_{tot}. The results for optimal storage of all three variations for all six price scenarios is shown in Figure 5.4.

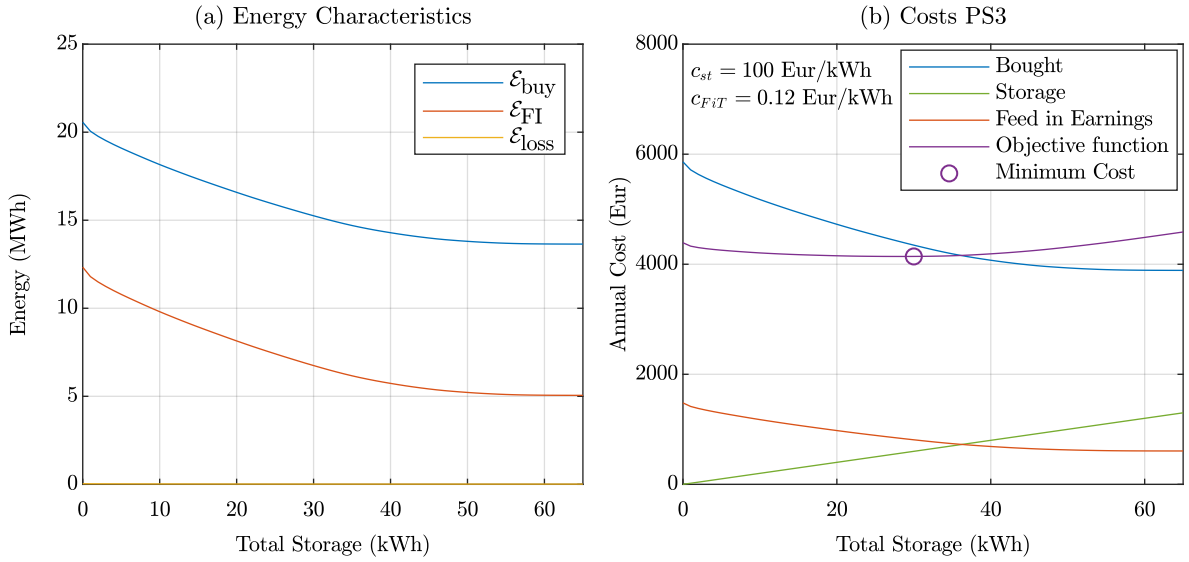

Figure 5.3: *Results of subsystem optimisation of CS1 aggregated over all days of the year shown in plot (a), plot (b) shows an example of the objective function for PS3*

There are several points to be made about Figure 5.4. Firstly, it shows that both approximations yield relatively accurate results in most cases, particularly looking at PS2, 3 and 4. PS1 is an interesting case because the Two Stage method seems to be outperformed by the sample day method. This is because E^*_{tot} is so small that the granularity inherent to the Two Stage method is the cause of inaccuracy. For PS1 E_{tot} according to the annual planning is 1.5kWh, which gets rounded up to 2kWh in the Two Stage algorithm. This is not a major cause for concern as the general conclusion to be drawn is that storage is not very profitable for PS1. If necessary, a more precise result can be achieved by including more steps between 1kWh and 2kWh in $\mathcal{E}_{tot}$.

Besides the exception for PS1, it is clear that the Two Stage algorithm yields results that are much closer to the annual optimisation, particularly for larger amounts of storage such as in PS5 and PS6. The placement is also very close, with all single node errors below 0.2kWh.

It is possible to gain some insight into the results of the sample day method, by plotting the equivalent energy characteristics $\mathcal{E}$, of the sample days versus those of the Two Stage algorithm. This is shown in Figure 5.5, where the energy characteristics are compared in plot (a) and an example of the objective function for PS5 is evaluated in plot (b).

It is immediately clear that the sample days have more PV than the annual average, which is reflected in the fact that $\mathcal{E}_{FI}$ is higher even for 0 storage. However the shape remains the same until around 35kWh and this is why the results for optimal storage are similar for the price scenarios used for this work. Upon closer examination of the sample days, the reason for the difference in total storage can be identified. The energy characteristics for the sample days are much less smooth, having distinct gradients where the Two Stage characteristics are more gradual. The kinks are a result of fewer troughs and peaks, due to the reduced time range of the simulation. Figure 5.5(a) explains why some of the results for total storage are very close (such as PS3), as for this amount of storage the curves coincide very well.

Figure 5.5 also explains why for CS1 the accuracy of the sample day method decreases for high

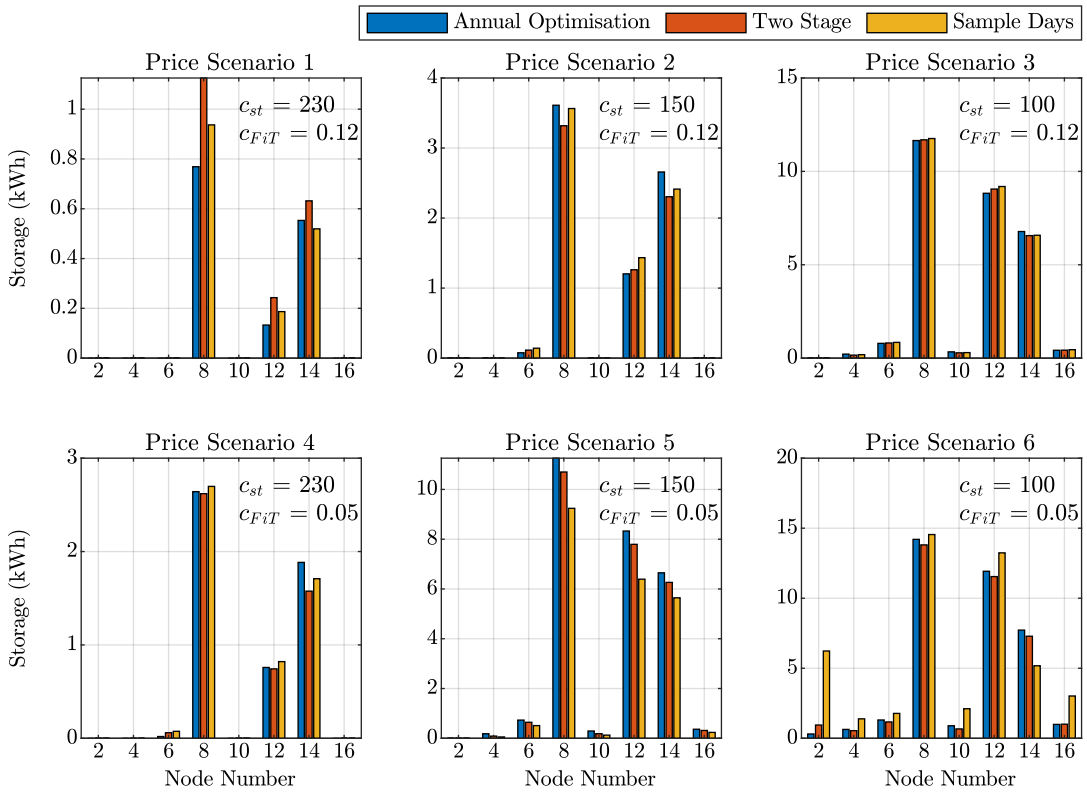

Figure 5.4: *CS1 results for optimal storage comparing the annual problem, Two Stage problem and the use of only the sample days*

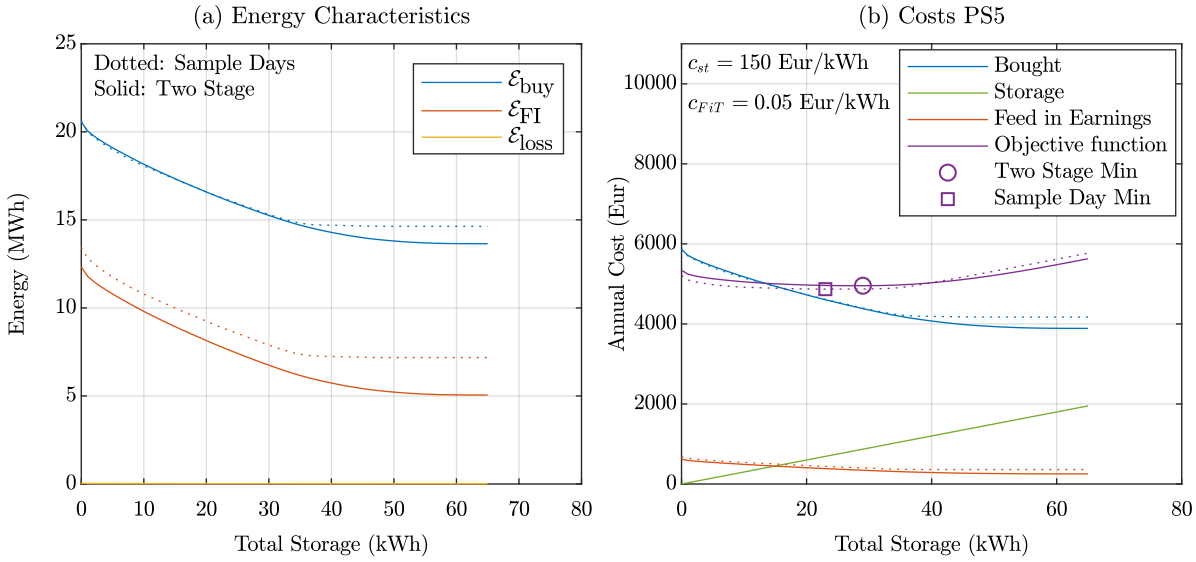

Figure 5.5: *Case study 1: Energy characteristics of the whole year in a solid lines, and dotted lines for the sample days in plot (a). Plot (b) shows the objective function evaluation for PS5*

amounts of storage like PS5 and PS6. The deviation to the energy characteristics of the Two Stage algorithm increases for higher amounts of storage. This is because the sample days contain a smaller variety of peaks and troughs for the storage to even out, at some point (around 35 kWh) the sample days do not offer any more opportunities for self-consumption of PV, and therefore the curves flatten out.

Verification of Two Stage Results

Before moving on to the second case study, it is worth confirming that the four requirements of system behaviour in section 5.1 are met. As some of the methods are applied to results rather than general system behaviour, the Two Stage results for PS3 are considered.

- ✓ **Requirement 1**: It is important to check the independence of the energy characteristics to price if the total storage is fixed. This can be tested by fixing E_{tot} to a random value and optimizing all daily problems with different price scenarios. For CS1 this requirement is fulfilled, because the energy characteristics are identical for each result.
- ✓ **Requirement 2**: Testing the independence of days of the year is slightly more complicated. In Section 4.3.1 it was confirmed for CS1 by simulating the system with and without inter-day load shifting, and confirming that the optimal storage result is the same. Since one of the strengths of the Two Stage planning algorithm is that it can be applied to systems that are too large for the annual optimisation, another method of verification is required. One way of testing the robustness of the results, is to run a receding horizon control (RHC) simulation with a window of 48 hours. The results for CS1 show no significant difference between the amount energy bought and sold.
- ✓ **Requirement 3**: Ensuring that losses are a small component of the cost function can be confirmed simply by calculating them, firstly as a percentage of the energy characteristics, secondly for the cost function. For CS1 the calculation shows that the losses are a maximum of 0.11% of the bought energy, and 0.23% of the feed-in energy. For PS3, the cost of losses are an average of 0.12% of the total cost, and a maximum of 0.22%. These values clearly show that losses are minor compared to the other cost components, both in total energy and in monetary value, and therefore will not influence the optimal storage much.
- ✓ **Requirement 4**: Confirming that the same nodes suffer from overvoltage is not necessary for CS1, as there are no active grid constraints. For a grid with active constraints however, this requirement can be checked by examining the over-voltage that occurs without any storage. It is also implicitly confirmed by the receding horizon control simulation used to verify Requirement 2, as it checks if fixed placement changes the energy characteristics.

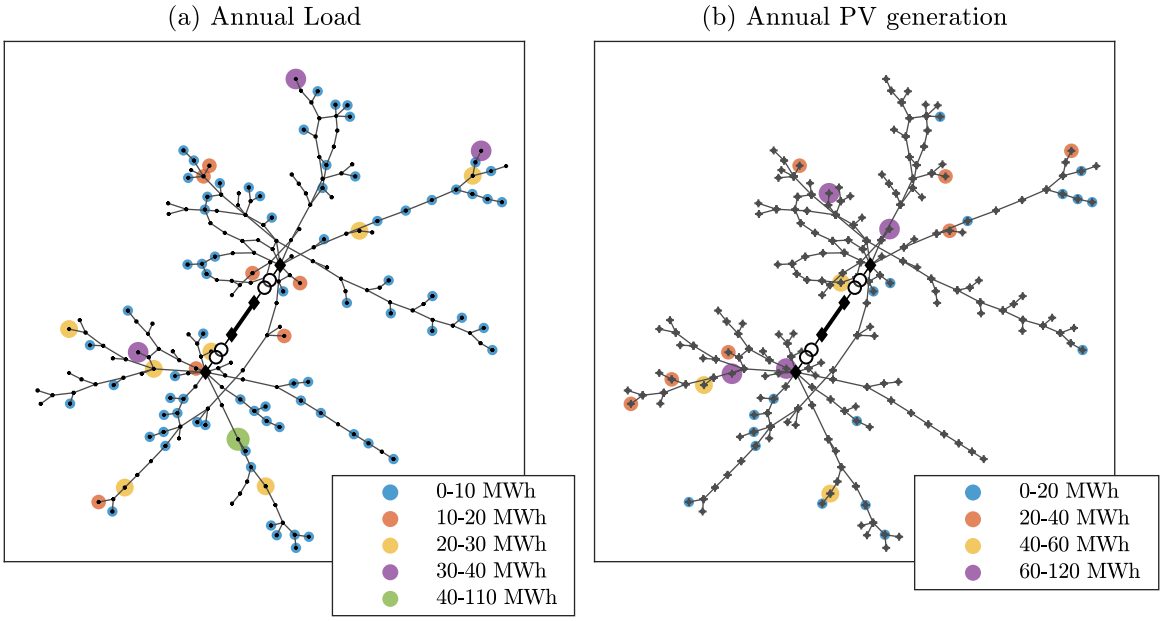

Figure 5.6: *The non-geographical topology of the Case Study 2 grid, showing the annual load (a) and annual PV generation (b)*

5.4 Case Study 2 : Hittistetten grid

Case Study 2 (CS2) is based on a real distribution grid in Bavaria. The grid model was obtained from the local distribution operator Stadtwerke Ulm, and processed by the Hochschule Ulm in the context of the project ESOSEG [134]. The location of the distribution grid is a suburb of the city of Ulm, called Hittistetten. The Hittistetten grid is already at the network limits in terms of voltage issues and overcurrent due to large amounts of PV generation and is therefore a highly relevant case study to examine the possible benefits of energy storage in the grid. Since the voltages vary much more than those of CS1, it is also important to verify the PF approximation and to ensure the network limits are maintained.

The grid itself is much larger and more meshed than CS1. A non-geographical representation of the grid, based on the cable lengths is shown in Figure 5.6. The grid has two substations with a 10kV MV link between them, indicated by the thicker black lines in the figure. Although the grid has a meshed structure for redundancy, it is usually operated radially. There is one large load of 110 MWh/year indicated by the green marker in Figure 5.6 (a), and four large PV installations between 77 MWh/year and 108 MWh/year indicated by the purple markers in Figure 5.6 (b). The loads are mostly residential, with a few industrial and commercial loads as well. The total annual load is 767 MWh, and the total PV generation is 886 MWh.

The residential load profiles were generated using the REM, based on measured annual loads provided by Stadtwerke Ulm. An annual REM simulation is performed for 5000 households, and profiles matching the annual loads are selected without repetition. Several of the load nodes in the network are connected to multiple residences, and for these nodes a random selection of profiles are aggregated to make up the correct annual load. The PV feed-in is also based on the real installed capacity that is already present in the system.

Both the Two Stage and the sample day algorithms are applied to CS2, and the results are

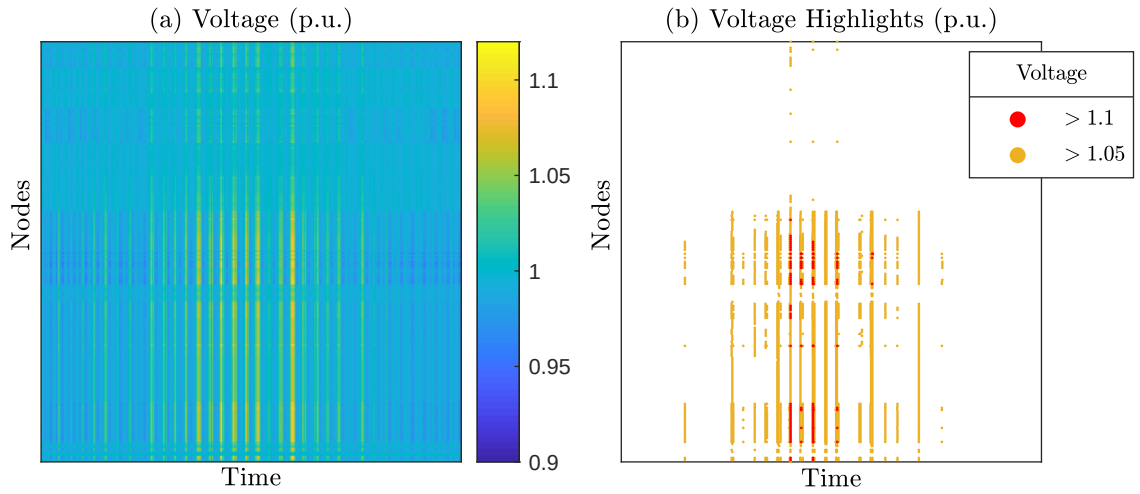

Figure 5.7: *The node voltages of the Case Study 2 grid with no storage, using a colormap to depict all the voltages in (a), and instances of over-voltage highlighted in (b)*

compared to show the adequacy of the sample days in approximating trends. Before the results are presented, it is useful to examine the way in which the grid is reaching its limitations.

Network Limits

CS2 is a useful case study, as the high penetration of PV currently causes the network to reach its limits during instances of high feed-in. Although both current limits and voltage limits are active, overvoltage is by far the most significant problem. Currently, violations are avoided through curtailment of PV and reactive power compensation. Reactive power compensation is neglected in this study, as the objective is to investigate if battery storage may be able to provide an alternative to curtailment.

Commonly, voltage limits in the grid are 0.9 pu - 1.1 pu, and the slack bus is assumed to be a constant 1 pu. This is only valid however if there are no voltage drops in the transmission system. In reality, the slack bus for the distribution system may deviate from 1. In this case the acceptable voltage range for the distribution system may be more constrained. Particularly since PV feed-in tends to coincide regionally, high PV feed-in in this distribution grid is likely to result in overvoltage not only in the local distribution grid but in surrounding grids as well, resulting in overvoltage at the MV connection node.

The selected sample days do include instances of voltage issues if all PV is fed into the network without curtailment. Node voltages above 1.05 pu are common, and violations of 1.1 pu also occur. Including all profiles for PV and load, the calculated voltages using the ACPF are shown in Figure 5.7. It can be seen that overvoltage is a particular problem at certain time instances due to excess PV.

The high PV feed-in also results in violations of line limits, overcurrent issues are also present in the network, with 10 branches exceeding their power limits for short times.

5.4.1 Case Study 2 Results

The Two Stage algorithm is applied to CS2, and the placement stage was carried out for the 6 different price scenarios used for CS1 shown in Table 4.5. The storage size vector used is: $\mathcal{E}_{tot} = [0kWh, 10kWh, ..., 1500kWh]$, with $n_{E_{tot}} = 151$. It is important to include 0kWh in the simulation, as it informs about how much curtailment is avoided by adding storage.

The results are more difficult to visualise compared to CS1 because of the increased range of storage, and number of nodes. One way of representing the results is using the map that was used in Figure 5.6, as shown in Figure 5.8 for PS1-6. There is a lack of preciseness due to the 20kWh bins of storages used in the maps, nevertheless it is useful for drawing conclusions.

A number of observations can be made when comparing the results presented in Figure 5.8 to the indication of PV and Load in Figure 5.6. Firstly, there are four large PV generation plants in the network, indicated by the purple markers in figure 5.6 (b). Large storage quantities are consistently placed at or near the two large PV installations in the upper half. The nodes in the lower half are assigned less storage in general. Particularly the PV node near the substation is rarely assigned storage. This could be because by being so close to the substation, overvoltage is not an issue and it is more profitable to spread the storage further out in the grid where losses can be saved.

Besides the nodes with high PV, there is also a strong correlation between lines with more PV generation that seem to have much more storage. In this context 'line' refers to the connected nodes that lead to the substation. For example the line left of the lower substation has multiple nodes with significant PV production, and in PS2-6 this line is populated with many storage units, even at nodes that do not have a lot of PV or loads themselves.

The link between storage and load is not as significant as the link between storage and PV. The nodes with large loads do not necessarily receive high amounts of storage. Large loads can lead to high power flow. Since losses follow a square relationship with power flow, the loss minimisation term in the cost function may place storage near large loads for peak reduction. It seems that besides matching storage to PV, the result is generally that more storage is placed at the end of lines.

Particularly for radial lines the storage is placed at the end of the lines, and this indicates that the voltage issue is more crucial than the line current issue when placing storage units for CS2. The end of the lines will experience more voltage fluctuation as they are furthest from the slack bus, however the lines nearest the substation have larger currents and therefore storage in these node is more helpful for reducing losses.

Similarly to the assessment carried out on CS1 using Figure 4.4, the same properties are plotted for CS2 as shown in Figure 5.9. It is interesting to compare the properties of CS1 and CS2. The first thing to note is that the self-supply exceeds to the self-consumption for CS2, which only indicates that the total generation in the whole distribution grid is higher than the total load. This makes it more difficult to increase the self-consumption as there is less overlap between the two without load shifting, and therefore more storage capacity is needed to shift it.

The second observation is that although the order has not changed in terms of price scenario versus total amount of storage, the rates at which they change is rather different. For example the difference between PS2 and PS5 is very large for CS1, and relatively much smaller for PS2.

(a) Two Stage Results PS1

(b) Two Stage Results PS2

(c) Two Stage Results PS3

(d) Two Stage Results PS4

(e) Two Stage Results PS5

(f) Two Stage Results PS6

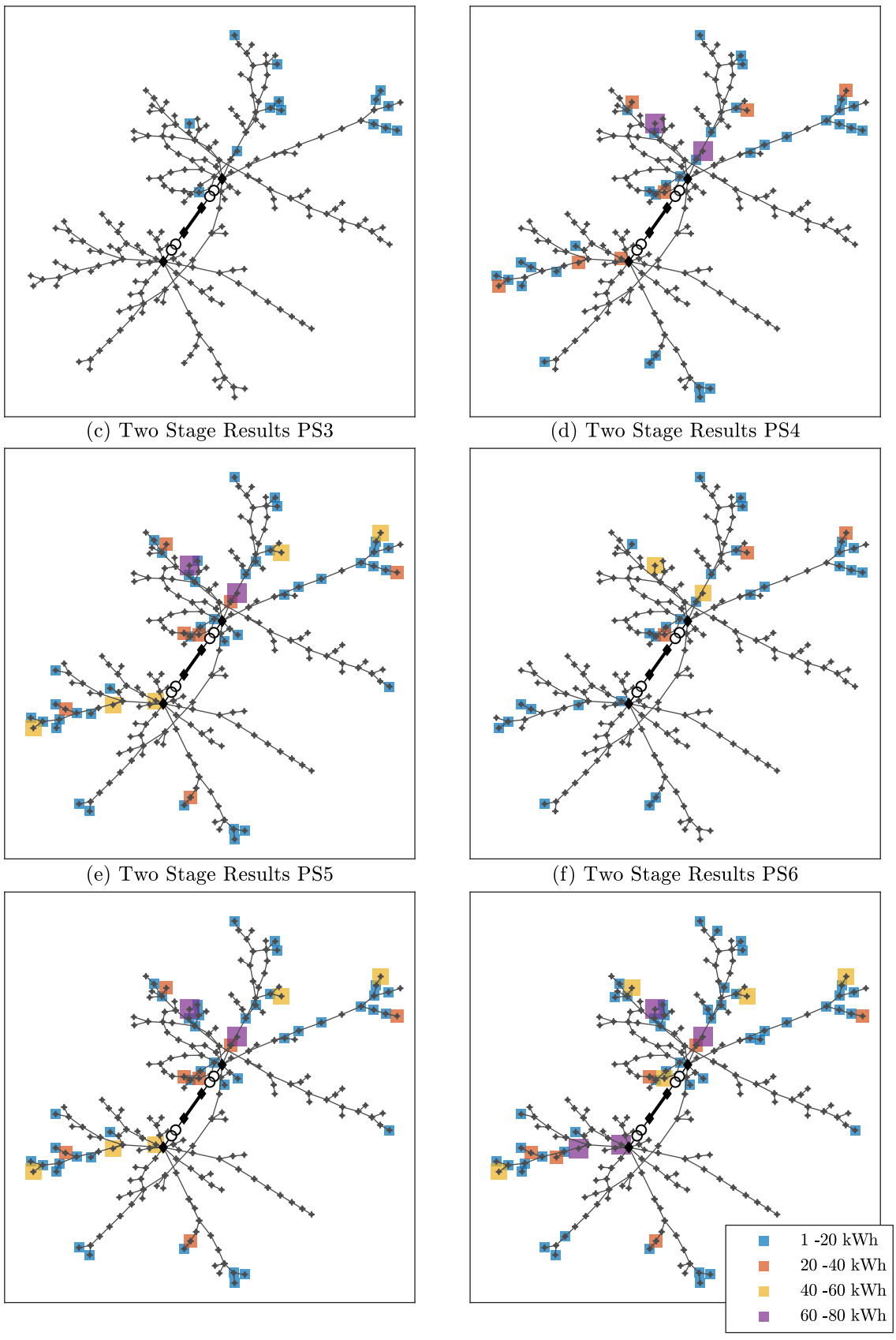

Figure 5.8: *Storage planning using the Two Stage planning algorithm for price scenarios 1-6*

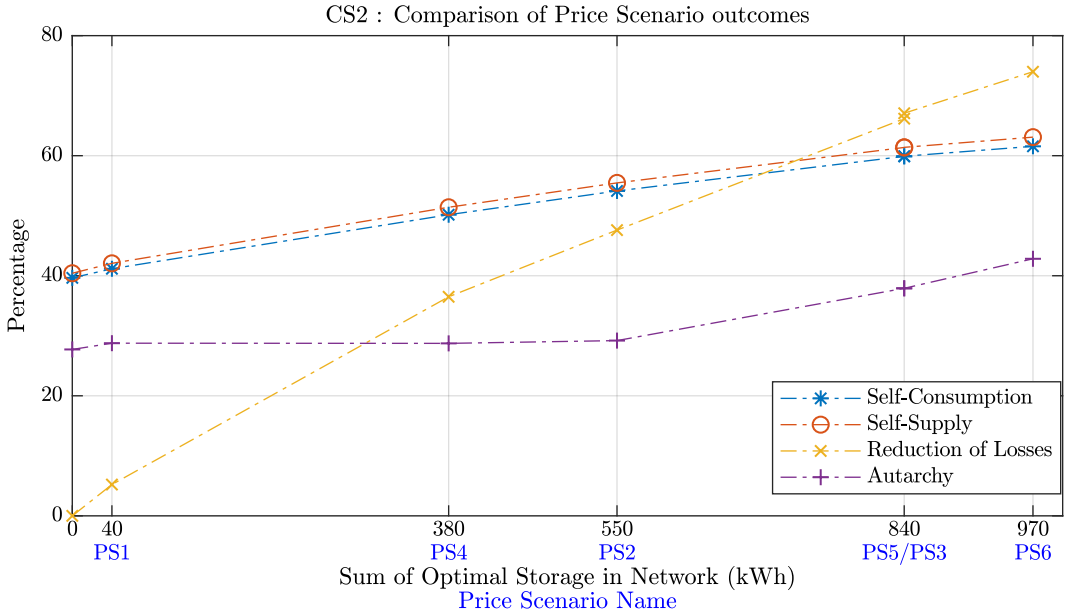

Figure 5.9: *Comparison of the Case Study 2 properties for the Two Stage Simulation*

Furthermore PS5 and PS3 result in exactly the same amount of total storage for CS2. This implies that the cost sensitivities to FiT and storage price are different for the two case studies. This is shown in greater detail in chapter 6.2.

The increases in self consumption and self supply percentagewise are less for CS2 than for CS1, however the improvement in autarchy and losses is greater in CS2. Particularly for PS3, PS5 and PS6, where the amount of storage is $\geq$ 840 kWh, the autarchy is much higher. Losses are also significantly improved.

Sample Day results

The Two Stage algorithm for CS2 is time consuming. Although the sizing stage is carried out only once to evaluate any price scenario, any other analysis regarding network parameters or profile properties requires an entirely new simulation. For some of the investigations the sample day method can be used, therefore it is helpful to evaluate its results compared to the Two Stage method. Figure 5.10 shows the results of the sample day planning compared to the Two Stage algorithm. It is immediately clear that the sample days systematically underestimate the amount of optimal storage compared to the Two Stage, which means that it is not a good estimate for the total amount of storage in general. However it does reflect the trend, i.e. the difference between the cost scenarios.

Figure 5.10(b) shows that the nodal distribution is extremely close to the Two Stage algorithm, as the total storage discrepancy is spread quite evenly between nodes. This is not a surprising result, as the same sample days are used as for the placement stage of the Two Stage algorithm.

As was done for CS1 in Figure 5.5, the energy characteristics of the sample days can be plotted and compared to the Two Stage algorithm energy characteristics. This is shown in Figure 5.11, showing that the results are quite different than for CS1. Clearly in this case the sample days have much less PV than average, as well as a little more load. It is significant that the shapes

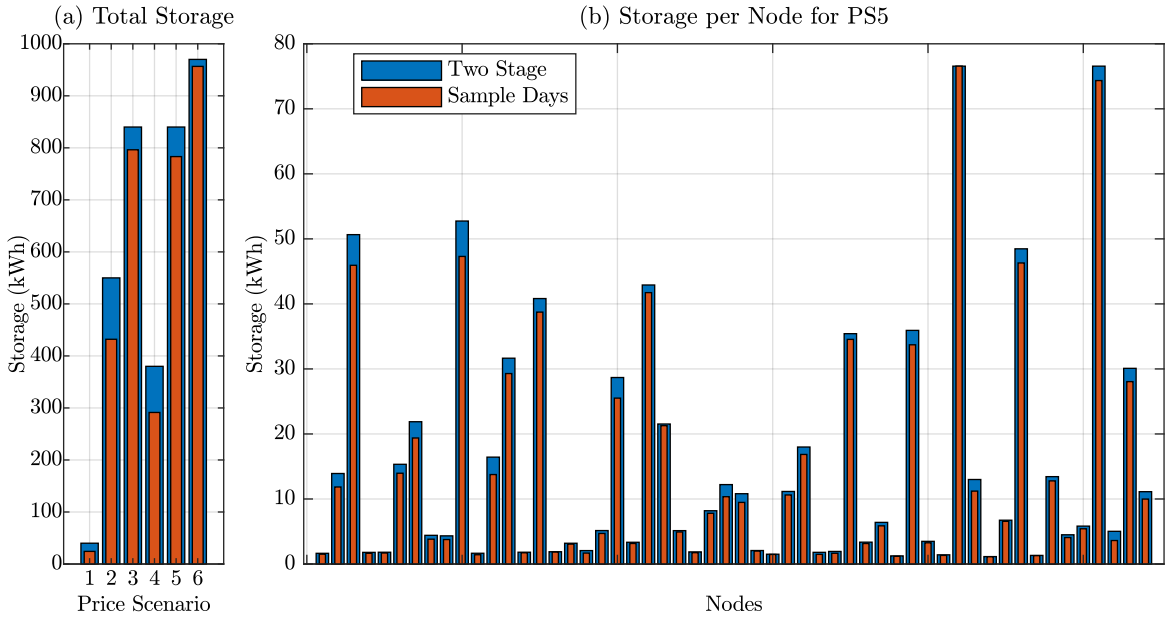

Figure 5.10: *Comparison of results using the Two Stage algorithm compared to using the sample days. Plot (a) shows the difference in total storage for each of the price scenarios, and plot (b) shows the amount of storage per node for PS5 as an example*

are very similar for both, which is why in plot (b) in fact the minimum cost is obtained in a relatively similar point. Unlike CS1, the sample days for CS2 do not necessary get less accurate for larger amounts of storage and can therefore be used more consistently.

Figure 5.11 shows quite clearly why the sample days generally underestimate the amount of optimal storage. The curves for $\mathcal{E}_{\text{buy}}$ and $\mathcal{E}_{\text{FI}}$ are almost identical only shifted up and down respectively. The result is that the objective function curve has the same shape except shifted up for the sample days, and therefore the storage component is a slightly smaller portion. This results in the minimum being shifted slightly to the left, i.e. a smaller amount of storage.

It is very useful to use the sample days for an initial indication of trends, followed by the Two Stage algorithm for more precise evaluations of the total storage. Judging by these results using sample gives a good representation of placement, and an adequate representation of trends for total storage. It is not considered to offer a good approximation of total optimal storage.

5.5 Modelling inaccuracies and approximations

Various simplifications are utilised for all three versions of the planning algorithm, particularly regarding the grid equations. To ensure that all the limits are adequately met, and that the approximations are not severe enough to strongly impact the results for optimal storage, it is useful to verify them. Three simplifications are investigated in the following pages.

Section 5.5.1 examines the linearisation of the power flow equations for active and reactive line power. The purpose is to assess the errors in bus voltage and bus angles, particularly to ensure that the limits are not violated. The second simplification, addressed in section 5.5.2 assesses the hyperplane approximation of apparent power magnitude in order to maintain the line limits.

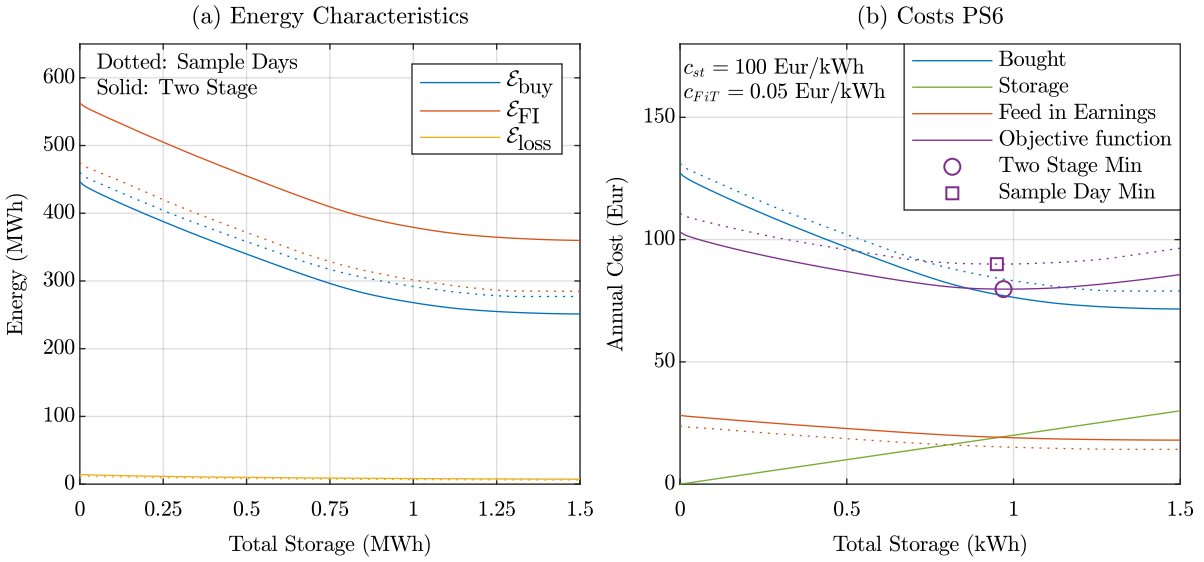

Figure 5.11: *Energy characteristics of the whole year in a solid lines, and dotted lines for the sample days in plot (a). Plot (b) shows the objective function evaluation for price scenario 6*

Finally section 5.5.3 investigates if it is possible to obtain similar results for optimal storage by neglecting the battery degradation in order to speed up the algorithm. Although degradation is an important aspect to consider for an operational algorithm, it is not clear if it will impact the planning of optimal storage. This is investigated by comparing results with and without a degradation mode.

For the simulations in this section, the sample day method is applied to CS2. This is sufficient as the sample days contain active voltage and line limits, for a simulation without curtailment. Therefore, the ability of the algorithm to maintain the limits can be demonstrated. CS1 is not used for verification, as the network constraints are not active.

5.5.1 Power Flow Approximation

The purpose of the approximation for power flow in a line shown in equations 2.33 and 2.34 is to linearise power flows, so as to incorporate them as linear conditions within an optimisation problem. Naturally this results in approximation errors, which can be verified by comparing the variables resulting from the optimisation problem to those calculated using the ACPF. For this the open source Matlab tool 'MATPOWER' is used, for solving steady state power system simulations [135]. MATPOWER solves ACPFs iteratively, solving the full line flow equations 2.23 and 2.24.

By adding the storage power P_{st} to the active loads at the respective nodes and subtracting PV, the net load at each node can be obtained and given to MATPOWER, which can then run an ACPF. The results give the accurate values for bus angles and voltages, as well as P_{gen} and Q_{gen}.

Figure 5.12 shows the bus voltage and angle errors for CS2 results for PS4. It is clear that the voltage errors follow a roughly a quadratic relationship with the voltage, which makes sense given the quadratic nature of the power flow equations. There also seems to be some correlation with the nodes, as the nodes in dark blue are shown to have relatively higher errors in part (a). The

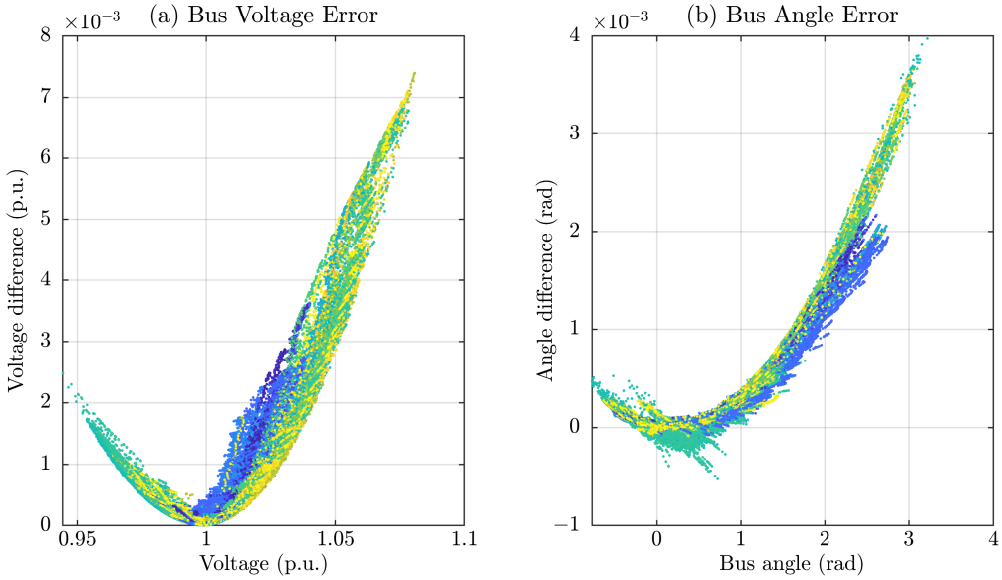

Figure 5.12: *The errors in bus voltage (a) and angle (b) are plotted as a function of the true voltage and angle respectively. The plot colour are scaled to the nodes, to see if there is a correlation between nodes and error*

angle errors are lower, and more varied than the voltage errors. Similarly to the voltage errors, they are node dependent. This is judged by the clustering of the turquoise plots with a negative angle error, and plot (a) indicates that these are nodes with undervoltage.

What is interesting to note is that the voltage error seems to be always positive, this means the approximation always gives a higher voltage than the real value. This is helpful information as it indicates that the upper voltage limits are more crucial and should be verified more carefully. In this case however the margin is high, and the distance to the upper voltage limit 1.1 p.u. is always sufficient. However this is not guaranteed for every simulation result and therefore the voltage should always be verified.

The accuracy is sufficient, and significantly better than the DC approximation would be, therefore the approximation is deemed to be acceptable for voltage and angle errors. The inaccuracies of the other variables such as P_{gen}, Q_{gen}, P_l and Q_l are even less severe than for voltage and angles.

5.5.2 Line Limits

The hyperplane approximation of the apparent power, and the leaving out of losses, results in errors in line power. The method used to enforce the line limits is described in Section 4.2.2. The method is conservative, and always overestimates the apparent power. To gain more insight, an example of active constraints is examined. Figure 5.13 shows active, reactive and apparent power flow in a line on a day where high PV feed-in causes the active power in the line to be very high.

There are several things to note. Firstly, the approximation is much more successful as the apparent power approaches the limit. The reason for this is clear from Figure 4.1, as the approximation errors for active and reactive power are very low near the limit. This is helpful, because the approximation allows the power to reach very close to the limit. For this approximation, an

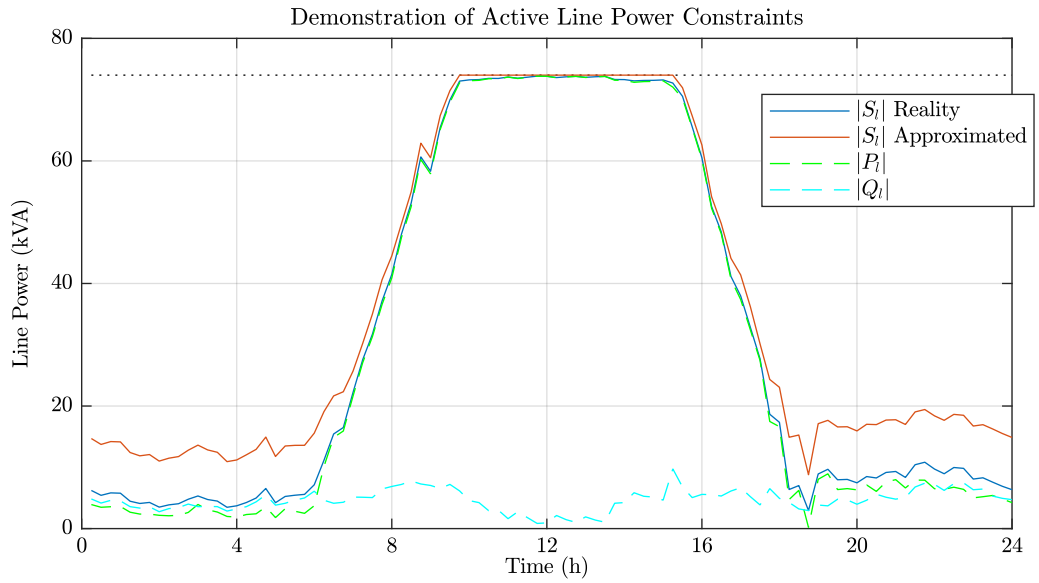

Figure 5.13: *Demonstration of the line power for a branch in the Case Study two sample day simulation on a day where the line constraint is active*

accurate representation of low powers is unnecessary.

The second point is that the high apparent power in the line is caused predominantly due to active power flow, and this is true for all the cases in CS2 where the line constraints are active. For many cases it is acceptable to neglect the line limits if it can be shown using MATPOWER that the line constraints are not active. This is particularly valid for the sensitivity studies that will take place in later chapters, as it can significantly speed up the iterations without damaging the integrity of the system limits.

Thirdly, line losses are absent from this plot, the reason is because they are so low that they cannot properly be visualised on the plot. For this branch the system losses add up to 0.6% of the active power, and so it is valid to neglect them from the calculation of line limits. Losses are however extremely important within the cost function as they allow the storage to be located most efficiently.

5.5.3 Battery Degradation

The impact of the degradation map is investigated to justify the neglect of the degradation in the sizing stage of the Two Stage algorithm. The effect of including the minimisation of degradation in the cost function on the outcome of optimal storage is examined, by taking the same price scenario (PS4) and running it excluding the degradation cost term. The degradation is then post-calculated using the degradation map applied to the charging power, SoE and battery capacity. The results of the sample day method applied to CS2 are shown in Figure 5.14.

The first thing that Figure 5.14 (a) shows is that the total storage is identical, and the effect on placement is minor as the results are very similar. The difference is seen in the smaller units. The algorithm without degradation has 40 battery units, whereas when degradation is included there are only 36. Four of the smaller batteries are suboptimal when degradation is taken into account. This makes sense when examining the degradation map shown in Figure 2.5, which

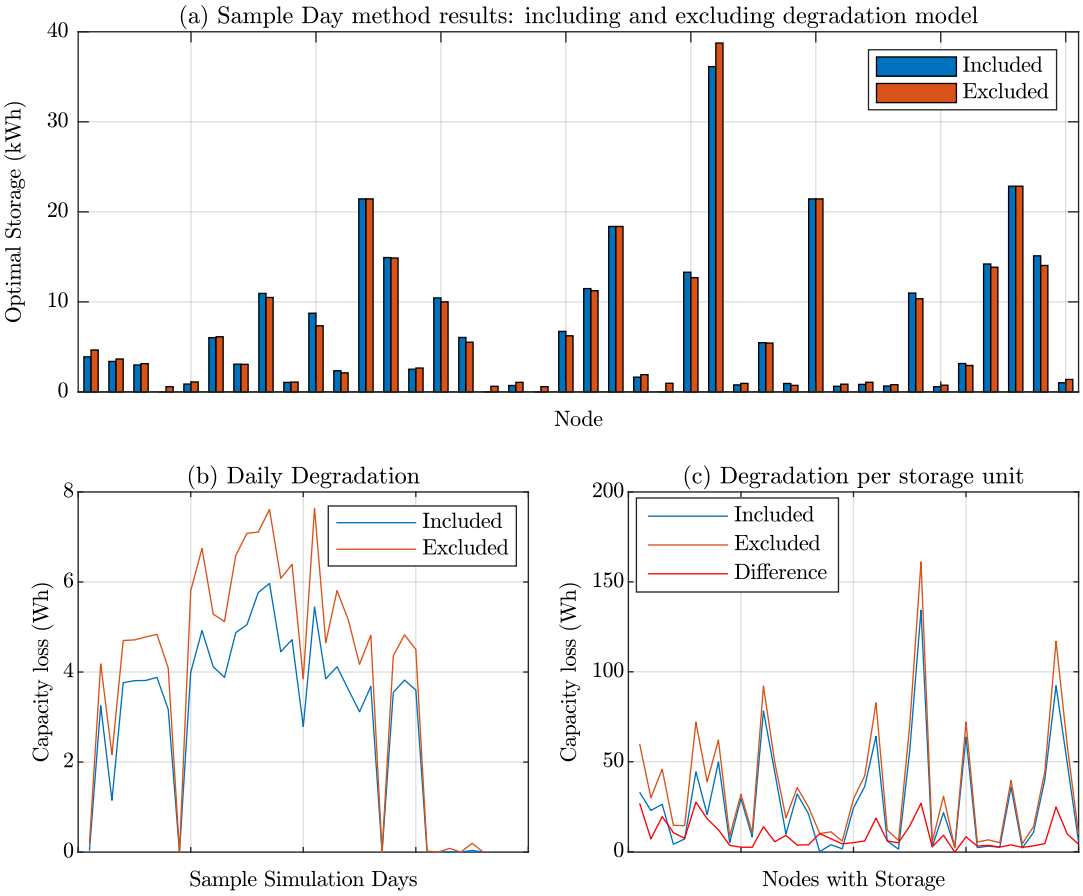

Figure 5.14: *The effect of the degradation on the planning result is demonstrated firstly in plot (a) with a comparison of optimal storage capacity when the degradation model is included and excluded. Plot (b) shows the total degradation for each of the sample days, and part (c) shows the difference in degradation per storage unit*

shows the degradation normalised to the capacity size. The steepness of the planes increases at higher operational ranges, and so it makes sense to apply smaller charging and discharging powers a larger unit to remain within the shallow plane where degradation is less.

Plots (b) and (c) show that the total degradation calculated is significantly lower when the degradation is included in the optimisation. From the plots it is clear that the savings are achieved more by certain units, independently of their size. The daily savings do not vary too much, and so it is more dependent on the operational strategy.

5.6 Time Resolution

So far in this thesis all simulations have been performed using a 15 minute time resolution. For a better understanding of the planning algorithm, it is worth comparing various time resolutions to examine their effect on optimal storage. Using the case studies, the three time resolutions that are tested are 1 minute, 15 minutes and 60 minutes.

It has been shown in chapter 2 that residential load profiles can look very different from 1 minute to 15 minute, and even more so from 15 minutes to 60 minutes, as shown in Figure 3.12. The main difference is that the spikiness is not represented for lower time resolutions.

Higher time resolutions result in larger optimisations problems, and therefore more computationally intensive algorithms. It has been previously stated that optimisation problems scale badly with the number of variables. Moving from a 1 minute to 15 minute time resolution, the necessary variables are 15 times less. Moving from 15 minutes to 60 minute requires 4 times less variables. The visual representation in Figure 3.12 shows a much more severe difference between 15 minute and 60 minutes for a single household. This is because most household loads are much shorter than 60 minutes, but can be captured well with 15 minutes. Although inaccuracy of load profiles increases with higher time resolutions, other dynamics are more robust. PV profiles for example, do not change significantly with the time resolution, as a one hour resolution is able to capture the important dynamics.

Within the context of planning, the objective is determining the required energy capacity, and short term spikes may have a smaller effect as they do not require much capacity to store. Furthermore, the planning algorithm charges the battery with perfect knowledge of load and PV. This is never the case for actual operation of a battery, as loads and generation can be difficult to predict. The optimality of the planning results are therefore only guaranteed for a hypothetical situation where the consumption and generation can be perfectly predicted.

Since the required capacity is the main outcome, short term spikes are relatively unimportant compared to longer periods of excess production. For high PV feed-in in distribution grids, longer times of excess production over several hours are likely to dominate the use of storage.

To investigate how time resolution impacts the optimisation results, the Two Stage algorithm is performed on CS1 for all three time resolutions. This yields the matrices $\mathcal{M}$ and energy characteristics $\mathcal{E}$, for each time resolution. The notation for the time resolution investigation includes a label of time resolution for $\mathcal{M}$, for example $\mathcal{M}_{\text{buy},60}$ refers to the bought energy matrix for the 1 hour time resolution simulation. Capital delta (Δ) is used to refer to the comparison of matrices $\mathcal{M}$. For example, $\Delta\mathcal{M}_{15-1}$, and $\Delta\mathcal{M}_{60-15}$ refer to the differences between these matrices for

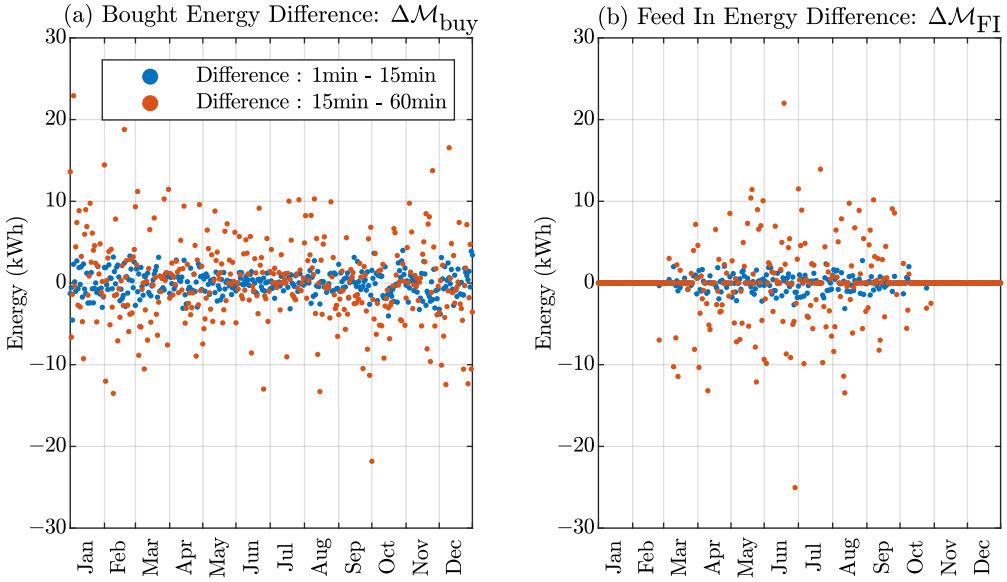

Figure 5.15: *Difference in a single row of $\mathcal{M}_{buy}$ and $\mathcal{M}_{FI}$ for the Two Stage algorithm performed with the different time resolutions. The row depicted above is characterised by: $E_{tot} = 34kWh$*

each time resolution.

It is found that the energy characteristics $\mathcal{E}$ are almost identical, therefore they are not plotted. This means that the results for annual optimal storage will be extremely similar, indicating that all three time resolutions are suitable and produce the correct results. More insight can be gained by examining the individual optimisation results, $\mathcal{M}_{\text{buy}}$, $\mathcal{M}_{\text{FI}}$ and $\mathcal{M}_{\text{loss}}$.

It is useful to examine the values of a single row of $\Delta\mathcal{M}_{\text{buy}}$ and $\Delta\mathcal{M}_{\text{FiT}}$ for both time resolution comparisons. This is shown in Figure 5.15, where all days of the year for one size of E_{tot}, in this case 34kWh. The results show that there are significantly more differences between the 60 minute and the 15 minute time resolution results. The daily variations do not obviously seem to be skewed positively or negatively, both variations seem to centre around 0 and this explains why the energy characteristics $\mathcal{E}$ do not change.

The fact that the 60 minute to 15 minute resolution results in many more errors over the days is interesting because the relative amount of data lost is much less than the difference between 15 minutes and 1 minute. This can be explained by the load characteristics. Chapter 3 showed that many event based household loads have durations of less than 60 minutes. Although there are also many activities with durations of less than 15 minutes, the reduced time length also means that the energy consumption is less. As a simple example, a 10 W load approximated from 1 minute as 15 minutes has an error in energy consumption of 2.3Wh, whereas approximated from 15minutes to 60 minutes is a 7.5Wh difference.

Figure 5.15 shows that although there are differences between the subproblems of the Two Stage algorithm when using different time resolutions, they may not have a significant impact on the result for optimal storage due to averaging effects. To verify this, the mean and standard deviation of $\Delta\mathcal{E}_{\text{buy}}$, $\Delta\mathcal{E}_{\text{FI}}$ and $\Delta\mathcal{E}_{\text{loss}}$ are plotted against E_{tot} for each of the characteristics. The results are shown in Figure 5.16.

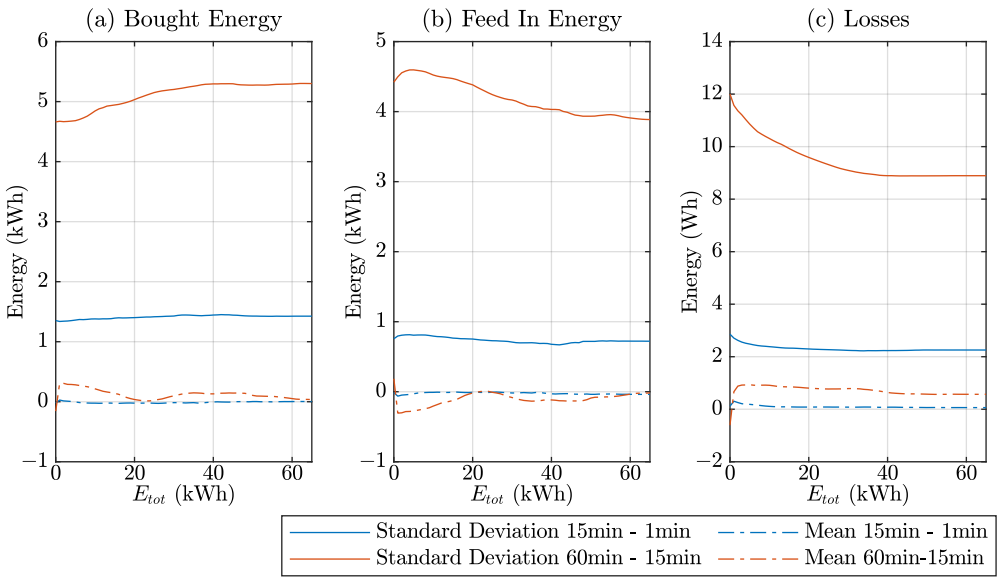

Figure 5.16: *Standard deviation and mean for the difference between the matrices* $\mathcal{M}_{buy}$, $\mathcal{M}_{FI}$ *and* $\mathcal{M}_{loss}$ *for each of the rows*

The results show that the mean for the difference between 15 minutes and 1 minute is always zero, which implies that the energy characteristics $\mathcal{E}$ will be very close or identical, resulting in the same results for optimal storage. Although the mean for the difference between the 60 and 15 minutes has more variation, it is still relatively small and does not affect the energy characteristics much. Figure 5.16 also shows the standard deviation for the 60 to 15 minutes difference to be much higher, meaning there is much more variation between most results and the mean.

It is not possible to carry out the Two Stage algorithm using a time resolution of 1 minute on CS2, as it is too time intensive. Comparing the difference between the Two Stage algorithm using 15 minutes and 1 hour shows an even smaller difference than for CS1. This can be explained due to the increased averaging effect of more loads.

To summarize the results of the investigation into time resolution, the Two Stage algorithm shows on that on a daily basis, the dynamics show minor differences between 15 minute and 1 minute time resolutions, and slightly more significant differences between 60 minutes and 15 minutes. These errors are random, and over the 365 days average out to have an insignificant effect on the sizing. A time resolution of 15 minutes captures the most important dynamics of residential loads, and a time resolution of 1 hour captures the most important dynamics of PV profiles. Since self-consumption of excess PV is the main financial benefit of storage, the 1 hour results are considered sufficient. When more details are required for examining the dynamics within a day, for example examining voltage issues, a 15 minute resolution may yield more accurate and detailed information.

Chapter Summary

In this chapter a heuristic alternative to the annual optimal planning algorithm is presented that can be applied to much larger networks, named the Two Stage algorithm. The applicability of this algorithm is discussed, and prerequisites for system behaviour are identified. The results are verified using the same case study as the annual algorithm (CS1). A second case study (CS2) is introduced with more complexities and active constraints that allow various modelling approximations to be verified.

- The Two Stage algorithm decomposes the optimal planning algorithm into a sizing problem and a placement problem that are executed sequentially. The sizing algorithm breaks down the large annual problem into many subproblems, firstly by decomposing the annual problem into daily problems, and secondly by iterating the daily problems over a range of fixed total storage values. Within the considered range of cost scenarios, the output of the sizing stage is independent of costs and can be used to evaluate optimal storage at any cost scenario. The placement stage involves fixing the total storage as determined by the sizing algorithm, and optimising over a number of sample days to obtain the optimal locations for battery units.
- The same sample days used for the placement stage can also be used for both sizing and placement to approximate optimal planning results. This method is referred to as the sample day algorithm.
- Using the case study presented in the previous chapter, the results for both the Two Stage algorithm and the sample day algorithm are compared to the annual problem from chapter 4. Both algorithms are shown to approximate the optimal results well, although the Two Stage algorithm outperforms the sample days consistently.
- The sub-optimality of the sample day method is shown to result from a lack of variety in troughs and peaks for the storage within the shorter duration.
- The Two Stage algorithm has the additional benefit of producing outputs that are independent of costs, and can therefore be used to evaluate a wide array of price scenarios at once. Cost independent results are useful for analysis, as the full results for optimal storage are highly sensitive to prices.
- Various modelling approximations are investigated in more detail, including:
  - The effect of the power flow linearisation on the errors in bus voltages and angles. The approximation is shown to be acceptable by comparing the optimisation results to those of the full AC power flow
  - the hyperplane approximation is shown to be effective in enforcing the limits on apparent power, by demonstrating an active constraint on a line
  - The inclusion of battery degradation is shown to have a negligible effect on optimal sizing, and a minor effect on optimal placement
- The results for optimal storage using three commonly used time resolutions are compared: 1 minute, 15 minute and 60 minute. The difference between 1 minute and 15 minutes is shown to be minor. The important dynamics are mostly captured by a 15 minute time resolution and the remaining differences average out throughout the year. The difference between 15 minute and 60 minutes is more significant in terms of dynamics, although the averaging effect is still very strong and results in negligible differences in optimal storage results.

Chapter 6

Cost Analysis

The algorithms used in chapters 4 and 5 determine the amount of storage at each node that minimises the total monetary cost for the network as a whole. For this type of welfare evaluation, the amount of optimal storage is strongly affected by the ratio of the various prices used in the objective function. In this case the electricity price, the cost of battery storage and the Feed-in Tariff (FiT) for renewables. Real world prices are highly variable and unpredictable parameters, as they generally vary from year to year, between countries and based on the application. Electricity prices and FiTs are determined by regulation and can be interdependent, as is the case in Germany. Battery prices are more market driven, and are changing rapidly due to technical advancements and push from the automotive industry.

For this reason it is very difficult to make general and definitive statements about the economic profitability of storage. The investigations in this work focus on using simulations of one year to gain insight into the profitability of storage in the short term. The objective of this work is not to predict future prices and make conclusive calculations on where storage should be installed, rather to gain insight into how certain trends might affect the profitability and use of battery storage.

Even though prices are changeable, there are some pronounced trends that can be investigated through simulations. It should be noted, that for a complete investigation of profitability, storage needs to be compared with other technologies that offer similar benefits. One commonly investigated option for load shifting is Power to Heat. This refers to the control of electrically powered heat pumps that use thermal storage or the internal storage of building stock, to offer flexibility. Another common contender is the use of batteries in electric vehicles (EV) attached to charging stations to offer flexibility. These options have great potential, however they involve many limitations. Implementation of heat pumps is limited by their application potential, as it is generally only possible for new buildings, or recently renovated buildings. EV charging for load shifting is not a very mature technology, and is an expensive investment for the end user. Battery storage is currently the only technology that can be implemented without significant change in infrastructure and investment from the end-user. It is therefore reasonable to investigate the profitability of storage without considering competing technologies.

6.1 Feed-in Tariff

Feed-in tariffs (FiT) are a highly important factor in determining the economic viability of storage in distribution networks. High FiTs reduce the financial incentive to increase self-consumption of locally generated energy by load shifting. FiTs have generally been introduced to increase distributed renewables. FiTs were essential for incentivising distributed generation, as it offered

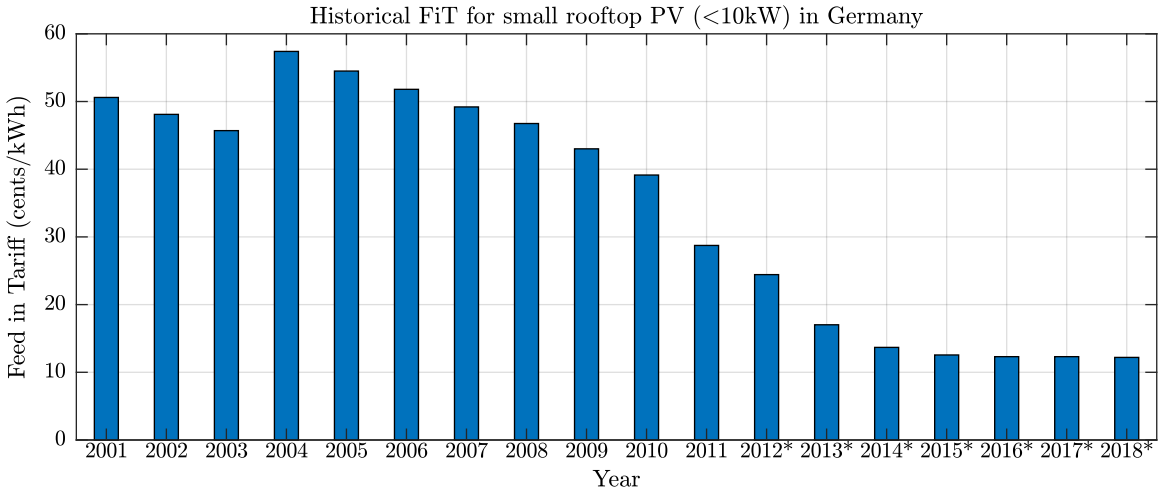

Figure 6.1: *Historical values for the FiT in Germany since their introduction in 2001, since after 2012 the FiT varies slightly between months, a corrected annual value is used for this graphic [6]*

financial benefit beyond simply reducing energy bills. This is particularly true for PV as the coincidence of household load and PV generation is usually quite low. Until recently, battery storage was too expensive to be considered profitable for load shifting.

Renewable energy support schemes vary significantly within Europe. In most countries, FiTs are offered, sometimes in combination with subsidies and tax incentives. FiTs themselves can be characterised by the amount, cap, and eligibility period. The amount, given in €/kWh, can vary with size of installation, location, and type of renewable energy. Many countries implement a cap to limit the amount of compensation that can be offered for renewable generation, and there are many ways to implement this. For example, Austria sets an overall annual support budget for renewable electricity, whereas in France there is an annual cap on each installation calculated by peak installed capacity multiplied by 1500 hours of full load [6]. Eligibility period refers to the term of guaranteed compensation. In Europe they generally vary between 10 and 25 years, in many countries the eligibility period is 20 years (including Germany, France, and Portugal) [136].

As PV installation costs have decreased, the FiTs have also decreased consistently since their introduction at various rates. As one of the global leaders in solar power production, and by far the largest producer of solar power in Europe [137], Germany is an important country to consider. Germany's FiTs are dependent on plant size and type of renewable generation, reflecting their respective costs. The first German FiT (EEG) was introduced in 2000 and it has been amended several times. It has also been extremely successful at increasing the amount of renewables, particularly distributed PV, in the system. The development of the FiT in Germany for small rooftop PV (<10kW) is shown in Figure 6.1. The FiTs for PV are reducing faster than those for any other type of renewable energy [138]. The EEG has undergone many revisions since 2000, with a defining revision taking place in 2017 which aimed to control the growth of RES by defining an expansion corridor [138]. Under the EEG 2017, self consumed PV energy is taxed above a nominal power of 10kW, increasing the PV electricity generation cost.

The mechanism for renewable compensation works by reflecting the cost within the electricity price. In 2018 the EEG portion amounted to 23% of the final electricity price. A key feature of the EEG is that it guarantees a term of 20 years, which ensures that owners of PV installations

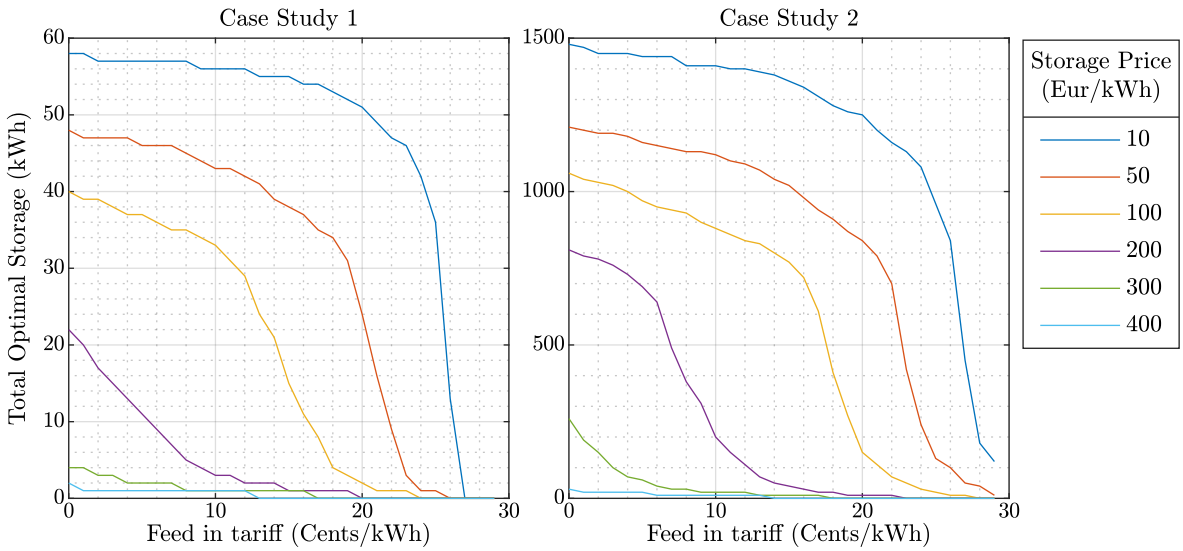

Figure 6.2: *Results for the planning algorithm applied to Case Study 1 and Case Study 2 for a range of storage costs and FiTs. The total optimal storage in the network is plotted against the FiT*

have investment security. Currently, the end of the 20 years is coming up for the first set of beneficiaries who received very high FiTs.

The projections for lowering FiTs, results in a higher incentive to self-consume energy that has been locally generated. Since storage can assist with increasing self-consumption, it is useful to investigate the effect of FiT on the total optimal storage (E_{tot}). This can be easily performed using the energy characteristics $\mathcal{E}$ produced by the sizing stage of the Two Stage algorithm, shown in Algorithm 2. The method for calculating E_{tot} by calculating the objective function can be repeated across the range of FiTs.

Figure 6.2 shows how total optimal storage changes with FiT for a range of storage prices, both for CS1 and CS2. The dependency of the curve on total storage is immediately clear, judging by how different the curves are in each sub-plot.

From Figure 6.2, it is clear that optimal storage does not have a linear relationship with FiT. For lower storage prices, ($\leq$€ 100) there seems to be a plateau where the FiT hardly affects the optimal storage even as it approaches 0. Clearly, storage prices between € 10 and € 50/kWh are unrealistic and unlikely to become available in the near future, but they are included in the plot to show the plateau behaviour. For higher storage prices the amount of optimal storage increases slowly but more consistently with lowering FiT. For high storage prices ($\geq$ € 300/kWh), the FiT does not matter much, there is very little economic incentive to use storage at all.

The trend is similar for CS1 and CS2, although batteries seem to be more profitable for CS2 in general. This can be seen as lower a FiT results in relatively more storage even for high storage prices like € 300/kWh. Furthermore at a storage cost of € 100/kWh there is a relatively strong case for storage at a FiT of € 0.16/kWh already, whereas for Case Study 1 it requires the FiT to be less than €0.12/kWh. The difference between the case studies is related to the fact that PV penetration is higher in CS2.

A few general statements can be made regarding FiT sensitivity. Firstly, the FiT sensitivity is

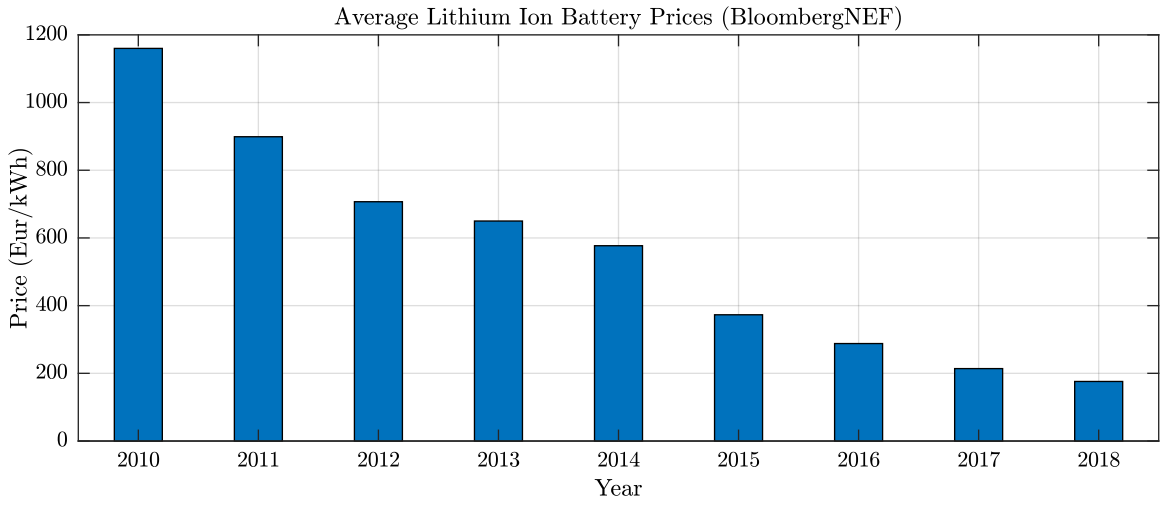

Figure 6.3: *Bloomberg New Energy Finance calculations for average price of Lithium Ion Batteries [7]*

highly dependent on storage prices. For many storage prices, there is a region of steep increase followed by a region of more gradually increase. This indicates that at some point the additional storage does not yield much marginal benefit. The fact that the plateaus are at different levels depending on the storage prices is investigated more in Section 6.2.

6.2 Battery prices

It has already been shown in this thesis that battery prices are important for planning cost optimal storage. Unfortunately, it is difficult to formulate a realistic battery price model. The continuous battery model does not reflect reality in terms of representing available buying options. Nevertheless, it is useful for simulations, particularly for examining trends. Although the discrete price model can be used to reflect more realistic current prices, it does not help with examining trends. For example if the simulations in Section 6.1 on FiT sensitivity would have used a discrete price battery model using todays prices, the analysis would have been less clear. The following paragraphs address trends in battery prices, and simulations for sensitivity to battery prices using the continuous price model.

Lithium Ion batteries have seen some of the highest growth, out of all the battery chemistries available on the market. Lithium Ion batteries are used within various industries, the largest of which is passenger electric vehicles (EV). The EV market is the strongest driver for lowering battery prices [131]. Electric busses and consumer electronics are also a growing market although not as large as personal vehicles. Solar batteries fall under the category of stationary storage, along with grid support storage and community storage.

To add some insight, it is worth trying to understand the trend in battery prices in more detail. Studies universally state that battery prices have significantly decreased in the last 10 years, and are expected to fall further. One of the most commonly cited sources is the Bloomberg New Energy Finance database, from which the cost patters for lithium ion batteries are accessible at [7]. The Bloomberg study uses the average price of all lithium ion batteries sold, across all industries and for both industrial and end user customers. The prices published, along with

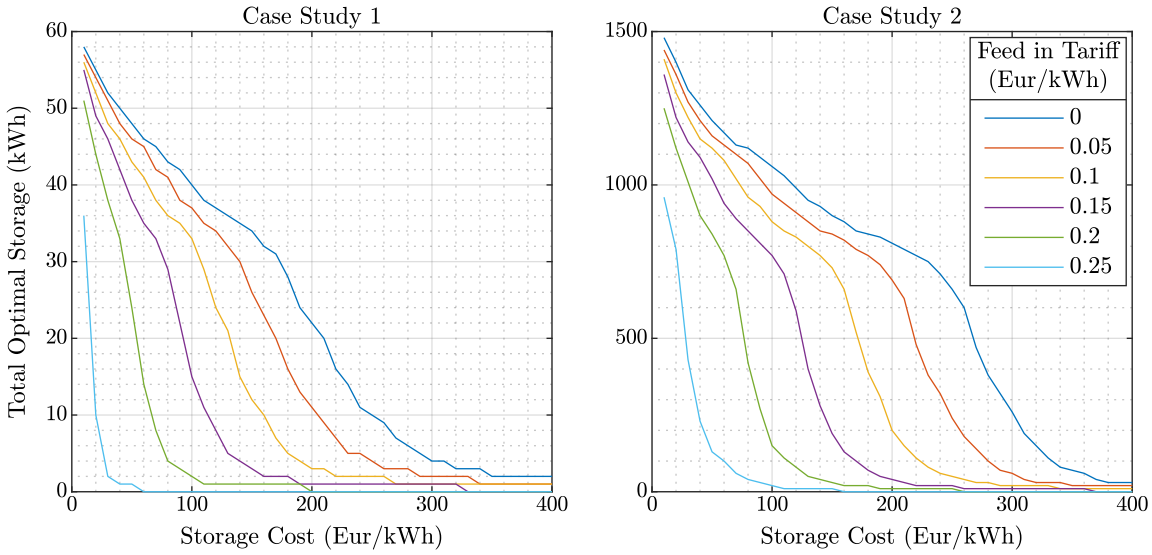

Figure 6.4: *Case Study 1 and Case Study 2 sensivity of total optimal storage to storage cost assuming a battery lifetime of 5 years*

future projections are shown in Figure 6.3. The Bloomberg study also found that lithium prices were rather insensitive to short term fluctuations in underlying metal prices (lithium, nickel, cobalt and aluminium).

Another commonly cited study in 2015 [139] addresses ways in which lower prices can be achieved. Two major recommendations are intelligent policy makingm, and R&D in materials research. The recommendations are based on various data sources, including the progress of battery storage prices with the number of relevant patents, and global R&D spending.

Although the average lithium ion battery prices are reducing rapidly, the prices that are accessible to private customers buying solar batteries are not reflected by the Bloomberg prices. The per kWh prices determined by Bloomberg are heavily skewed by large scale electric vehicle buyers like Tesla and Volkswagen, and the bargaining power of individuals buying stationary batteries is much less. For this reason it is necessary to perform a market study to determine the actual available offers for commercial solar batteries. This topic will be addressed in section 6.3.

Since the studies indicate clearly that the average cost of lithium ion batteries is decreasing and likely to continue doing so, it is useful to examine the effect this has on optimal storage using the continuous price model. For various FiTs the price sensitivity is shown in Figure 6.4 for CS1 and CS2. The results are interesting as they are more regular and predictable than the sensitivity to FiT shown in Figure 6.2.

The annual planning algorithms in this theses are based on 20% of the capital cost of storage. This can be interpreted as a linear depreciation using a lifetime of 5 years. Since many battery lifetimes are upto 10 years, 20% is a rather conservative calculation. Since the prices are changing so rapidly, and future predictions of load and PV are also very uncertain, the focus of this techno-economic study is short term profitability. For this reason a linear depreciation over 10 years was avoided, and a more conservative number was used.

Visually it is also clear that for CS2 there is a broader spread of viable price ranges, confirming

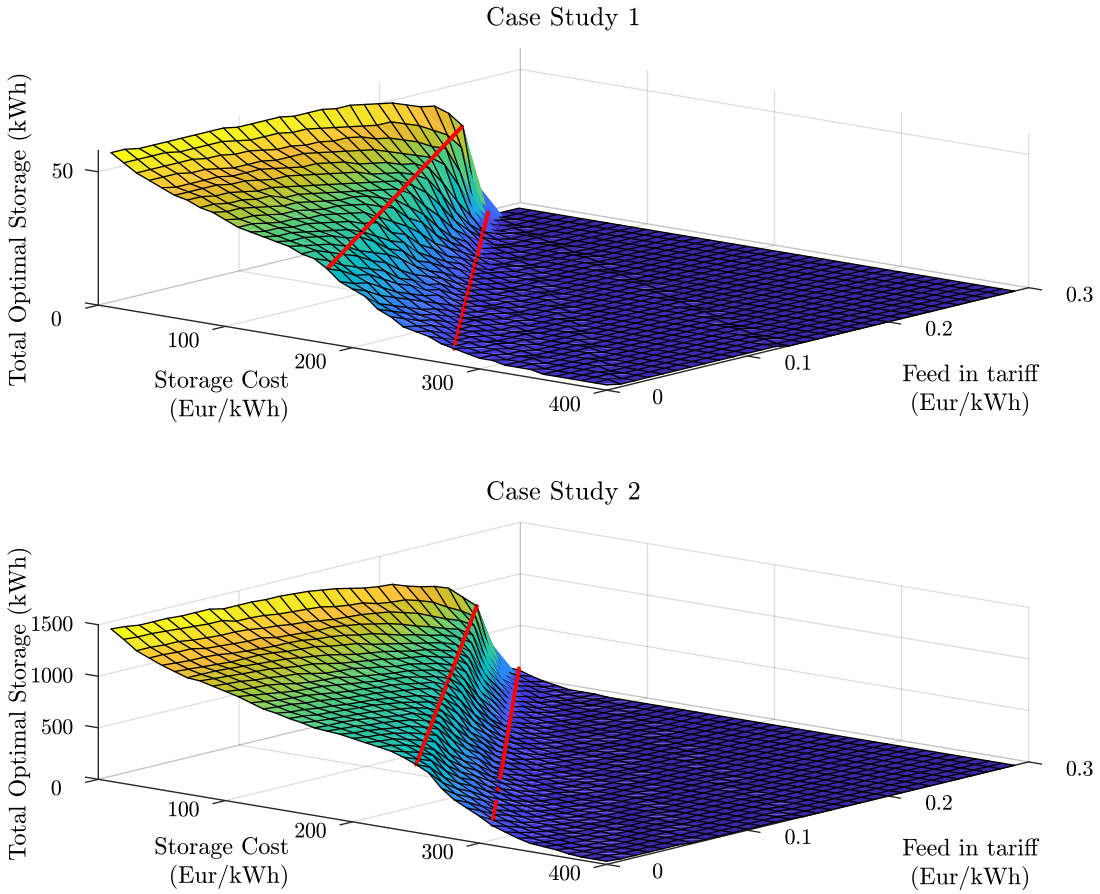

Figure 6.5: *Surface plot of optimal storage results for Case Study one varying both the FiT and storage cost, based on 20% of capital cost of storage*

once again that more PV results in a stronger financial case for storage. Depending on the FiT the gradient crosses a threshold of where the profitability increases rapidly until it reaches around 28 kWh - 35 kWh for CS1 and 750 kWh for CS2. Then there is a section with a slower gradient that increases till the maximum. For both case studies the result seems to converge for low storage costs, where the FiT does not have much relevance unless it's very high. This is likely due to the reduced opportunities throughout the year to use the high storage capacity. Fewer opportunities for load shifting such large quantities means that the FiT is less important, as the potential profits of additional storage are low anyway.

Since FiT and storage cost sensitivity are so interlinked, the results of the Two Stage algorithm can be used to construct a cost sensitivity surface, as shown in Figure 6.5. The cost surface is extremely useful for visually comparing different simulation outcomes, as it yields much more insight than the optimal storage for a single price scenario. The cost surfaces are used extensively in Chapter 7, and the ability to construct them is one of the major strengths of the Two Stage algorithm.

Figure 6.5 clearly visualises the existence of two gradient areas, where the turning point seems to be around 28-35 kWh for CS1 and 750 kWh for CS2. A likely cause of this is that number of peaks and troughs exceeding this value are less numerous, and therefore marginally less profit is gained from additional storage. Secondly for higher FiTs (more than € 15/kWh), storage prices

need to drop extremely low to add any significant value. Profitability of batteries are therefore only achievable in situations where FiTs are lower than this. For very low FiTs (less than 5 cents/kWh), the amount of optimal storage increases much more gradually.

The investigations into sensitivity to FiT and storage costs have highlighted a number of points. The combined trends of lowering storage prices and FiTs result in higher economic viability of battery storage. The current FiT does not result in a strong case for battery storage for the case studies. The next section will touch on the realistic prices that are available for stationary storage, showing current prices are higher than €500/kWh. Using a depreciation of 20% of the capital costs per annum is conservative, and batteries not being profitable. Although a linear depreciation over 10 years would result in a 10% annual cost, poor predictions into future profitability make this a questionable approach.

Lowering the FiT, not only increases the viability of storage by making self-consumption more profitable, it also makes the profitability of storage increase more gradually with falling prices. Significantly reduced FiTs are therefore key to the success of battery storage used purely for self-consumption.

Finally, it is clear that there is no single price point at which storage becomes profitable as it is highly case study specific. There is strong indication from these results that the profitability of storage highly depends on the amount of PV in the system. This is investigated in chapter 7.2.

6.3 Realistic Solar Home Battery Options

Since the continuous price model is not a realistic reflection of the prices available for batteries in the market, the planning algorithm can incorporate the discrete price model in order to assess the optimal choice out of a discrete series of size options and associated prices. The MIQP implementation is demonstrated using CS1. The issue with the discrete model is that the introduction of integer variables results in an extremely slow algorithm that is unsuitable to use with larger networks like CS2. Furthermore, using discrete prices makes it very difficult to compare the different price options of various suppliers. In the following pages an overview of the various suppliers of new batteries is provided, as well as a short investigation into second life options for batteries.

Market Study Solar Lithium Ion Batteries

In this section the prices offered by a few of the major suppliers of solar home batteries are investigated. Furthermore, the limitation of using an optimisation algorithm to choose between different suppliers is shown. The various prices and suppliers that will be discussed are shown in Figure 6.6.

The most well known installation for solar home batteries is the Tesla Powerwall [140], which was announced in 2015 with a pilot project. As of March 2019 the only battery size available 13.5kWh. Although the battery comes with a built in inverter it is not possible to purchase the battery alone. The Powerwall comes with many supplementary technologies including control software and an app. It is difficult to compare the cost of the Powerwall to other battery manufacturers, although the battery and inverter costs are €6850 which is competitive with the other

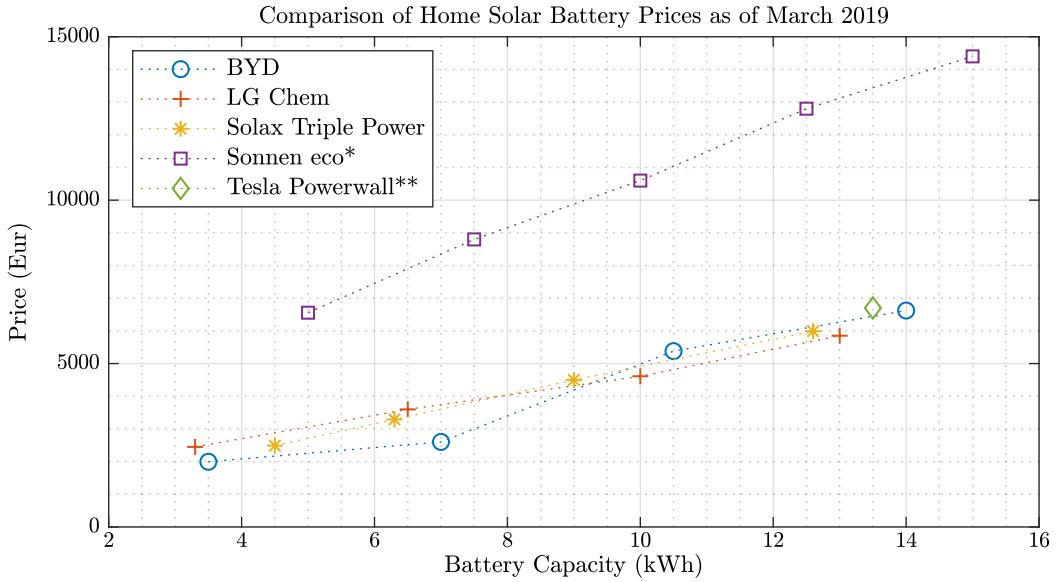

Figure 6.6: *Price comparison of some of the major suppliers of lithium ion batteries for solar applications, prices available with online retailers on 21.03.2019. *Sonnen eco batteries have an built in inverter, and it was not possible to find the price of the battery alone. **The Tesla Powerwall cannot be bought as a standalone battery, the entire system equipment cost €8800, although this does not include mandatory installation costs*

battery manufacturers, the additional hardware costs €2000 and installation costs are estimated to be between €1100 and €3300. Nevertheless the Tesla Powerwall is the most established product in the field of solar batteries.

Another popular supplier, particularly in Germany, is Bavaria based company Sonnen, of which the most competitive range is the Sonnen *eco*. Again, the Sonnen product range is very difficult to compare that of the other companies as the batteries come with a built in inverter and many other features. The Sonnen system is modular with units of 2.5kWh, and more units can be retrofitted based on the needs of the customer. Installation is region dependent and no price estimation is published. It also offers the possibility to participate in a community tariff that can reduce electricity prices by utilising the excess PV of others in the community.

Another interesting company is Solax, which offers a range of technologies supporting solar installations, such as inverters and batteries. The batteries are compatible with their inverters which have a very wide price range depending on their specifications. Solax only offers 2 sizes of batteries of 4.5kWh and 6.3kWh, of which upto 4 of the same units can be connected in parallel.

The other two companies shown in Figure 6.6: BYD and LG Chem are supplied without inverters. For all three the most commonly recommended inverter is the SMA Sunny Island which costs upwards from €1860 depending on the size and specifications.

It is important to understand that the planning algorithm using the discrete price model is still a purely cost based optimisation and has no way to evaluate the non-financial relative merits of each battery manufacturer. Therefore when choosing between two manufacturers it will always choose the cheapest. From the information above it is clear that there are many more factors to consider when choosing battery supplier besides the prices. Sonnen has a very expensive

Table 6.1: *Comparison of Home Battery Lines*

	BYD	LG Chem	Solax	Sonnen	Tesla
Battery line Name	Battery Box	RESU	Triple Power	Eco	Powerwall
Size Range (kWh)	2.5-13.8	3.3 - 13	4.5-25.2	5-15	14
Price Range (€/kWh)	473-570	450-742	475-553	960-1311	507
Warranty (years)	10	10	10	10	10
Max Continuous Power (kW)	2.5-13.8	5	2.5-5	1.5-3.3	5
Cell chemistry	LFP	NMC	NMC	LFP	NMC
Round trip Efficiency	0.95	NA	0.95	0.98	0.9
Depth of Discharge	100	100	90	100	96
Built in Inverter	No	No	No	Yes	Yes

range, but offers many services along with the modular battery and an expected lifetime of 20 years. The Tesla hardware is extremely competitive, but does not offer any variety of sizes or any modularity, and the installation costs may be disproportionately high. The Solax batteries are modular but only in a limited way. When considering any of the manufacturers above, great consideration should be taken in understanding the associated costs of additional hardware and installation. A number of such properties are listed in Table 6.1.

It is not within the scope of this work to determine the best battery manufacturer, and it is important to note that the algorithm in chapters 4 and 5 are sizing and placement algorithms. They are more suitable to select the sizes and locations of battery units once a suitable manufacturer has been selected. For discrete price models it is also useful to keep the number of options small because MILPs and MIQPs scale badly with the number of integer variables. For each size option a vector of integer variables the length of the number of candidate nodes is required. For a reasonable optimisation problem size, it is only suitable to use the planning algorithm to decide which sizes are most profitable after a manufacturer or battery series has been decided upon.

One more aspect that is difficult to incorporate into the modelling, but can dramatically effect the profitability of battery storage is the availability of external funding. There are many countries where governments offer subsidies or other finance options for battery storage in conjunction with renewable generation. In Germany the main source of finance is the KfW (Kreditanstalt für Wiederaufbau), who have a program regarding renewable energy (KfW 270), and additionally a specific credit program for battery storage until the end of 2018 (KfW 275). Currently, there is still the option to include battery storage under the KfW 270 program although the available funds may be less. In Germany there are also local programs that may offer grants for battery installation. For example, the Bavarian program called EnergieSystemHaus, which offers a €1000 - €3000 technology bonus grant for grid supportive PV including batteries. Incorporating grants into the optimisation is not reasonable as the exact grant accessibility is very specific to each installation.

Second Life Batteries

Besides buying new solar home batteries from any of the manufacturers listed in 6.1, another interesting market segment is the second life market for batteries which have experienced a first life in the electric vehicle industry. This market is still extremely young, with no conclusive patterns or trends that allow clear predictions to be made on the future. A number of major studies have been carried out to investigate the industry both quantitatively and qualitatively.

A major report was published by Circular Energy Storage which is not freely available, although some of the conclusions were summarized and published by the Global Battery Alliance and are freely available at [141]. An older report published by NREL in 2016 is more focussed on barriers to second life use with a specific re-purpose application of grid support and peak shaving [142].

Second life batteries are generally re-purposed either for commercial home storage systems, or for grid support. One commonly proposed use is reinforcement of charging infrastructure for EVs to reduce the burden on the grid. The alternative to reuse is recycling, where chemicals such as Lithium, Cobalt, Nickel and Graphite are extracted from the batteries for raw material use in new batteries. This process is costly and does result in some waste, therefore the second life could still be considered a more cost effective option. From an environmental perspective, it is more sustainable to utilize the batteries for an additional number of years before recycling.

The process of remanufacturing involves several stages including: removal of the battery from the EV, performance of a quality analysis on the components, any required adjustments, and the redeployment itself. Many of these stages are costly, and require infrastructure that would probably be provided by the battery manufacturer. A detailed cost analysis was undertaken by the NREL study [142], although the uncertainty is large as it depends on the future development of the market.

There are many stakeholders in the second life market that have various economic interests. The EV manufacturers have an incentive for second life storage, as the battery is still the single largest cost component of the EV, and a second life would reduce the cost hurdle of EV. On the other hand, re-manufacturing batteries for other applications does incur costs which would be overtaken by the re-manufacturer. Nonetheless many EV manufacturers are investing in second life schemes and demonstrations [141].

The NREL study found that there was little economic benefit for owners of EVs to replace batteries before the lifetime of the vehicles themselves. The lifetime is estimated to be 15 years with a reduced battery capacity of 70%. The other consideration is that a battery replacement is also an upgrade for the vehicle, particularly considering the rapid improvements that taking place in the battery market. Being able to drive longer distances between charges may be a good incentive for EV owners to replace their battery when it is still in a reasonably healthy condition. This may result in a large flood in the market of batteries with 5-7 years of use [141].

Buyers of home energy storage may be able to procure second life batteries at a lower cost than new batteries. However, as with any second hand purchase, there is a risk attached as the capacity and lifetime are perceived as unknown. Furthermore, it is acknowledged that the rapid reduction in battery costs is a barrier to the second life market.

The use of second life batteries could result in many environmental and economic benefits. It is currently unclear to which extent second life batteries can be expected to enter the market in terms of volume, price and application. There are some critical steps that could be taken to increase the uptake of second life batteries, such as a standardization of manufacturing of batteries that include onboard diagnostics of battery health. Furthermore, there are policies that can be implemented to provide impetus to the market, as investigated in [143].

There is much to be investigated regarding the second life market, and the studies cited provide much more insight. For the purpose of this work it is sufficient to state that second life

batteries offer a potential source of low cost batteries, that can profitably be used to increase self-consumption. The uncertain future of the second market make it difficult to investigate the planning aspect more concretely.

MILP simulation

To investigate the functioning of the discrete price model, a number of simulations are carried out using the LG Chem battery range, plotted in Figure 6.6. The sample day algorithm is used, as an annual problem with integer variables is too computationally intensive. The Two Stage algorithm is not compatible with the discrete price model. The LG Chem selection for battery sizes and prices is shown in table 6.2.

Table 6.2: *LG Chem Battery Range*

$\mathcal{S}$ - Capacity (kWh)	3.3	6.5	10	13
$\mathcal{P}$ - Price (€)	2450	3598	4612	5853
Price per kWh (€)	742	553	461	450

Table 6.2 shows that the battery price per kWh varies with the unit size. This makes comparison of results to the continuous price simulation very difficult. For example, using the cost surface in Figure 6.5, the CS1 optimal storage for a FiT of € 0.05/kWh and storage price of €742 is 1kWh. Amongst the discrete storage options, 1kWh is not listed. The discrete price optimisation results show a 3.3kWh unit at node 13. This is an interesting result as 13 is not even a storage node for the continuous version. This is likely because the continuous model would have divided the storage between nodes 14 and 16, but since the division was not possible, a single unit was placed at node 13. What is interesting is that 3.3kWh is more economical than no storage at all.

Based on the results for the price scenarios in Figure 4.3, the continuous price model does places units of 6.5kWh or greater for price scenarios 3, 5 and 6. This means that the price needs to be lower than 300 €/kWh for an FiT of 5cents/kWh. The results of the discrete simulation can be compared to the continuous one by reducing the real prices in 6.2 by 60% and optimising the system with an FiT of € 0.05/kWh. This means a unit of 3.3kWh costs 300 €/kWh. The result is quite different from the continuous price model, as it places a 3.3kWh at node 13 same as 100 the previous simulation.

The discrete price implementation takes between 8 and 18 hours per simulation using the sample day method for CS1. For CS2 it is not possible to do a network level optimisation using MILP. The results only show that current prices result in a very low amount of storage. This does not mean that there is no case for storage at current prices, only that there is no case for distribution level energy saving.

Chapter 7

Scenario Analysis

The algorithms presented in Chapter 5, as well as the method of constructing cost surfaces presented in Chapter 6 can be used to analyse various scenarios that affect optimal planning of battery storage. In this chapter, a number of scenarios are investigated using the Two Stage and sample day algorithms applied to CS1 and CS2. Comparison results often reference the base case, which refers to the results of the Two Stage algorithm presented in Chapter 5. Section 7.1 addresses the topic of changing grid parameters with two investigations. Firstly, the effect of line upgrades of problematic branches, and secondly the modification of the slack bus voltage. Section 7.2 investigates the effect of increasing PV feed-in, both by scaling the total PV in the grid, and by introducing one large new installation in the grid. Finally in Section 7.3, the topic of placement strategies is addressed. Three different placement scenarios are compared, to generate insight into the difference between centralized and decentralized storage.

7.1 Grid parameters

The two grid issues that are investigated are overcurrent and over-voltage. Both issues occur in the CS2, for system simulations without any storage or curtailment. PF calculations applied to CS2 over a year show that there are 10 branches that exceed their current rating if PV is not curtailed. Overvoltage has been shown to be a time-related issue in Figure 5.7, affecting many nodes in the system.

The location of the branches that suffer from overcurrent is shown in Figure 7.1(a). It is clear that there are certain lines that are more problematic than others, and that the issue is mostly concentrated closer to the substation. This makes sense, as these branches carry current from multiple PV sources whose peaks coincide with one another. As shown in Figure 7.1 (b), overvoltage affects a significant portion of the grid. Nodes that reach voltage levels above 1.1 pu are located entirely in the upper half of the network, and concentrated towards the end of the lines. The entire upper half of the network reaches voltage levels above 1.05 pu, along with many nodes in the lower half. This indicates that if the tolerance for voltage fluctuation reduces, due to a higher slack bus voltage, the grid is likely to face severe issues.

From the frequency of constraint violations, it is clear that overcurrent is a minor issue compared to overvoltage. The results in Chapter 5 show that the planning algorithm manages the constraints by introducing storage and curtailing PV depending on the prices. A closer look at the storage outcome, for example in Figure 5.8, shows a strong correlation between storage placement and overvoltage.

Having shown that the planning algorithm effectively eliminates the grid issues of overcurrent

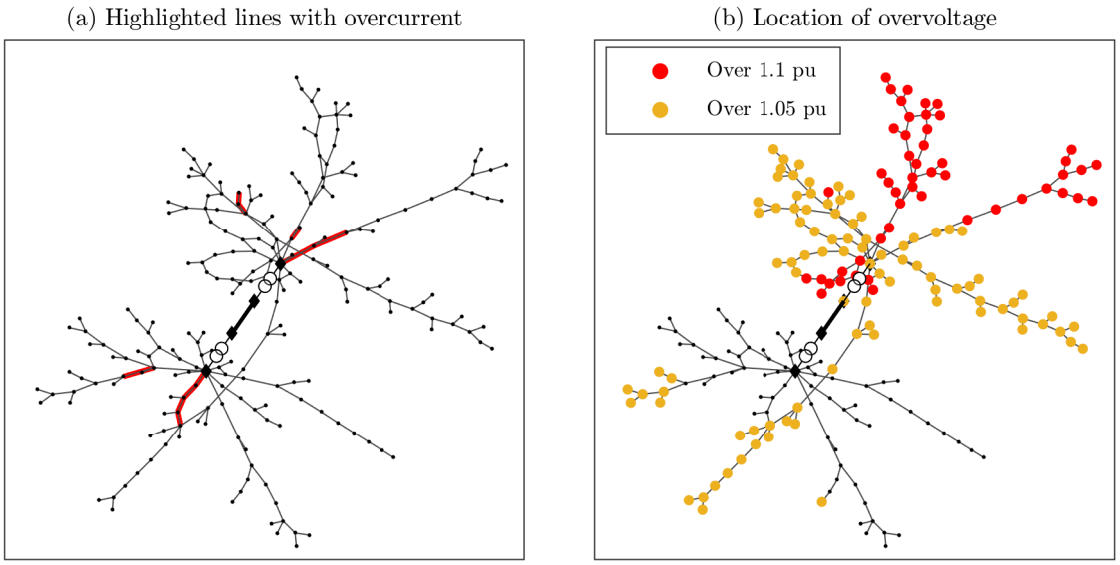

Figure 7.1: *In a PF simulation with no storage and no curtailment, plot (a) shows the lines that have overcurrent and plot (b) shows the location of nodes that face overvoltage*

in Section 5.5.2 and overvoltage in Section 5.5.1, it follows that the algorithm can shed light on the effect of changes in the grid parameters on the optimal storage. The two scenarios that are simulated in this section, are line upgrades and an adjustment of the slack bus voltage.

Line upgrades are implemented by modifying the lines highlighted in Figure 7.1 (a) by doubling their power rating, and halving the resistance and reactance. This represents an identical parallel line being laid next to the existing one, for a very simple representation of a line upgrade. The objective is to identify whether this will reduce the amount of optimal storage in the network.

The change in voltage setpoint is implemented by adjusting the slack bus voltage to 1.05 pu. This means that the constraint of the upper limit of node voltage (1.1 pu) is much more severe. The possibility of a change in slack bus voltage is not only high, it is also likely to coincide with times of high PV feed-in. Although the slack bus voltage may be as high as 1.07 pu [144], it is shown that even raising it to 1.05 pu has a significant impact on optimal storage.

Since the planning algorithms in this thesis use an objective function that aims to reduce curtailment as much as possible, it is worth first examining the effect on curtailment of upgrading lines and increasing the voltage setpoint. Curtailment can be calculated by running an MPOPF on CS2 without any storage, thereby identifying how much PV needs to be curtailed in order to maintain the network limits. The results are shown in Figure 7.2. The base case has a little curtailment in the summer months, that sums up to 0.5% of the total PV generation. Line upgrades do reduce the curtailment slightly, although the effect is minor. The change in voltage setpoint has a more significant impact, and the simulation results in the curtailment of 9.6% of total PV generation. More importantly, the curtailment is much more spread throughout the year.

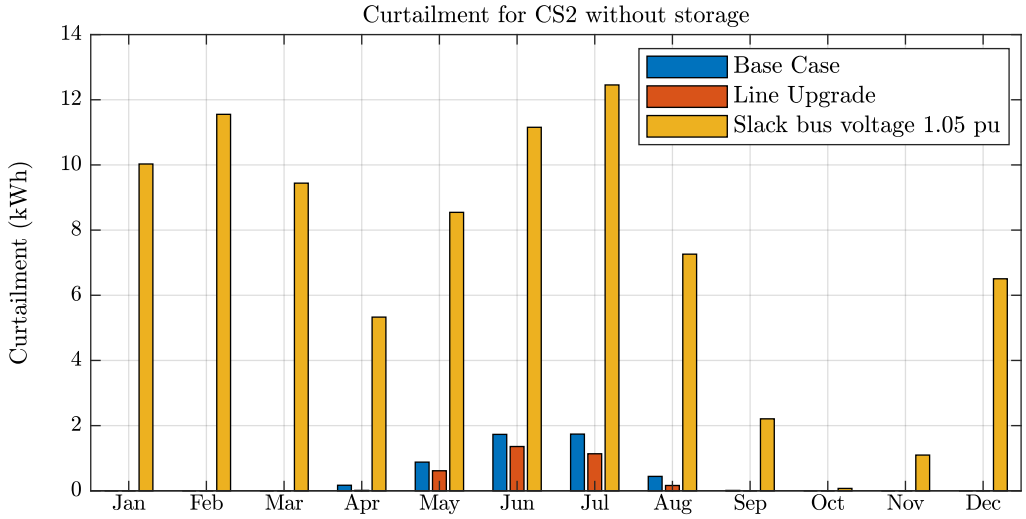

Figure 7.2: *Optimal Power Flow with no storage in the network results in curtailment of PV to maintain limits*

7.1.1 Effect of Line Upgrades

The line upgrades are implemented by doubling the apparent power rating, and halving the resistance and reactance of the problematic branches indicated in Figure 7.1. The Two Stage algorithm is applied to CS2 with line upgrades, and the total optimal storage calculated for all six price scenarios. The system upgrade is effective, as the MPOPF without storage has no more active line constraints. The curtailment shown in Figure 7.2 for the line upgrade is due to voltage constraints. The total optimal storage and curtailment for the upgraded system is detailed in Table 7.1. The curtailment should be compared to the MPOPF without any storage, which is 0.4%. Line upgrades reduce voltage at some nodes, as the line resistances are higher and there is less voltage difference across those lines. For CS2, this is the reason that curtailment reduces from 0.5% to 0.4%.

Table 7.1: *Line upgrade simulation for all six price scenarios, including the total storage and the storage increase compared to the base case in chapter 3, and the total curtailment.*

PS	Storage Cost €/kWh	Feed-In Tariff €/kWh	Total Network Storage kWh	Storage Decrease Percentage	Curtailment Percentage (max 0.4%)
1	230	0.12	24	2.1	0.24
2	150	0.12	406	5.9	0
3	100	0.12	775	2.6	0
4	230	0.05	277	4.8	0
5	150	0.05	775	1.0	0
6	100	0.05	957	0	0

The difference in optimal storage between the line upgrade simulation and the base case is relatively minor, with the highest difference in total storage being 5.9% for PS2. The curtailment is already completely eliminated with the 589 kWh in PS2, and after this there is not a lot of incentive to significantly increase the amount of storage compared to the base case.

The main conclusion that can be drawn from these simulations is that for this particular case study, line upgrades will not make a big difference to the optimal storage as they do not signif-

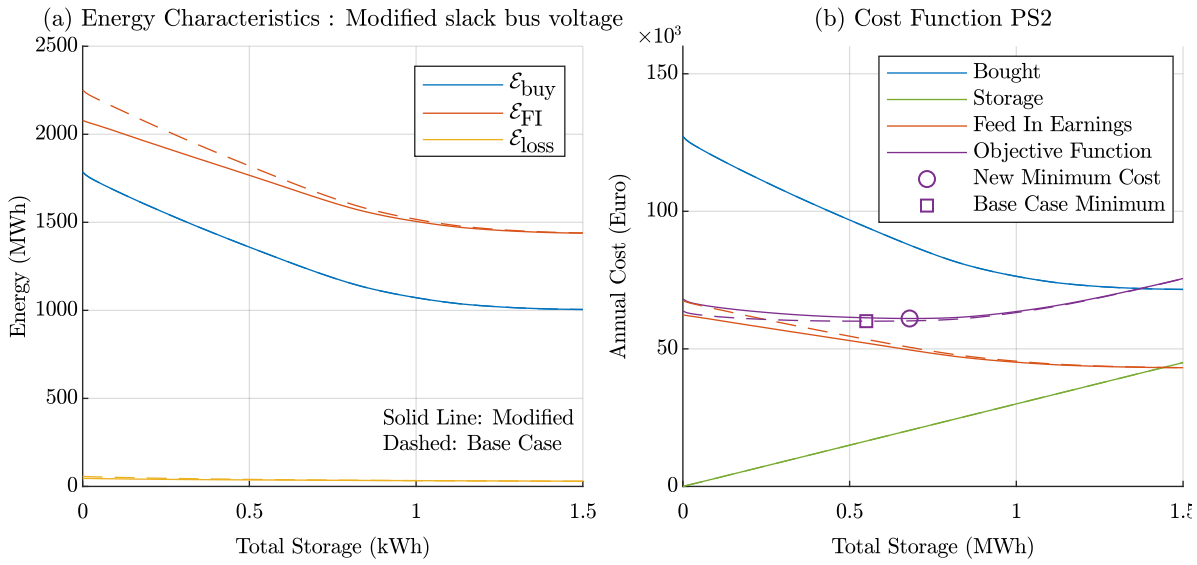

Figure 7.3: *Results of the Two Stage algorithm for the energy characteristics (a), and an evaluation of the cost function for PS2 in (b). The dashed lines show the corresponding results for the base case results*

icantly change the amount of PV that can be used. There is a small reduction in the amount of storage for the more expensive scenarios, as slightly less storage is required to eliminate curtailment. A different grid where the line current capacity is severely limiting the amount of PV would likely have different results.

7.1.2 Increased slack bus voltage

An increase in slack bus voltage during times of high feed-in is a likely scenario, as there is likely to be voltage rise in the medium and high voltage grid levels [144]. For CS2, a change in the slack bus voltage has a significant effect on the amount of curtailment, as shown in Figure 7.2. This has a significant effect on the optimal planning result, as the opportunity cost of curtailment (i.e. feed-in earnings) is a component of the cost function.

Since the sample days have a lower than average requirement for curtailment, using the sample day algorithm skews the results. Furthermore, it is interesting to examine the cost sensitivity of the system with a different slack bus voltage. For this reason the Two Stage algorithm was applied CS2 with a slack bus voltage of 1.05 pu.

The sizing stage results give the energy characteristics $\mathcal{E}$ as a function of the total storage in the system. Similarly to the base case, a range of total storage was used from 0-150kWh, with 10kWh increments. In Figure 7.3 the energy characteristics are compared to those of the base case. It is immediately obvious that the curtailment can be seen in the gap between $\mathcal{E}_{\mathrm{FI}}$ for the modified simulation and the base case. For the base case, $\mathcal{E}_{\mathrm{FI}}$ has an identical shape to $\mathcal{E}_{\mathrm{buy}}$, indicating that the storage shifts energy from being fed into the grid to being locally used. For the modified simulation, the shape of $\mathcal{E}_{\mathrm{FI}}$ is different, indicating that less PV feed-in enters the system. With higher amounts of storage, the difference in $\mathcal{E}_{\mathrm{FI}}$ between the two simulations reduces.

An example of the impact the change in $\mathcal{E}_{\mathrm{FI}}$ has on the objective function value is shown in Figure 7.3 for PS2. The difference in the feed-in earnings propagates to the value of the objective function, resulting in a new optimal storage of 550 kWh. From Figure 7.3(a) it is clear that at 550 kWh there is a significant difference in $\mathcal{E}_{\mathrm{FI}}$ between the two simulations.

Figure 7.3 indicates that the effect of increasing the slack bus voltage on optimal storage will be significant for scenarios where the total amount of storage is low ($<$ 550 kWh), as this is where there the difference in curtailment is most significant. In other words, there may be scenarios where storage is not very financially viable for the base case but for the increased slack bus voltage case it becomes viable due to reduction of curtailment. This can be further examined by determining the total optimal storage for each of the Price Scenarios, as shown in Table 7.2. Even though the optimal storage is calculated using the Two Stage algorithm, the curtailment in 7.2 refers to the curtailment seen during the sample days. This is because the curtailment compared here is a result of the placement stage.

The results mostly confirm that the differences are higher for smaller amounts of total storage, with PS1 showing a 175% increase in storage to the base case. The results reduce significantly going to 2% or less for PS3, PS5 and PS6. This can be explained by examining the difference in curtailment. Without storage, the MPOPF over the sample days shows that 4.33% curtailment is required to maintain limits. The difference between PS4 and PS6 for example is only 0.02% in curtailment despite there being 130kWh more storage in the system.

Table 7.2: *Modified slack bus voltage simulation results including aggregate network storage, the comparison to the base case in chapter 5, and the total curtailment.*

PS	Storage Cost €/kWh	Feed-In Tariff €/kWh	Total Network Storage kWh	Storage Increase Percentage	Curtailment Sample Days Percentage (max 4.33%)
1	230	0.12	110	175	2.74
2	150	0.12	680	23	0.53
3	100	0.12	860	2	0.42
4	230	0.05	430	13	1.25
5	150	0.05	840	0	0.54
6	100	0.05	990	2	0.44

Impact on Cost Sensitivity

To get a better idea of the relationship between increased slack bus voltage and the cost sensitivity, the energy characteristics calculated by the Two Stage algorithm are used to construct a surface plot of the cost sensitivity, similarly to Figure 6.5. The result is shown in Figure 7.4 (a).

The shape of the surface has not significantly changed compared to the base case in Figure 6.5 (b), the upper threshold is exactly the same, 1.48 MWh. This is expected as Figure 7.3(a) shows that the difference between the simulations are most pronounced for low levels of storage. The range of viable storage costs has also not significantly changed, with little to no financial case for battery storage if it costs more than 300 €/kWh. On the other hand, the sensitivity to the FiT has changed significantly. For the base case there was almost no case for storage for high FiTs, above 0.2 €/kWh, even if storage is very cheap.

A graphical representation of the difference is shown in Figure 7.4(b), which plots a surface of the difference between the cost sensitivities. The result confirms that the sensitivity to FiT has

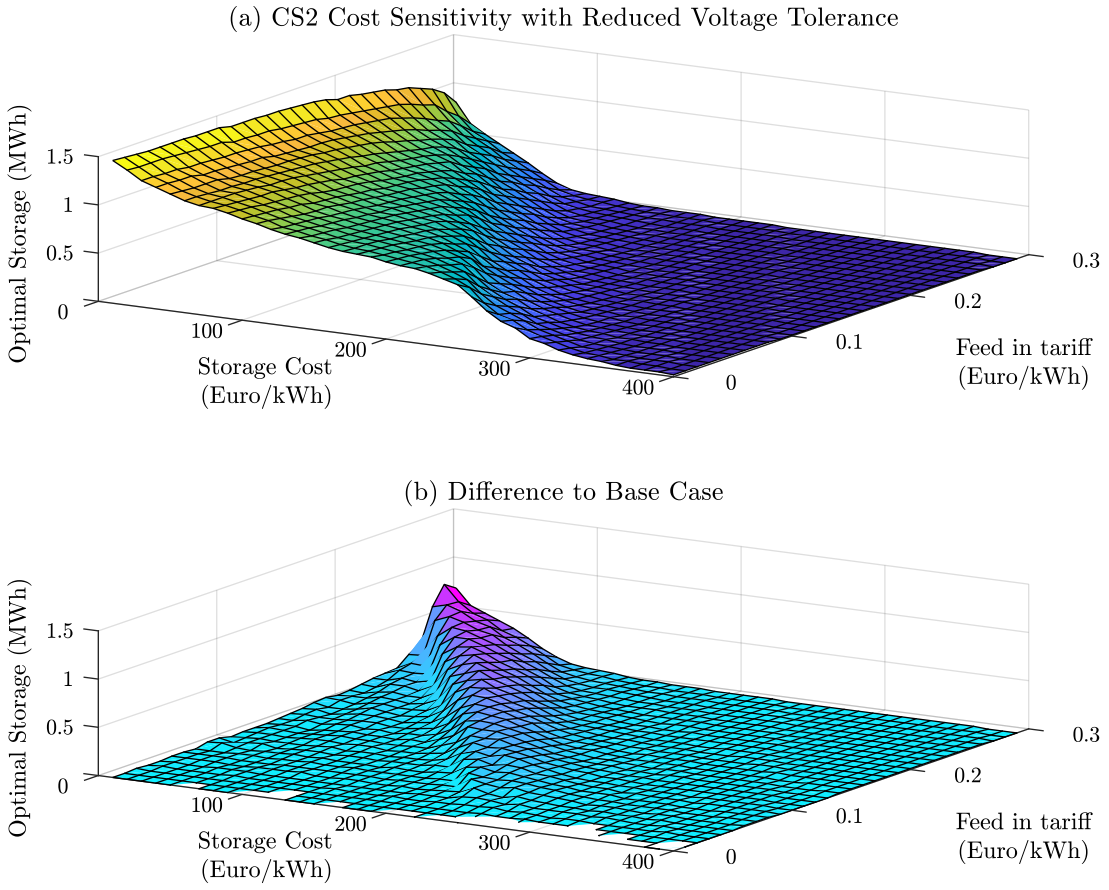

Figure 7.4: *Cost Sensitivity of the simulation with reduced voltage tolerance (a) and the difference to the base case (b)*

changed, as for higher FiTs there is now a case for storage where previously there was not. One way of interpreting this result, is that under certain cost conditions, there is a new financial case for battery storage to reduce curtailment, whereas under the previous conditions the major case for battery storage was increasing self-consumption.

The difference is highly dependent on the costs. The highest difference is seen at an FiT of 0.28€/kWh, which is unrealistically high. Even for the currently realistic FiT €0.12/kWh, a increase in slack bus voltage results in a much more financially attractive case for small amounts of storage (<110kWh).

As storage gets more expensive, the difference is eliminated, and the upfront storage cost outweighs the potential profit from reducing curtailment. This can also be seen in terms of the energy characteristics and cost function breakdown in Figure 7.3. For PS2, the feed-in earnings are still a significant portion of the objective function. If the storage cost were to be much higher, the storage curve would have a much higher gradient and dominate the shape of the objective function, with the feed-in earnings being relatively insignificant.

For the results in Figure 7.3 and Table 7.2 no other measures against voltage rise are included in the simulation. This is because the goal is to investigate the effectiveness of battery storage to alleviate overvoltage issues. In reality, another practical measure against overvoltage is reac-

tive power compensation using PV inverters. Since PV installations are generally connected to the grid using inverters anyway, the benefit of this approach is that no additional hardware is required.

A simple comparison is carried out by allowing each PV node to supply the grid with reactive power. It is assumed that every PV installation is equipped with an inverter that can operate at a power factor of 0.95. This translates to an allowed reactive power injection in the range of ±33% of the active power feed-in. The Two Stage algorithm is applied to CS2 with this additional degree of freedom, and with a slack bus voltage of 1.05 pu. The results show that the energy characteristics are identical to those of the base case presented in Chapter 5, meaning that the additional storage to avoid curtailment is not required if reactive power compensation is available for free. In reality this form of reactive compensation is not completely without cost, as additional inverter capacity is likely to be required. However, the purpose of this simulation is not to compare batteries to reactive power compensation, but rather to definitively show that if alternative, cheaper measures are employed to reduce overvoltage, the effect of an increased slack bus voltage on optimal storage is negligible.

Impact on Placement

So far the impact of changing the slack bus voltage on the sizing stage has been investigated, i.e. the difference in total storage E^*_{tot}, including the difference in cost sensitivity. A difference in results is also observed for placement within the network. The amount of optimal storage in the network, even if it remains the same as the base case, is relocated. Instead of minimising losses, it is now used to maintain voltage limits. This can best be demonstrated by plotting the network storage for the two cases for a price scenario where there is very little difference in the total storage. The effect of modifying the slack bus voltage is shown by plotting the optimal storage for PS1-3 in 7.5 and PS4-6 in 7.6 for both the base case and the modified results.

It is clear that there is a significant difference in the placement of the storage within the network. Firstly, battery capacity has been relocated from the lower half of the network to the upper half for PS2-6. This is because the upper half has shown to suffer from overvoltage in Figure 7.1 (b). The second point to be made is that the storage is much more distributed. All the modified results have more storage nodes, even if the total storage has not significantly changed. This is particularly clear for PS3 and PS5, where the modified simulation results have fewer large units (>40 kWh), but more units in total.

Finally, it is also clear that as the amount of storage increases the difference in placement also reduces. The relocation of storage from the lower to the upper half is most noticeable in PS 1, 2, and 4. For PS6 both the sizing and the planning results are almost identical. This is because the amount of storage in the network is high enough to cope with the voltage issues anyway.

Sine the placement algorithm was only carried out for the six price scenarios, these were also used to ensure the effectiveness of the voltage approximation for the reduced voltage tolerance. All the results are verified using MATPOWER to ensure that the actual voltages remain within the limits, despite the approximation error. This is an important step, as unlike the base case simulations, every single one of the modified simulations include active voltage constraints.

The conclusions based on the results of these simulations are that reducing the voltage tolerance can change the amount of optimal storage only when the amount of curtailment can be signifi-

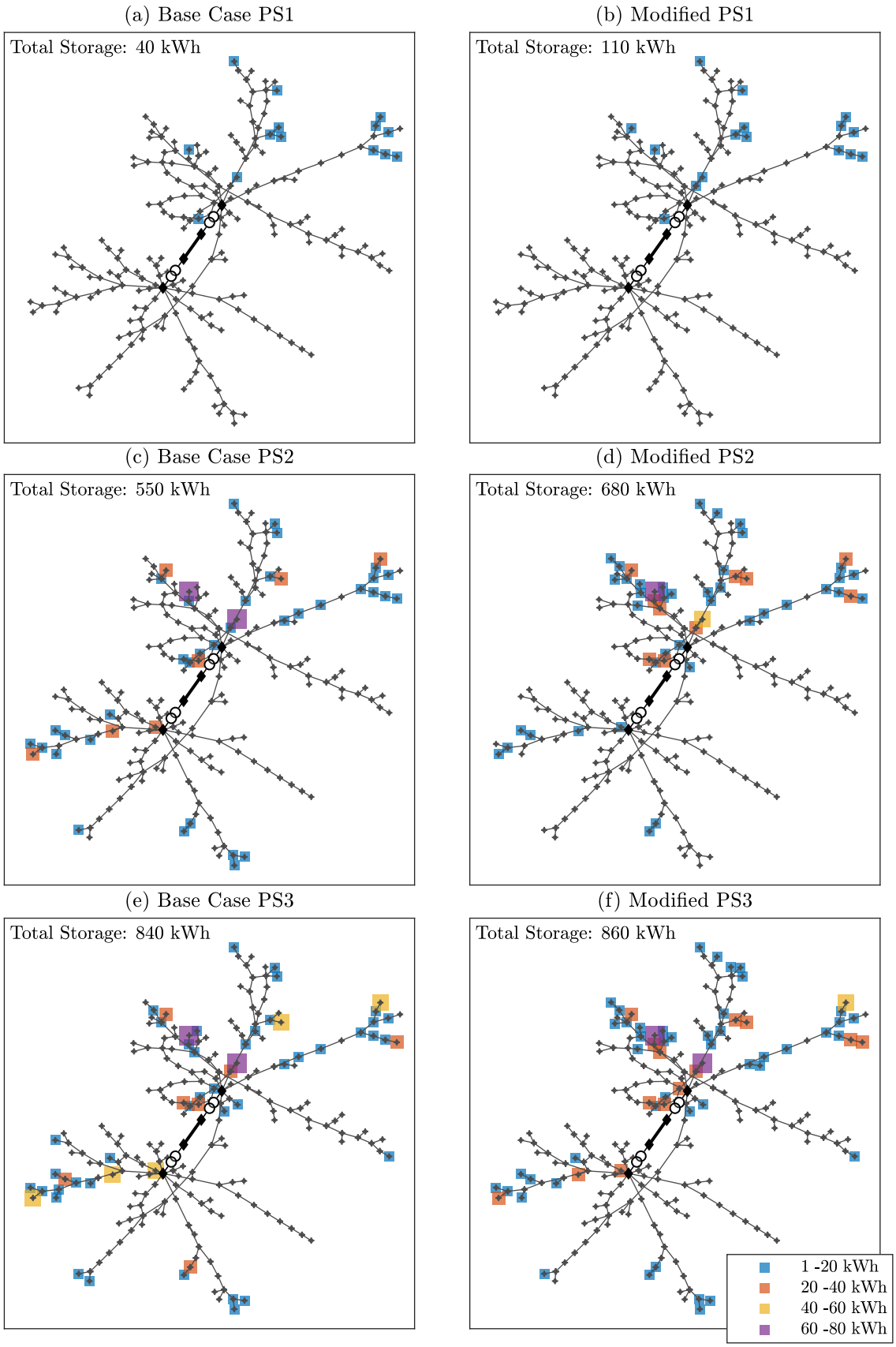

Figure 7.5: *Effect of modifying the slack bus voltage to 1.05 pu in for PS1-3*

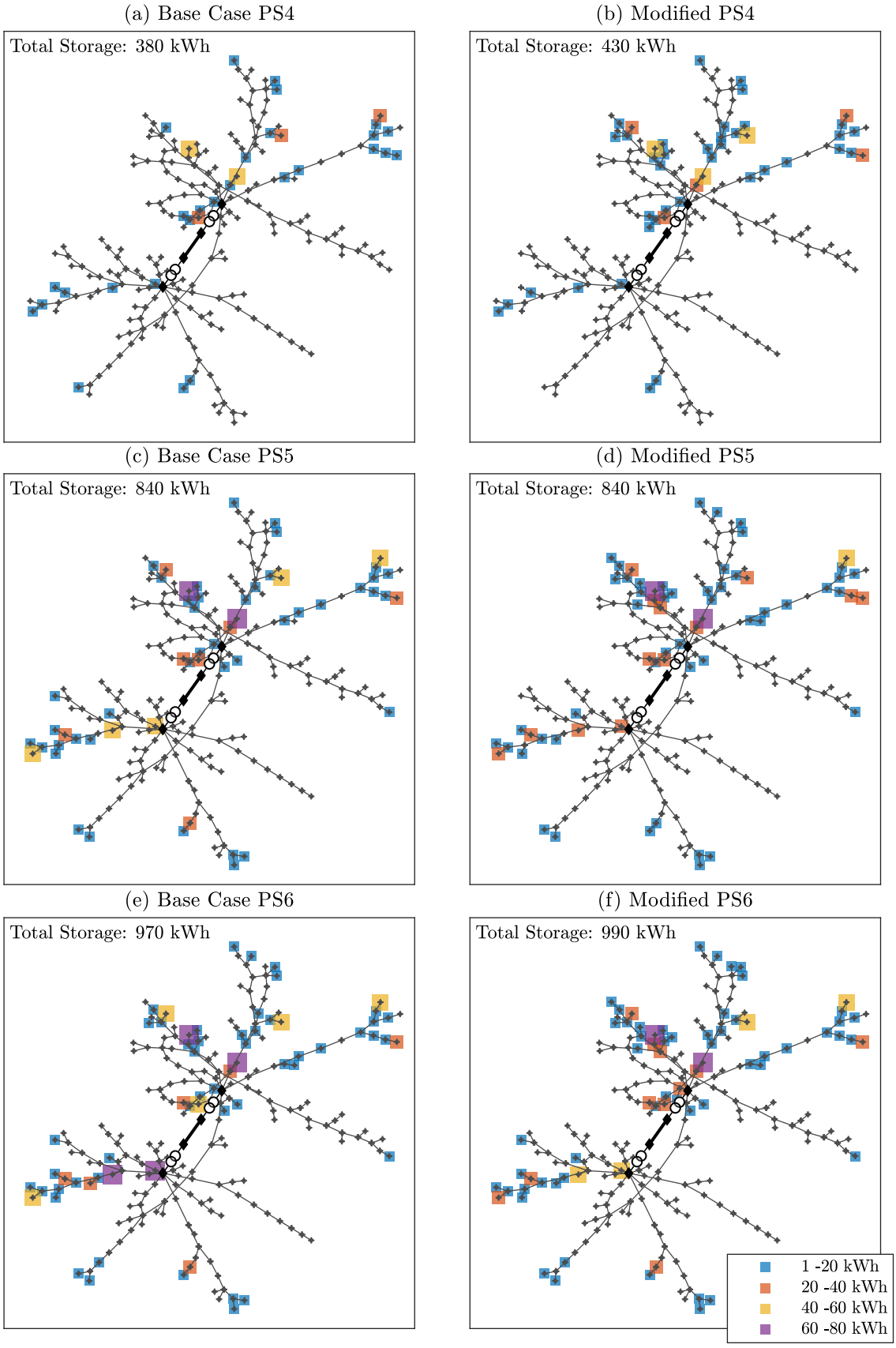

Figure 7.6: *Effect of modifying the slack bus voltage to 1.05 pu in for PS4-6*

cantly improved. Where active constraints are significantly limiting the amount of PV that can be utilised in the grid, storage may provide a financially attractive solution if no cheaper alternative is available. The price scenario is very significant in this assessment. With current price scenarios, it is still cheaper to allow some curtailment to take place rather than to drastically increase the amount of storage in the network.

To encourage grid support using distributed storage, a financial incentive can be offered to make batteries more financially viable. For distributed storage with a main purpose of increasing the amount of self-consumption, an additional income for voltage support could result in synergy potential as increasing self-consumption in itself helps reduce the voltage issues. This is reflected in the fact that as the amount of storage in the grid increases due to the profitability, the results for the base case and the modified slack bus voltage simulations become very similar.

Relocation of storage to more problematic nodes can assist with maintaining limits, as the cost savings from integrating more PV is much more significant than reducing losses. Network simulations including grid constraints can help to identify the nodes which will benefit most from additional storage.

7.2 PV Feed-in

It is commonly assumed that increasing PV will increase the need for storage in the system in order to increase self-consumption and reduce the load on the grid. Since the amount of distributed PV is likely to increase in many locations, it is worth examining this effect in more detail by performing the optimal planning algorithm with various amounts of PV. In the following pages a series of simulations is carried out for both CS1 and CS2 to investigate the relationship between total amount of PV in the grid and total optimal storage. In Section 7.2.1, the existing PV generation profiles are multiplied by a series of scaling coefficients, and the sizing stage of the Two Stage algorithm is carried out for each iteration. In Section 7.2.2 the effect of adding a large PV installation to a single node is investigated.

7.2.1 Total Grid PV Feed-in

The results are presented in Figure 7.7, plot (a) showing the results for CS1 and plot (b) for CS2. The results for CS1 are generated using a step size for $\mathcal{E}_{tot}$ of 1 kWh, which is why the results are slightly granular. The step size used for the CS2 results is 25 kWh, or 0.025 MWh. The Two Stage algorithm for CS2 is still rather time consuming, and therefore it was not extended beyond a scaling coefficient of 4. The results are close enough to those of CS1 to assume that the progression is the similar.

Figure 7.7 also includes an annotation at the point where total annual PV generation equals total active load. This varies between the two cases, as for CS1 it is 1.36, and for CS2 it is 0.86. This means that for CS2, the base case total PV already exceeded the total annual load. Since it has also been shown that the battery is generally used for intra-day savings, there are still many days where load exceeds PV, and therefore this statistic is not too important. The statistic that would create a boundary condition is the scaling factor where daily PV equals daily load for every day of the year. This scenario is very unrealistic, as daily variation in PV generation is so high that it would result in huge amounts of curtailment during the summer months.

The results shown in Figure 7.7 show that an increase in PV has a non-linear effect on the amount of optimal storage. For most price scenarios there is a steep increase in the amount of storage, and then after a certain point there is a more gradual, approximately linear increase.

The gradient of the near-linear increase seems to depend on the FiT more than on the storage cost, judging by Figure 7.7 (a). PS1, PS2 and PS3 end up with a similar gradient, which is higher than that for PS4, PS5 and PS6. The implication is that the higher the FiT, the more sensitive optimal storage is to the amount of PV in the system. This is a logical result, as when FiTs are higher there is generally more to be gained by reducing curtailment for feed-in earnings, instead of purely self-consumption.

In plot (b) there are even intersections between the lines, e.g. after the coefficient of 2.2 the total storage for PS3 is higher than that for PS6, where the FiT is lower. This is an interesting result, as it is contradictory to the price sensitivity analysis performed in chapter 6.1. Figure 6.2 clearly shows a negative correlation between FiT and optimal storage. In fact examining the cost surfaces a change in shape is detected at a certain point that explains the difference. Although the PV scenario's that will result in this reversal are highly unrealistic, it is still interesting to examine.

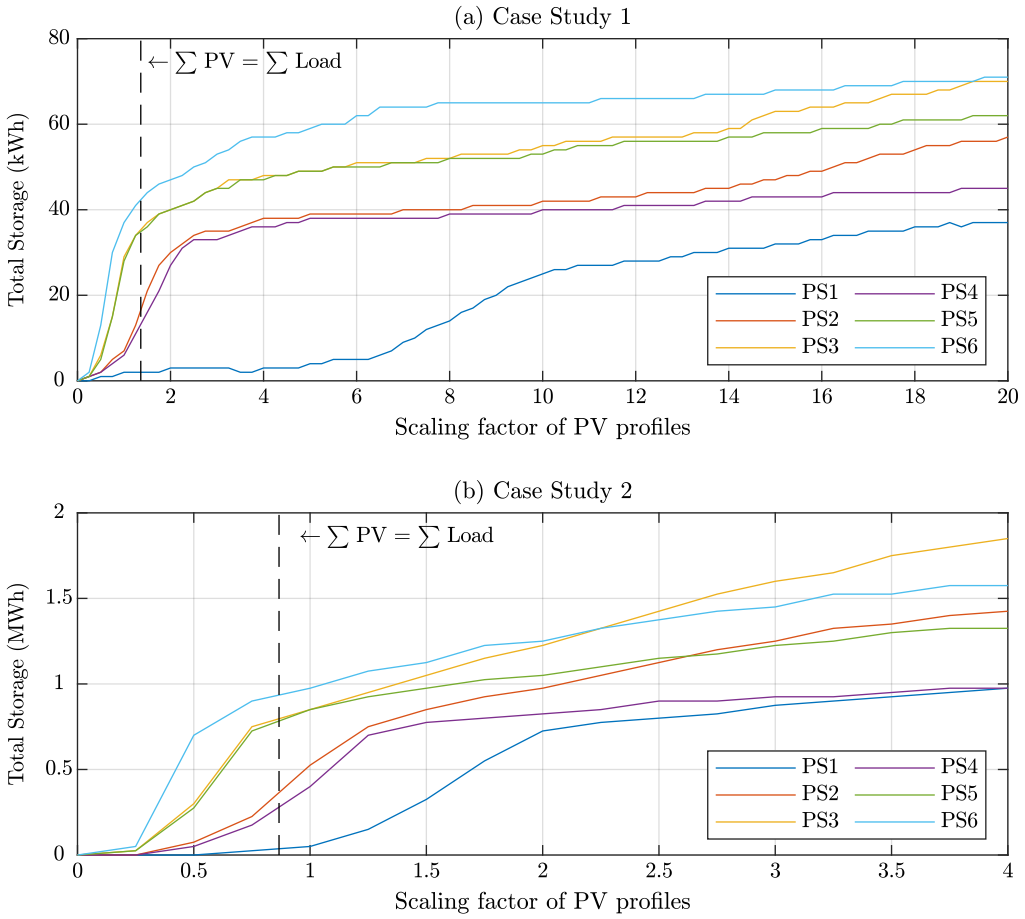

Figure 7.7: *Change in optimal storage as PV is scaled for CS1 in plot (a) and CS2 in plot (b)*

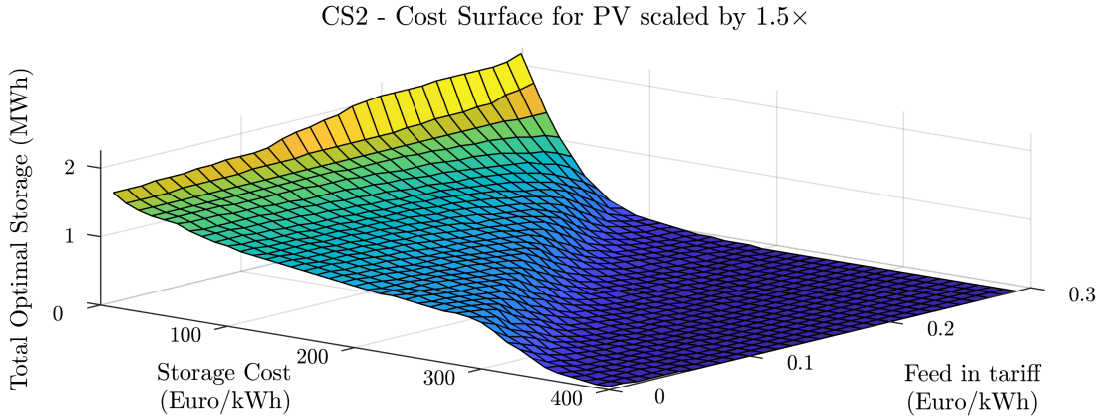

Figure 7.8: *Cost Sensitivity surface plot CS2 for a PV scaling factor of 1.5*

For CS2 the change in shape is seen earliest at a PV coefficient of 1.5, for which the cost surface is shown in Figure 7.8. Although the difference is only seen in the area of very high FiT and low storage costs, it still changes the shape compared to the base case shown in Figure 6.5.

This behaviour does increase with even higher amounts of PV in the grid, it is not too important to consider as the scenarios become unrealistic. CS2 already has a very high amount of PV, and even if it were to double, these effects are not relevant for any realistic price scenarios. Although the trend is that storage costs are lowering, which increases this effect, it is counteracted by the trend of reducing FiT.

A more relevant characterisation is of the sensitivity to PV increase with no FiT as shown in Figure 7.9. In this case total optimal storage is shown to have a very steady and predictable response to PV increase, with a steep increase and then a levelling off where increasing PV does not result in much more storage. The level of the plateau is dependent on the storage cost, as in each case the amount of intraday energy shifting is determined by the investment cost.

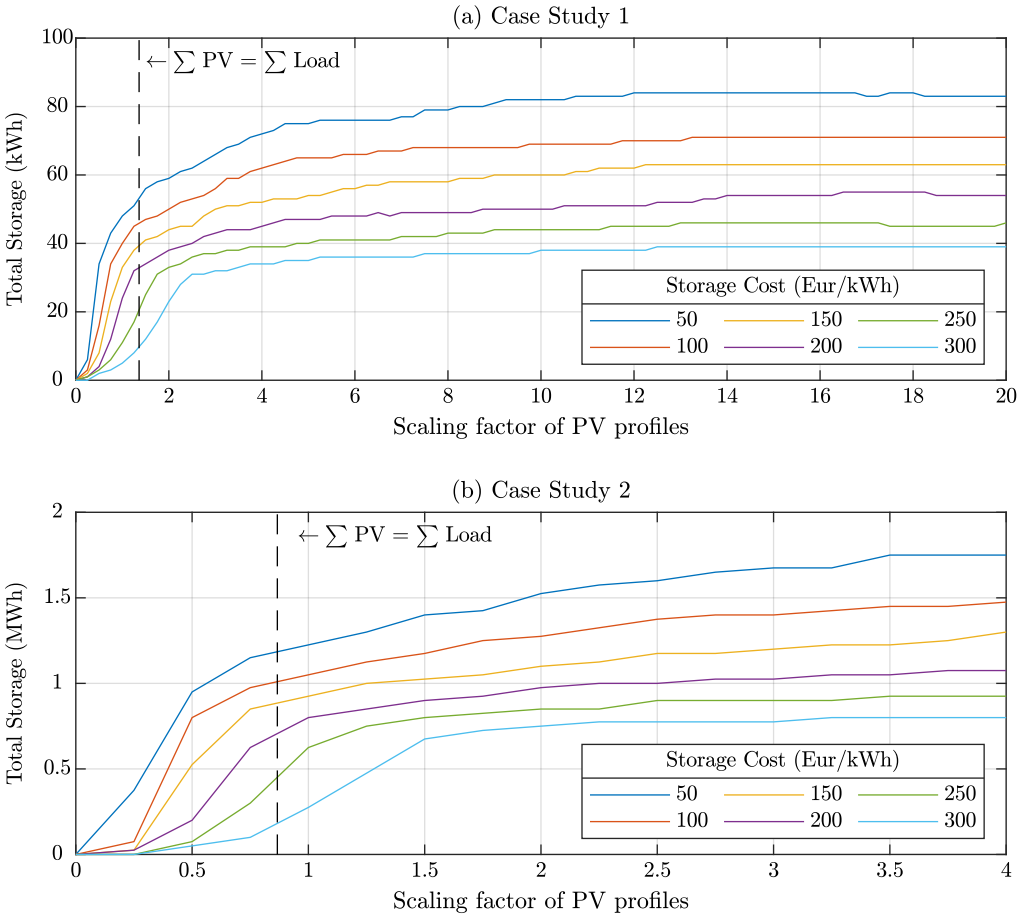

Figure 7.9: *Sensitivity to PV scaling without a FiT, for a range of storage costs*

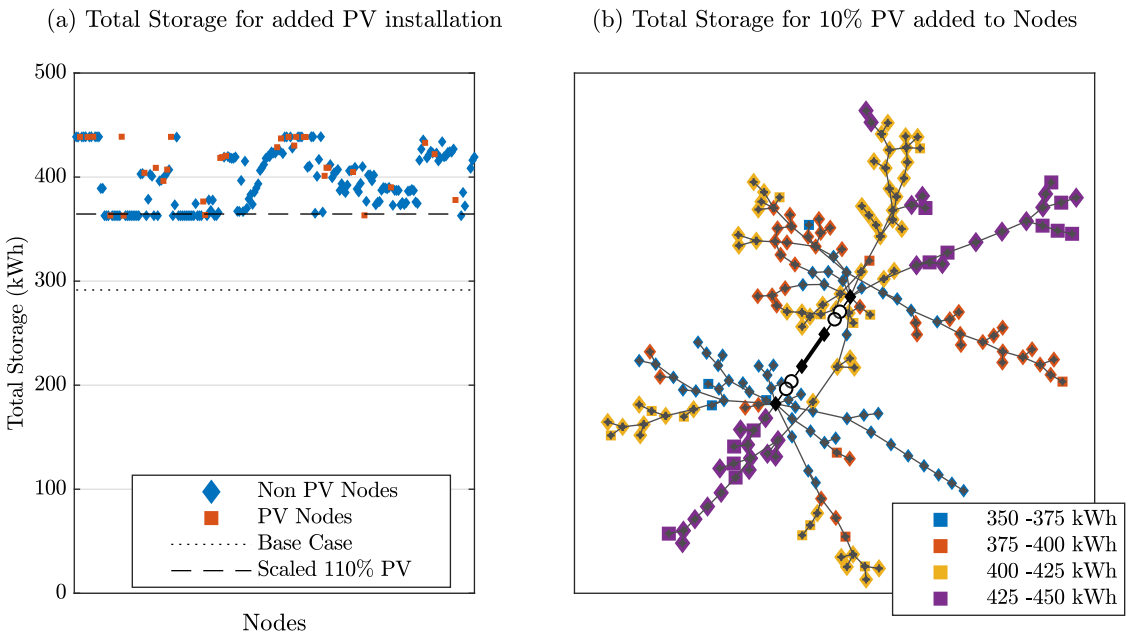

Figure 7.10: *Results of adding a 95 kWp PV installation to each node in the network besides substation nodes, using the sample day algorithm for CS2 with PS4. Plot (a) shows the total optimal network storage, against the node to which the PV is added. Plot (b) classifies the total network storage in 4 bins and indicates the total storage results for the respective nodes. The diamond plots are nodes that previously had no PV, and the square plots indicate nodes with existing PV, to which the 95 kWp installation is added*

7.2.2 PV increase in single nodes

In Section 7.2.1, the effect of scaling the total PV generation of all installations in the network is examined. In this section, the effect of adding one large PV installation to a single node in the network is examined. It is shown that the location of the new installation has a significant effect on the total optimal storage. The purpose is to understand if the total storage is sensitive to total PV or if it more sensitive to PV in certain locations.

The results are obtained by performing the sample day algorithm 207 times, each time adding a large PV installation to a different node in the network. The four substation nodes are not included. The sample day algorithm is chosen, due to the large number of iterations required. An installation that generates 10% of the sample day PV generation is added, which corresponds to a 95 kWp PV panel, producing a total of 7.8 MWh over the 36 sample days. This is a large installation for this network, as for the base case, the largest PV panel in the system is 115 kWp.

The results are shown in Figure 7.10, where plot (a) shows the total optimal storage, distinguishing between nodes that have PV for the base case and those that do not. This is also compared against the total optimal storage yielded by scaling the PV by 110%, adding the same amount of total PV energy in the system evenly to all PV nodes, as in Section 7.2.1. Firstly, it is clear that the scaled PV gives the lower bound on optimal storage that can be achieved by adding a single installation. Secondly, it is clear that the difference between nodes is significant. A maximum difference of 75 kWh of storage is seen, which is a 20% difference.

Finally, plot (a) does not indicate that existing PV in the system has a significant effect on the

increase in total storage. The average difference between the PV nodes and non PV node is only 5%. This indicates that location within the network could be a more significant factor. This is confirmed by plot 7.10(b), which shows the total optimal storage against the node to which the PV is added. Clearly there are strings that are much more sensitive to PV than others, with the location of existing PV being relatively insignificant. Interestingly there is no particular correspondence to the overvoltage issues, as there are lines in the lower have which are also highly sensitive to PV. This could be because the strings in the lower half had less PV in the base case, and so a large added installation is not covered by the existing PV.

The strings that are less sensitive to PV increase in the upper half either already have significant storage in the base case or are close to the substation, and are therefore minimally affected by overvoltage. In the lower half the strings that are less sensitive are generally less affected by network limits. The four nodes that previously had the highest PV generation are some of the least sensitive to the increase. This makes sense as the storage and network is already prepared to deal with high PV feed-in from the base case.

The main conclusion of this section is that the main impact of PV increase, is the overall increase, however the location can also make a difference. This depends on many factors, such as the previous amount of storage installed in the neighbourhood of the node, and the level to which it is facing network overload.

7.3 Placement Scenarios: Centralized Storage

In all the simulations so far the emphasis has been on decentralized storage, and every node in the low voltage network has been considered a candidate node for storage besides substation nodes. The nodes on either side of the transformer have been excluded, as this could be considered centralized. In fact the practicalities of the candidate nodes has not been considered at all, therefore it is worth examining some other placement scenarios. This can be enforced by reducing the number of candidate nodes, and adjusting the connective matrix C_{st} to ensure that the only the correct nodes are considered.

Three placement scenarios are simulated, with varying effects on the optimal storage:

- **Placement Scenario 1** - Reflects centralized storage, where only the low voltage sides of the substations are candidate nodes for storage. This could reflect a scenario where large grid support storage is installed at the substation and managed by the DSO.
- **Placement Scenario 2** - Allows storage only at the top of the lines, i.e. nodes that are connected to the low voltage substation nodes.
- **Placement Scenario 3** - Links storage to PV, therefore the candidate nodes for storage are those that also have PV production. This is a more traditional decentralized storage scenario, where PV and storage are managed together.

A number of simulations are carried out for each of the placement scenarios. To evaluate CS1, the sample day algorithm was carried out for each of the price scenarios. For CS2, the results are more interesting since the grid is so much larger and curtailment may factor into the results. The Two Stage algorithm was carried out on an hourly basis for each of the scenarios. Since for CS2 the issue of curtailment due to overvoltage is an issue, it is relevant to see how centralized

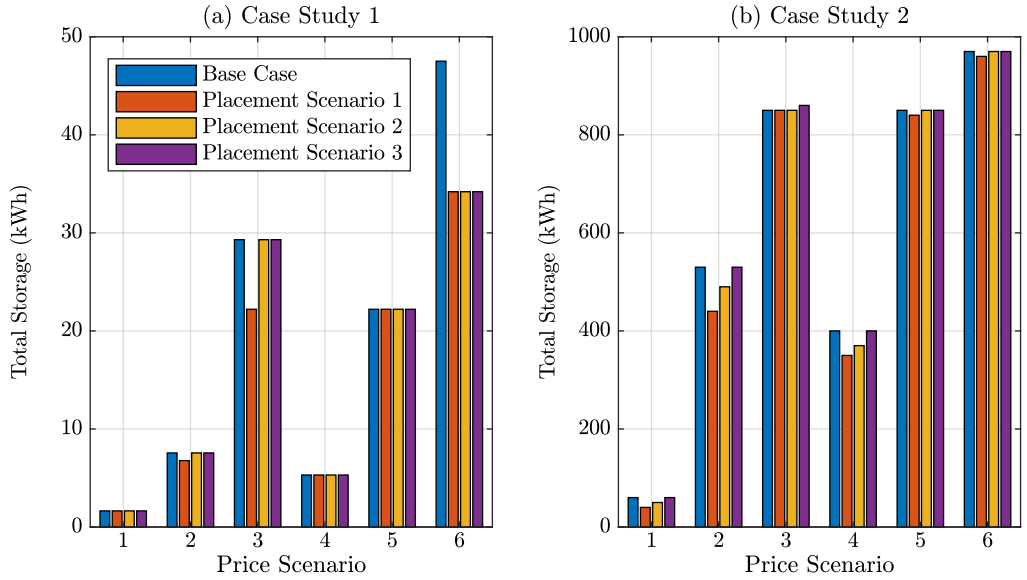

Figure 7.11: *The effect of the placement scenarios on the total storage for each of the price scenarios, for CS1 (a) and CS2 (b)*

storage can support the network compared to decentralized storage.

Another important point to note in this case, is that the price of storage is kept fixed per kWh, which is not very realistic. Larger storage installations for grid support would likely have a lower price per kWh. Furthermore, the control strategy of a centralized battery may be more straightforward.

The total storage can be compared using a bar chart of the placement scenarios for the price scenarios used in this work. The results can be seen in Figure 7.11 for both CS1 and CS2. In general the results are very similar to the base case for all the price scenarios, particularly price scenario 5. The only significant difference is seen for CS1- PS6, for CS2 the results hardly vary. The differences to the base case are particularly low for placement scenario 3. This indicates that given free choice of all nodes in the network, the storage is best placed near the PV. Now it is confirmed however, that reducing the number of candidate nodes does not significantly impact the results if the PV nodes are included.

The most severe difference is seen for placement scenario 1, i.e. centralized storage. The general result is that optimal centralized storage is slightly less than optimal decentralized storage. To investigate this further, the energy characteristics of all the placement options are compared for CS2, with extremely similar results. In fact $\mathcal{E}_{\text{buy}}$ and $\mathcal{E}_{\text{FI}}$ are almost identical. The only visually identifiable difference is for $\mathcal{E}_{\text{loss}}$, which is shown in Figure 7.12.

The results in Figure 7.12 are consistent with the results for total storage in Figure 7.11. The more centralized the storage is, the less it is able to reduce line losses. This is a logical result, as at times of high PV feed-in a lot of current has to travel to the substation. Losses are proportional to the square of the active power, which explains the significant difference between placement scenarios 1 and 2.

The reason that placement scenario 3 is more effective at reducing losses than even the base sce-

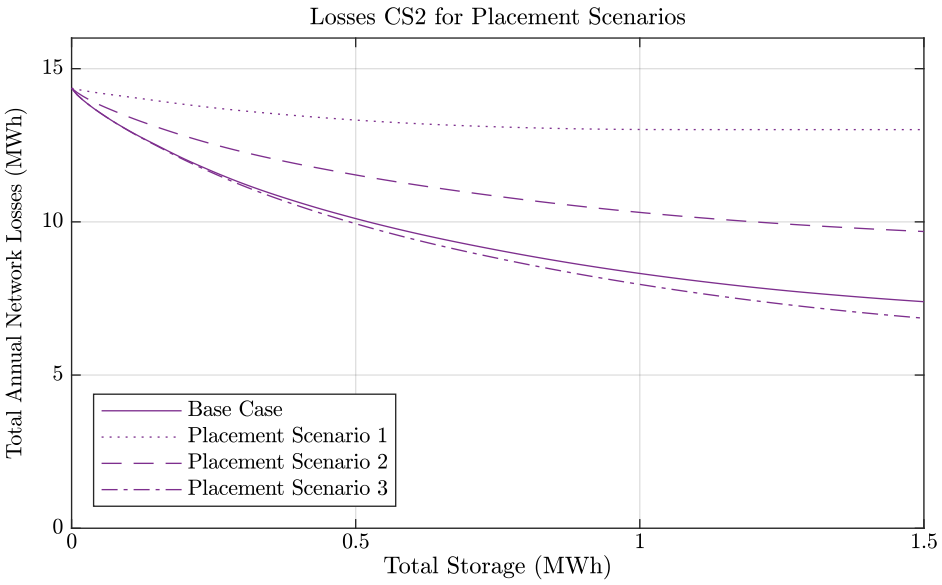

Figure 7.12: *Annual total network losses for each of the placement scenarios plotted against the total storage in the network*

nario, is that for the placement scenarios the constraint on the charging and discharging power is relaxed to counteract the reduced number of storage units. In the base case the storage power is limited to 10kW per unit, to encourage the distributed storage aspect. For placement scenario 3, the algorithm is able to more efficiently place storage at the PV nodes.

The higher losses for placement scenario 1 and 2 results in lower levels of optimal storage in general, as the saving of network losses allow for a slightly more profits resulting from the storage. Since in this case the $\mathcal{E}_{\text{buy}}$ and $\mathcal{E}_{\text{FI}}$ are the same, this is the only effect on total storage and it is relatively minor.

Modified Slack Voltage

The results comparing the base case have shown that the placement has a relatively minor effect on the total storage. Although decentralized storage has a significant impact on network losses, within the base case there is little to no impact on the curtailment. To examine the effect of centralized storage on a network which is severely limited by the overvoltage, the slack bus voltage is increased to 1.05 pu. It has already been shown in section 7.1.2 that increasing the slack bus voltage causes the cost surface to change as storage can help increase the total amount of PV in the system. In the following pages it is examined if the same effect applies to centralized storage.

Firstly, it is useful to see the energy characteristics of the various placement scenarios and compare them to the modified slack bus results with unrestricted placement, i.e. the simulation performed in section 7.1.2. The Two Stage algorithm was performed on CS2 at an hourly time resolution using all the placement scenarios. The results for all of the energy characteristics are shown in Figure 7.13.

Figure 7.13 plots all the energy characteristics for the various placement scenarios, as well as the

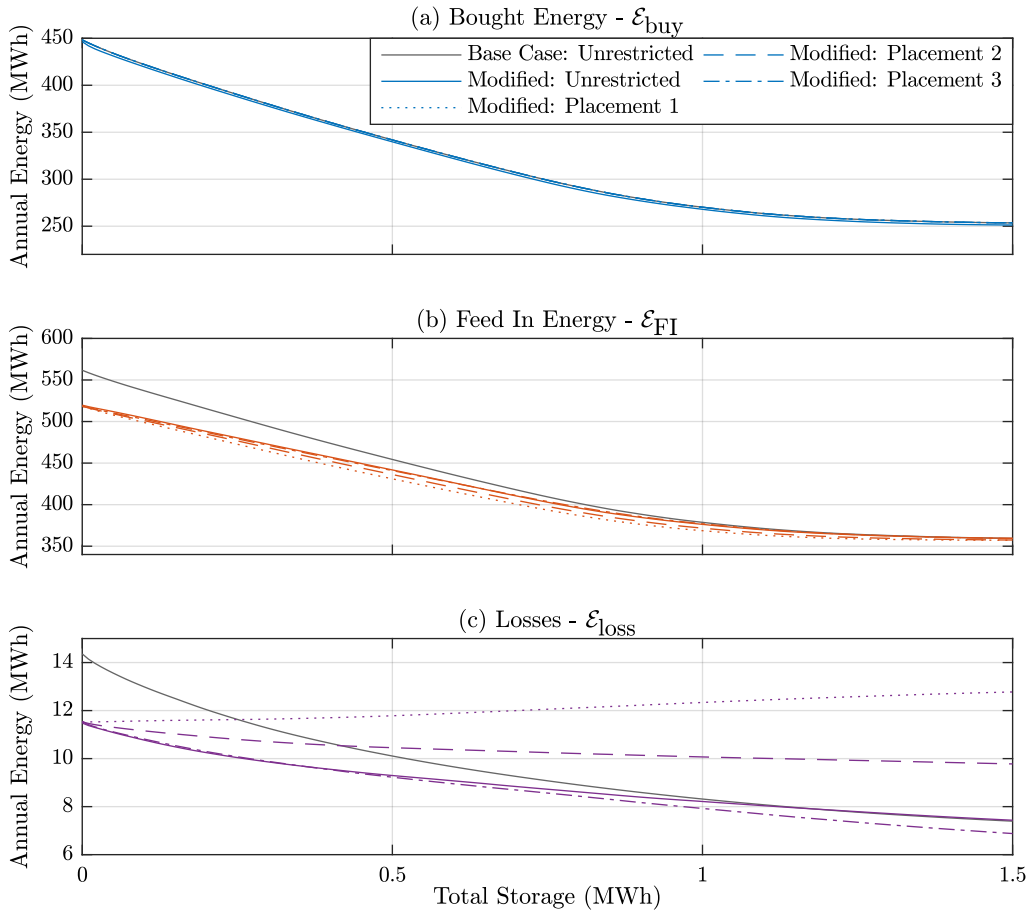

Figure 7.13: *Energy characteristics for the various placement scenarios with a slack bus voltage of 1.05 pu*

(a) Surface Difference Placement Scenario 1: Modified - Base slack bus voltage

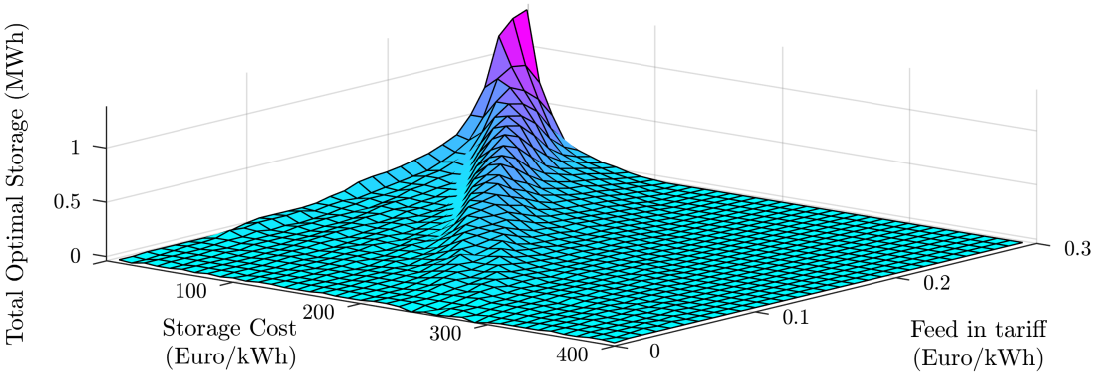

(b) Surface Difference Modified: Placement 1 - Unrestricted Placement

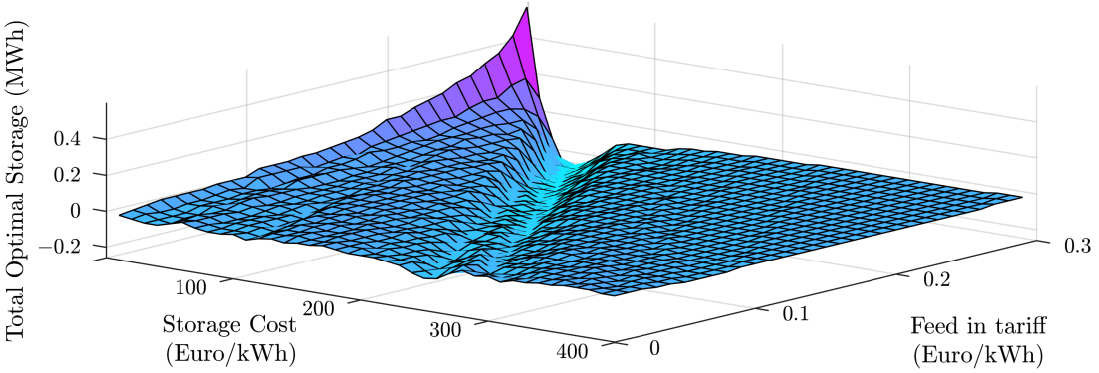

Figure 7.14: *Cost Surface difference plots showing in plot (a) the effect of reducing the voltage tolerance for centralized storage, subtracting the normal voltage tolerance results from the reduced. Plot (b) shows the difference between centralized and distributed storage by subtracting the surface for free placement from placement scenario 1. The free placement surface is shown in Figure 7.4(a)*

.

unrestricted placement results. For reference, the base case with the slack bus voltage of 1 pu is also included. The results show that there is very little impact on $\mathcal{E}_{\text{buy}}$ in plot (a). As the storage increases the $\mathcal{E}_{\text{buy}}$ reduces as more of the PV is used locally, and for this it does not matter where the storage is placed.

A slightly more noticeable difference is seen for $\mathcal{E}_{\text{FI}}$, where the more centralized the storage is, the less PV is fed back into the grid. The result is most significant for medium amounts of storage, between 400kWh and 1000kWh in the system.

The losses are very similar to the case without reduced voltage tolerance, shown in Figure 7.12. placement scenario 3 has a slightly improved performance, due to the higher power limits on the individual storage units. What is interesting here is that placement scenario 1 (centralized) actually ends up reversing the curve and ends up with more losses than if there was no storage at all. This is because large centralized storage can increase PV self-consumption, but it requires large currents to be transmitted up and down the distribution grid, resulting in high losses.

Figure 7.4 demonstrates the impact of increased slack bus voltage on the cost surface. In order

to assess the impact this has on optimal storage, it is helpful to plot the cost surface difference plots, as in Figure 7.4(b). In Figure 7.14, two cost surface difference plots are given.

Firstly in (a) the effect of increasing the slack bus voltage to 1.05 pu is shown for centralized storage, which initially does not seem very different from the equivalent decentralized version in Figure 7.4(b). To understand the difference, the cost surfaces are compared for modified slack bus voltage simulations using placement scenario 1 minus the unrestricted placement in 7.14 (b).

Figure 7.14 (b) shows that the centralized version has less optimal storage than the decentralized storage for most price scenarios. Particularly the peaks that were seen in Figure 7.4 are shown to be less spread out, by the wells in the plot. Only for a very low storage cost is more storage profitable when centralized. In other words, reducing the voltage tolerance increases the profitability of storage, and decentralized storage is more effective than centralized storage.

To summarize the results on placement strategies, some insight has been gained on the difference between centralized and distributed storage by simulating different placement scenarios. Firstly, if curtailment is required to maintain network limits, the placement scenario has very little impact on the optimal storage. Out of the three cost components, the only significant difference is in losses. Centralized storage results in much higher system losses as the PV has to be transmitted up and down the grid.

The difference in cases where the voltage constraints cause curtailment of PV is more significant. By plotting the energy characteristics, it is shown that the same amount of storage results in less feed-in energy for centralized storage. This is a very logical result, as the voltage issues can be reduced by less line loading, which distributed storage enables.

If costs are the same, the best result is obtained when decentralized storage is enabled, particularly when large storage units are installed at PV nodes. In fact larger storage at PV nodes performs slightly better than totally decentralized storage.

The simulations in this section do not take into account the fact that larger storage units can cost less per kWh. Therefore these results cannot be used to state clearly that centralized storage is less profitable. It has already been shown in section 6.2 that storage costs are complicated to model, as they are changing rapidly and different manufacturers and types of storage have very different offers. What can be shown, is that although the same amount of storage in a decentralized fashion can be much more effective at alleviating grid overload, centralized storage can offer most of the same benefits. Only when curtailment is a big issue, a significant improvement can be achieved with distributed storage.

Chapter 8

Conclusion and Outlook

8.1 Summary

This thesis has presented a number of modelling tools and techniques, along with analysis based on simulations using the models.

A detailed description is given of a residential electricity demand model (REM), that generates household electricity profiles at a high time and spatial resolution. The REM uses a combination of bottom up, activity based modelling and top down modelling to generate highly detailed load profiles for a synthetic population that can be broken down into the various load categories. The profiles can be generated on a per second basis or per minute basis, and for lower time resolutions the profiles should be generated on a minute basis and then downsampled. The REM was built to be extremely flexible, and to generate profiles for a wide range of applications. The REM is considered as a contribution of this thesis, as it documents the model in its entirety, and a significant validation is performed. The level of detail, though excessive for this study, is likely to be useful for studies on operation.

The REM is used to assign load profiles to two case study grids used for the main body of work, which is focussed on optimal planning of battery storage in a distribution grid. The storage planning algorithms developed in this thesis utilise a number of models from literature that are briefly mentioned here. The grid model is based on a linearisation from [76], which is shown to provide a good estimation of voltages and angles as verified using MATPOWER. The battery model used, is the well established KiBaM [1], which includes the charge recovery effect and the rate capacity effect. The model is discretised for use in the multiperiod optimisation.

These elements are integrated into an optimisation problem that considers all nodes in the grid as candidate nodes for battery storage. The objective function includes the annualised cost of storage per kWh at 20% of capital cost, the cost of bought energy for the whole grid, the earnings from feed-in energy, and the network losses. This is a welfare optimisation, assuming that there are no conflicts between stakeholders, and that the objective is shared for all stakeholders. The result of this annual optimisation problem gives the optimal capacities and locations of battery storage in the grid. This basic optimisation problem is time consuming, and is highly sensitive to feed in tariffs and storage prices. Since these vary significantly both geographically, and over time, only limited insight can be gained from these results.

Two case studies are presented, a simple grid (CS1) used mostly for the validation of the method, and a more complex grid (CS2) for more detailed analysis. The basic algorithm is unable to perform annual optimal planning for CS2 due to the problem size. A novel methodology to perform optimal planning of batteries in a distribution grid model is derived, referred to as the Two Stage

algorithm, that can be applied to large grids such as CS2.

One of the contributions of this thesis is the development of the Two Stage planning algorithm, named as such because it splits up the planning problem into a sizing and placement problem. For the sizing stage, the annual problem is decomposed into daily problems. Leaving the amount of storage per node open, the total storage for the whole network is fixed and optimised for each daily subproblem, extracting the results for total bought energy, total feed in energy and total losses. Along with the storage costs, these are all the cost function components. This methodology exploits the fact that the optimal total storage is dependent on the relationship between the costs, and that placement has an insignificant impact on the total network storage. Furthermore, for the daily problem, the placement and charging behaviour are independent on prices for a fixed amount of total storage.

The results of this step come in the form of matrices for the bought energy, feed in energy, and losses for each daily subproblem, and for each value for total network storage. This can then be used to construct the objective function for any price scenario, to obtain the optimal total network storage, thus completing the sizing stage of the algorithm.

The placement stage is performed by optimising over sample days, with a fixed amount of total storage determined by the sizing stage. The sample days are selected by optimising every 10-11 chronological days and choosing the individual day with the closest results, resulting in 36 sample days to represent the year. The results are verified using the basic annual optimisation problem described above, for a simple radial grid (CS1) yielding highly accurate results.

There are two major advantages to the Two Stage algorithm. Firstly, the results can be immediately evaluated for all price scenarios. Secondly, since the problem is decomposed into many small subproblems, it can be performed on much larger and more complicated networks, and on smaller grids like CS1 it gives an approximation of the results in a fraction of the time.

The Two Stage algorithm is applied to a more complex grid (CS2), which has a large amount of PV and faces network limits, mostly due to overvoltage. The results show that batteries can significantly improve the overvoltage and thereby reduce curtailment of PV. The grid approximation is then tested, by evaluating the complete grid equations and comparing the results. The approximation is accurate and the errors are relatively small, the limits are still effectively maintained for the simulations in question. This method does not guarantee the limits for any situation, and the voltage should be checked for results that are close to the limits.

The Two Stage algorithm and the case studies are used to investigate a number of aspects of planning storage in distribution grids. First, the effect of the simulations time resolution are examined, by evaluating the results for CS1 on a minute, 15 minute and hourly basis. Although the daily subproblems are shown to have much more significant differences between the 15 minute and hourly simulations, they average out over the year, thereby giving the same results for total optimal storage. The difference between 1 minute and 15 minutes is much less, even though data loss is more. All three time resolutions are therefore judged to be adequate for the annual planning problem.

The Two Stage algorithm is used to perform a cost analysis on the case studies, where various cost trends are examined. Using realistic costs are difficult since there are many factors that are related to battery costs. Using discrete prices may yield more realistic results, but it is very

slow and many other decision factors would go into actually buying storage than simple cost optimality.

Various scenarios are simulated using the developed storage planning variations. Firstly, the effect of changing network parameters is shown to only have a significant effect on the optimal storage if it leads to curtailment. Secondly increasing PV is shown to lead to more optimal storage, although the marginal benefits are less. Finally various placement scenarios are investigated, showing that for a welfare optimisation the differences are minor unless network issues result in curtailment. For reducing network losses it is best to have storage near the major PV nodes.

This thesis does not include the additional costs that are associated with a battery storage implementation, such as inverter costs and controller costs. It also assumed that it is always possible to coordinate all the storage units in the grid to achieve the best results.

8.2 Conclusions

The investigations in this thesis have shown that the results of a welfare optimisation on a distribution grid is extremely case study specific. They show that there is no universal price point at which batteries becomes viable. The results in this study have made it clear that the main dynamic that determines the profitability of battery storage, is the absorption of excess energy during the PV generation peak during the day, and its release at other times of the day. Although this may seem like an obvious result, it has some important implications. The reasons for this conclusion are basically, that with the cost function used, there is very little sensitivity to any factor besides cost unless it impacts curtailment. For example, the time resolution is shown to affect the results of the daily subproblems, but has no effect on the total optimal network storage. This is because when a lot of PV is installed, particularly for a larger quantity of households, the household peaks are still less than the PV peaks. The results may look different if the PV peaks are closer is size to the household peaks, however this is an unrealistic scenario with current PV projections.

The clearest proof is in the comparison of the CS2 network with a modified slack bus voltage compared to the base case. The reduced voltage tolerance results in much more curtailment of PV which can be counteracted with battery storage. This makes battery storage generally more profitable, and at certain price points therefore the optimal storage is increased. Placement has a similar effect, although the network losses vary significantly depending on the placement strategy, the effect on total optimal storage is only noticeable if the overvoltage is resulting in curtailment. If a cheaper alternative to overvoltage is provided, such as reactive power compensation from PV inverters, the effect on the optimal storage is eliminated.

The first general implication of this for battery storage in distribution networks, is that to encourage battery storage to achieve any other objectives different price incentives are required. For example, although peak reduction does happen to some degree due to network loss optimisation, a price incentive for lowering peaks would increase this significantly. The same applies for voltage management. Current battery prices do not make it profitable to implement battery storage simply to lower voltage, and a separate price incentive would be needed.

Another clear statement based on the results is that autarchy is extremely difficult to achieve

with only PV and storage, since the PV dynamic is so time constrained, the storage requirements would be enormous. To achieve autarchy at a reasonable cost, other sources of energy generation besides PV would be required.

Some general inferences can be made based on the cost analysis. Trivially, the cheaper that batteries become, the more storage is economical as the benefits are generally marginally reducing. Considering all the cost surfaces that have been plotted in this thesis, a common feature is a region of sharp increase followed by a flattening as the storage increases, however the price point at which this is reached depends highly on the feed in tariffs. Moreover with the current FiT, the battery prices required to enter this region are unrealistically low. If the FiT were to be eliminated, then the storage prices do not have to drop much from their current values to be significantly more profitable for some distribution grids like CS2. The future implication is that as both storage prices and feed in tariffs reduce, a point will come where storage becomes a lot more economic quickly. This growth is not exponential and at some point the effect of reducing prices will become marginally less.

This is explained by the fact that larger amounts of storage in the grid can be used to absorb large amounts of excess PV during the day, and discharge at night. The frequency of this need during the year will reduce, so that the large capacity is only infrequently utilised.

The cost analysis showed that current prices are still too high for storage to be significantly profitable. However, if feed in tariffs were to reduce or be eliminated, the storage prices would not have to drop much for storage to be highly profitable additions to the grid to utilise PV locally. Furthermore, the placement study has made it clear that the best locations for storage is simply near PV installations, both for keeping node voltage low and reducing losses.

Seeing the price trends, in terms of lowering feed in tariffs, lowering storage prices and the growing market of second life batteries, confirm that battery storage is a highly promising technology for distribution grids. Including batteries in distribution grids, with existing market models make it profitable to use storage to use excess locally generated PV. More sophisticated market models and pricing are required for encouraging use of batteries for other purposes. Models such as the one presented in this thesis, which use welfare optimisation, can show the potential of batteries for the whole system, providing insight into the factors that can effect the profitability of batteries.

8.3 Outlook

As in any publication with a focus on describing a model, it is always possible to state ways in which a model can be extended or improved to gain better results. In this case one aspect in which this model is limited, is that it neglects any practical conflicts or ownership issues regarding storage. It assumes that the distribution grid is free of use for the storage, and the interests of the grid as a whole are shared by all battery owners and operators. A more sophisticated set of constraints and cost functions that reflect multiple stakeholders would create much more insight into the potential of battery storage. The second major limitation of this model, is the simplistic price model that neglects other costs. The discrete price model is more realistic, but its use in further analysis is limited due to computational difficulty, and its limitation in comparing different competing offers by any factor other than price.

Another improvement to this thesis lies in the method of selecting sample days, the method used in this system was experimental. A more scientific, statistics based approach may yield much better results in terms of accuracy, or reduce the sample days required for faster results.

Any model can be extended and developed further to reflect reality better, however the purpose should be clear. It is therefore also necessary to comment on further studies that can expand on the conclusions drawn here as well as use the models developed.

Firstly, the simulations in this study analyse the use of batteries as the only source of flexibility in the distribution grid, however many other flexible technologies are also being developed. An analysis of the competition with other technologies, such as power to heat, or other flexible industrial loads could also yield in important insight into the future success of batteries. Finally this study only deals with the sizing of batteries where PV is existing already. By adding reasonable pricing for PV, and a similar model for PV capacity, the model used can easily be extended to size PV along with batteries, to gain insight into profitable combinations.

Bibliography

[1] J. F. Manwell and J. G. McGowan, "Lead acid battery storage model for hybrid energy systems," *Solar Energy*, vol. 50, no. 5, pp. 399 – 405, 1993.

[2] P. Fortenbacher, *On the Integration of Distributed Battery Storage in Low Voltage Grids*. phdthesis, ETH Zurich, 2017.

[3] EnergieAgentur.NRW, "Erhebung "wo im haushalt bleibt der strom?" stromverbrauchsanteile verschiedener anwendungsbereiche in ein- bis fünf-personen-haushalten - 2015 und 2011 im vergleich," Nov. 2015.

[4] S. S. Manuel Frondel, Nolan Ritter, "Stromverbrauch privater haushalte in deutschland: Eine ökonometrische analyse," Aug. 2015.

[5] M. Lindner, C. Aigner, R. Witzmann, F. Wirtz, I. Berber, M. Gödde, and R. Frings, "Aktuelle musternetze zur untersuchung von spannungsproblemen in der niederspannung," in *14. Symposium Energieinnovation*, 2016.

[6] International Energy Agency (IEA), "Photovoltaic power systems programme annual report 2017," May 2018.

[7] L. Goldie-Scot, "A behind the scenes take on lithium-ion battery prices." BloombergNEF, Mar. 2019.

[8] Statistischer Amt München, "Die privathaushalte in den stadtbezirken am 31.12.2017 nach der haushaltsgrösse," 2017.

[9] Destatis Statistisches Bundesamt, "Durchschnittliche wohnfläche pro person nach haushaltstyp," 2011.

[10] United Nations Framework Convention on Climate Change (UNFCCC), "Paris agreement." Online, 2015.

[11] International Energy Agency (IEA), "Co2 emissions from fuel combustion: Overview 2019," 2019.

[12] Federal Ministry of Economics and Technology (BMWi), "Energy concept for an environmentally sound, reliable and affordable energy supply," Sept. 2010.

[13] International Energy Agency (IEA), "World energy outlook 2018 : Executive summary," 2018.

[14] Bundesnetzagentur, "EEG in Zahlen 2017."

[15] O. Edenhofer, "Renewable energy sources and climate change mitigation," tech. rep., Intergovernmental Panel on Climate Change, 2012.

[16] Gurobi Optimization, LLC, "Gurobi optimizer reference manual." http://www.gurobi.com, 2019.

[17] IBM, "CPLEX." https://www.ibm.com/analytics/cplex-optimizer.

[18] MATLAB, *MATLAB:2018b*. The Mathworks Inc., 2018.

[19] J. Löfberg, "Yalmip : A toolbox for modeling and optimization in matlab," in *In Proceedings of the CACSD Conference*, (Taipei, Taiwan), 2004.

[20] B. Battke, T. S. Schmidt, D. Grosspietsch, and V. H. Hoffmann, "A review and probabilistic model of lifecycle costs of stationary batteries in multiple applications," *Renewable and Sustainable Energy Reviews*, vol. 25, pp. 240 – 250, 2013.

[21] M. K. Matthias Resch, Jochen Bühler and A. Sumper, "Impact of operation strategies of large scale battery systems on distribution grid planning in germany," *Renewable and Sustainable Energy Reviews*, vol. 74, pp. 1042–1063, 2017.

[22] H. Hesse, M. Schimpe, D. Kucevic, and A. Jossen, "Lithium ion battery storage for the grid : A review of stationary battery storage system design tailored for applications in modern power grids," *Energies*, vol. 10, no. 12, 2017.

[23] G. Delille, B. Francois, and G. Malarange, "Dynamic frequency control support by energy storage to reduce the impact of wind and solar generation on isolated power system's inertia," *IEEE Transactions on Sustainable Energy*, vol. 3, pp. 931–939, Oct 2012.

[24] S. Bradbury, A. Laguna-Estopier, and D. P. Papadopoulos, "Smarter network storage - electricity storage in gb: Final evaluation of the smarter network storage solution (sdrc 9.8)," Dec. 2016.

[25] D. I. Stroe, V. Knap, M. Swierczynski, A. I. Stroe, and R. Teodorescu, "Operation of a grid-connected lithium-ion battery energy storage system for primary frequency regulation: A battery lifetime perspective," *IEEE Transactions on Industry Applications*, vol. 53, no. 1, pp. 430–438, 2017.

[26] D. Greenwood, K. Lim, C. Patsios, P. Lyons, Y. Lim, and P. Taylor, "Frequency response services designed for energy storage," *Applied Energy*, vol. 203, pp. 115 – 127, 2017.

[27] A. Zeh, M. Müller, M. Naumann, H. C. Hesse, A. Jossen, R. Witzmann, and J. V. Mierlo, "Fundamentals of using battery energy storage systems to provide primary control reserves in germany," *Batteries*, vol. 2, no. 3, 2016.

[28] C. Goebel, H. Hesse, M. Schimpe, A. Jossen, and H. A. Jacobsen, "Model-based dispatch strategies for lithium-ion battery energy storage applied to pay-as-bid markets for secondary reserve," *IEEE Transactions on Power Systems*, vol. 32, pp. 2724–2734, July 2017.

[29] A. Zeh, M. Müller, H. C. Hesse, A. Jossen, and R. Witzmann, "Operating a multitasking stationary battery storage system for providing secondary control reserve on low-voltage level," in *International ETG Congress 2015; Die Energiewende - Blueprints for the new energy age*, 2015.

[30] H. Pandzic and I. Kuzle, "Energy storage operation in the day-ahead electricity market," in *2015 12th International Conference on the European Energy Market (EEM)*, 2015.

[31] A. D. Giorgio, A. Giuseppi, F. Liberati, and A. Pietrabissa, "Controlled electricity distribution network black start with energy storage system support," in *2017 25th Mediterranean Conference on Control and Automation (MED)*, pp. 781–786, July 2017.

[32] A. I. Stan, M. Swierczynski, D. I. Stroe, R. Teodorescu, and S. J. Andreasen, "Lithium ion battery chemistries from renewable energy storage to automotive and back-up power applications," in *2014 International Conference on Optimization of Electrical and Electronic Equipment (OPTIM)*, 2014.

[33] WEMAG, "Wemag-batteriespeicher testet erfolgreich schwarzstart nach blackout." Online, Aug. 2017.

[34] M. Naumann, R. C. Karl, C. N. Truong, A. Jossen, and H. C. Hesse, "Lithium-ion battery cost analysis in pv-household application," *Energy Procedia*, vol. 73, pp. 37 – 47, 2015. 9th International Renewable Energy Storage Conference, IRES 2015.

[35] C. Goebel, V. Cheng, and H. A. Jacobsen, "Profitability of residential battery energy storage combined with solar photovoltaics," *Energies*, vol. 10, July 2017.

[36] J. von Appen, T. Stetz, M. Braun, and A. Schmiegel, "Local voltage control strategies for pv storage systems in distribution grids," *IEEE Transactions on Smart Grid*, vol. 5, pp. 1002–1009, March 2014.

[37] S. Barcellona, L. Piegari, V. Musolino, and C. Ballif, "Economic viability for residential battery storage systems in grid-connected pv plants," *IET Renewable Power Generation*, vol. 12, no. 2, pp. 135–142, 2018.

[38] G. Merei, J. Moshövel, D. Magnor, and D. U. Sauer, "Optimization of self-consumption and techno-economic analysis of pv-battery systems in commercial applications," *Applied Energy*, vol. 168, pp. 171 – 178, 2016.

[39] A. Oudalov, D. Chartouni, and C. Ohler, "Optimizing a battery energy storage system for primary frequency control," *IEEE Transactions on Power Systems*, vol. 22, pp. 1259–1266, Aug 2007.

[40] X. Luo, J. Wang, M. Dooner, and J. Clarke, "Overview of current development in electrical energy storage technologies and the application potential in power system operation," *Applied Energy*, vol. 137, pp. 511 – 536, 2015.

[41] N. Nasiriani, G. Kesidis, and D. Wang, "Optimal peak shaving using batteries at datacenters: Characterizing the risks and benefits," in *2017 IEEE 25th International Symposium on Modeling, Analysis, and Simulation of Computer and Telecommunication Systems (MASCOTS)*, 2017.

[42] N. Wade, P. Taylor, P. Lang, and P. Jones, "Evaluating the benefits of an electrical energy storage system in a future smart grid," *Energy Policy*, vol. 38, no. 11, pp. 7180 – 7188, 2010. Energy Efficiency Policies and Strategies with regular papers.

[43] A. Lahyani, P. Venet, A. Guermazi, and A. Troudi, "Battery/supercapacitors combination in uninterruptible power supply (ups)," *IEEE Transactions on Power Electronics*, vol. 28, pp. 1509–1522, April 2013.

[44] I. Atzeni, L. G. Ordonez, G. Scutari, D. P. Palomar, and J. R. Fonollosa, "Demand-side management via distributed energy generation and storage optimization," *IEEE Transactions on Smart Grid*, vol. 4, pp. 866–876, June 2013.

[45] D. Connolly, H. Lund, P. Finn, B. Mathiesen, and M. Leahy, "Practical operation strategies for pumped hydroelectric energy storage (phes) utilising electricity price arbitrage," *Energy Policy*, vol. 39, no. 7, pp. 4189 – 4196, 2011. Special Section: Renewable energy policy and development.

[46] K. Bradbury, L. Pratson, and D. Patino-Echeverri, "Economic viability of energy storage systems based on price arbitrage potential in real-time u.s. electricity markets," *Applied Energy*, vol. 114, pp. 512 – 519, 2014.

[47] F. Wankmueller, P. R. Thimmapuram, K. G. Gallagher, and A. Botterud, "Impact of battery degradation on energy arbitrage revenue of grid-level energy storage," *Journal of Energy Storage*, vol. 10, pp. 56 – 66, 2017.

[48] X. Tan, Y. Wu, and D. H. K. Tsang, "Optimal energy trading with battery energy storage under dynamic pricing," in *2014 IEEE International Conference on Smart Grid Communications (SmartGridComm)*, 2014.

[49] R. Poudineh and T. Jamasb, "Distributed generation, storage, demand response and energy efficiency as alternatives to grid capacity enhancement," *Energy Policy*, vol. 67, pp. 222 – 231, 2014.

[50] K. Spiliotis, S. Claeys, A. R. Gutierrez, and J. Driesen, "Utilizing local energy storage for congestion management and investment deferral in distribution networks," in *2016 13th International Conference on the European Energy Market (EEM)*, pp. 1–5, June 2016.

[51] S. Vazquez, S. M. Lukic, E. Galvan, L. G. Franquelo, and J. M. Carrasco, "Energy storage systems for transport and grid applications," *IEEE Transactions on Industrial Electronics*, vol. 57, pp. 3881–3895, Dec 2010.

[52] F. Geth, J. Tant, R. Belmans, and J. Driesen, "Balanced and unbalanced inverter strategies in battery storage systems for low-voltage grid support," *IET Generation, Transmission Distribution*, vol. 9, no. 10, pp. 929–936, 2015.

[53] M. Muller, L. Viernstein, C. N. Truong, A. Eiting, H. C. Hesse, R. Witzmann, and A. Jossen, "Evaluation of grid-level adaptability for stationary battery energy storage system applications in europe," *Journal of Energy Storage*, vol. 9, pp. 1 – 11, 2017.

[54] D. B. Richardson, "Electric vehicles and the electric grid: A review of modeling approaches, impacts, and renewable energy integration," *Renewable and Sustainable Energy Reviews*, vol. 19, pp. 247 – 254, 2013.

[55] K. Clement-Nyns, E. Haesen, and J. Driesen, "The impact of charging plug-in hybrid electric vehicles on a residential distribution grid," *IEEE Transactions on Power Systems*, vol. 25, pp. 371–380, Feb 2010.

[56] O. Veneri, L. Ferraro, C. Capasso, and D. Iannuzzi, "Charging infrastructures for ev: Overview of technologies and issues," in *2012 Electrical Systems for Aircraft, Railway and Ship Propulsion*, 2012.

[57] C. Capasso and O. Veneri, "Experimental study of a dc charging station for full electric and plug in hybrid vehicles," *Applied Energy*, vol. 152, pp. 131 – 142, 2015.

[58] F. Ciccarelli, A. D. Pizzo, and D. Iannuzzi, "An ultra-fast charging architecture based on modular multilevel converters integrated with energy storage buffers," in *2013 Eighth International Conference and Exhibition on Ecological Vehicles and Renewable Energies (EVER)*, 2013.

[59] H. Ding, Z. Hu, and Y. Song, "Value of the energy storage system in an electric bus fast charging station," *Applied Energy*, vol. 157, pp. 630 – 639, 2015.

[60] D. Wu, C. Jin, P. Balducci, and M. Kintner-Meyer, "An energy storage assessment: Using optimal control strategies to capture multiple services," in *2015 IEEE Power Energy Society General Meeting*, 2015.

[61] A. Zeh, M. Müller, H. C. Hesse, A. Jossen, and R. Witzmann, "Operating a multitasking stationary battery storage system for providing secondary control reserve on low-voltage level," in *International ETG Congress 2015; Die Energiewende - Blueprints for the new energy age*, 2015.

[62] B. Cheng and W. B. Powell, "Co-optimizing battery storage for the frequency regulation and energy arbitrage using multi-scale dynamic programming," *IEEE Transactions on Smart Grid*, vol. 9, pp. 1997–2005, May 2018.

[63] E. Sortomme and M. A. El-Sharkawi, "Optimal power flow for a system of microgrids with controllable loads and battery storage," in *2009 IEEE/PES Power Systems Conference and Exposition*, 2009.

[64] A. Malhotra, B. Battke, M. Beuse, A. Stephan, and T. Schmidt, "Use cases for stationary battery technologies: A review of the literature and existing projects," *Renewable and Sustainable Energy Reviews*, vol. 56, pp. 705 – 721, 2016.

[65] L. D. Robinson and R. E. Garcia, "Dualfoil.py: Porous electrochemistry for rechargeable batteries," Oct 2015.

[66] M. Doyle, T. F. Fuller, and J. Newman, "Modeling of galvanostatic charge and discharge of the lithium/polymer/insertion cell," *Journal of the Electrochemical Society*, vol. 140, no. 6, pp. 1526–1533, 1993.

[67] S. Gold, "A pspice macromodel for lithium-ion batteries," in *The Twelfth Annual Battery Conference on Applications and Advances*, 1997.

[68] C. F. Chiasserini and R. R. Rao, "Energy efficient battery management," *IEEE Journal on Selected Areas in Communications*, vol. 19, pp. 1235–1245, July 2001.

[69] J. Manwell and J. McGowan, "Extension of the kinetic battery model for wind/hybrid power systems," in *Proceedings of the 5th European Wind Energy Association Conference (EWEC '94)*, pp. 284 – 289, 1994.

[70] J. Manwell and J. McGowan, "Evaluation of battery models for wind/hybrid power system simulation," in *Proceedings of the 5th European Wind Energy Association Conference (EWEC '94)*, pp. 1182–1187, 1994.

[71] D. Rakhmatov and S. Vrudhula, "An analytical high-level battery model for use in energy management of portable electronic systems," in *IEEE/ACM International Conference on Computer Aided Design. ICCAD 2001. IEEE/ACM Digest of Technical Papers*, 2001.

[72] M. Jongerden and B. Haverkort, "Which battery model to use?," *IET software*, vol. 3, 2009.

[73] B. Xu, J. Zhao, T. Zheng, E. Litvinov, and D. S. Kirschen, "Factoring the cycle aging cost of batteries participating in electricity markets," *IEEE Transactions on Power Systems*, vol. 33, pp. 2248–2259, March 2018.

[74] M. Ecker, N. Nieto, S. Käbitz, J. Schmalstieg, H. Blanke, A. Warnecke, and D. U. Sauer, "Calendar and cycle life study of li(nimnco)o2-based 18650 lithium-ion batteries," *Journal of Power Sources*, vol. 248, pp. 839 – 851, 2014.

[75] G. Andersson, "Power system analysis," Sept. 2012.

[76] H. Yuan, F. Li, Y. Wei, and J. Zhu, "Novel linearized power flow and linearized opf models for active distribution networks with application in distribution lmp," *IEEE Transactions on Smart Grid*, vol. 9, pp. 438–448, Jan. 2018.

[77] A. Jambagi, M. Kramer, and V. Cheng, "Residential electricity demand modelling: Activity based modelling for a model with high time and spatial resolution," in *2015 3rd International Renewable and Sustainable Energy Conference (IRSEC)*, Dec 2015.

[78] G. B. A. Grandjean, J. Adnot, "A review and an analysis of the residential electric load curve models," *Renewable and Sustainable Energy Reviews*, vol. 16, no. 9, pp. 6539 – 6565, 2012.

[79] L. G. Swan and V. I. Ugursal, "Modeling of end-use energy consumption in the residential sector: A review of modeling techniques," *Renewable and Sustainable Energy Reviews*, vol. 13, no. 8, pp. 1819 – 1835, 2009.

[80] D. J. Aigner, C. Sorooshian, and P. Kerwin, "Conditional demand analysis for estimating residential end-use load profiles," *The Energy Journal*, vol. 5, no. 3, pp. 81–97, 1984.

[81] R. Bartels, D. G. Fiebig, M. Garben, and R. Lumsdaine, "An end-use electricity load simulation model: Delmod," *Utilities Policy*, vol. 2, no. 1, pp. 71 – 82, 1992.

[82] C. Wang, G. Grozev, and S. Seo, "Decomposition and statistical analysis for regional electricity demand forecasting," *Energy*, vol. 41, no. 1, pp. 313 – 325, 2012. 23rd International Conference on Efficiency, Cost, Optimization, Simulation and Environmental Impact of Energy Systems, ECOS 2010.

[83] F. McLoughlin, A. Duffy, and M. Conlon, "Characterising domestic electricity consumption patterns by dwelling and occupant socio-economic variables: An irish case study," *Energy and Buildings*, vol. 48, pp. 240 – 248, 2012.

[84] L. Magnano and J. Boland, "Generation of synthetic sequences of electricity demand: Application in south australia," *Energy*, vol. 32, no. 11, pp. 2230 – 2243, 2007.

[85] B. Stephen, A. J. Mutanen, S. Galloway, G. Burt, and P. Järventausta, "Enhanced load profiling for residential network customers," *IEEE Transactions on Power Delivery*, vol. 29, pp. 88–96, Feb 2014.

[86] R. Yao and K. Steemers, "A method of formulating energy load profile for domestic buildings in the uk," *Energy and Buildings*, vol. 37, no. 6, pp. 663 – 671, 2005.

[87] M. Stokes, *Removing barriers to embedded generation: a fine-grained load model to support low voltage network performance analysis.* phdthesis, De Montfort Universtiy, 2005.

[88] J. Paatero and P. Lund, "A model for generating household electricity load profiles," *International Journal of Energy Research*, vol. 30, pp. 273–290, 2006.

[89] C. F. Walker and J. L. Pokoski, "Residential load shape modelling based on customer behavior," *IEEE Transactions on Power Apparatus and Systems*, vol. PAS-104, pp. 1703–1711, July 1985.

[90] A. Capasso, W. Grattieri, R. Lamedica, and A. Prudenzi, "A bottom-up approach to residential load modeling," *IEEE Transactions on Power Systems*, vol. 9, pp. 957–964, May 1994.

[91] M. M. Armstrong, M. C. Swinton, H. Ribberink, I. Beausoleil-Morrison, and J. Millette, "Synthetically derived profiles for representing occupant-driven electric loads in canadian housing," *Journal of Building Performance Simulation*, vol. 2, no. 1, pp. 15–30, 2009.

[92] I. Richardson, M. Thomson, and D. Infield, "A high-resolution domestic building occupancy model for energy demand simulations," *Energy and Buildings*, vol. 40, no. 8, pp. 1560 – 1566, 2008.

[93] I. Richardson, M. Thomson, D. Infield, and A. Delahunty, "Domestic lighting: A high-resolution energy demand model," *Energy and Buildings*, vol. 41, no. 7, pp. 781 – 789, 2009.

[94] I. Richardson, M. Thomson, D. Infield, and C. Clifford, "Domestic electricity use: A high-resolution energy demand model," *Energy and Buildings*, vol. 42, no. 10, pp. 1878 – 1887, 2010.

[95] J. Widén, M. Lundh, I. Vassileva, E. Dahlquist, K. Ellegård, and E. Wäckelgård, "Constructing load profiles for household electricity and hot water from time-use data – modelling approach and validation," *Energy and Buildings*, vol. 41, no. 7, pp. 753 – 768, 2009.

[96] J. Widén, A. M. Nilsson, and E. Wäckelgård, "A combined markov-chain and bottom-up approach to modelling of domestic lighting demand," *Energy and Buildings*, vol. 41, no. 10, pp. 1001 – 1012, 2009.

[97] J. Widén and E. Wäckelgård, "A high-resolution stochastic model of domestic activity patterns and electricity demand," *Applied Energy*, vol. 87, no. 6, pp. 1880 – 1892, 2010.

[98] Molitor, K. Togawa, S. Bolte, and A. Monti, "Load models for home energy system and micro grid simulations," in *2012 3rd IEEE PES Innovative Smart Grid Technologies Europe (ISGT Europe)*, Oct 2012.

[99] D. Fischer, A. Härtl, and B. Wille-Haussmann, "Model for electric load profiles with high time resolution for german households," *Energy and Buildings*, vol. 92, pp. 170 – 179, 2015.

[100] Bayerisches Landesamt für Statistik, "Ausstattung privater haushalte mit ausgewählten langlebigen gebrauchsgütern in bayern," June 2017.

[101] Stadtwerke Ulm/ Neu-Ulm Netze GmbH, "Lasprofile SH0 2018," 2018.

[102] fdz der Statistischen Ämter des Bundes und der Länder, "Zeitbudgeterhebung," 2001-2002. eigene Berechnungen.

[103] fdz der Statistischen Ämter des Bundes und der Länder, "Zeitbudgeterhebung," 2012-2013. eigene Berechnungen.

[104] R. Stamminger, "Synergy potential of smart appliances," resreport, University of Bonn, Nov. 2008.

[105] E. U. Calculator, "Electricity usage of a stove top," 2018.

[106] A. Ridi, C. Gisler, and J. Hennebert, "Acs-f2 – a new database of appliance consumption signatures," in *In the 6th International Conference of Soft Computing and Pattern Recognition (SoCPaR)*, pp. 145–150, 2013.

[107] S. Barker, A. Mishra, D. Irwin, E. Cecchet, and P. Shenoy, "Smart*: An open data set and tools for enabling research in sustainable homes," in *Proceedings of the 2012 Workshop on Data Mining Applications in Sustainability (SustKDD 2012)*, (Beijing, China), Aug. 2012.

[108] E. Palacios-Garcia, A. Chen, I. Santiago, F. B.-O. no, J. Flores-Arias, and A. Moreno-Munoz, "Stochastic model for lighting's electricity consumption in the residential sector. impact of energy saving actions," *Energy and Buildings*, vol. 89, pp. 245 – 259, 2015.

[109] Statista, "Average annual electricity consumption of computer products in households in england in 2011 (in kilowatt-hours/year)." Online, June 2012.

[110] N. Terry, J. Palmer, D. Godoy, S. Firth, and A. T. Tom Kane, "Further analysis of the household electricity survey: Lighting study (final report)," May 2013.

[111] A. Reinhardt, P. Baumann, D. Burgstahler, M. Hollick, H. Chonov, M. Werner, and R. Steinmetz, "On the accuracy of appliance identification based on distributed load metering data," in *Proceedings of the 2nd IFIP Conference on Sustainable Internet and ICT for Sustainability (SustainIT)*, pp. 1–9, 2012.

[112] H. Pihala, "Power signatures of home appliances based on non-intrusive appliance load monitoring (nialm) method," tech. rep., SGEM (Smart Grids and Energy Markets), 2012.

[113] M. G. Nipun Batra, "Indian dataset for ambient water and energy," 2013.

[114] S. Makonin, "Ampds2: The almanac of minutely power dataset (version 2)," 2016.

[115] LASS (Laboratory for Advanced Software Systems), "Umass trace repository," 2017.

[116] Department of Energy and Climate Change, "Household electricity survey," 2012.

[117] H. Pandzic, Y. Wang, T. Qiu, Y. Dvorkin, and D. S. Kirschen, "Near-optimal method for siting and sizing of distributed storage in a transmission network," *IEEE Transactions on Power Systems*, vol. 30, no. 5, pp. 2288–2300, 2015.

[118] C. Thrampoulidis, S. Bose, and B. Hassibi, "Optimal placement of distributed energy storage in power networks," *IEEE Transactions on Automatic Control*, vol. 61, no. 2, pp. 416–429, 2016.

[119] S. Wogrin and D. F. Gayme, "Optimizing storage siting, sizing, and technology portfolios in transmission-constrained networks," *IEEE Transactions on Power Systems*, vol. 30, no. 6, pp. 3304–3313, 2015.

[120] A. Castillo and D. F. Gayme, "Profit maximizing storage allocation in power grids," in *52nd IEEE Conference on Decision and Control*, pp. 429–435, 2013.

[121] S. Bose, D. F. Gayme, U. Topcu, and K. M. Chandy, "Optimal placement of energy storage in the grid," in *2012 IEEE 51st IEEE Conference on Decision and Control (CDC)*, pp. 5605–5612, Dec 2012.

[122] M. Nick, R. Cherkaoui, and M. Paolone, "Optimal planning of distributed energy storage systems in active distribution networks embedding grid reconfiguration," *IEEE Transactions on Power Systems*, vol. 33, no. 2, pp. 1577–1590, 2018.

[123] S. Mashayekh, M. Stadler, G. Cardoso, and M. Heleno, "A mixed integer linear programming approach for optimal der portfolio, sizing, and placement in multi-energy microgrids," *Applied Energy*, vol. 187, pp. 154 – 168, 2017.

[124] S. Bolognani and S. Zampieri, "On the existence and linear approximation of the power flow solution in power distribution networks," *IEEE Transactions on Power Systems*, vol. 31, no. 1, pp. 163–172, 2016.

[125] S. Bahramirad and H. Daneshi, "Optimal sizing of smart grid storage management system in a microgrid," in *2012 IEEE PES Innovative Smart Grid Technologies (ISGT)*, 2012.

[126] A. Aichhorn, M. Greenleaf, H. Li, and J. Zheng, "A cost effective battery sizing strategy based on a detailed battery lifetime model and an economic energy management strategy," in *2012 IEEE Power and Energy Society General Meeting*, 2012.

[127] Y. Ru, J. Kleissl, and S. Martinez, "Storage size determination for grid-connected photovoltaic systems," *IEEE Transactions on Sustainable Energy*, vol. 4, no. 1, pp. 68–81, 2013.

[128] H. Nazaripouya, Y. Wang, P. Chu, H. R. Pota, and R. Gadh, "Optimal sizing and placement of battery energy storage in distribution system based on solar size for voltage regulation," in *2015 IEEE Power Energy Society General Meeting*, 2015.

[129] G. Carpinelli, F. Mottola, D. Proto, A. Russo, and P. Varilone, "A hybrid method for optimal siting and sizing of battery energy storage systems in unbalanced low voltage microgrids," *Applied Sciences*, vol. 8, no. 3, 2018.

[130] M. Motalleb, E. Reihani, and R. Ghorbani, "Optimal placement and sizing of the storage supporting transmission and distribution networks," *Renewable Energy*, vol. 94, pp. 651 – 659, 2016.

[131] C. Curry, "Lithium ion battery costs and market." Bloomberg New Energy Finance, July 2017.

[132] K. Poncelet, H. Hoschle, E. Delarue, A. Virag, and W. D'haeseleer, "Selecting representative days for capturing the implications of integrating intermittent renewables in generation expansion planning problems," *IEEE Transactions on Power Systems*, vol. 32, pp. 1936–1948, May 2017.

[133] I. J. Scott, P. M. Carvalho, A. Botterud, and C. A. Silva, "Clustering representative days for power systems generation expansion planning: Capturing the effects of variable renewables and energy storage," *Applied Energy*, vol. 253, p. 113603, 2019.

[134] Technical University of Munich (TUM), "ESOSEG," 2019.

[135] R. D. Zimmerman, C. E. Murillo-Sanchez, and R. J. Thomas, "Matpower: Steady-state operations, planning, and analysis tools for power systems research and education," *IEEE Transactions on Power Systems*, vol. 26, pp. 12–19, Feb 2011.

[136] European Commission, "RES LEGAL Europe." http://www.res-legal.eu/.

[137] IRENA, "Renewable capacity statistics (2018)," tech. rep., International Renewable Energy Agency (IRENA), 2018.

[138] F. ISE, "Aktuelle fakten zur photovoltaik in deutschland." Download, Feb. 2019.

[139] N. Kittner, F. Lill, and D. M. Kammen, "Energy storage deployment and innovation for the clean energy transition," *Nature Energy*, vol. 2, no. 17125, 2017.

[140] Tesla, "Powerwall." https://www.tesla.com/powerwall.

[141] H. E. Melin, "The lithium ion battery end of life market. a baseline study," Jan. 2019.

[142] J. Neubauer, K. Smith, and A. P. E. Wood, "Identifying and overcoming critical barriers to widespread second use of pev batteries," techreport NREL/TP-5400-63332, National Renewable Energy Laboratory, Feb. 2015.

[143] G. Reid and J. Julve, "Second life-batteries as flexible storage for renewables energies," techreport, Bundesverband Erneuerbare Energien e.V. (BEE), Apr. 2016.

[144] Ront.Info, "Der regelbare ortsnetztransformator: Die wirtschaftliche alternative zu netzausbau." https://ront.info/.

Appendix A

REM Background Data

Breakdown of residential loads depending on household size [3].

	Household Category (HC)				
Load Category (LC)	1	2	3	4	5+
Office	17.95	13.93	13.17	12.66	12.36
TV/Audio	14.68	12.86	13.23	11.63	11.43
Refrigeration	17.78	13.14	11.08	10.11	8.60
Cooking	11.07	12.21	10.78	10.73	9.72
Lighting	10.74	10.19	10.00	10.39	11.77
Circulation Pump	5.80	6.74	7.04	7.76	7.69
Drying	2.34	5.22	7.44	8.93	9.44
Dishwashing	2.81	5.14	6.33	6.94	7.02
Washing Machine	4.19	4.75	5.4	5.67	6.09
Freezing	3.06	5.39	5.51	5.86	5.99
Miscellaneous	9.58	10.43	10.02	9.33	9.89